ISAS - INTERNATIONAL SCHOOL
FOR ADVANCED STUDIES

A Study of BL Lacertae Objects in the Far Ultraviolet Spectral Band based on IUE Observations

Thesis submitted for the degree of
Magister Philosophiae

Astrophysics Sector

Candidate:
Elena Pian

Supervisor:
Prof. Aldo Treves

October 1992

TRIESTE

ISSA - SCUOLA
TERNAZIONALE
SUPERIORE
STUDI AVANZATI
TRIESTE
Strada Costiera 11

Table of Contents

Introduction 1

1. The analysis of observational UV data 4

1.1 The *International Ultraviolet Explorer* 5

1.2 IUE performance and running 6

1.3 Data-quality limitations 9

1.4 The GEX method of spectra extraction 12

2. IUE observations of BL Lac Objects 15

2.1 Target objects 17

2.2 The UV to IR spectral flux distribution of four BL Lacs . . . 21

2.3 The ultraviolet continuum of five BL Lacs 29

3. IUE monitoring of the BL Lac Object PKS 2155-304 32

3.1 Observations and data reduction 35

3.2 Results 38

3.3 Correlation analysis 41

3.4 Comparison with previous results and discussion 42

Conclusion 45

Acknowledgments 47

References 48

Figure Captions 54

Tables 117

Appendix A: Multifrequency observations of BL Lac Objects 142

Appendix B: IUE monitoring of PKS 2155-304 170

Appendix C: Notes on IUE data reduction software 183

Introduction

Early in the study of quasars and Active Galactic Nuclei (AGN) it was discovered that the optical brightness of some sources varied by a magnitude or more. Further studies in the past two decades revealed that there is a class of objects in which emission variability is accompanied by high and variable polarization and flat radio spectra. These characteristics are found in sources with emission lines (Optically Violently Variable quasars) and without emission lines (BL Lacertae Objects). Collectively, these sources are referred to as *blazars*, a term which resumes the characteristic of violent optical flaring and stresses the likely common nature of the non thermal activity in host objects which may differ in other properties.

BL Lacs have pointlike optical images, show continua which steepen gradually from the radio through the UV, optical emission which is dominated by a highly polarized, featureless continuum, strong non thermal radio emission and extremely strong and rapid variability at all observed wavelengths, whose amplitude carries important information about the size of the emitting region.

The present study is based on the observation and reduction of ultraviolet (UV) data of BL Lac objects taken from the *International Ultraviolet Explorer* (IUE), the longest living satellite in the far–UV energy band, being at work since 1978.

The far–UV band has, with respect to the optical, the important advantage of a lesser contamination by starlight. This enables a reliable determination of the non thermal continuum.

The IUE observatory is very well suited to regular monitoring of AGN because of its ease of scheduling, efficient geosynchronous orbit, precise photometric calibration (better than 5%) and stability, and broad wavelength coverage.

IUE has operated for more than 13 years, having gathered over 4500 spectra of some 500 AGN since its launch. Edelson *et al.* (1991*b*) listed 41 BL Lac Objects for a total of 471 extracted spectra contained in the IUE archive as part of the project of extracting line and continuum fluxes for all IUE observations of AGN, focussing the analysis on individual spectra.

Kinney, Bohlin, and Blades (1991) constructed an UV atlas of 69 quasars, blazars and Seyfert 1 galaxies by combining over 1000 low–resolution spectra drawn from over a decade of observations contained in the IUE data archive. The purpose of the work was to provide a uniformly extracted and calibrated set of UV spectra of the highest possible signal–to–noise ratio for quasars and blazars observed with IUE. They concluded that quasars and blazars in their sample undergo substantial UV variation, which is considerably larger than optical, and they vary more at short UV wavelengths than at long UV wavelengths.

The present thesis describes the UV continuum characteristics of a list of nine BL Lacs with weak UV emission and the UV variability properties of the strong emitting BL Lac source PKS 2155–304. Both studies have been conducted in collaboration with other groups.

The IUE observational data have been reducted and analysed within *MIDAS*, the software package for data reduction, which has been recently implemented at S.I.S.S.A. to allow local analysis of IUE data. The IUE spectra are extracted with the GEX method described in Chapter 1.

The local implementation of GEX is described in the handbook contained in

Appendix C, as well as other *MIDAS* procedures locally developed and not contained in the general handbook which is provided from ESO with the distributed package. These additional available procedures represent the result of the effort to facilitate the use of *MIDAS* and to realise a "user–friendly" global and complete scheme for the IUE data reduction and analysis. They were developed and documented in Milan at the Istituto di Fisica Cosmica e Tecnologie Relative del CNR (I.F.C.T.R.) by Dott. Lucio Chiappetti, who made them available to implementation at S.I.S.S.A..

The thesis work is divided as follows: in the first Chapter a review is proposed of the characteristics of IUE, also containing a description of the GEX method of spectra extraction; the second Chapter is devoted to the study of nine BL Lacs observed with IUE. Four of them have been observed for the first time in the UV band and they have been quasi–simultaneously observed also in the optical and IR bands. The overall spectra, from IR to UV are reported and studied. The third Chapter reports the results of the IUE monitoring performed during November 1991 on the BL Lac object PKS 2155–304. The monitoring which was part of an observing program extending also to the optical and X–ray energy ranges and aimed to study the variability properties of the object, revealed strong variations in the flux and remarkable changes in the spectral shape of the UV continuum.

Three appendices are added. The first two report the text of the articles in which the data and results would be published, and the third one contains a handbook for the use of the *MIDAS* reduction system facilities currently available at S.I.S.S.A.. The handbook has been adapted from an internal report of I.F.C.T.R. prepared by Dott. Lucio Chiappetti.

Chapter 1

The analysis of observational UV data

IUE two–dimensional images of the extragalactic objects under study have been examined and reduced to one–dimensional spectra files with the GEX spectra extraction method and then fitted to a simple power–law. The extraction procedure, as well as the integration of fluxes on short wavelength bands and the realization of spectral flux distribution files have been implemented within the *MIDAS* software package for astronomical data analysis. Appendix C contains a description handbook of the *MIDAS* routines and procedures locally available and running on an UNIX system.

The fitting routine runs on an IBM machine in Milan. A general description of the routine and of its implementation will be given in Appendix C as well.

Followingly are exposed the working and observing conditions of the IUE satellite (Sections 1.1 and 1.2), then are briefly illustrated the general data reduction procedures (Sections 1.3 and 1.4).

1.1 The International Ultraviolet Explorer

The *International Ultraviolet Explorer* was launched successfully on 26 January 1978, from Cape Canaveral, Florida, as a realization of a joint project of ESA, NASA and SERC. The satellite was developed to provide a general facility for observing UV spectra of astronomical sources over the wavelength range from about 1150 Å to 3200 Å. The satellite has been placed in geosynchronous orbit over the Atlantic Ocean at a mean distance of about 35,000 km from the Earth and is operated for 16 h each day from the US ground observatory located at the Goddard Space Flight Center (GSFC) near Washington, D.C., and for the remaining 8 h by ESA, from European ground observatory located near Madrid.

A high spectral resolution of the order of 0.2 Å is available to study the atmospheric characteristics of bright stars and planets and a lower resolution of about 6 Å to obtain information on faint sources. The spectra of the objects under study have all been taken in low resolution.

Two requirements were fundamental in determining the design of the scientific instrument and of the spacecraft to support it: first, the instrument should be able to record simultaneous data over large spectral ranges and, second, the spacecraft should be able to take maximum advantage of the observer's real–time judgement concerning the quality and content of his data. The first suggests a spectrograph using an imaging system, such as a television camera, capable of integrating the spectrum. To achieve adequate resolution, the total spectrum must be splitted into two ranges, from 1150 Å to 1950 Å and from 1900 Å to 3000 Å, and so two cameras are required to record the full spectral range. The second requires good communication between the spacecraft and the observer so a geosynchronous orbit was chosen (Boggess *et al.*, 1978).

1.2 IUE performance and running

The long- and short–wavelength spectrographs of IUE each have one primary and one redundant camera, which integrate the spectrograph image in SEC vidicon detectors. Exposures are controlled by the on–board computer, which gives reliable exposure length control in units of 0.4096 sec. At the conclusion of the exposure, the image, a 768 × 768 pixel array, is scanned and transmitted to the ground. The video signal from the potassium chloride SEC target is digitized into one of 256 discrete levels (0 to 255 Data Numbers, or DN) by an eight–bit analog–to–digital converter. An "optimum" exposure level is approximately 200 DN, due to non–linear camera response at higher DN levels. All exposure–level information is lost above 255 DN. Overexposures are measured with respect to "optimum" levels. All four television cameras are of identical construction and, since they are only sensitive to visible light, are preceeded by UV–to–visible converters (UVCs) (Harris and Sonneborn, 1987).

The Short–Wave Prime (SWP) camera is the most used and least problematic camera. Its role as the standard short–wavelength camera has remained unchanged throughout the history of the project to date. The SWP camera provides complete wavelength coverage from 1150 to 1975 Å in low dispersion. Since mid–1979 its sensitivity has decreased by less than 1 % per year at any wavelength, although a rather rapid decrease of about 6% was observed at 1550 and 1850 Å during the first year after launch.

The Short–Wave Redundant (SWR) camera has suffered from intermittent failure of its read–out section since launch and has never been made available for Guest Observer use. Some images were taken during the commissioning period, however.

Until 16 October 1983, the Long–Wave Prime (LWP) camera was, despite its name, the back–up long–wavelength camera due to the frequent scan control malfunction of its read–out section. However, on that date it was promoted to standard (default) long–wavelength camera due to the "flare" problem which has developed in the LWR camera (see below). The LWP camera provides complete wavelength coverage from 1910 to 3300 Å in low dispersion. Due to the improved behaviour of the camera with increased usage and implementation of a "bad scan detection" software patch, the scan control malfunction no longer presents a problem. No change of sensitivity with time has been apparent to date. In terms of both sensitivity and signal–to–noise ratio S/N the LWP is the better camera longward of 2500 Å. While serving as the long–wavelength back–up camera, the LWP camera was made available in 1981 to Guest Observers having programs for which these characteristics were particularly important.

The Long–Wave Redundant (LWR) camera was the standard long–wavelength camera for the first 5.5 yr of Guest Observer operations. The LWR camera provides complete wavelength coverage from 1900 to 3300 Å in low dispersion. The flare discharge in the camera's UVC, which produces a bright patch near the lower rim of an image, has been contaminating long exposure images since April 1983. The serious and steadily worsening impact of this anomaly was recognized in September 1983, and prompted the switch to the LWP as default long–wavelength camera in October 1983. Tests have shown, however, that with a 10% reduction in the UVC operating voltage, flare–free images can be obtained.

IUE target acquisition and telescope pointing control during exposures, rely on the Fine–Error Sensor (FES) in the scientific instrument. The actual spacecraft pointing control and slewing is performed by the on–board computer (OBC). The

FES provides the only means of mapping the telescope field of view and measuring stellar positions and brightnesses. FES star tracking data is also used by the OBC for automatic offset guiding during exposures. The most important aspects of the FES operations with regard to the quality of IUE spectral data are the accuracy with which a target can be centered in the spectrograph apertures and the pointing precision of the tracking, or offset–guiding mode. The large apertures are approximately 10 × 20 arcsec ovals; the small apertures are 3 arcsec diameter circles.

The FES "prime" mode is used to measure the position of an object's center of light and its brightness. The FES positional resolution is about 0.26 arcsec, so that an object brighter than about $m_{1'} = 13.5$ can be centered in an aperture with an error of less than 0.5 arcsec. The photometric calibration of the FES brightness measurements is a function of time, $B - V$, and FES tracking mode. While the FES was not designed to function as a photometer, it has often been used as such. The FES signal (counts) measured at the time of a given observation are recorded on the observing "scripts" at GSFC and VILSPA and have been entered in the Merged Log of IUE Observations.

The acquisition of targets invisible (in visual light, $m_{1'} > 13.5$) to the FES is one of the most difficult type of observations routinely carried out by the IUE spacecraft. Such objects are acquired by blind–offset techniques, where the telescope is maneuvered a short distance to the invisible target from a nearby star. Blind–offset maneuvers performed with the three–gyro control system had errors less than 1 arcsec for slews less than 10 arcmin, and errors less than 2.5 arcsec for slews less than 30 arcmin. Similar maneuvers performed on the two–gyro/Fine Sun Sensor control system have errors less than 2 arcsec for slews less than 15 arcmin.

The indication that a blind–offset acquisition was performed for a particular spectral image will be found on the GSFC observing script or the VILSPA observing log. The GSFC observing scripts usually contain the name and coordinates of the offset star used for the blind–offset.

The sensitivity of the IUE cameras is determined by the quantum efficiency of the UVC photocathode, which is highly wavelength dependent, and the photoelectron sensitivity of the remaining system which is dependent on position in the image. The sensitivity of the SWP camera increases with wavelength, apart from a dip near 1500 Å. The LWR and LWP cameras both have sensitivities which peak near 2800 Å.

The spectral and spatial resolution achievable with IUE data are limited by the size of the point spread function (PSF) in the camera image plane. In general this varies with wavelength and is dependent on camera used, dispersion mode and telescope focussing conditions.

1.3 Data-quality limitations

The quality of IUE data is limited by several phenomena and artifacts which are common to all cameras. The most important of these from the user's point of view are:

1) Reseau marks. These marks appear on images as small dark dots, 2 to 3 pixels square, in a regular array. They provide a reference grid to enable correction during processing for the geometric distortion of the image by the camera electron optics. A spectral order falling on a reseau gives rise to a very narrow "absorption" feature in the processed spectrum. Reseaux are flagged in extracted spectral files

and plots; on photowrites their regular spacing usually facilitates their separation from real absorption features.

2) Image blemishes. There are a number of permanent "hot–pixels" on the target of all cameras. These appear as bright spots on the images and produce false narrow "emission" features where they coincide with spectral orders. Random bright spots also appear in IUE images due to radioactive decay of atoms in the UVC phosphor; their number increases with exposure time. Many random features are caused by cosmic–ray hits in the UVCs. These can leave streaks or comet–like patterns on an image, which will give rise to spurious spectral features when they intersect an order or contaminate the adjacent background (Harris and Sonneborn, 1987).

3) Phosphorescence. After the end of an exposure, the UVC continues to emit some light with an intensity proportional to the exciting exposure level and a power–law decay with time. A more serious problem occurs when there is phosphorescence after an overexposed spectral image or even a series of many optimum exposures. The data bank contains many examples of long–exposure images contaminated by residual "ghost" spectral orders originating in this way which produce spurious features in the processed data.

4) Radiation–induced background. This builds up uniformly over the image area during an exposure and is the result of Cerenkov photons produced in the camera faceplate by high–energy electrons from the outer Van Allen Belt.

5) Microphonics and data corruption. Particularly LWR images, may be contaminated by a narrow band of microphonic noise (up to 100 DN) cutting horizontally across the image.

Also there are limitations imposed on the data accuracy by the hardware.

The S/N of IUE data is camera dependent and varies greatly with exposure level and wavelength. Up to a signal level of about 200 DN, the S/N increases roughly linearly with exposure level. Beyond this the camera target begins to saturate and the extra exposure time required per DN increase in signal leads to a disproportionate increase in noise level.

The S/N can be enhanced by averaging several spectra. However, due to small–scale spatial variations in camera gain and imperfect photometric correction by the ITF, some "fixed–pattern" noise is generally apparent in IUE data. Since adding spectra will not reduce this non–random noise component, the improvement in S/N obtained by co–adding spectra is therefore not as great as would be expected if the noise were purely statistical.

Finally, errors due to the effects of bad pointing may be not negligible in extragalactic observations. Because the targets are faint ($m_V \gtrsim 13$), source acquisition is generally by blind offset from a nearby bright star. Such offsets are generally good to 1-2″, although, in a few cases, mistakes in the positions of sources or other problems could cause the pointing to be off by much more. One would tend to expect larger errors for those objects having relatively distant offset stars ($r > 30'$), and for those offsets done since 1985 under the somewhat less accurate "two–gyroscope" system. Unfortunately, the IUE Merged Log of Observations and the spectra themselves contain little or no information on the accuracy of the pointing, so the magnitude of this effect is difficult to assess (Edelson *et al.*, 1991*b*).

1.4 The GEX method of spectra extraction

The IUE Spectral Image Processing System (IUESIPS) has been designed to provide the Guest Observer with spectral data reduced from the raw images in an accurate and standard manner and as free of instrumental effects as possible. The principal image processing steps have remained qualitatively the same during the mission. These steps include implicit correction for geometrical distortion of the camera system by reference to the reseau grid superposed on each image; photometric correction of the image, by means of pixel–by–pixel intensity transfer functions (ITFs), which correct for sensitivity variation across the SEC vidicon detector and its non–linear response; wavelength calibration of the spectral orders with analytical dispersion relations determined from on–board platinum–neon lamp spectral images; extraction of spectral flux as a function of wavelength from the photometrically corrected image and reduction of the extracted spectral flux to an absolute flux system by means of absolute calibrations obtained from observations of photometric standard stars.

The image is transformed from the initial array of 8–bit raw signal data numbers (DN) to an array of 16–bit *linearized* flux numbers (FN) by means of an "intensity transfer function" (ITF). This is necessary since the signal stored on the potassium chloride camera target is a non–linear function of exposure, especially at high exposure levels. Furthermore, the form of the response varies from one pixel to another. Hence an ITF actually consists of a set of FN/DN transformation curves, one for each pixel in the image.

Once the wavelength–calibration dispersion relations are known, the positions of the orders in the geometrically corrected reference frame are determined. To extract each order, the dispersion relations must be mapped back into the photo-

metrically corrected raw–image space. For low–dispersion images the mapping is done for each pixel. Low–dispersion spatially–resolved extracted spectra are generated by passing a numerical slit along the dispersion direction, and calculating the extracted flux values every $\sqrt{2}/2$ pixels along and approximately perpendicular to the dispersion direction. Extracting data from the image in this way is equivalent to forming an appropriately weighted average of the four surrounding pixels for each pixel in the appropriate portion of the photometrically corrected image. For large aperture observations the size of the extraction slit in the spatial dimension is controlled by the extraction type, such as point source, trailed, or extended source extraction as selected by the observer. The extraction of fluxes in the spatial direction is along lines of constant wavelength. For images processed prior to 1 October 1985, 110 lines are extracted in the spatial direction and averaged in pairs to produce the 55 line spatially–resolved image file. Images processed after this date omit the pair–wise averaging and have spatially resolved files which have 110 lines. This is referred to as the "extended line–by–line" extraction. Slit–integrated spectra are formed by adding 9 (point source) or 15 (extended source) lines of the spatially resolved data and then subtracting background, that is the sum of two 5–line wide swaths on either side of, and separated by 5 lines from, the central 9 lines. It has long been recognized that this does not produce the best S/N, particularly for a faint signal above a high background. Also, the determination of the background is not reliable since it does not take into account its smooth change over the camera face. Moreover, the IUESIPS extraction procedure does not discriminate between cosmic ray hits and photons, so that spurious emission features arise.

For these reasons, other extraction techniques have been developed, and one

of these is the Gaussian extraction (GEX) method described by Urry and Reichert (1988), which assumes the cross–dispersion profile is a Gaussian. GEX consists of two passes on the line–by–line file, one coarse and one fine. The first pass, GEX1, fits a linear background plus a Gaussian to a series of cross–cuts (signal perpendicular to the dispersion direction). All fit parameters are stored in a table. In an intermediate step, the Gaussian widths are fitted to a quadratic, allowing for a smoothly changing focus along the spectrum. The second pass, GEX2, uses the same Gaussian–plus–linear–background model, but calculates only the height of the Gaussian for each cross–cut, taking the appropriate linear background coefficients and Gaussian centers from the table and imposing Gaussian widths determined from the quadratic fit. The width and height of the Gaussian determine its area and thus the flux at that particular cross–cut.

The extraction procedure produces spectra in units of time–integrated net FN. Conversion to absolute flux units requires multiplication by $S_\lambda^{-1}/\mathrm{t}$, where S_λ^{-1} is the "inverse sensitivity function" in units of 10^{-14} erg cm^{-2}Å^{-1} FN^{-1}, and t is the exposure time in seconds. Officially adopted S_λ^{-1} curves for each camera to give absolutely calibrated time-integrated fluxes in units of 10^{-14} erg cm^{-2} s^{-1}Å^{-1} are those of Bohlin and Holm (1980) for the SWP camera and Cassatella, Lloyd, and Gonzales Riestra (1988) for the LWP camera, which have been used in the present analysis. Other calibration curves are available, such as the SWP curve of Bohlin *et al.* (1990), which is used as well from many observers and differs from the one of Bohlin and Holm (1980) of about a 5%. A correction is often made by some observers for degradation in the sensitivity of the cameras, which has not been taken into account in this work.

Chapter 2

IUE observations of BL Lac Objects

We analysed the spectra of nine BL Lac Objects, six radio–selected and three X–ray–selected, observed between 1984 and 1989 from IUE at VILSPA.

Some of them have been obtained through our own observations (PKS 0118–272, PKS 0301–243, PKS 1538+149, H 0323+022, PKS 0048–097, PKS 0422+004 and PKS 0521–365) and for the other two (H 1722+119 and H 0414–009) spectra have been retrieved from the IUE archive and re–extracted with the GEX method. Also two archival spectra of H 0323+022 have been retrieved.

For three of these BL Lacs, PKS 0118–272, PKS 0301–243 and PKS 1538+149, the presented IUE observations are the first obtained thus far. They have been selected for observation with IUE for being among the most optically bright sources of the catalog of Impey and Tapia (1988, 1990), including a complete sample of radio–selected objects for which they performed optical polarimetry.

These objects have been quasi–simultaneously studied both in the optical and IR bands and the results of this multifrequency study in which I have been responsible of the UV data analysis, will appear in a paper reproduced in Appendix A.

Four other objects (H 0323+022, PKS 0048–097, PKS 0422+004 and PKS

0521–365) had been already observed by us with IUE and the present observations were gained as part of the long–term multiwavelength monitoring program in which the sources have been included several years ago. H 0323+022 has been quasi–simultaneously observed in the optical and IR bands and the results are presented in Section 2.2, as well as in Appendix A.

Finally, H 1722+119 and H 0414–009 enter our program of long–term monitoring of the sources and of study of the surrounding nebulosity (see Falomo, Melnick and Tanzi, 1990; Falomo and Tanzi, 1991). Here we do not present our observations but we extract and analyse archival spectra.

Figure 2.1 contains all the IUE extracted spectra, which are mostly so far unpublished. The UV spectrum of H 0323+022 is of higher quality than reported before. The data are not dereddened. Overimposed are the best fit power–law curves. When SWP and LWP simultaneously taken spectra were available for an object, they have been plotted together, forming a combined spectrum, and in those cases the overimposed curve corresponds to the fit of both spectra with a unique power–law. The results of fitting the UV continua with a simple power–law are listed in Table 2.3..

In the next Section will be given a brief review of the previous observations of the objects under study in various energy bands. In Section 2.2 the results of the multifrequency observations are reported and in Section 2.3 the UV continuum parameters will be discussed.

2.1 Target objects

PKS 0118-272

The optical magnitude ranges between $m_V = 15.5$ and $m_V = 17.0$ (Condon, Hicks, and Jauncey, 1977; Thompson, Djorgovski, and De Carvalho, 1990). The polarization has been measured by Impey and Tapia (1988, 1990) who report the value of 17.4%. IR optical photometry is given by Adam (1985), Tanzi *et al.* (1989), Allen *et al.* (1982), Ballard *et al.* (1990) and Mead *et al.* (1990), who also observed a high and constant polarization. The X–ray flux observed by the *Einstein* satellite is 0.14 μJy at 1 keV (Ledden and O' Dell, 1985). An absorption redshift $z = 0.559$ was recently determined by Falomo (1991) from an intervening absorption feature attributed to the MgII doublet.

PKS 0301-243

The optical magnitude ranges between 16.0 and 17.0 (Condon, Hicks, and Jauncey, 1977; Pica *et al.*, 1980, 1988). Optical polarimetry by Impey and Tapia (1988, 1990) gave an average polarization of 10.6%. Near–IR observations were gathered by Allen *et al.* (1982), Wright, Ables, and Allen (1983) and Bersanelli *et al.* (1992). Thus far there is no X–ray detection, nor a redshift estimate.

PKS 1538+149

The optical identification ($m_V = 15.5$) and the spectroscopic confirmation are due to Wills and Wills (1974) who have been led to recognize it as a BL Lac object. Optical monitoring of the source by Kinman (1976) and Pica *et al.* (1988)

evidenced a variability in the visual band of almost 2 mag ($17.2 \leq m_V \leq 19$) and a weaker one in the blue band (Kidger, 1988). The maximum optical polarization measured by Impey and Tapia (1990) was of 20%. The results of *IRAS* far–IR observations are reported by Impey and Neugebauer (1988) who also give the overall energy distribution which is peaked in the far–IR. Observations in the millimetric spectral range are reported by Edelson (1987) and near–IR measurements have been performed by Allen *et al.* (1982) and Bersanelli *et al.* (1992). The X–ray flux detected by *Einstein* is 0.15 μJy at 1 keV (Ledden and O'Dell, 1985). The redshift $z = 0.605$ is reported by Stickel *et al.* (1991).

H 0323+022

The flaring X–ray source H 0323+022 was independently noted by Doxsey *et al.* (1981) and Piccinotti *et al.* (1982) because of its dramatic variability and is well studied at all frequencies (Feigelson *et al.*, 1986, and references therein). The redshift $z = 0.147$ has been measured by Filippenko *et al.* (1986). The near–IR flux emission has been studied by Ballard *et al.* (1990). The visual magnitude ranges from 15.5 to 17.5 (Doxsey *et al.*, 1983; Feigelson *et al.*, 1986 and Pica *et al.*, 1988) with short term fluctuations.

The X–ray flux in the energy range 2–10 keV varied by about a factor of 3 between $\simeq$ 1 μJy and 3 μJy with an occasional flare up to 10 μJy during a 6 month period (Doxsey *et al.*, 1983), whereas the *Einstein* IPC data exhibited a 60 seconds dip of a factor of $\sim$ 11 at X–ray energies greater than 0.6 keV but not at 1/4 keV. The data following the 60 seconds dip showed that the X–ray emission at 1 keV varied smoothly between 4.8 and 6.4 μJy. *GINGA* observations by Ohashi (1989) in the range 2–30 keV yielded a dramatic variation of the flux in 5 hours from 1.1 μJy to 0.4 μJy.

H 1722+119

This BL Lac object is a strong and persistent X–ray source originally discovered by *Uhuru* (Forman *et al.*, 1978) and located by the HRI instrument on the *Einstein Observatory*. The *Einstein* HRI and MPC observations indicate a steep X–ray spectrum with a power–law energy index near 1.3. Brissenden *et al.* (1990) demonstrated that the source observed with the HRI is the correct identification of the *HEAO 1* LASS detection (Wood *et al.*, 1984). They also performed radio, IR and optical observations, finding an optical magnitude $m_{\rm V} = 15.77$, a featureless optical spectrum and no evidence of host galaxy, which puts the object at a redshift $z > 0.1$. The optical–IR polarization reaches a maximum of 17%. Radio measurements reveal a variable, compact source with increasing emission from 1985 to 1988. IUE archival spectra of the source were retrieved (the same we have extracted and analysed): extrapolation of the UV flux to the X–ray energy range is a factor of 2 smaller than the X–ray flux.

PKS 0048–097

This flat spectrum radio–source is strongly variable at radio and optical wavelengths (Stull, 1972; Falomo *et al.*, 1988, and references therein). Adam (1985) reports the UBV photometry of the source and Impey and Neugebauer (1988) studied it in the far–IR. Bersanelli *et al.* (1992) report about the near–IR monitoring of the object. The first IUE observations of PKS 0048–097 were obtained on 1987 January 7 and 8, when the object was in a moderately high optical state ($m_{\rm V} \approx 15.5$). Quasi–simultaneous optical–IR spectrophotometry allowed deriving the overall energy distribution from $\sim 10^{14}$ to $\sim 2.5 \times 10^{15}$ Hz. It was noted that the LWP data appeared to deviate significantly from the general trend, which could

be ascribed to a rapid variation of the UV emission in both intensity and spectral slope. The source has been observed also in the X–ray domain with *Einstein.*

PKS 0422+004

The strongly variable radio–source PKS 0422+004 was identified by Bolton, Shimmins, and Merkelijn (1968) with a starlike counterpart ($m_{\rm V} \approx 17$), whose featureless optical spectrum and variable optical polarization revealed its BL Lacertae nature. The object has been monitored both in the optical (Pica *et al.*, 1980) and in the near–IR (Allen, Ward, and Hyland, 1982; Bersanelli *et al.*, 1992). It was observed by Falomo *et al.* (1989) with IUE on 1987 August 31–September 1, when the visual magnitude of the object was $m_{\rm V} = 16.2$, and again ~ 4 months later (1988 Jan 10) during an active state ($m_{\rm V} = 15.6$). Quasi–simultaneous optical to IR observations allowed to conclude from the shape of the overall spectrum that it remarkably steepens between the optical and the UV frequencies. The extrapolated UV flux to the X–ray band is a factor of ~ 2 less than the flux observed from *Einstein.*

H 0414–009

This BL Lac object was first detected by *HEAO 1*, and identified in *Einstein Observatory* X–ray images. The polarization of Impey and Tapia (1988) confirmed the BL Lac classification. Halpern *et al.* (1991) show that there are no emission lines in the 1200–9000 Å range, and the spectrum can be decomposed into starlight and power–law components. They report a redshift $z = 0.287$, which makes H 0414–009 one of the most luminous X–ray emitters. The UV flux is very weak, as deduced from the SWP spectrum analysed by Halpern *et al.*, and from the

two LWP spectra studied by George (1988). He found marginal evidence for variability with a decrease of $\sim 30\%$ in one week. We extracted and analysed one of these spectra. Falomo and Tanzi (1991) report the results of multifrequency observations on this object including the UV band. They refer both SWP and LWP fluxes.

PKS 0521-365

This source was discovered in the NRL LASS *HEAO 1* experiment and identified as a BL Lac object by Schwartz *et al.* (1979). The bright BL Lac nucleus ($m_V = 16$) is hosted by a relatively isolated elliptical radiogalaxy at a redshift $z = 0.055$, characterized by a prominent radio and optical jet (Macchetto *et al.*, 1991, and references therein). Optical spectroscopy is reported by Falomo, Tanzi, and Treves (1989), optical and IR observations are reported by Tanzi *et al.* (1989) and optical polarimetry by Luna (1990). Far–IR measurements are due to Impey and Neugebauer (1988) and near–IR to Bersanelli *et al.* (1992).

The first IUE observations of the object had been made from Danziger *et al.* (1983). Edelson *et al.* (1991*b*) report the results of the analysis of archival IUE spectra of the object.

2.2 The UV to IR spectral flux distribution of four BL Lacs

Multifrequency spectra of blazars reveal that the nearly universal flat radio spectrum steepens in the millimeter or submillimeter region and there is a smooth connection between the IR, optical, and UV regions. Along with the variability data, this suggests that the UV radiation, like the IR and optical emission, is

produced by the synchrotron or synchrotron self–Compton process.

Because an extrapolation of the UV continuum to higher frequencies does not generally coincide with the X–ray flux, rather passing below it, the X–ray emission may be produced by another mechanism, as the inverse Compton process (Bregman, Maraschi, and Urry, 1987).

The continuous steepening of the flux distribution between the IR and the UV domain suggests that the overall spectrum of BL Lacs cannot be described by a single power–law, but more complex forms, like broken power–laws (e.g. Landau *et al.*, 1986; Cruz-Gonzales and Huchra, 1984; Ballard *et al.*, 1990; Brown *et al.*, 1989) should be used depending on the considered energy range. Spectral "breaks" are seen to occur between near–IR and optical or between optical and UV frequencies (*e.g.* Ghisellini *et al.*, 1986). These observed "features" may be intrinsic to the non–thermal emission component or be due to other causes like reddening, a contribution from the host galaxy and/or lack of simultaneity among observations in different bands. The contribution of starlight from the galaxy, if non negligible with respect to the non–thermal emission, produces a steepening of the energy distribution in the optical and a flattening in the near–IR, while reddening introduces a steepening of the continuum at optical–UV frequencies. For instance the spectral break observed in some objects between near–IR and optical is completely removed when proper reddening corrections are applied (*e.g.* Tanzi *et al.*, 1989).

A detailed study of the spectral shape of the non thermal component is important in order to understand the physics of the emission region.

Here will be reported the results of quasi–simultaneous (within days) UV, optical and near–IR observations of four BL Lac objects obtained in the course of

a systematic multifrequency study of BL Lacs (see *e.g.* Tanzi *et al.*, 1986; Falomo *et al.*, 1988, 1989; Treves *et al.*, 1989; Falomo and Treves, 1990). Table 2.1 contains a journal of observations.

The sources were centered in the blind offset mode in the large aperture ($10'' \times 20''$ oval) at coordinates measured on a blue POSS paper copy or on ESO plates and observed using both the SWP and the LWP cameras.

Bidimensional images have been reduced with the GEX extraction method described in Section 1.4, which is particularly efficient in detecting signal from weak and faint sources like the ones we are handling with.

The spectrum of PKS 1538+149 was at the limit of detectability, but still clearly visible in the line–by–line spectrum. For this case only the extraction criteria of Urry and Reichert have been relaxed: the default procedure first makes a fit of the background and computes the rms of the residuals around this fit in the region where signal is expected, then proceeds to signal extraction only if the average signal is $>$ rms/2. In our case we have loosened this constraints to be $>$ rms/3 to give evidence to the very faint signal.

The extracted net fluxes are converted to absolute flux using the IUE calibration of Bohlin and Holm (1980) for the SWP spectra and the calibration of Cassatella *et al.* (1988) for the LWP spectra.

For each spectrum the flux was averaged in wavelengths bands of 50 or 100 Å after rejecting flaws and features arising onto the continuum. The region below 1250 Å in the SWP spectra has been systematically avoided during this selection, because it is affected from the geocoronal Lyman α emission line and the region below 2400 Å has been as well rejected because the signal–to–noise ratio is here very poor.

The error associated to these averaged fluxes is the standard deviation σ divided by $\sqrt{N/3}$, where N is the number of pixels contained in each selected wavelength band. The factor 3 by which it is reduced takes into account the correlation between the pixels (Edelson *et al.*, 1991*b*).

Table 2.2 contains for each spectrum the averaged UV fluxes in the selected wavelength bands with relative errors. Also the exposure times (in seconds) used in gathering every image are given.

Using an iterative, chi–squared minimization fitting routine, the dereddened and undereddened IUE spectra were fitted to a simple power–law model of the form:

$$F_\lambda = F_0 \left(\frac{\lambda}{\lambda_0} \right)^{-\alpha_\lambda} \quad . \tag{2.1}$$

The fit parameters are the normalization, F_0, at fiducial wavelength λ_0, and slope α_λ. The definition of power–law slope seen most often in the literature is the energy index, α_ν, where $F_\nu \propto \nu^{-\alpha_\nu}$, which is related to α_λ via $\alpha_\nu = 2 - \alpha_\lambda$.

The interval of confidence at the 90 % level associated to the spectral index has been evaluated after Avni (1976) and Lampton *et al.* (1976).

The fluxes have been also dereddened for those objects for which the extinction A_V is different from zero.

Table 2.3 summarizes the results of the fitting both for undereddened and dereddened SWP and LWP spectra. Reduced chi–squared values relative to the fit are also listed. The fitted spectral indices are given in terms of the energy index, α_ν, but the fitting was done in wavelength space, with no resampling to frequency space.

In case both SWP and LWP simultaneous or quasi–simultaneous observations

were available for an object, the averaged SWP and LWP fluxes have been fitted together with a single power–law. This procedure reduces considerably the uncertainties on the fitted flux and spectral index, though it can suffer from a possible "mismatch" of the spectra due to the lack of perfect simultaneity, so that the absolute values of fitted flux and spectral index are not as reliable as for the fits to individual SWP and LWP spectra. Table 2.4 contains the parameters of the fit on combined spectra.

Optical spectrophotometry of the sources was obtained at the European Southern Observatory (ESO) 1.5m telescope equipped with a Boller and Chivens spectrograph and CCD detector. Spectra were taken at a resolution of $\approx$ 15 Å (FWHM) through a long slit of 8 arcsec width. Standard reduction procedures were applied to obtain flux calibrated spectra. From repeated observations of standard stars (Stone 1977; Baldwin and Stone, 1984) during each night, we derive a photometric accuracy better than 10 %. To increase the signal–to–noise ratio we obtained fluxes at intervals spaced of $\sim$ 100 Å binning the spectra over bands of 100 Å.

J,H,K and L photometry was obtained (see Table 2.1) at the ESO 2.2m telescope (+ InSb photometer). A 15 arcsec circular aperture with chopper throw of 20 arcsec in the E–W direction was used. Statistical 1-σ errors are less than 0.1 mag in all bands. Conversion to flux units is made according to the zero–magnitude fluxes given in Bersanelli, Bouchet and Falomo (1991).

A composite spectral flux distribution was constructed for each object from quasi simultaneous IR, optical and UV observations. Errors in the UV were computed combining the statistical errors of each band with a 10% systematic error. Data were corrected for interstellar reddening using A_V as deduced from the hy-

drogen column density (Stark *et al.*, 1984) and assuming $N_H/E_{B-V} = 5.8 \times 10^{21}$ (Bohlin, Savage and Drake 1978). The interstellar extinction curve of Savage and Mathis (1979) for the optical–UV region and its extension to the IR by Whittet (1988) were used. The adopted values of A_V are given in Table 2.3. Figures representing the overall spectra are at the end of Appendix A.

a) PKS 0118–272

The spectral flux distribution of PKS 0118–272 is reported in Fig. 3 of Appendix A. We find that a single power–law of $\alpha_\nu = 1.17 \pm 0.03$ is a good representation of the non thermal emission from 8×10^{13} to 1.2×10^{15} Hz. There is no spectral signature in the spectral flux distribution of the presence of a host galaxy.

b) PKS 0301–243

The overall spectral flux distribution of PKS 0301–243 from 1.2×10^{14} to 2.4×10^{15} Hz (see Appendix A, Fig. 4) can be described by a single power–law of index $\alpha = 1.01 \pm 0.03$ ($\chi^2_\nu \sim 1.9$). Although the data appear to be consistent with a single powe–law model there are some deviations which could be real.

The near–IR to optical region exhibits a small curvature. Spectral indices in the optical and near–IR regions indicate that some curvature (break ?) may be present at 5×10^{14} Hz ($\alpha_{opt} = 1.17 \pm 0.04$; $\alpha_{IR} = 0.83 \pm 0.22$). This could arise from the thermal contribution due to the host galaxy. To test this hypothesis we decomposed the spectrum into a power–law plus an elliptical galaxy (assuming $z = 0.2$). We find the data are well fitted ($\chi^2_\nu \sim 0.9$) by the model with $\alpha_\nu = 0.84$ and a galaxy contributing 10% of total flux at 5500 Å. This corresponds to a galaxy of $M_V \sim -22$.

c) PKS 1538+149

This is the faintest source among those observed and in fact it is at the limit of detectability with IUE. In the observed spectral range (1.2×10^{14} to 1.2×10^{15} Hz) the dereddened spectral flux distribution (see Appendix A, Fig. 5) is consistent with a simple power–law model of $\alpha = 1.33 \pm 0.08$ ($\chi^2_\nu \sim 0.2$). We note, however, that a fit to the optical spectrum alone gives a significant steeper spectral index ($\alpha \sim 1.8$). This steeper value was repeatedly observed also at different other epochs (Falomo *et al.*, 1992).

d) H 0323+022

The X–ray selected BL Lac object H 0323+022 (Doxsey *et al.*, 1983) is known to reside in a giant elliptical galaxy of $M_V \sim -22$ (Feigelson *et al.*, 1986; Fillipenko *et al.*, 1986) which contributes substantially to the observed flux in the near–IR and optical range. Our overall spectrum (see Fig. 6 of Appendix A) shows in fact a clear signature of a stellar population which flattens the energy distribution in the near–IR with respect to the optical.

To study the non thermal component, we decomposed the UV–optical to IR spectral flux distribution into a giant elliptical superposed onto a single power–law emission. We assumed the standard elliptical of Yee and Oke (1978) with the near–IR colors of Arimoto and Yoshii (1987) for the thermal component and a single power–law ($f_\nu \propto \nu^{-\alpha}$) for the non thermal source.

We found that the observations can be well fitted by the superposition of the (standard) elliptical galaxy, contributing 25% of the observed flux at 5500 Å, plus a flat non thermal component of spectral index $\alpha_\nu = 0.78$. The absolute magnitude of the host galaxy as derived from the decomposition of the spectral flux

distribution is $M_V = -21.6$ assuming $H_0 = 50$. This decomposition is consistent with that performed by Filippenko *et al.* (1986) using only optical spectrum and indicates that the non thermal component described by a flat power–law extends from 2×10^{14} to 5×10^{15} Hz.

The source was observed with IUE at previous epochs (see Figure 2.1 and Table 2.3). It is apparent that no significant variability of spectral shape is present within the errors in the combined spectra, but a little fading of the source from 1984 to 1988 seems to be evident followed by a brightening from 1988 to 1989.

A significant spectral hardening is evident in the long–wavelength UV range (LWP) from 1988 to 1989, but no correspondent flux variation is seen within the errors.

In all cases observed the spectral flux distribution is well accounted for either by a single power–law ($f_\nu \propto \nu^{-\alpha}$) or by a power–law plus an elliptical galaxy. The large polarization observed in the optical together with the continuity of the spectral shape strongly suggests that in the entire IR to UV range the dominant emission mechanism is synchrotron radiation. There is no clear signature in the overall spectra observed of a steepening of the non thermal continuum, indicating that energy losses of relativistic electrons would occur at higher frequencies than UV.

It may be noticeable that the slope for H 0323+022, $\alpha_\nu = 0.87$, which is an X–ray selected object is flatter than that of PKS 0301–243, which instead is radio–selected. This agrees with the findings based on the examination of archival data of a collection of 33 IUE observed BL Lacs (Maraschi *et al.*, 1986; Ghisellini *et al.*, 1986) and confirmed by Bersanelli *et al.* (1992) for a large set of homogeneous IR measurements of BL Lacs.

The power–law which describes the non thermal component in the IR–UV domain can be extrapolated to the X–ray band and compared with the observed flux. In the case of PKS 1538+149 and H 0323+022 the extrapolation is consistent, within the uncertainty, with the *Einstein* fluxes at 1 keV. The expected flux for PKS 0118–272 is a factor $\sim$ 5 higher than the observed one, which may be attributed to a steepening of the spectrum or to non simultaneous observations. We note that the optical–UV observations were taken during a high state of the source. Finally, the extrapolated flux for PKS 0301–243 is $\sim$ 2.7 μJy at 1 keV. Therefore the source should be successfully detected with the *ROSAT* satellite.

2.3 The ultraviolet continuum of five BL Lacs

Five objects have been observed from IUE. The spectra of two of them (H 1722+119 and H 0414–009) have been retrieved from the IUE archive, whereas the other three (PKS 0422+004, PKS 0048–097 and PKS 0521–365) have been observed by us. We have extracted the spectra with the GEX method and presented them in Figure 2.1.

The same technique as described in Section 2.2 has been used to analyse and fit the spectra. In Table 2.2 are listed the averaged fluxes in selected bands with the errors, in Table 2.3 are given the results of the fit on separate SWP and LWP fluxes and in Table 2.4 are reported the parameters for the fitted combined spectra.

a) H 1722+119

The results of our extraction and fitting on the spectra of H 1722+119 of 1986 September are approximately consistent with those of Brissenden *et al.* (1990).

The reduction of the 1987 May data is slightly disagreeing.

b) PKS 0048–097

For PKS 0048–097 we gathered on 1988 August only SWP data, so that a comparison with the previous year observations of Falomo *et al.* (1988) is only possible for a restricted range of frequencies. The flux in the short–wavelength range presents a weakening from 0.83 to 0.27 erg s^{-1} cm^{-2} $Å^{-1}$ and the shape of the spectrum correspondingly steepens, as expected in BL Lac objects. Consistently with Falomo *et al.* (1988), we did not apply any dereddening correction to the data.

c) PKS 0422+004

PKS 0422+004 has a very steep SWP spectrum and a flat, or even inverted LWP one. This can possibly cause a mismatch between the two flux distributions and then give problems in fitting the combined spectrum, from which we derive a fitted flux at 2000 Å which is higher than the fluxes pertaining to the separated IUE ranges.

With respect to the observations of Falomo *et al.* (1989) we observe a steepening of both SWP and LWP spectral indices and a decreasing flux, whereas in the combined spectral flux distribution a flattening can be seen.

The sharp difference between the slopes of the two IUE spectral flux distributions generates a marked "concave down" spectral shape which suggests a break or curvature in the UV spectrum.

d) H 0414–009

The source H 0414–009 is too faint for any significant signal to be revealed through the usual GEX extraction. The criteria of extraction have then been modified for this object, as for PKS 1538+149, in the way described in Section 2.2. The extracted spectrum, represented in Fig. 2.1, is clearly visible, though very faint. The fitting parameters are consistent, within the large errors, with those reported by George (1988) (see Table 2.3). The LWP flux is $\sim$ 50% lower than that reported by Falomo and Tanzi (1991), which means the source presents a strong long–term variability in the UV band.

e) PKS 0521–365

We have only a long–wavelength IUE spectrum for PKS 0521–365, described by a fitting power–law of slope $\alpha_\nu = 0.96$, which is poorly constrained. The data, as suggested from Kinney, Bohlin, and Blades (1991) and according with Danziger *et al.* (1983) have not been corrected for any reddening extinction. The source was in a low emission state during this observation, with a flux of 0.36 $\pm$0.01 mJy at 2800 Å, as can be argued from the archival LWP observations listed by Edelson *et al.* (1991*b*). Danziger *et al.* (1983) found a slope for the combined SWP + LWP spectrum of 0.5 and a flux at 2000 Å of 0.25 mJy.

All the nine analysed objects show weak emission, the maximum UV flux being exhibited from H 1722+119 ($\sim$ 1.2 mJy) and their spectral shapes are very widely distributed, spectral indices ranging from $\sim$ –4 to $\sim$ +4.

A little evidence of predominance of flat SWP spectra in X–ray–selected objects rather than in radio–selected may be seen, but the list is not sufficiently numerous to statistically test theoretical models of the UV emission of BL Lacs.

Chapter 3

IUE monitoring of the BL Lac Object PKS 2155-304

The brightest known BL Lacertae object at UV wavelengths is PKS 2155–304, which has been detected as a relatively intense (10 μJy at 3.6 keV) X–ray source by *HEAO 1* (Schwartz *et al.*, 1979, and references therein). The identification with a blue stellar object showing a featureless optical continuum, together with the 5% optical polarization, suggested its BL Lac nature. The radio counterpart was recognized as the Parkes source 2155–304.

The radial brightness profile of the surrounding nebulosity is consistent with that of an elliptical galaxy of effective radius of 4.″5 which, assuming an absolute magnitude typical of luminous ellipticals, puts the object at the redshift $z \sim 0.1$ (Falomo *et al.*, 1991).

The object appeared since the first observations to be variable in all the energy bands. PKS 2155–304 is the most well–observed BL Lac in the UV domain, but it is actually one of the least strongly variable in this energy range (Edelson, 1992).

Archival plates of PKS 2155–304 (Griffiths *et al.*, 1979) reveal that the optical magnitude varied between $m_v = 12.4$ and $m_v = 14$ with flares of the duration of months. On October 1989, Carini and Miller measured, at a distance of few days, the optical magnitudes $m_v = 13.46$ and $m_v = 13.59$, which are approximately in

accord to the average value resulting from the monitoring of Miller and McAlister (1983).

Maraschi *et al.* (1986) examined all the UV spectra of PKS 2155–304 taken with IUE in the time interval 1978–1984. Use of combined spectra, extending from 1200 Å to 3200 Å, has been made in order to substantially reduce the uncertainty on the derived spectral index. This procedure, which has been followed also for the analysis exposed in the present thesis work, has the drawback of being possibly subject to errors due to intraday variability, which causes mismatch in joining the flux distributions of two separated (SWP and LWP) IUE spectra.

In the considered time span ($\sim$ 6 years) the maximum observed variation in the UV flux was a factor of 2.5. The recorded UV variations were smaller than the maximum recorded optical ones, which may be due to the limited time coverage of the UV observations. Small but evident spectral variability has been found to be present in the UV range, the maximum variation of the spectral index derived from combined spectra being $(\Delta\alpha)_{comb} = 0.30 \pm 0.02$.

An indication of spectral correlation, in the sense that higher fluxes correspond to harder spectra, is present, with the suggestion that the correlation may be stronger on shorter time scales. An also stronger correlation is visible between changes in flux density and spectral index, in the sense that the spectrum hardened as the source brightened, as expected for non thermal processes where flux increases (decreases) result from acceleration (radiative losses) of the non thermal electron population.

Urry *et al.* (1988) analysed the 64 spectra of PKS 2155–304 available at that time in the IUE archive. They calculated the mean spectral index for combined spectra to be $< \alpha >= 0.89 \pm 0.12$, which agrees with the value derivable from the

data of Maraschi *et al.* (1986) ($< \alpha >= 0.90 \pm 0.14$). The overall flux variation was a factor of $\sim$2 over 7 years, which is not so dramatic as the UV flux variation of other BL Lacs. In the X–rays, PKS 2155–304 varied by a factor of $\sim$10 during the same time period. The rising X–ray spectrum ad the relatively flat UV spectrum suggest a sharp change in spectral slope between 8×10^{16} Hz and 10^{17} Hz.

Unlike Maraschi *et al.* (1986), Urry *et al.* (1988) found no correlation between flux and spectral index, attributing the previous result to mis–calibration of some IUE spectra. They confirmed and improved the correlation between changes in flux and spectral index.

Edelson *et al.* (1991*a*, and references therein) performed a high density UV sampling, with sufficient time resolution and signal–to–noise to resolve small outbursts in the UV flux of BL Lac objects. From the analysis of 57 closely spaced IUE spectra they inferred clear evidence of a $\sim$ 12% drop in the UV flux of PKS 2155–304 over a 2 day period in 1989 October and a strong indication of a similar drop in a 5 hr period some three weeks later.

The decrease in the optical flux is of similar amplitude and sense to that observed in the UV suggesting that the optical and UV variations are correlated.

The IUE data were obtained in conjunction with simultaneous X–ray observations made with the *Ginga* satellite.

Up to November 1991, these were near the fastest variations which could have been detected with UV data, but they were still much slower (or weaker) than those which had been observed in the X–rays. The authors point out that these variations are orders of magnitude faster than Seyfert 1 UV variations. This suggests that a "standard" Seyfert 1 accretion disk may not be responsible for the UV emission from PKS 2155–304. An increase in UV intensity can be due to a

sudden injection or acceleration of radiating particles, while decreases in intensity could arise as a result of the aging of the electron population.

Simultaneous X–ray (EXOSAT), UV, and optical (ESO) observations in the temporal range from 1983 to 1985 showed an increase of the source variability with increasing energy and decreasing variability time scales, consistenlty with the predictions of the current theoretical models. The UV flux has been observed to undergo a doubling of its intensity (Treves *et al.*, 1989).

The complete absence of spectral features intrinsic to PKS 2155–304 combined with the large number of exposures in the archive, makes the object a unique probe of intervening absorption. For this reason Maraschi *et al.* (1988) co–added the available UV spectra taken prior to 1986 September with the aim of select features with equivalent widths $\lesssim 1$ Å. Most of the lines could be identified with expected interstellar species in our Galaxy. Two unidentified lines, at 1285 Å and 1414 Å, are tentatively explained respectively as intervening Lyα at $z = 0.057$ and C II λ1334 at the same redshift.

For a complete journal of observations of PKS 2155–304 up to November 1991, we refer to Edelson *et al.* (1991*b*).

3.1 Observations and data reduction

The change in spectrum with intensity is a strong diagnostic of the process which is responsible for the emission of AGN. For this reason observations with frequent and regularly spaced sampling are needed in all the wavelength bands.

In order to follow the short–term variability of PKS 2155–304 a monitoring program has been designed covering the month of November 1991 which

yielded high–quality simultaneous light–curves in the UV, optical and X–ray energy ranges.

X–ray observations were performed with the *ROSAT* spacecraft; the ground–based optical monitoring was supported from the Steward Observatory of the University of Arizona and it revealed strong daily variability in both flux and linear polarization. Particularly, PKS 2155–304 was near its historical photometric maximum during the last two weeks of November (Smith *et al.*, 1992).

Here will be presented the results of the IUE satellite observations.

In order to measure moderate time scale variations (days to a week) it has been scheduled at least one half IUE shift daily from 1 November to 29 November (except on November 8, due to a scheduling conflict). In order to study short–term variability, four and a half days in the middle of the campaign (10.7 - 15.3 November) were devoted to nearly continuous coverage using $\sim$3 shifts per day. A log of the 201 IUE low dispersion observations is given in Table 3.1.

The short–wavelength (SWP) and long–wavelength (LWP) IUE cameras were exposed alternately, with nominal integration times of 55 and 25 minutes, respectively. This allowed us to get two pairs of spectra during each half IUE shift, absent any operational problems.

As a result of this rigid schedule, some IUE exposures had to be longer or shorter than the nominal exposure times, typically by a few minutes but occasionally by much more. There are four SWP spectra (SWP 43048, SWP 43073, SWP 43088 and SWP 43165) which are really underexposed and have then been excluded from the correlation analysis, though they were fitted and the results appear in the presented light–curves. Exposure times for each IUE image are listed in Table 3.1.

The data analysis and reduction of the spectra has been made independently in two different ways by us and by the NASA/GSFC group of Urry *et al.*. The paper contained in Appendix B reports about the results of the NASA/GSFC data analysis and reduction, based on the SWET extraction of IUE spectra (Kinney, Bohlin and Neill, 1991). We used instead the Gaussian extraction (GEX) method, and report here the results, which are not significantly different from the former.

GEX gives a somewhat better signal–to–noise ratio than SWET for very low signal–to–noise data, but for well–exposed spectra systematic problems at the level of a few percent can occur because the true PSF is not precisely Gaussian. Moreover, unlike SWET, the GEX algorithms currently available do not produce an error vector.

The extracted net fluxes are converted to absolute flux using the IUE calibration of Bohlin and Holm (1980) for the SWP spectra and the calibration of Cassatella *et al.* (1988) for the LWP spectra.

The IUE spectra are dereddened using $E(B-V) = 0.034$ and the average Galactic curve from Seaton (1979). The dereddening correction has often been ignored by previous IUE observers of PKS 2155–304, but it makes a significant difference. The dereddened flux is 24% greater at 1400 Å, 17% greater at 2800 Å and 22 % greater at 2000 Å than the observed flux, and the fitted energy spectral index is typically 0.05 flatter in the SWP, 0.35 flatter in the LWP and 0.1 flatter in the combined spectra.

For each spectrum the flux was averaged in wavelength bands of 50 Å after rejecting flaws affecting the UV data and features arising onto the continuum. The uncertainty associated to these averaged fluxes is a statistical error calculated as explained in Section 2.2.

With the same fitting technique described in Section 2.2, the dereddened and undereddened IUE spectra were fitted to the simple power–law model of eq. 2.1. The wavelength ranges over which the data were fitted were 1250–1950 Å for the SWP camera (which excludes the geo–coronal Lyman α region) and 2125–2925 Å for the LWP camera.

Table 3.2 summarizes the results of the fitting both for undereddened and dereddened SWP and LWP spectra. Reduced chi–squared values relative to the fit are also listed.

The fitted spectral indices are given in terms of the energy index, α_ν.

Each SWP spectrum was jointed to an LWP spectrum taken close together in time and the combined spectral flux distribution was then fitted to a unique power–law. The advantage of this procedure is to reduce the uncertainties on the fitted parameters. Nevertheless, "mismatch" of spectra taken in different though very close epoques can make the fit less reliable, especially for very rapidly variable sources. Table 3.3 contains the parameters of the fit on combined spectra.

The chi–squared values, together with the small errors on the spectral indices ($\sim$ 5% for SWP and $\sim$ 10% for the LWP) and on fitted SWP and LWP fluxes ($\sim$ 1%) indicate that power–law fit is generally good.

Figure 3.1 contains the entire set of extracted combined spectra, each one with the fitting power–law curve overimposed. The data are not dereddened.

3.2 Results

Earlier studies on PKS 2155–304 revealed that flux variations could have "doubling time scales" as short as $\sim$ 10 days, but the light–curves were grossly

undersampled.

During the 1991 November monitoring campaign the intensity of the object increased by a factor of 2 over the month to roughly its historical maximum brightness. The total emitted UV power, calculated for a redshift $z = 0.1$ and assuming $H_0 = 50$ km s^{-1} Mpc^{-1} and isotropic emission, was of 1.3 $\times 10^{46}$ erg s^{-1} at this maximum point.

The light–curves for the full month and for the central period are shown in Figures 3.2,3,4,5,6,7,8. During the intensive monitoring, the UV flux varied by $\sim$30% in several distinct flares that are well–sampled apart from a possible dip during the 7–hour gap on 11 November. The width of these rapid flares is roughly half a day; if we define an exponential variability time scale as $\tau_D = \Delta t / \Delta ln F$, then values for these flares are less than 2 days. Such fast UV variations have been detected previously in only two blazars, PKS 2155–304 and Mrk 421, while slightly longer and/or lower amplitude flares have been seen in another three (3C 279, OI 158, and OD 26; Edelson *et al.*, 1992). There are no obvious differences between the time scales for flaring or decaying intensity. The depth of the dip during 12 November is unclear. The low SWP point comes from a very short exposure of only 13 minutes, so it should be considered uncertain, and no corresponding dip is seen in the LWP light–curve.

The fractional variability is comparable for the two bands: both light–curves undergo a doubling of flux, and the application of the variability test (Treves and Girardi, 1991) shows that in both bands the variance is about 14% of the mean flux. This is in contrast to the historical trends in other blazars, where long–term IUE monitoring indicates the SWP flux is more variable than the LWP flux (Edelson, 1992) and also to the previous findings about PKS 2155–304. Indeed,

we find a comparable variability in the two IUE ranges, contrary to Treves and Girardi (1991) who found a 23 % variability index in the SWP and 19 % in the LWP range, and to Edelson (1992) who gives a 25 % in the SWP and a 21 % in the LWP.

The variation of spectral index throughout the run is also shown (Figures 3.9,10,11,12,13,14,15,16). As observed even previously, the spectral index does not show so large amplitude variations as the flux does, and the SWP spectral index seems to vary more than the LWP one, though this is probably due to the larger errors affecting the LWP spectral indices.

The spectral index of the combined flux distributions is definitely weakly variable with respect to the independent behaviours of SWP and LWP indices.

The spectral shape in the UV band depends critically on the dereddening correction. When no correction is applied, the LWP spectral indices are systematically higher than the SWP spectral indices, as reported by Edelson (1992). This implies an unexpected flattening of the spectrum toward shorter wavelengths; that is, a "concave–up" shape in ν–F_ν space, in contrast to the overall "concave–down" shape of the radio through soft–X–ray spectrum. An excess at long wavelengths due to dilution by starlight is not expected, as the host galaxy for PKS 2155–304 detected in deep optical imaging (Falomo *et al.*, 1991) is too faint ($V \sim 16.5$) relative to the nuclear point source. The spectral curvature goes away, however, when a dereddening correction with $E(B-V) = 0.034$ is applied.

The flatness of the UV spectral index means that peak of the luminosity emitted from this BL Lac object is in the far–UV as noted by previous authors. PKS 2155–304 is one of the few extragalactic objects detected in the Rosat WFC survey (Pounds, 1991), indicating that its extreme UV luminosity must be consid-

erable.

3.3 Correlation analysis

The relation between flux density and spectral index could give important clues to the physical origin of the UV emission from BL Lac objects. If the UV is due to synchrotron emission, electron losses at high energies could cause the spectrum to soften as the flux decreases, and injection or reacceleration could make it flatten as the source brightens, so that one might expect flux and spectral index to be correlated.

Possible correlations between spectral shape and flux density were investigated by means of a linear regression fit of the type

$$logF_\lambda = a\ \alpha_\nu + b\ . \tag{3.1}$$

Errors in $logF_\lambda$ and α_ν are not taken into account. No significant correlation was found in none of the SWP, LWP and SWP + LWP cases. A similar fit has been performed with the aim of examining the correlation of the flux variation ΔF between successive observations and the corresponding variation of the spectral index. The model of a constant trend can be ruled out with a highly significance for the SWP case (P = 0.34 $\times 10^{-9}$) and a strong correlation is found between increasing flux and steepening spectrum.

Cross–correlations between SWP and LWP fluxes, between fluxes and spectral indices and auto–correlations of these quantities have been studied with the Discrete Correlation Function method, devised by Edelson and Krolik (1988). Only data pertaining to the intensive monitoring period have been used to carry out

the computation of the DCF.

Systematic errors arising in only four SWP spectra are not taken into account by the analysis procedure, which assumes that the exposures have similar properties.

The SWP and LWP light–curves are highly correlated, with no discernable lag (the upper limit is $\lesssim 0.1$ days), as is evident from Figure 3.17, where the DCF for LWP versus SWP is plotted. The cross–correlation function is asymmetric, in the sense of the short–wavelength emission leading the long–wavelength emission.

The auto–correlation functions of the SWP, LWP and SWP + LWP light–curves are shown in Figure 3.18,19,20. They seem to be modulated with a period of $\sim$0.7 days. This quasi–periodic behavior can be seen going through a full five cycles in the light–curves, if the first peak lies in the gap at 11.5 November.

The DCF method gives similar results in the three cases, and the behavior of the auto–correlation functions suggests the estimates of flux errors were about right.

Figures 3.21,22,23 report the DCF for the cross–correlation of the flux versus the spectral index. In the SWP, LWP and SWP + LWP cases a clear anti–correlation between the two quantities can be argued at a time lag of –1 day, meaning that a steepening or a hardening of the spectrum implies respectively a decrease or increase in flux preceeding it approximately of one day, which is physically not clearly explainable.

3.4 Comparison with previous results and discussion

Comparison with previous study of PKS 2155–304 since the time of the first

IUE observations allows to approximately describe its long–term behaviour though the data are are irregularly and sparsely distributed. The SWP and LWP fluxes are similar in their trend without a discernable lag.

A continuous decrease from 1979 May to 1980 May is followed by a rapid increase until 1980 December. The flux then decreased toward 1982 October and again enhanced undergoing almost a doubling between 1982 October and 1985 October with a flare on 1984 November 7, when the flux was $\sim$ 10 mJy in the SWP and $\sim$ 18 mJy in the LWP. The emission damped and then raised during 1986 September and no reliable data sampling is available for the successive three years period. During 1989 October the intensity increased and doubled, reaching a peak value of $\sim$ 8 mJy in the SWP and $\sim$ 15 mJy in the LWP, then decreasing toward the end of the month. A high flux state is registered in 1990 June, then another data sampling "gap" of almost two years does not allow to describe the flux behaviour prior to 1991 November. The present monitoring refers to an averagely high state of the source emission and registers in both IUE working ranges the highest UV fluxes ever observed for PKS 2155–304 up to October 1989. The light–curves at 1400 Å and 2800 Å referring to the preceeding review data (Edelson *et al.*, 1991*b*) are presented in Figure 3.24.

The UV flux of PKS 2155–304 varied during November 1991 between $\sim$ 7 and $\sim$ 14.5 mJy in the SWP and between $\sim$ 11 and $\sim$ 24 mJy in the LWP. The change in intensity occurring over a day (for example, around 13–14 November 1991) corresponds to $\Delta L/\Delta t \sim 5\times10^{40}$ ergs s^{-2}, which is just below the fiducial limit for Eddington–limited accretion with efficiency η (Fabian 1979), $\Delta L/\Delta t > 2\times10^{41}\ \eta$ ergs s^{-2}. Concerning this estimate only the UV luminosity, the flaring of the luminosity in all the energy bands surely exceeds this limit, suggesting relativistic

beaming.

Electron acceleration would cause spectral hardening with increasing intensity. The improvement in the correlation when one looks at *changes* in F and α indicates there is little long–term memory of spectral shape.

Finally, the significance of the periodicity in the auto–correlation of the UV flux is unclear. Were there only three peaks, it could be dismissed as almost certainly spurious. Signals with red power spectra frequently show spurious periodicity on a time scale $\sim 1/3$ of the duration of the data stream because there are too few large–amplitude components at low frequencies to achieve the Gaussian behavior of the central limit theorem. The fact that this period is closer to 1/5 of the intensively–sampled stream, and that the light–curve appears to show little power at other frequencies, tempts us to believe that it may be real. This period is not present in the extensive optical data taken by Miller in 1988 (private communication), which means, since we now know the optical and UV are closely related, that any periodicity is transitory.

Conclusion

I have analysed and presented homogeneously reduced UV data, thanks to the analysis methods imported in this institution and locally developed.

The IUE spectra and their fitted spectral parameters reported in Chapter 2 for nine BL Lac objects represent a means to study the UV continua of this class of sources and to improve the knowledge about the emission processes which are responsible of them.

From the multifrequency observations arises that the broad–band spectrum of BL Lacs seems to be related to the spectral shape in individual bands. This statement can be quantified with a correlation analysis between the various spectral indices. This correlation has been studied for 33 IUE observed blazars, partly derived from the list of Angel and Stockman (1980), by Ghisellini *et al.* (1986). One of the projects for future work will be to enrich this list with the newly observed objects and so update and improve the cited work.

The IUE monitoring of PKS 2155–304 described in Chapter 3 is the most important even performed on this source because of the great quantity of data gathered well close in time and represents a substantial improving for the study of the flux and spectral variations of this bright object and for the study of BL Lac emission variability in general, both from a phenomenological and theoretical point of view.

I intend to continue the study of the UV variability properties of PKS 2155–

304. To this aim, I will retrieve all the archival spectra of the object and re–extract them to construct a homogeneous complete set of spectra including those of the 1991 November monitoring. This entire data set will constitute a template to a systematic study of the continuum UV emission of PKS 2155–304 and of the behaviour of the possible emission and absorption lines overimposed on it.

Of great importance will be the cross–correlation analysis between the UV and the simultaneous *ROSAT* X–ray data of PKS 2155–304.

The results of this cross–correlation analysis will test the models which explain the origin of the high energy emission of blazars and will enlight the relation between the far–UV and the soft X–ray flux.

On the track of the UV variability study of BL Lacs I will be involved in an UV monitoring of the object 3C 279 and in a multifrequency observation program of two very bright and highly monitored sources, OJ 287 and Mkn 421, which will be observed with IUE on March 1993 and simultaneously in the radio, optical and IR bands.

This combined monitoring at several frequencies will allow to examine the characteristics of the source emission at all the energies and to study the overall continuum parameters in order to find evidence of a correlation between them.

Acknowledgments

I would like to thank Prof. Dennis Sciama, director of the Astrophysics Sector of S.I.S.S.A., who encouraged and allowed my collaboration with the University of Milan and gave me the opportunity to attend stimulating schools.

My greatest debt is to my supervisor at S.I.S.S.A., Prof. Aldo Treves, who directed my work with precise suggestions and comments and improved, with useful and fruitful discussions, my experience and competence in astrophysics.

I warmly thank Prof. Laura Maraschi, who invited me to a pleasant collaboration in Milan and helped me to develop an intuitive mind for the research.

I gratefully thank Dott. Lucio Chiappetti, who tirelessly taught and followed me during my getting started and working on data analysis systems, both in Milan at I.F.C.T.R. and here in Trieste via electronic communication.

I am very indebted to Dott. Antonio Lanza, who installed at S.I.S.S.A. the *MIDAS* software package and assisted me with great disponibility in my acquaintance with the local data analysis facilities.

I would like to thank all my colleagues of the Astrophysics Sector and all my friends of S.I.S.S.A., for always helping me with their presence and availability. Among all of them, I particularly thank Pasquale Pavone, a real computer expert, who helped me in achieving familiarity with the VAX machine and developed the "macro" file for the graphic frame of the thesis text.

References

Adam, G. 1985, *Astron. Astrophys. Suppl. Ser.*, **61**, 225.

Allen, D.A., Ward, M.J., & Hyland, A.R. 1982, *Mon. Not. R. astr. Soc.*, **199**, 969.

Angel, J.R.P., & Stockman, H.S. 1980, *Ann. Rev. Astron. Astrophys.*, **18**, 321.

Arimoto, N., & Yoshii, Y. 1987, *Astron. Astrophys.*, **173**, 23.

Avni, Y. 1976, *Astrophys. J.*, **210**, 642.

Baldwin, J.A., & Stone, R.P.S. 1984, *Mon. Not. R. astr. Soc.*, **206**, 241.

Ballard, K.R., Mead, A.R.G., Brand, P.W.J.L., & Hough, J.H. 1990, *Mon. Not. R. astr. Soc.*, **243**, 640.

Bersanelli, M., Bouchet, P., & Falomo, R. 1991, *Astron. Astrophys.*, **252**, 854.

Bersanelli, M. Bouchet, P., Falomo, R., & Tanzi, E.G. 1992, *Astron. J.*, in press.

Boggess, F.A. *et al.* 1978, *Nature*, **275**, 372.

Bohlin, R.C., & Holm, A.V. 1980, *IUE NASA Newsletter*, 10, 37.

Bohlin, R., Harris, A.W., Holm, A.V., & Gry, C. 1990, *Astrophys. J. Suppl. Ser.*, **73**, 413.

Bohlin, R.C., Savage, B.D., & Drake, J.F. 1978, *Astrophys. J.*, **224**, 132.

Bolton, J.G., Shimmins, A.J., & Merkelijn, J. 1968 *Australian J. Phys.* **21**, 81.

Bregman, J.N., Maraschi, L., & Urry, C.M. 1987, in *Exploring the Universe with the IUE Satellite*, ed. Y. Kondo, p.685.

Brissenden, R.J.V., Remillard, R.A., Tuohy, I.R., Schwartz, D.A., & Hertz, P.L. 1990, *Astrophys. J.*, **350**, 578.

Brown, L.M.J., *et al.* 1989, *Astrophys. J.*, **340**, 129.

Carini, M.T., & Miller, H.R. 1991, *Astrophys. J.*, submitted.

Cassatella, A., Lloyd, C., & Gonzales Riestra, R. 1988, *IUE ESA Newsletter*, 35, 225.

Condon, J.J., Hicks, P.D., & Jauncey, D.L. 1977, *Astron. J.*, **82**, 692.

Cruz-Gonzalez, I., & Huchra, J.P. 1984, *Astron. J.*, **89**, 441.

Danziger, I.J., Bergeron, J., Fosbury, R.A.E., Maraschi, L., Tanzi, E.G., & Treves, A. 1983, *Mon. Not. R. astr. Soc.*, **203**, 565.

Doxsey, R.E., McClintock, J.E., Petro, L., Remillard, R., & Schwartz, D.A. 1981, *Bull. Am. Astron. Soc.*, **13**, 558.

Doxsey, R.E., *et al.* 1983, *Astrophys. J.*, **264**, L43.

Edelson, R.A. 1987, *Astron. J.*, **94**, 1150.

Edelson, R.A., & Krolik, J.H. 1988, *Astrophys. J.*, **333**, 646.

Edelson, R.A., *et al.* 1991*a*, *Astrophys. J. (Letters)*, **372**, L9.

Edelson, R.A., Pike, G.F., Saken, J.M., Kinney, A., & Shull, J.M. 1991*b*, *Astrophys. J. Suppl. Ser.*, submitted.

Edelson, R.A. 1992, *Astrophys. J.*, submitted.

Edelson, R.A., *et al.* 1992, in preparation.

Elvis, M., Lockman, F.J., & Wilkes, B.J. 1989, *Astron. J.*, **97**, 777.

Fabian, A.C. 1979, *Proc. Roy. Soc.*, **366**, 449.

Falomo, R., Bouchet, P., Maraschi, L., Tanzi, E.G., & Treves, A. 1988, *Astrophys. J.*, **335**, 122.

Falomo, R., Bouchet, P., Maraschi, L. , Tanzi, E.G., & Treves, A. 1989, *Astrophys. J.*, **345**, 148.

Falomo, R., Tanzi, E.G., & Treves, A. 1989, in *BL Lac Objects*, ed. L. Maraschi,

T. Maccacaro & M.-H. Ulrich (Berlin: Springer), p. 72.

Falomo, R., Melnick, J., & Tanzi, E.G. 1990, *Nature*, **345**, 692.

Falomo, R., & Treves, A. 1990, *Publ. astr. Soc. Pac.*, **102**, 1120.

Falomo, R., Giraud, E., Maraschi, L. Melnick, J., Tanzi, E.G., & Treves, A. 1991, *Astrophys. J. (Letters)*, **380**, L67.

Falomo, R., & Tanzi, E.G. 1991, *Astron. J.*, **102**, 1294.

Falomo, R. 1991, *Astron. J.*, 102, 1991.

Feigelson, E.D., *et al.* 1986, *Astrophys. J.*, **302**, 337.

Filippenko, A.V., Djorgovski, S., Spinrad, H., & Sargent, W.L.W. 1986, *Astron. J.*, **91**, 49.

Forman, W., *et al.* 1978, *Astrophys. J. Suppl. Ser.*, **38**, 357.

George, I. 1988, Ph.D. thesis, University of Leicester.

Ghisellini, G., Maraschi, L., Tanzi, E.G., & Treves, A. 1986, *Astrophys. J.*, **310**, 317.

Griffiths, R.E., Tapia, S., Briel, U., & Chaisson, L. 1979, *Astrophys. J.*, **234**, 810.

Halpern, J.P., Chen, V.S., Madejski, G.M., & Chanan, G.A. 1991, *Astron. J.*, **101**, 818.

Harris, A.W., & Sonneborn, G. 1987, in *Exploring the Universe with the IUE Satellite*, ed. Y. Kondo, p.729.

Impey, C.D., & Neugebauer, G. 1988, *Astron. J.*, **95**, 307.

Impey, C.D. & Tapia, S. 1988, *Astrophys. J.*, **333**, 666.

Impey, C.D., & Tapia, S. 1990, *Astrophys. J.*, **354**, 124.

Kidger, M.R. 1988, *Publ. astr. Soc. Pac.*, **100**, 1248.

Kinman, T.D. 1976, *Astrophys. J.*, **205**, 1.

Kinney, A.L., Bohlin, R.C., & Blades, J.C. 1991, *Astrophys. J. Suppl. Ser.*, **75**,

645.

Kinney, A.L., Bohlin, R.C., & Neill, J.D. 1991, *Publ. of Astr. Soc. of Pac.*, **103**, 694.

Lampton, M., Margon, B., & Bowyer, S. 1976, *Astrophys. J.*, **208**, 177.

Landau, R., *et al.* 1986, *Astrophys. J.*, **308**, 78.

Ledden, J.E., & O'Dell, S.L. 1985, *Astrophys. J.*, **298**, 630.

Luna, H.G. 1990, *Astron. Astrophys. Suppl. Ser.*, **84**, 611.

Macchetto, F., *et al.* 1991, *Astrophys. J.*, **369**, L55.

Margon, B., & Jacoby, G.H. 1984, *Astrophys. J.*, **286**, L31.

Maraschi, L., Tagliaferri, G., Tanzi, E.G., & Treves, A. 1986, *Astrophys. J.*, **304**, 637.

Maraschi, L., Ghisellini, G., Tanzi, E.G., & Treves, A. 1986, *Astrophys. J.*, **310**, 325.

Maraschi, L., Blades, J.C., Calanchi, C., Tanzi, E.G., & Treves, A. 1988, *Astrophys. J.*, **333**, 660.

Mead, A.R.G., Ballard, K.R., Brand P.W.J.L., Hough, J.H., Brindle, C., & Bailey, J.A. 1990, *Astron. Astrophys. Suppl. Ser.*, **83**, 183.

Miller, H.R., & McAlister, A. 1983, *Astrophys. J.*, **272**, 26.

Ohashi, T. 1989, in *BL Lac Objects*, ed. L. Maraschi, T. Maccacaro & M.-H. Ulrich (Berlin: Springer), p. 96.

Pica, A.J., Pollock, J.T., Smith, A.G., Leacock, R.J., Edwards, P.L., & Scott, R.L. 1980, *Astron. J.*, **85**, 1442.

Pica, A.J., Smith, A.G., Webb, J.R., Leacock, R.J., Clements, S., & Gombola, P.P. 1988, *Astron. J.*, **96**, 1215.

Piccinotti, G., Mushotzky, R.F., Boldt, E.A., Holt, S.S., Marshall, F.E., Serlemit-

sos, P.J., & Shafer, R.A. 1982, *Astron. J.*, **253**, 485.

Pounds, K. A. 1991, in *Frontiers of X-Ray Astronomy*, in press.

Savage, B.D., & Mathis, J.S. 1979, *Ann. Rev. Astr. Astroph.*, **17**, 73.

Schwartz, D.A., Doxsey, R.E., Griffiths, R.E., Johnston, M.D., & Schwarz, J. 1979, *Astrophys. J. (Letters)*, **229**, L53.

Seaton, M.J. 1979, *Mon. Not. R. astr. Soc.*, **187**, 73.

Smith, P.S., Hall, P.B., Allen, R.G., & Sitko, M.L. 1992, *Astrophys. J. Suppl. Ser.*, submitted.

Stark, A.A., Heiles, C., Bally, J., & Linde, R. 1984, Bell Labs. privately distributed tape.

Stickel, M., Padovani, P., Urry, C.M., Fried, J.W., & Kühr, H. 1991, *Astrophys. J.*, **374**, 431.

Stone, R.P.S. 1977, *Astrophys. J.*, **218**, 767.

Stull, M.A., 1972, *Astron. J.* **77**, 13.

Tanzi, E.G., Falomo, R., Bouchet, P., Bersanelli, M., Maraschi, L., & Treves, A. 1989, in *BL Lac Objects*, ed. L. Maraschi, T. Maccacaro & M.-H. Ulrich (Berlin: Springer), p. 171.

Thompson, D.J., Djorgovski, S., & De Carvalho, R. 1990, *Publ. astr. Soc. Pac.*, **102**, 1235.

Treves, A. *et al.* 1989, *Astrophys. J.*, **341**, 733.

Treves, A., & Girardi, E. 1991, in *Lecture Notes in Physics*, N. 377, p. 175.

Ulrich, M-H. 1989, in *BL Lac Objects*, ed. L. Maraschi, T. Maccacaro, & M.-H. Ulrich (Berlin: Springer), p. 92.

Urry, C.M. & Reichert, G. 1988, *IUE NASA Newsletter*, 34, 96.

Urry, C.M., Kondo, Y., Hackney, K.R.H., & Hackney, R.L. 1988, *Astrophys. J.*,

330, 791.

Wandel, A., & Urry, C.M. 1991, *Astrophys. J.*, **367**, 78.

Wills, D. & Wills, B.J. 1974, *Astrophys. J.*, **190**, 271.

Whittet, D.C.B. 1988, in *Dust in the Universe*, eds. Bailey, M.E. & Williams, D.A., p. 25.

Wood, K.S., *et al.* 1984, *Astrophys. J. Suppl. Ser.*, **56**, 507.

Wright, A.E., Ables, J.G., & Allen, D.A. 1983, *Mon. Not. R. astr. Soc.*, **205**, 793.

Yee, H.K.C., & Oke, J.B. 1978, *Astrophys. J.*, **226**, 769.

Figure Captions

Chapter 2

Fig. 2.1 — IUE undereddened spectra of the BL Lac objects under study. Spectral flux distributions from SWP and LWP cameras have been combined (see also Table 2.3) where both were present. The fitting power–law curves have been overimposed.

Chapter 3

Fig. 3.1 — IUE undereddened spectra of PKS 2155–304. Spectral flux distributions from SWP and LWP cameras have been combined (see also Table 3.3) and represented with the fitting power–law curves overimposed.

Fig. 3.2 — UV light–curves of PKS 2155–304. The full light–curve, with fitted fluxes at 2800 Å (*open squares*) and 1400 Å (*filled circles*) on the same scale, in units of 10^{-14} erg s^{-1} cm^{-2} $Å^{-1}$. Both long– and short–wavelength fluxes doubled during the month, with no apparent lag. The data presented here and in the following figures have been dereddened considering $E(B-V) = 0.03$.

Fig. 3.3 — Same as in Fig. 2, except the fluxes are in mJy.

Fig. 3.4 — UV light–curve of PKS 2155–304 with fitted fluxes at 2000 Å in units of 10^{-14} erg s^{-1} cm^{-2} $Å^{-1}$.

Fig. 3.5 — Same as in Fig. 4, except the fluxes are in mJy.

Fig. 3.6 — Expanded view of the intensive monitoring period (1991 Nov 10 – 1991 Nov 15), during which IUE observations were nearly continuous. The fluxes at 1400 Å are plotted in mJy: many rapid flares, with duration of about half a day, have clearly been well–sampled. Five cycles of a quasi–periodic nature can be seen, but true periodicity cannot be established without a longer data train.

Fig. 3.7 — Expanded view of the intensive monitoring period. Light–curve of the LWP fluxes (2800 Å).

Fig. 3.8 — Expanded view of the intensive monitoring period. Light–curve of the combined spectra fluxes (2000 Å).

Fig. 3.9 — Variability of spectral indices. SWP energy spectral index, α_ν (SWP), over the full month. A horizontal line at $\alpha_\nu = 0.58$ indicates the mean spectral index value, averaged over the entire set of observations.

Fig. 3.10 — SWP energy spectral index during the intensive monitoring period.

Fig. 3.11 — LWP energy spectral index, α_ν (LWP), over the full month. A horizontal line at $\alpha_\nu = 0.78$ indicates the mean spectral index value averaged over the entire set of observations.

Fig. 3.12 — LWP energy spectral index during the intensive monitoring period.

Fig. 3.13 — SWP + LWP energy spectral index, α_ν (SWP + LWP), calculated from combined spectra, over the full month. A horizontal line at $\alpha_\nu = 0.72$ indicates the mean spectral index value averaged over the entire set of observations.

Fig. 3.14 — Same as in Fig. 13, except the view is expanded in the ordinate. The combined spectral index is not so remarkably variable as the SWP and the LWP ones. Moreover, it is affected by sensibly smaller errors.

Fig. 3.15 — SWP + LWP energy spectral index during the intensive monitoring period.

Fig. 3.16 — Same as in Fig. 15, except the view is expanded in the ordinate.

Fig. 3.17 — Cross–correlation of SWP (1400 Å) flux versus LWP (2800 Å). The SWP flux is leading the LWP one. The light–curves are highly correlated, with zero lag (with an upper limit of less than a few hours), and the curves are asymmetric in the sense of the short–wavelength emission leading the long–wavelength emission. Cross–correlation and auto–correlation functions (see also the next figures) computation has been restricted to the 5–day intensive monitoring period (since 10 to 15 November).

Fig. 3.18 — Auto–correlation function of SWP flux (1400 Å).

Fig. 3.19 — Auto–correlation function of LWP flux (2800 Å).

Fig. 3.20 — Auto–correlation function of SWP + LWP flux (2000 Å). All the three autocorrelation functions are very similar, and show a peak at a lag of about 0.7 days.

Fig. 3.21 — Correlations between flux and spectral index. F_{1400} versus α_{SWP}. Here and in the following two figures the spectral index leads the flux.

Fig. 3.22 — Cross–correlation of F_{2800} and α_{LWP}.

Fig. 3.23 — F_{2000} versus $\alpha_{SWP+LWP}$. In all the three cases (SWP, LWP and markedly for the combined) is visible an anticorrelation between the spectral index and the flux at a temporal lag of –1 day, meaning that an increase in α_ν implies a decrease in the flux and viceversa, as theoretically expected, and preceeds it of about one day.

Fig. 3.24 — Historical UV light–curves of PKS 2155–304 at 1400 Å and at 2800 Å (after Edelson *et al.*, 1991*b*).

Fig. 2.1

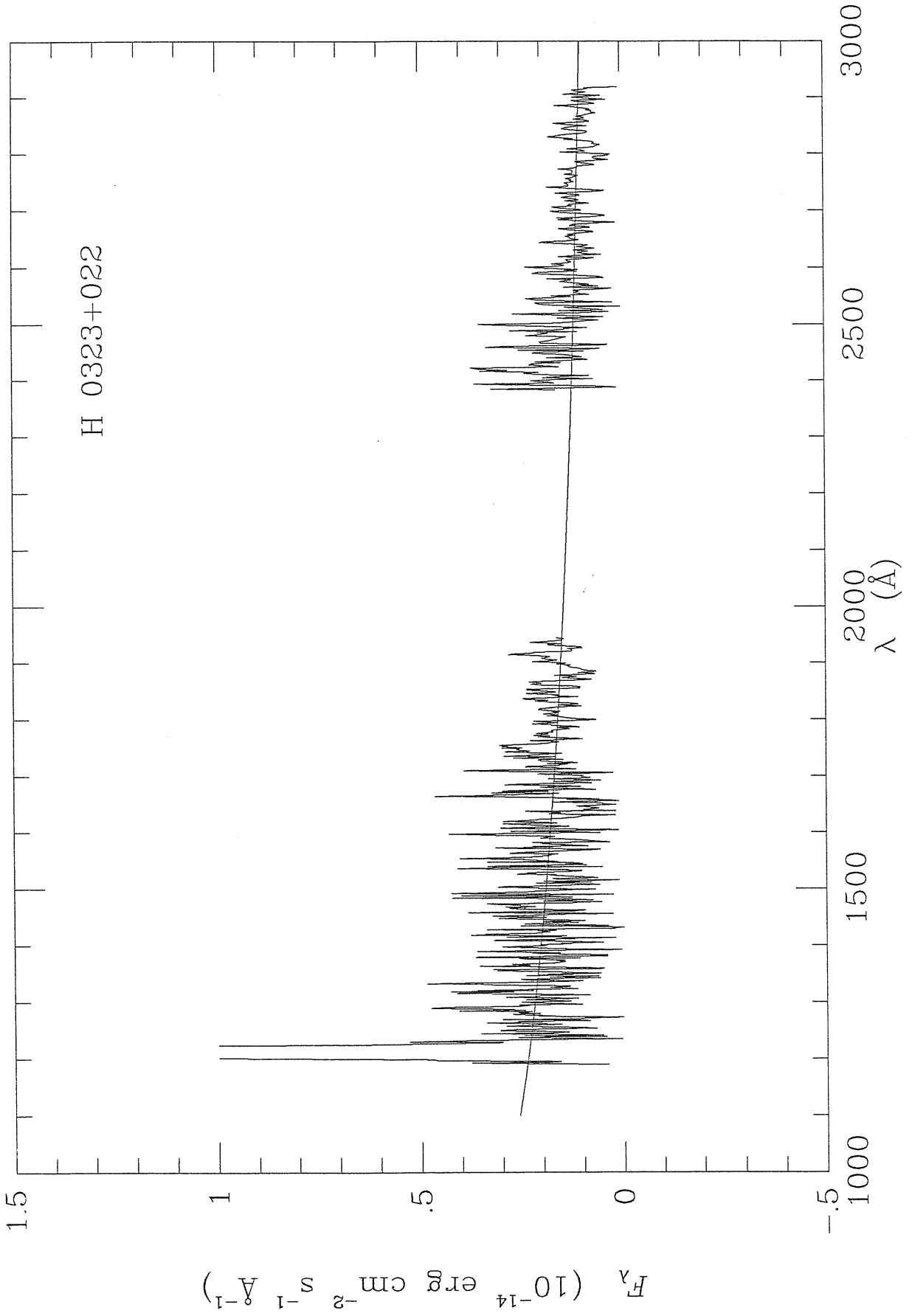
H 0323+022
1.5
1
.5
0
−.5
1000
1500
2000
2500
3000
λ (Å)
F_λ (10^{-14} erg cm^{-2} s^{-1} Å^{-1})

Fig. 2.1 (continued)

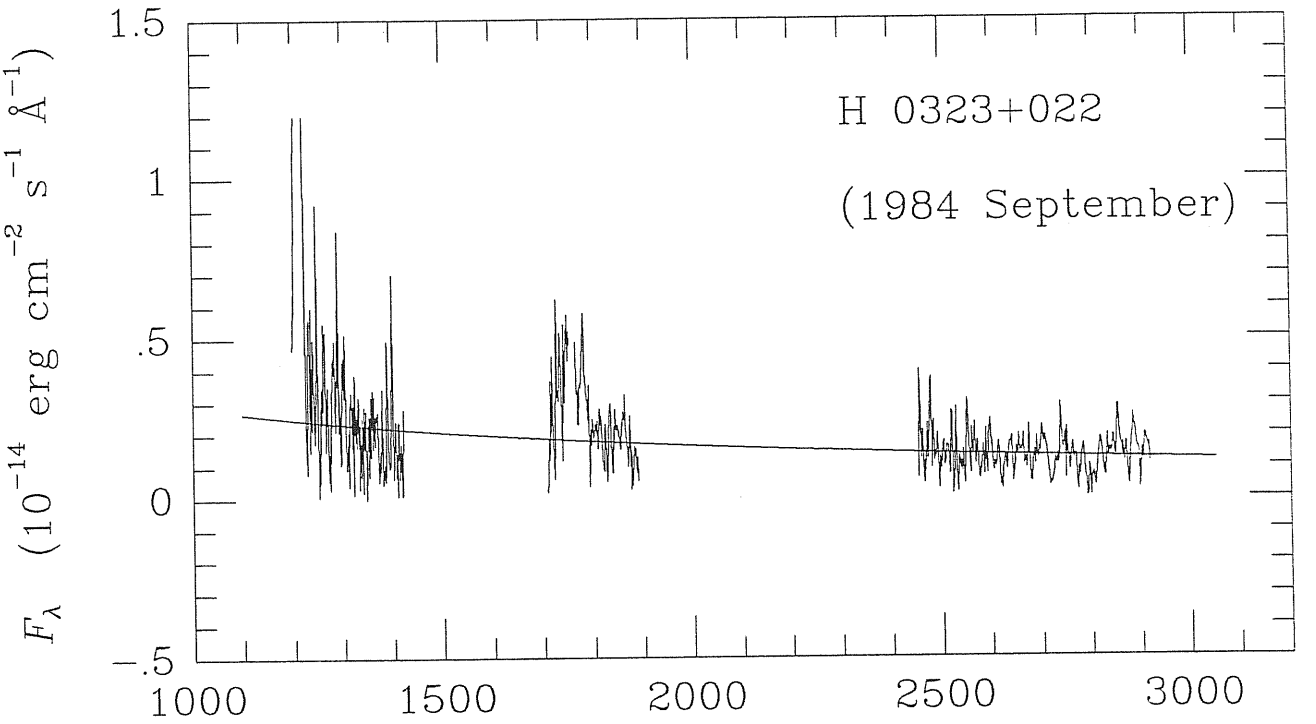

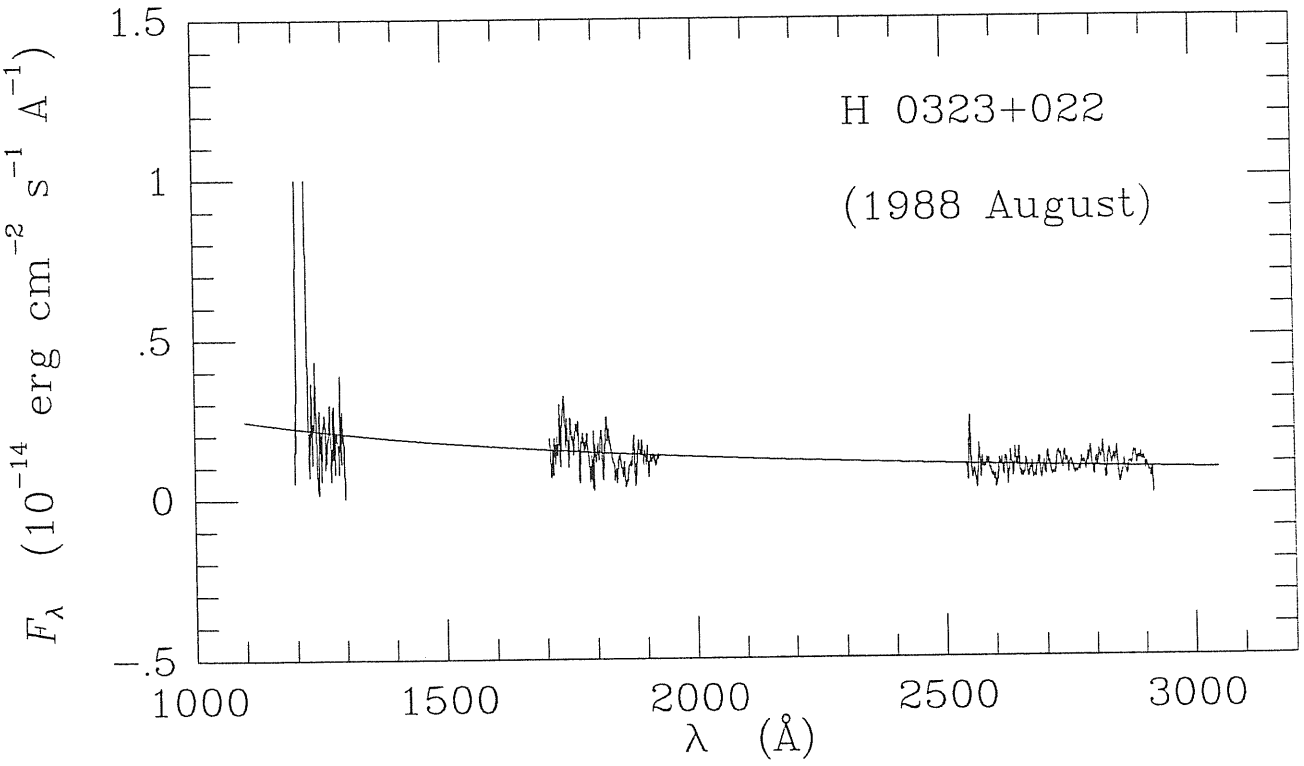

Fig. 2.1 (continued)

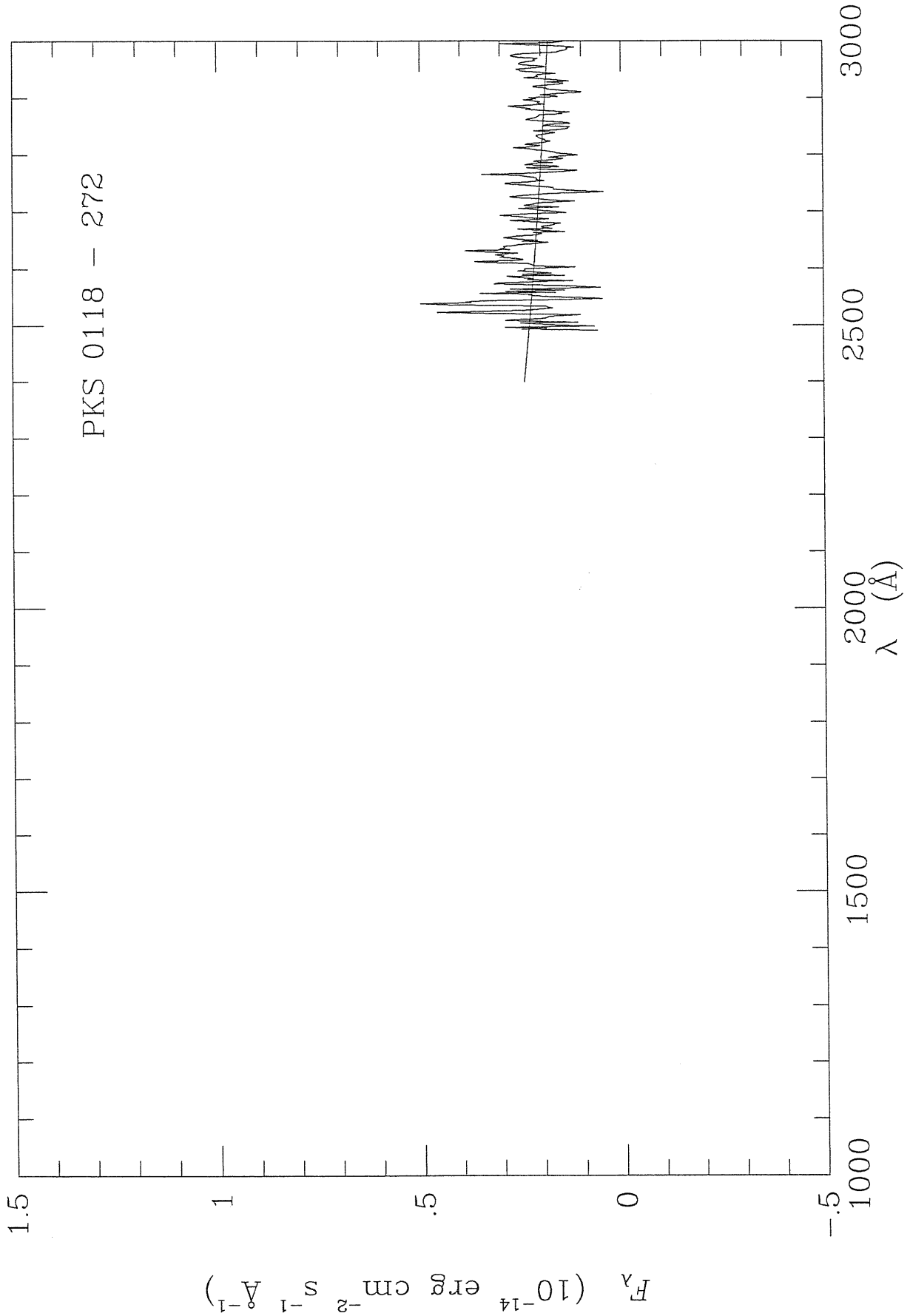

Fig. 2.1 (continued)

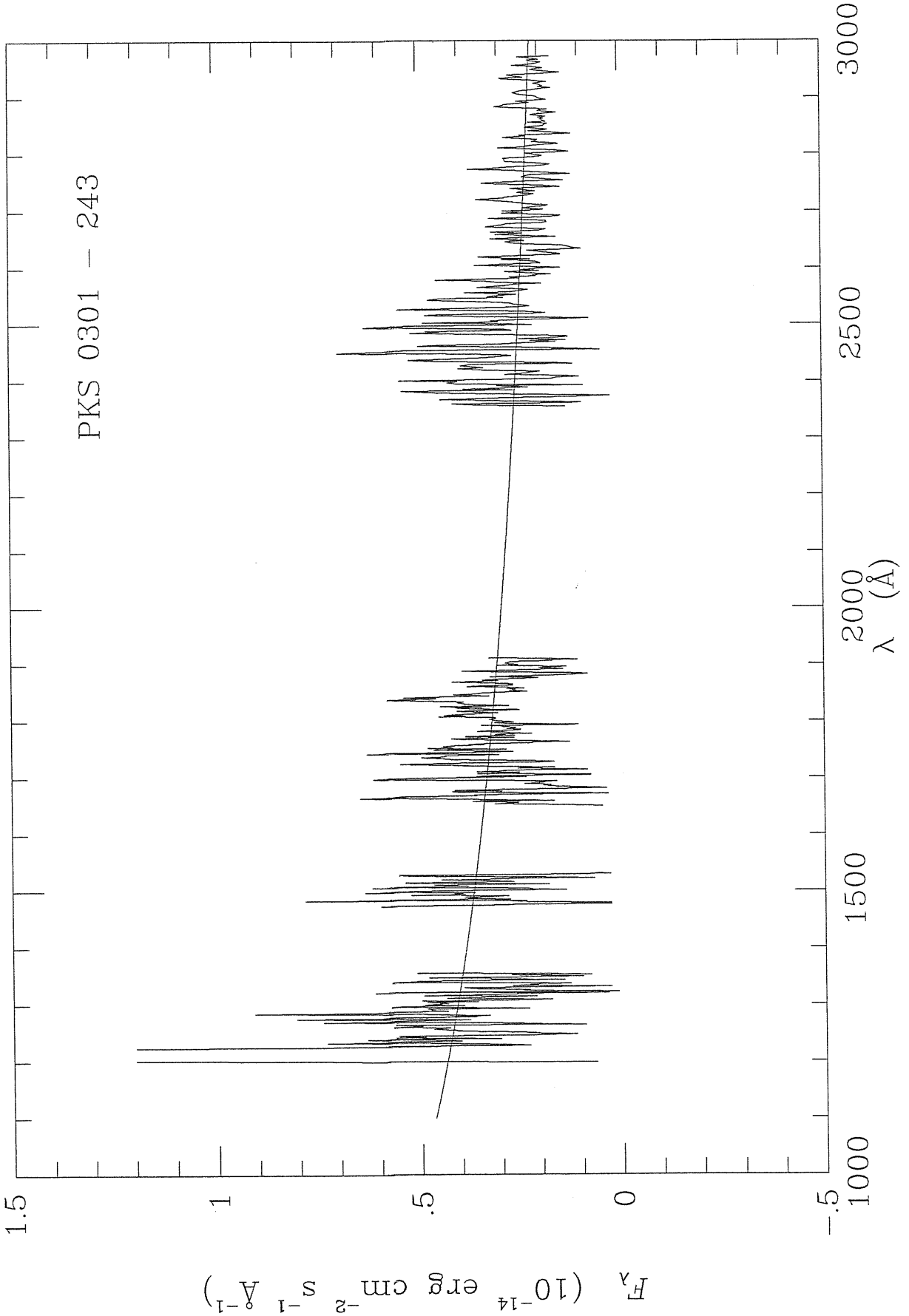

Fig. 2.1 (continued)

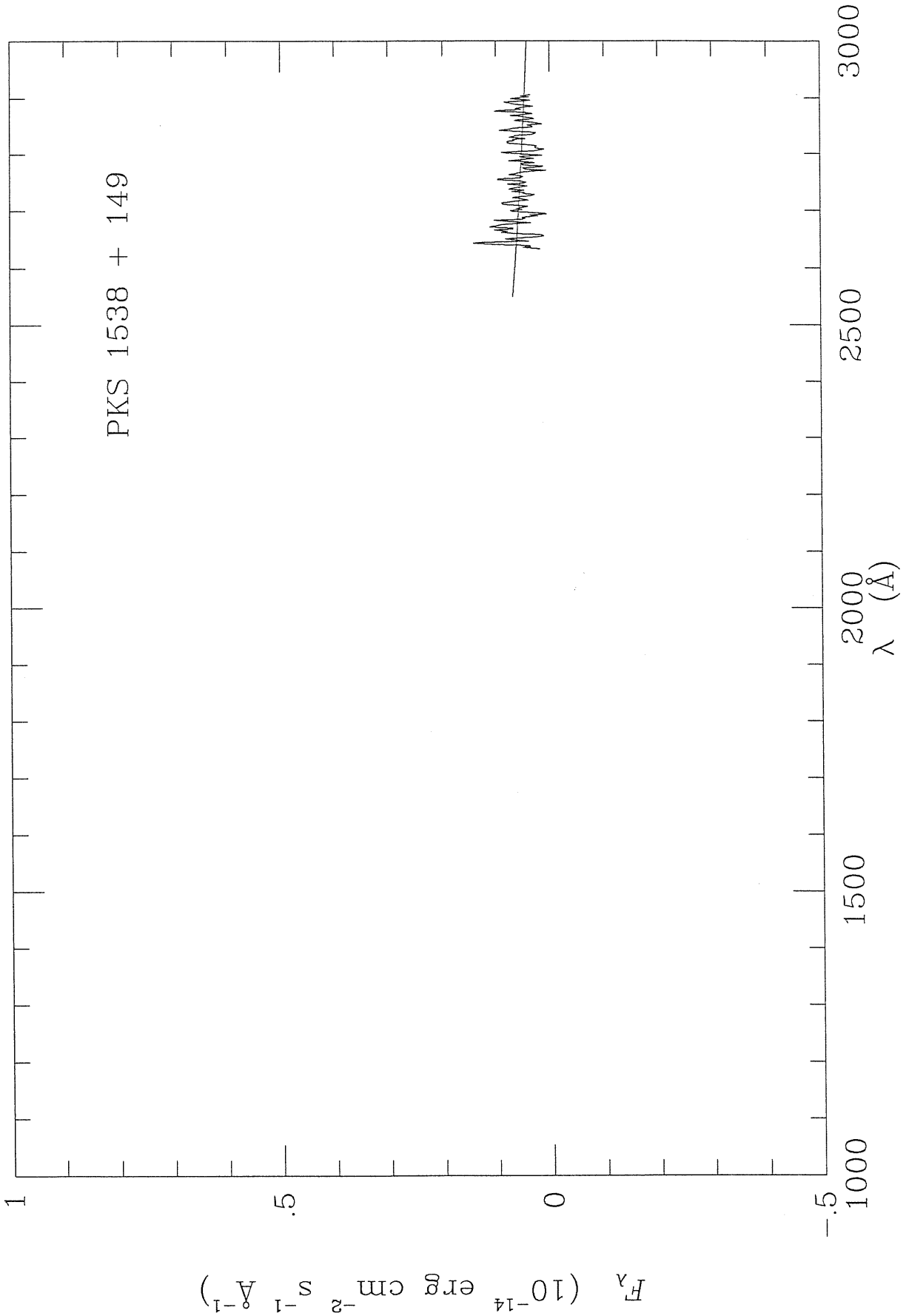

Fig. 2.1 (continued)

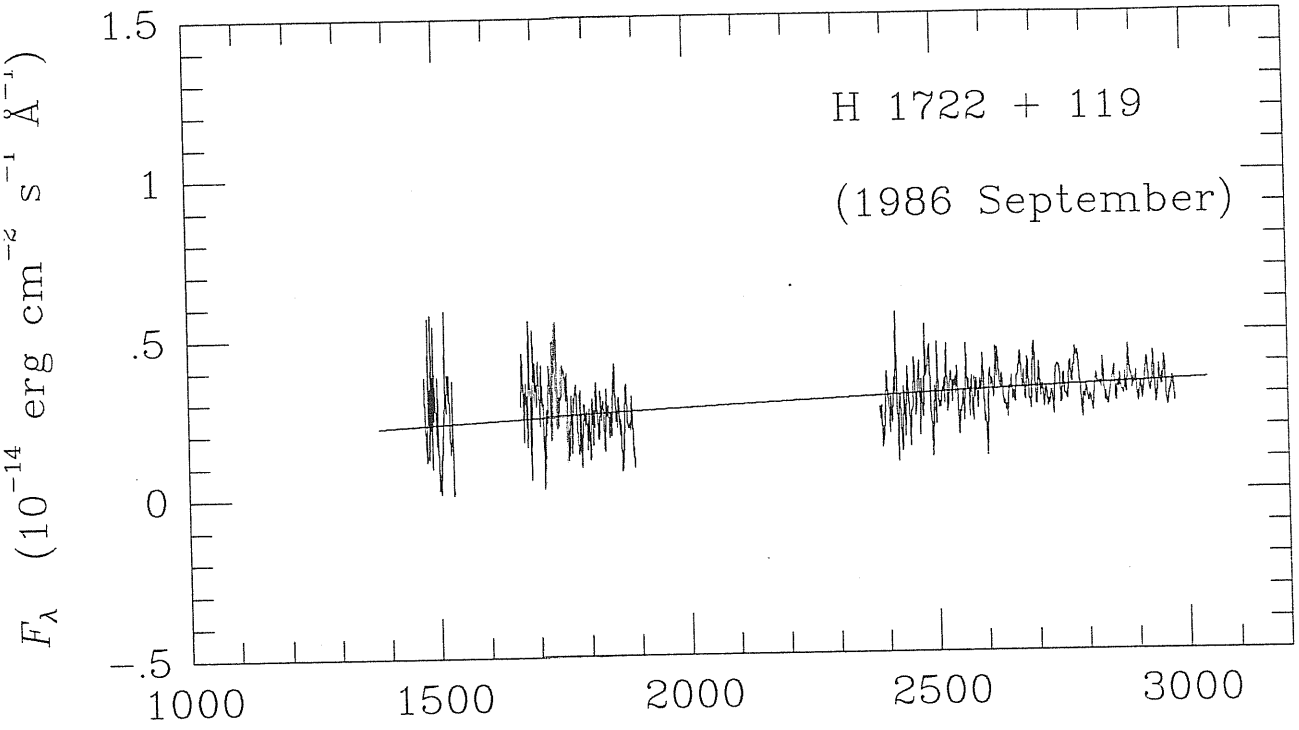

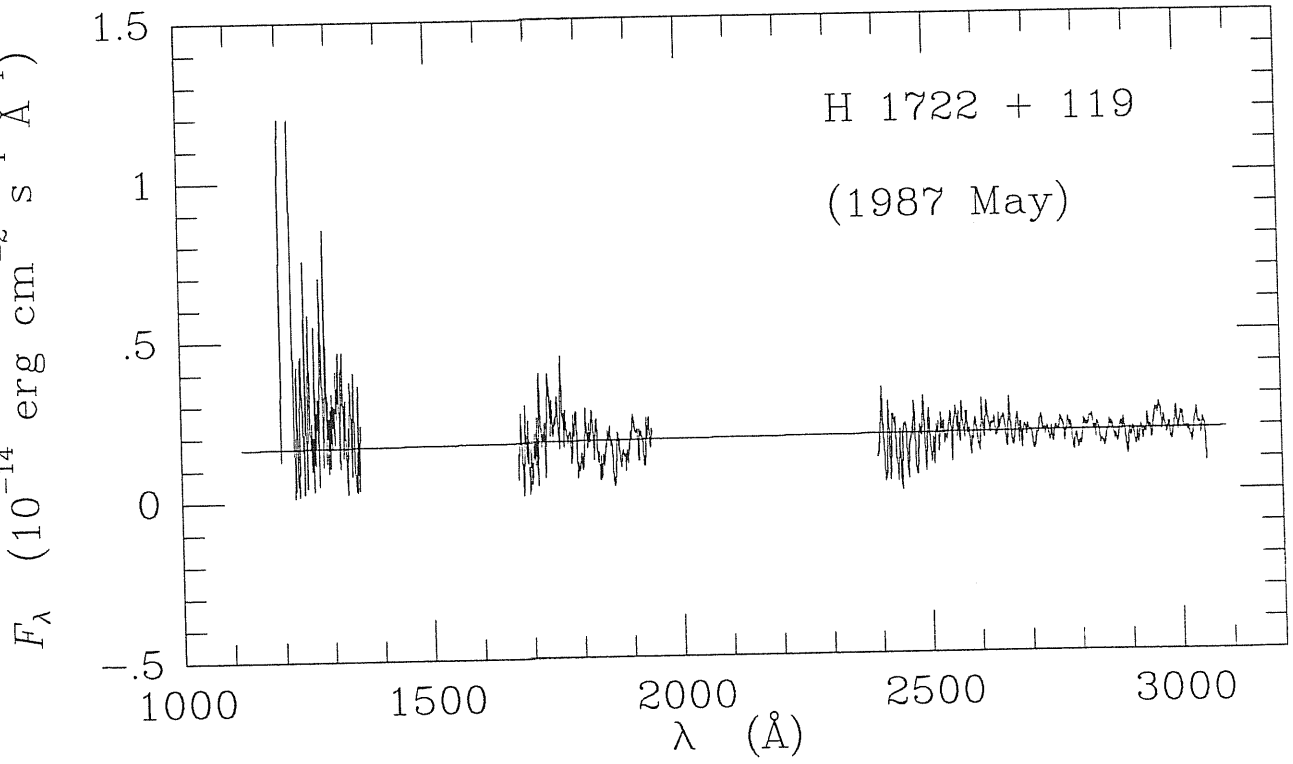

Fig. 2.1 (continued)

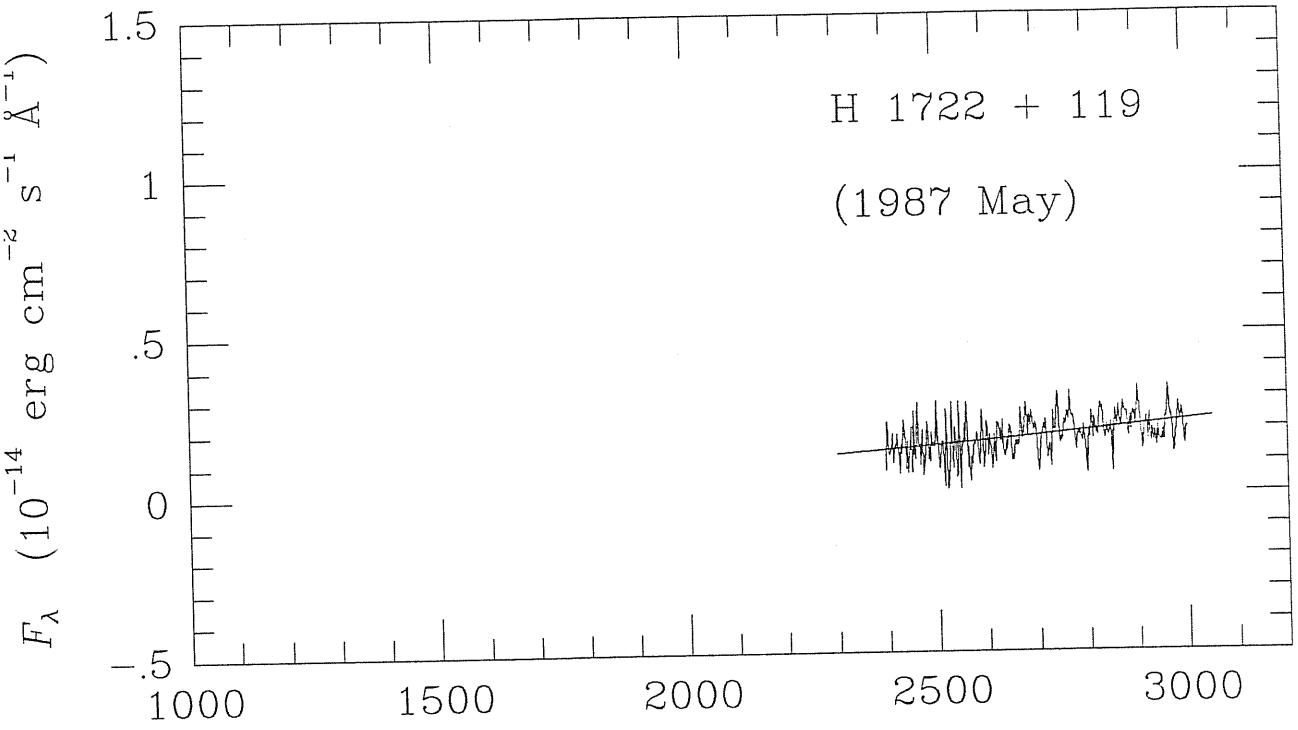

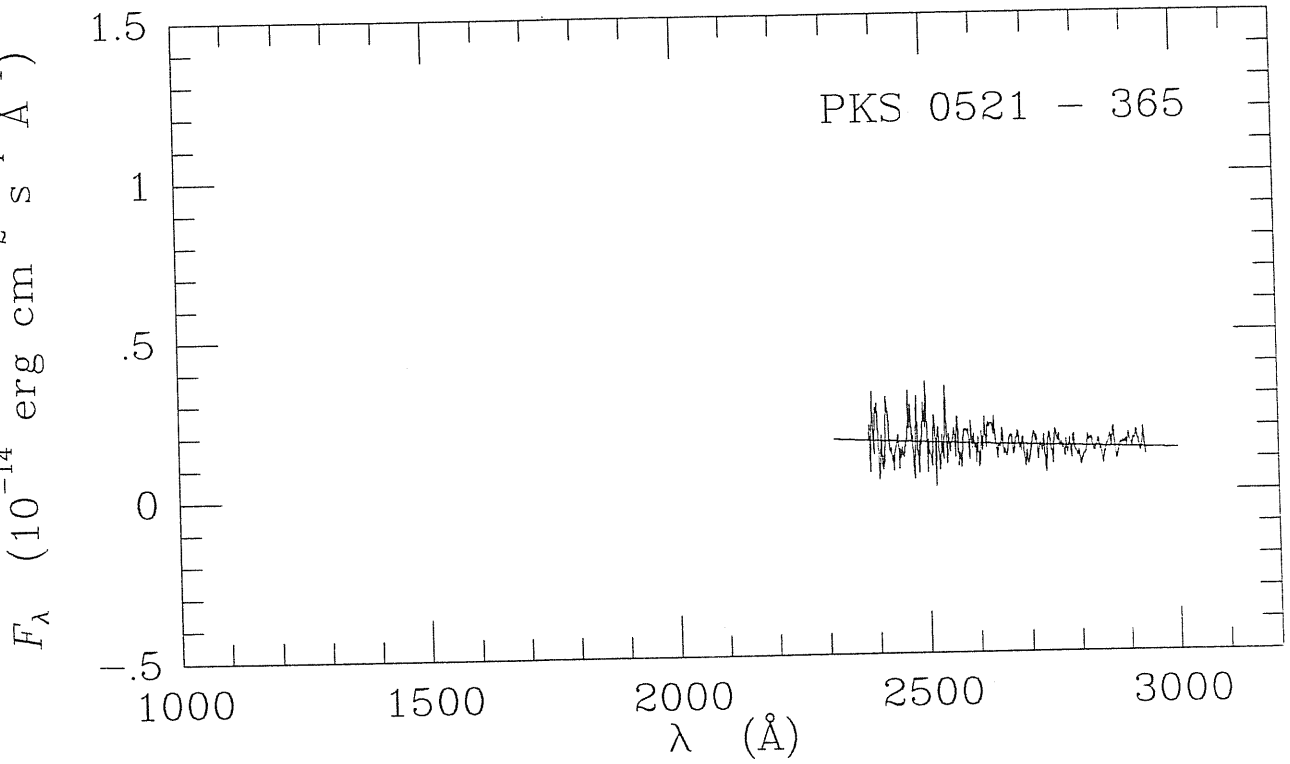

Fig. 2.1 (continued)

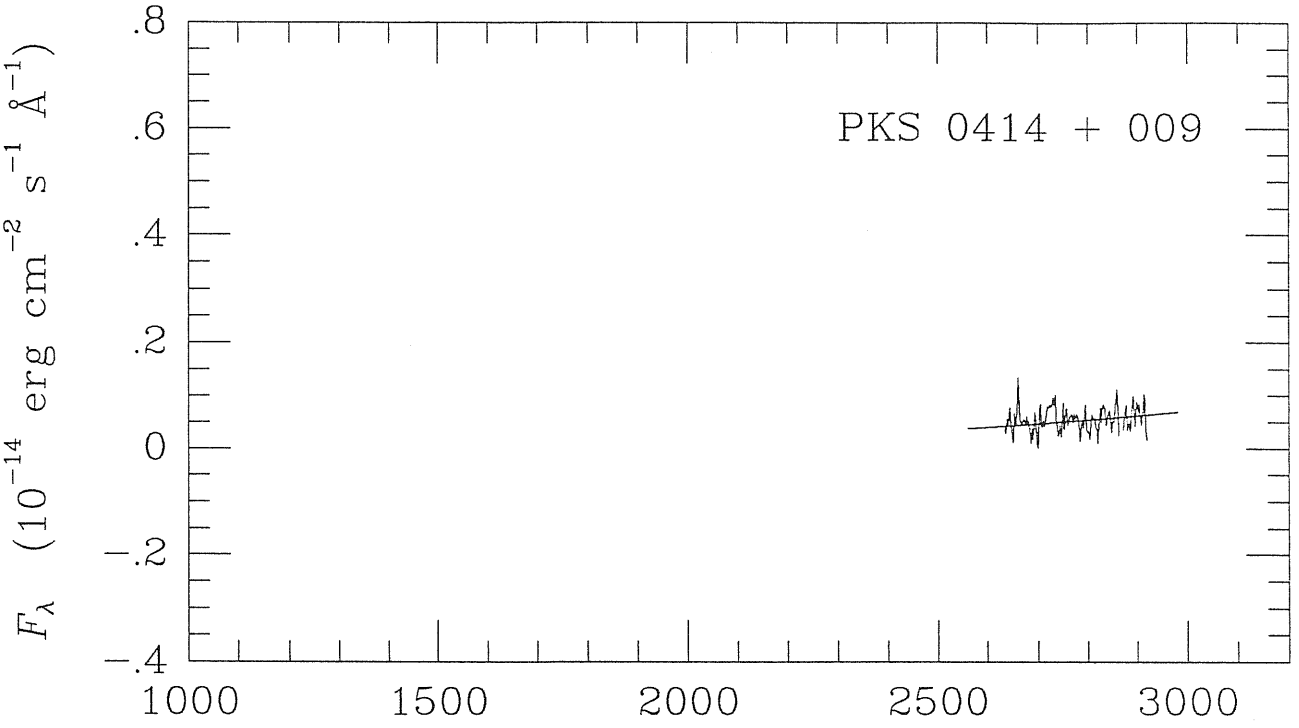

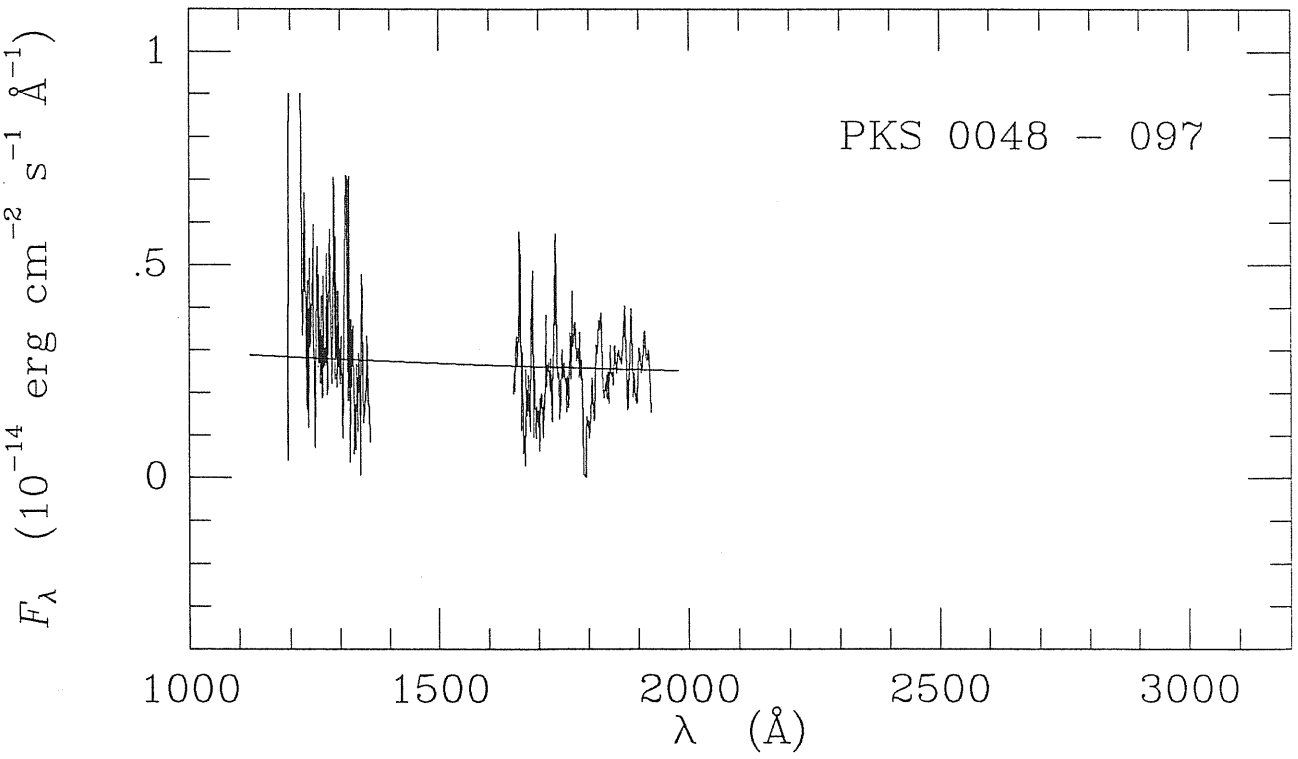

Fig. 2.1 (continued)

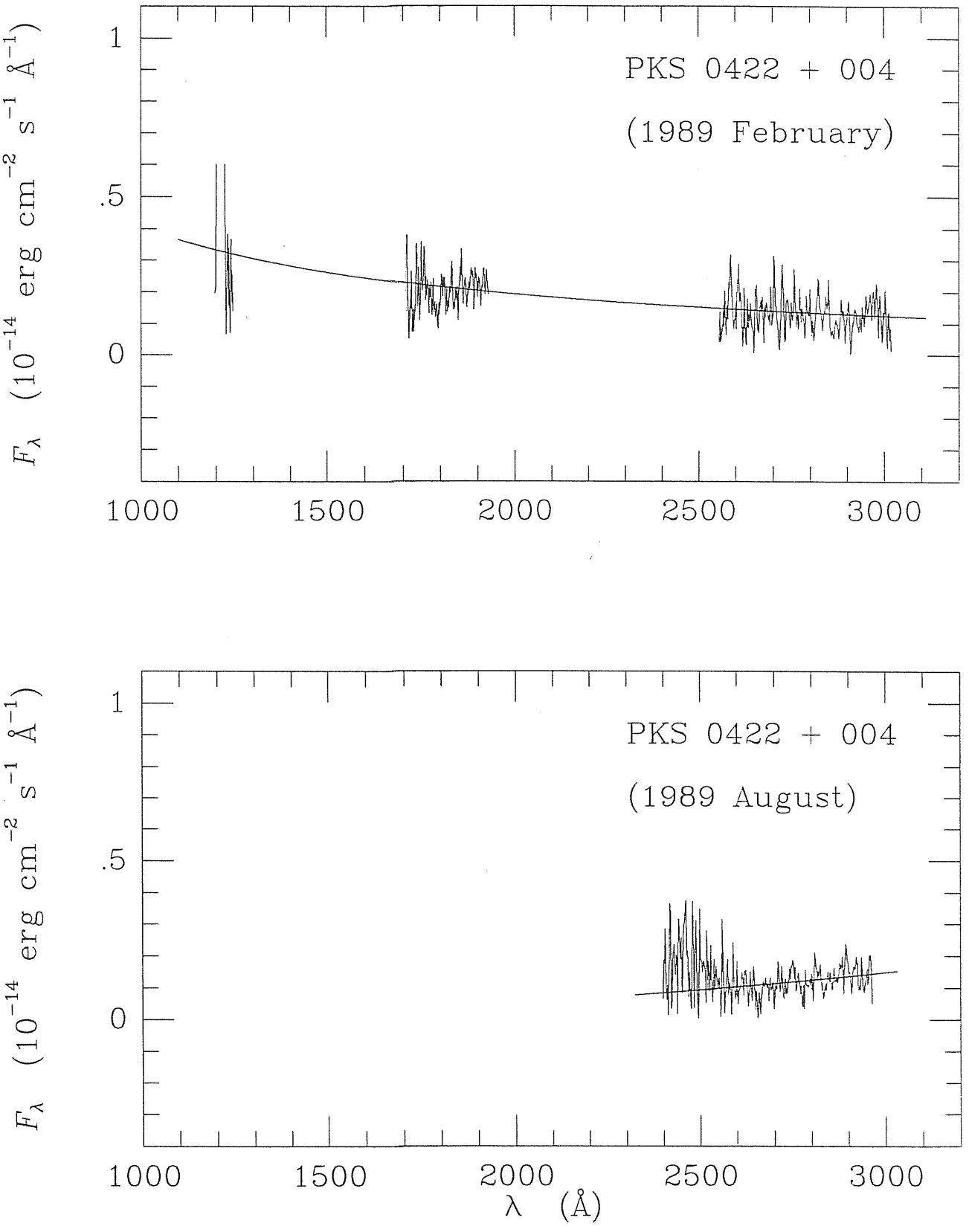

PKS 2155 − 304

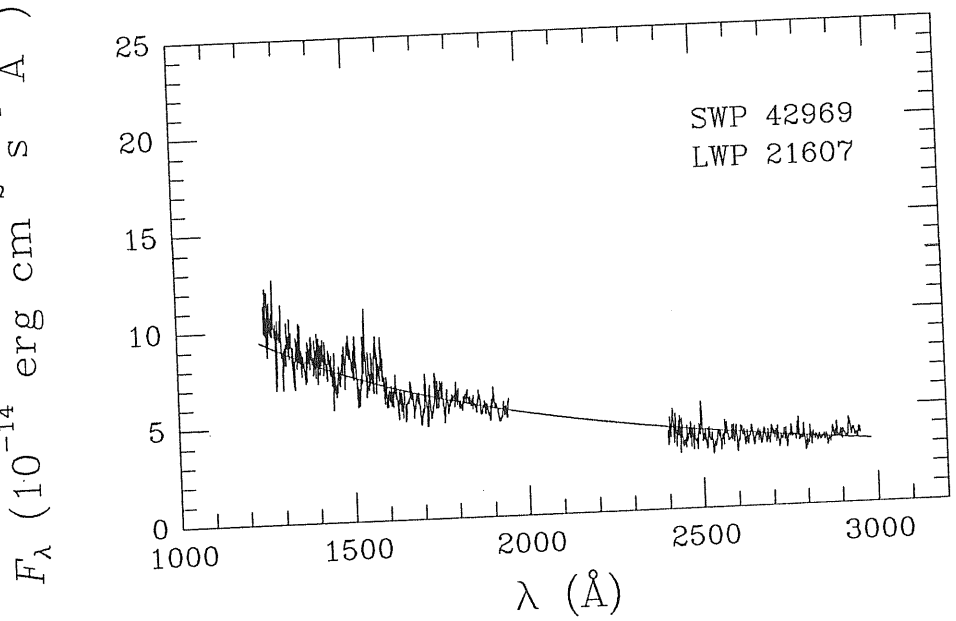

Fig. 3.1

Fig. 3.1 (continued)

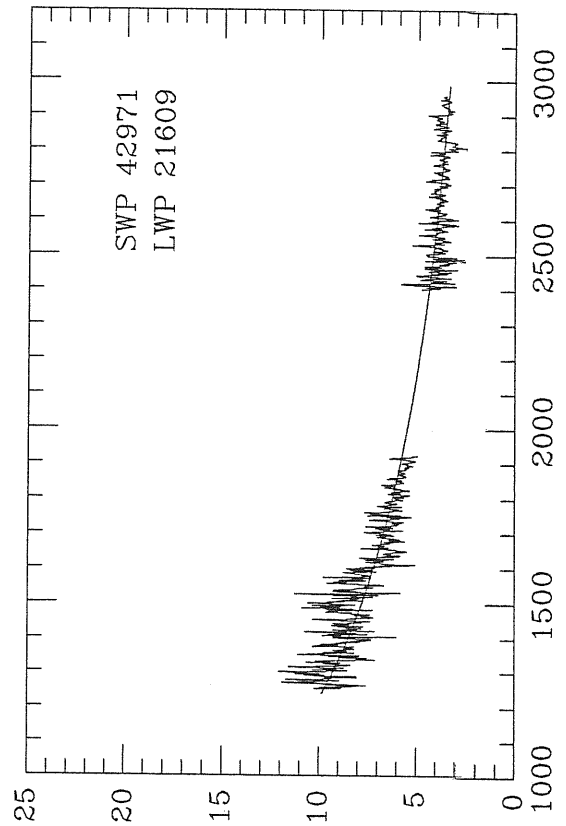

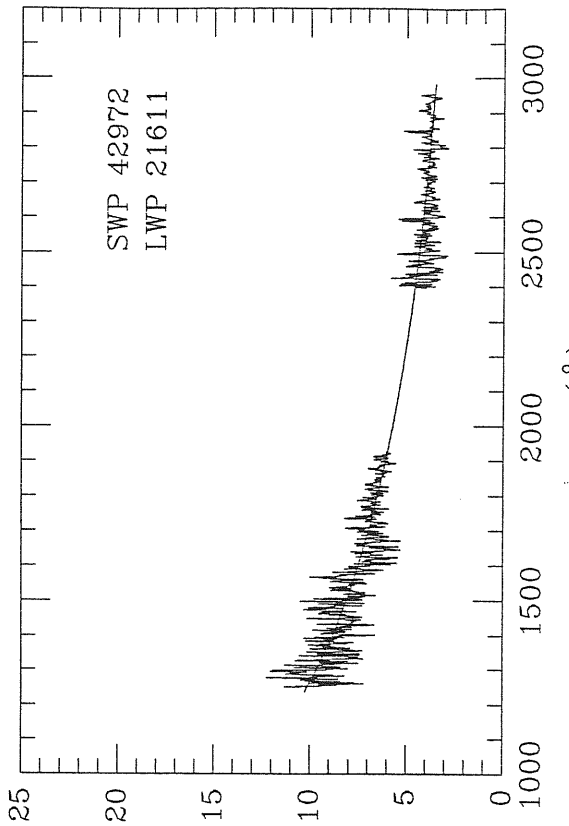

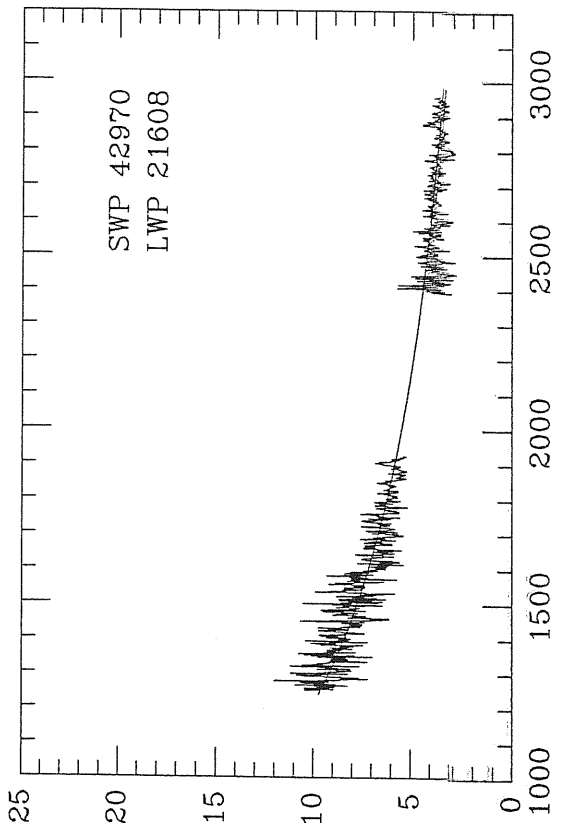

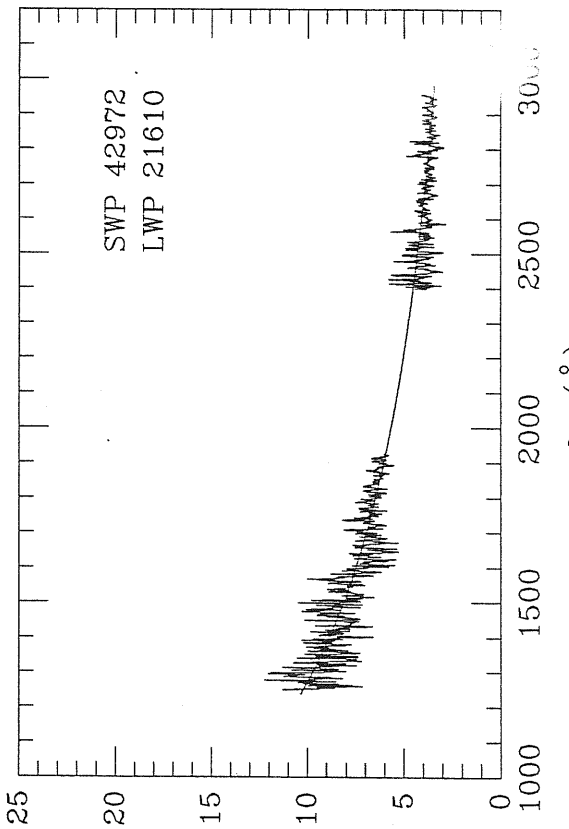

Fig. 3.1 (continued)

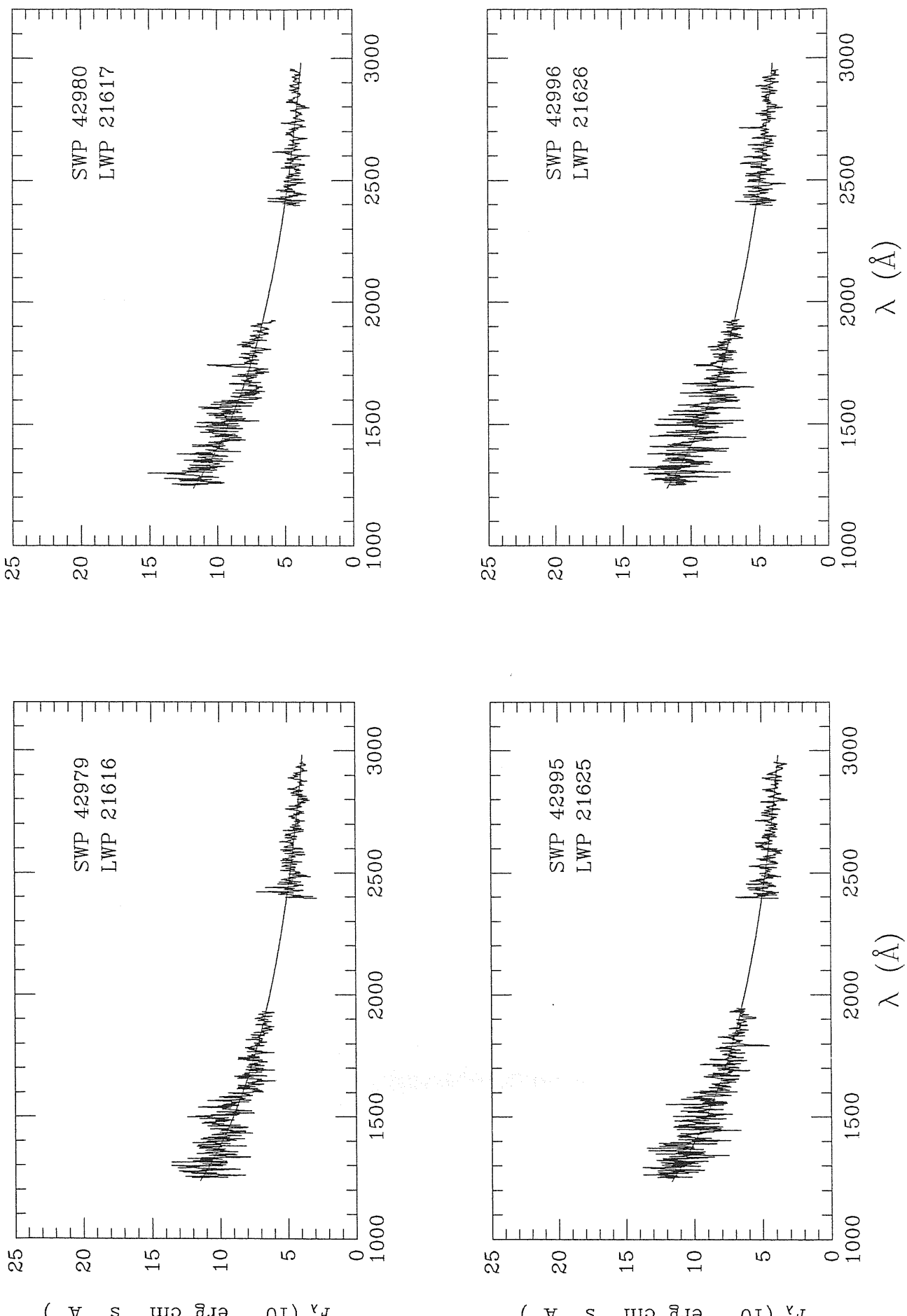

Fig. 3.1 (continued)

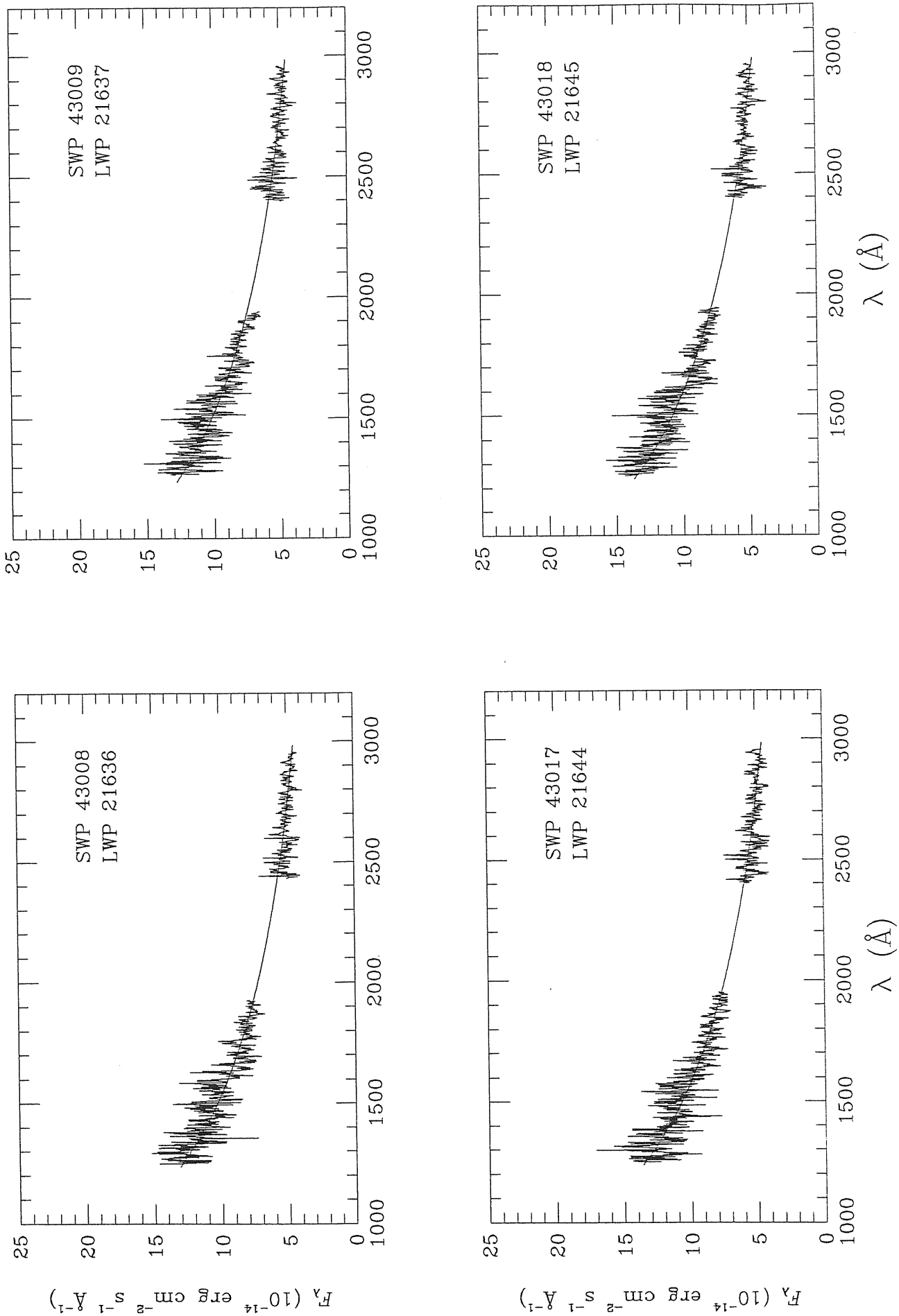

Fig. 3.1 (continued)

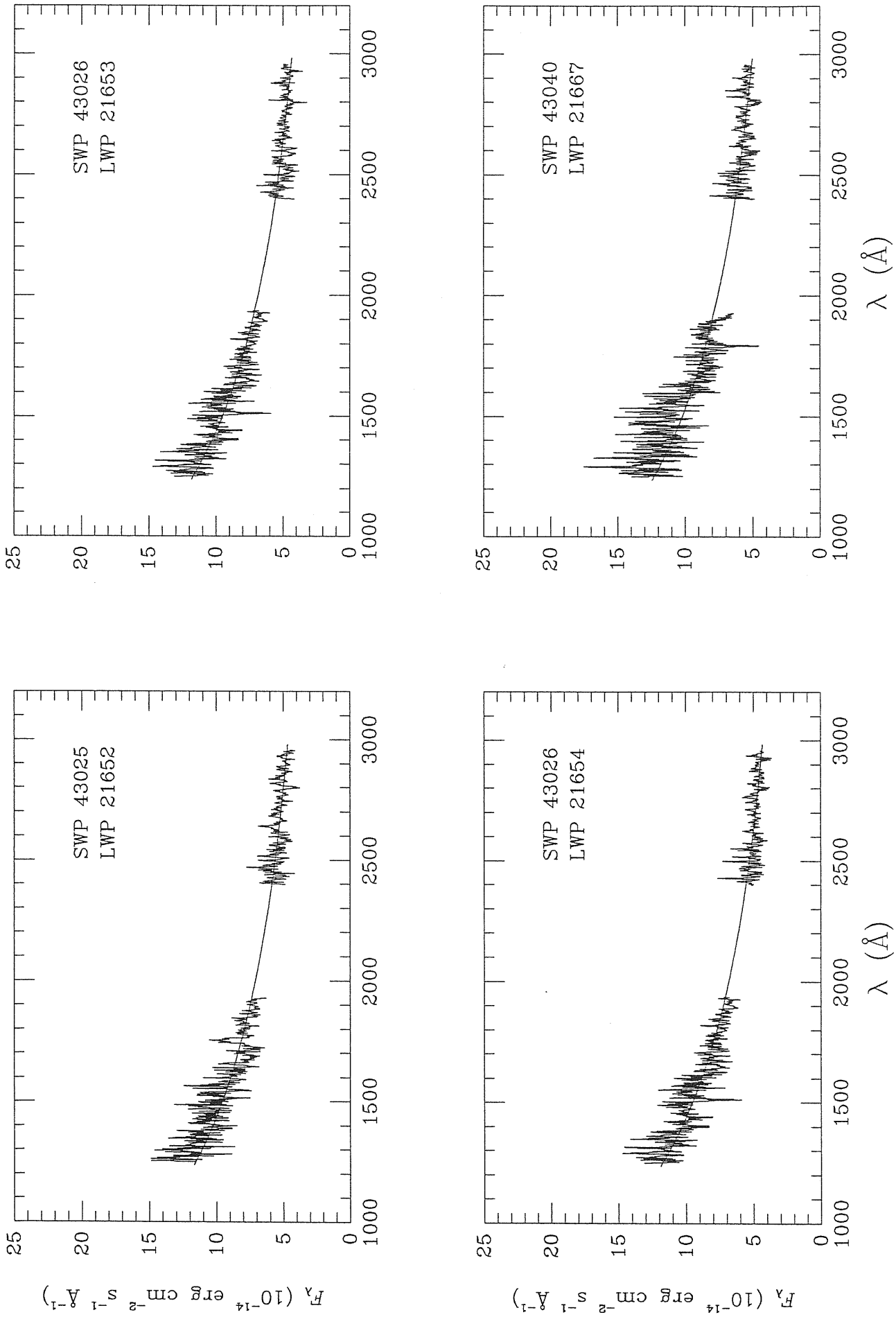

Fig. 3.1 (continued)

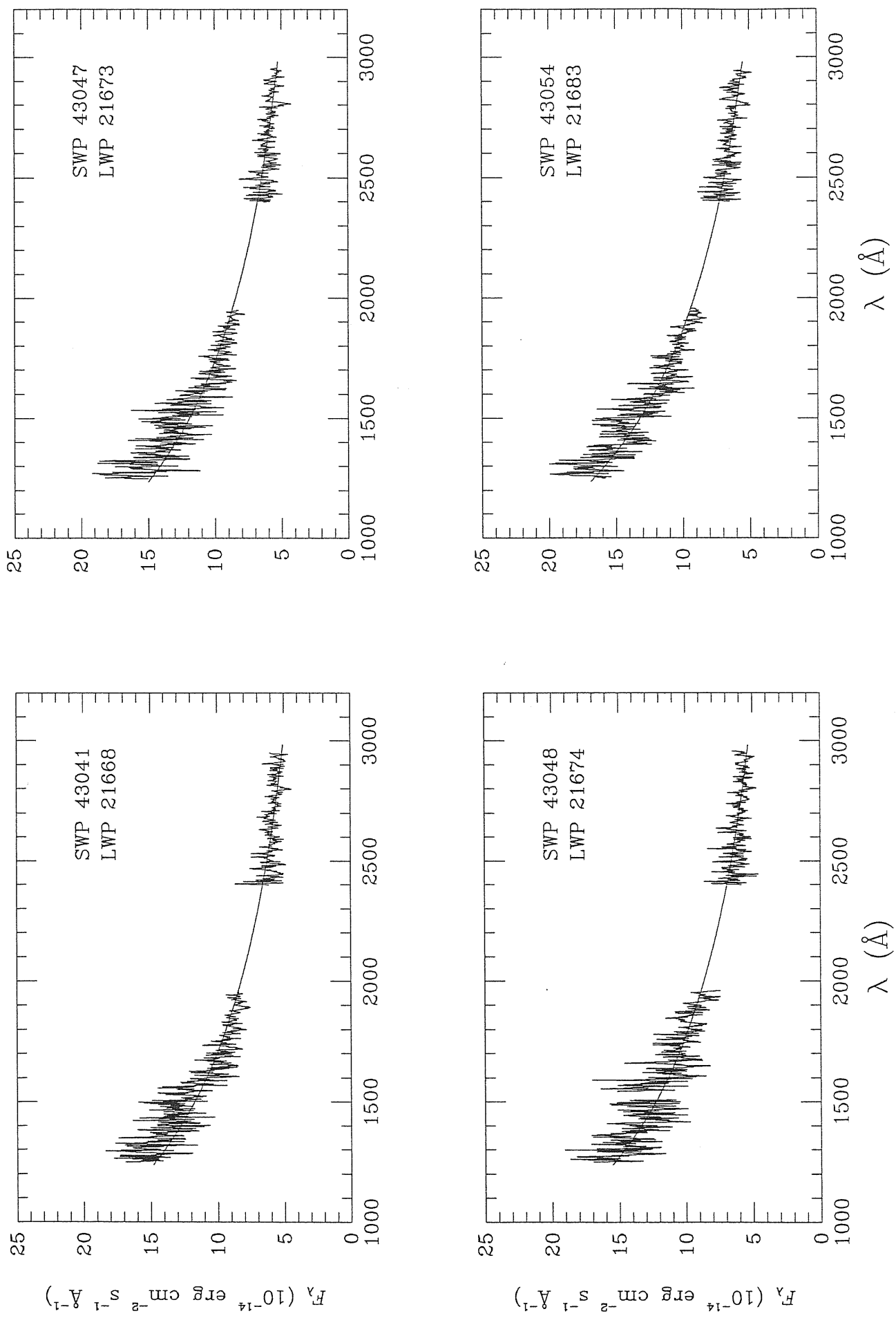

Fig. 3.1 (continued)

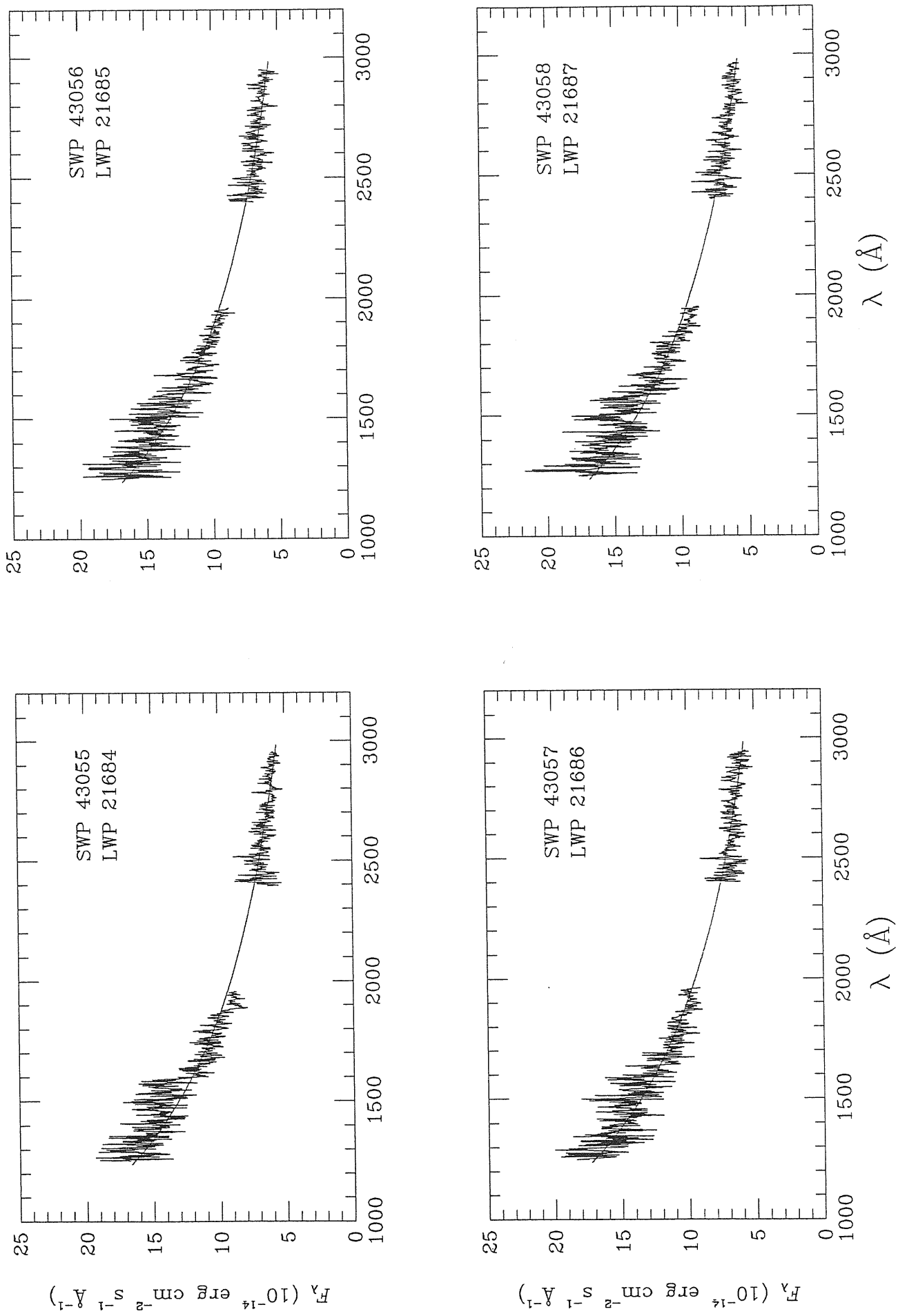

Fig. 3.1 (continued)

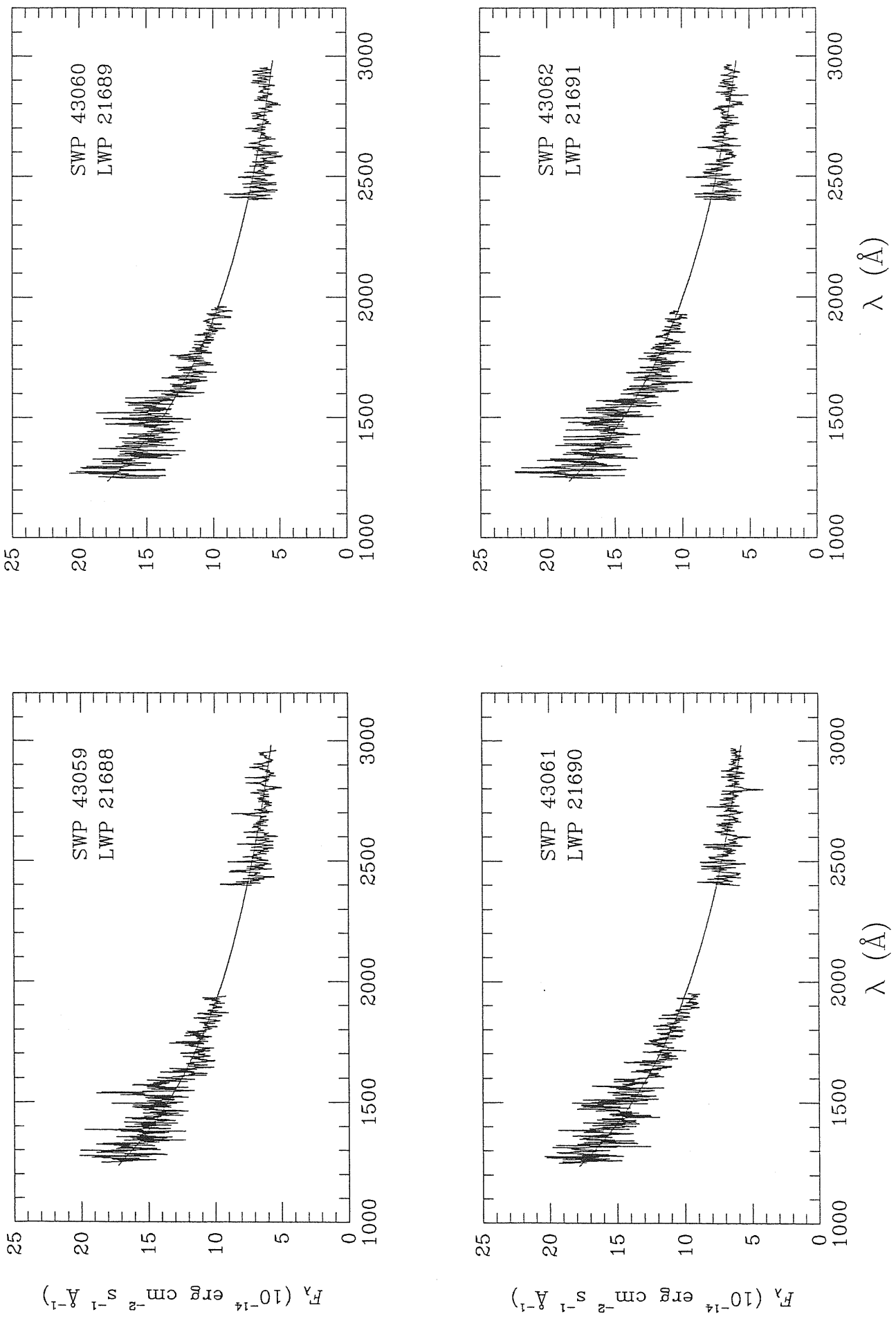

Fig. 3.1 (continued)

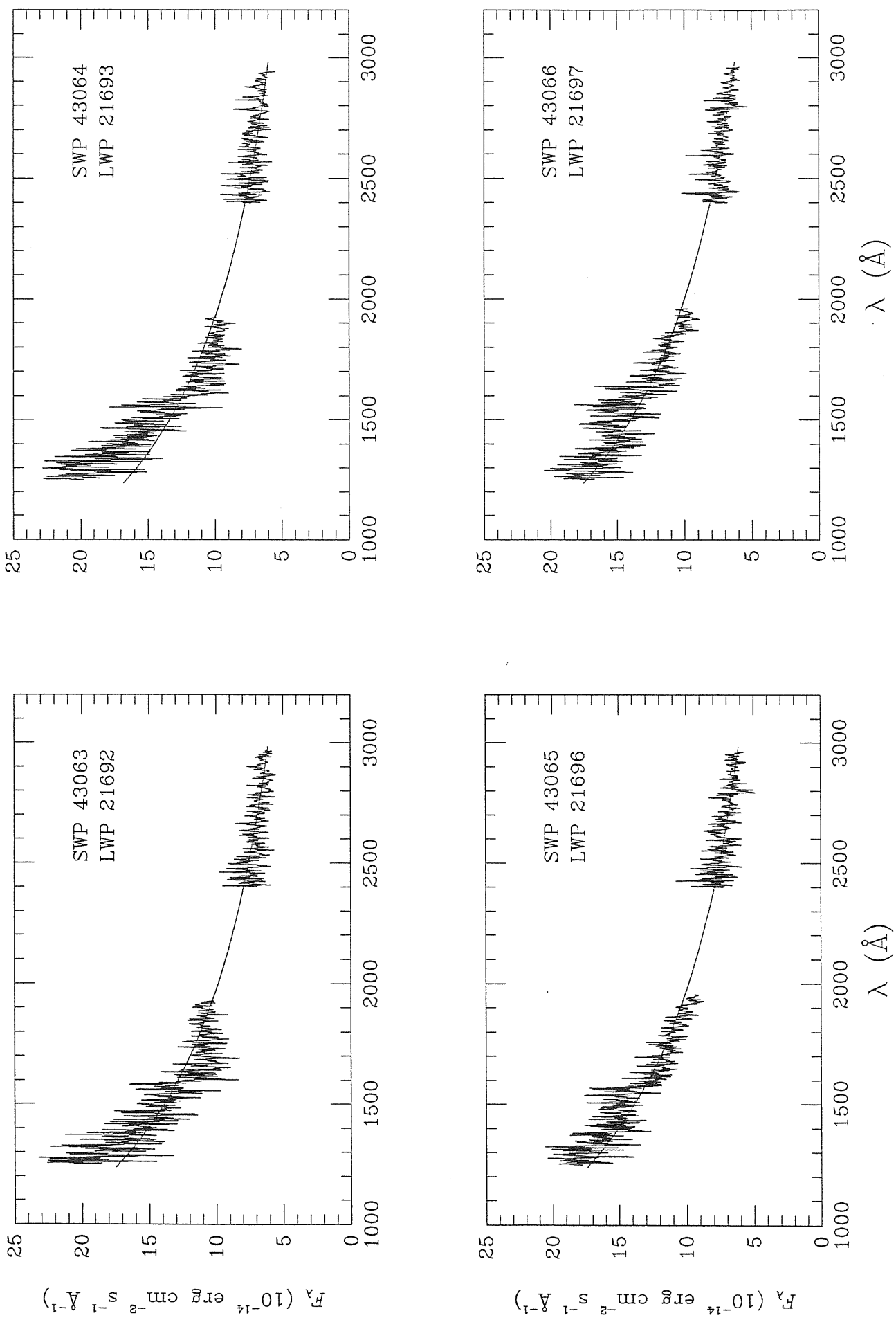

Fig. 3.1 (continued)

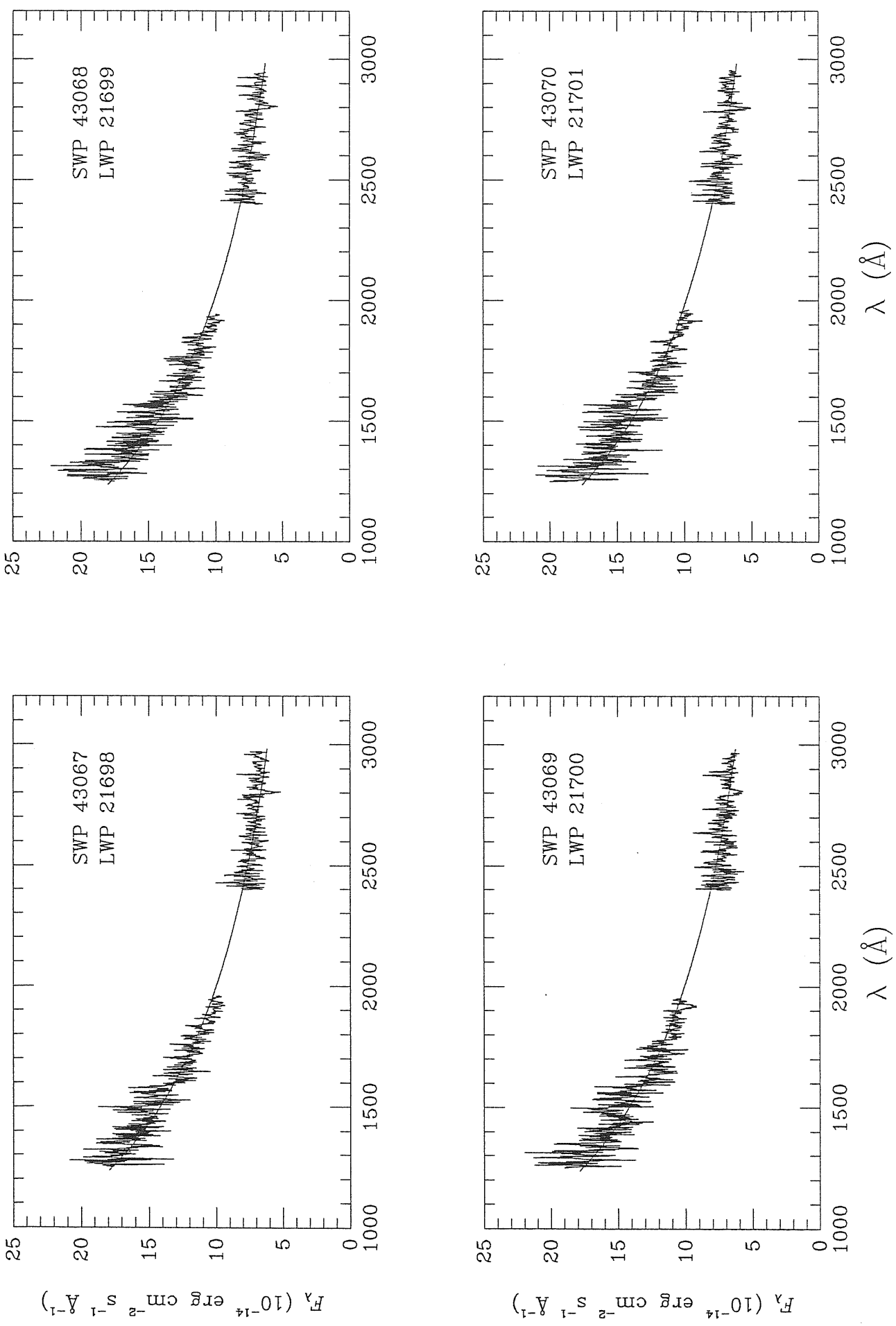

Fig. 3.1 (continued)

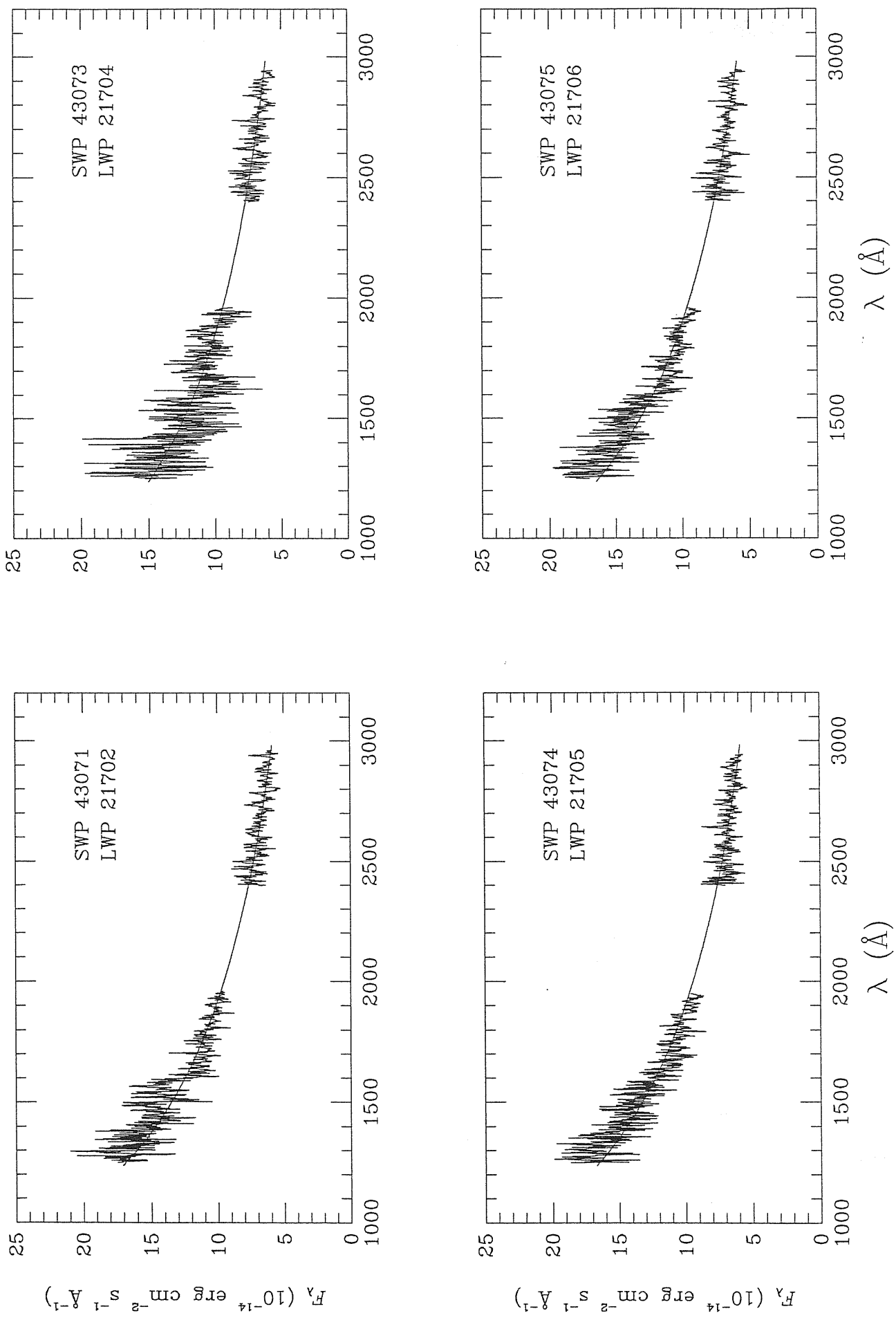

Fig. 3.1 (continued)

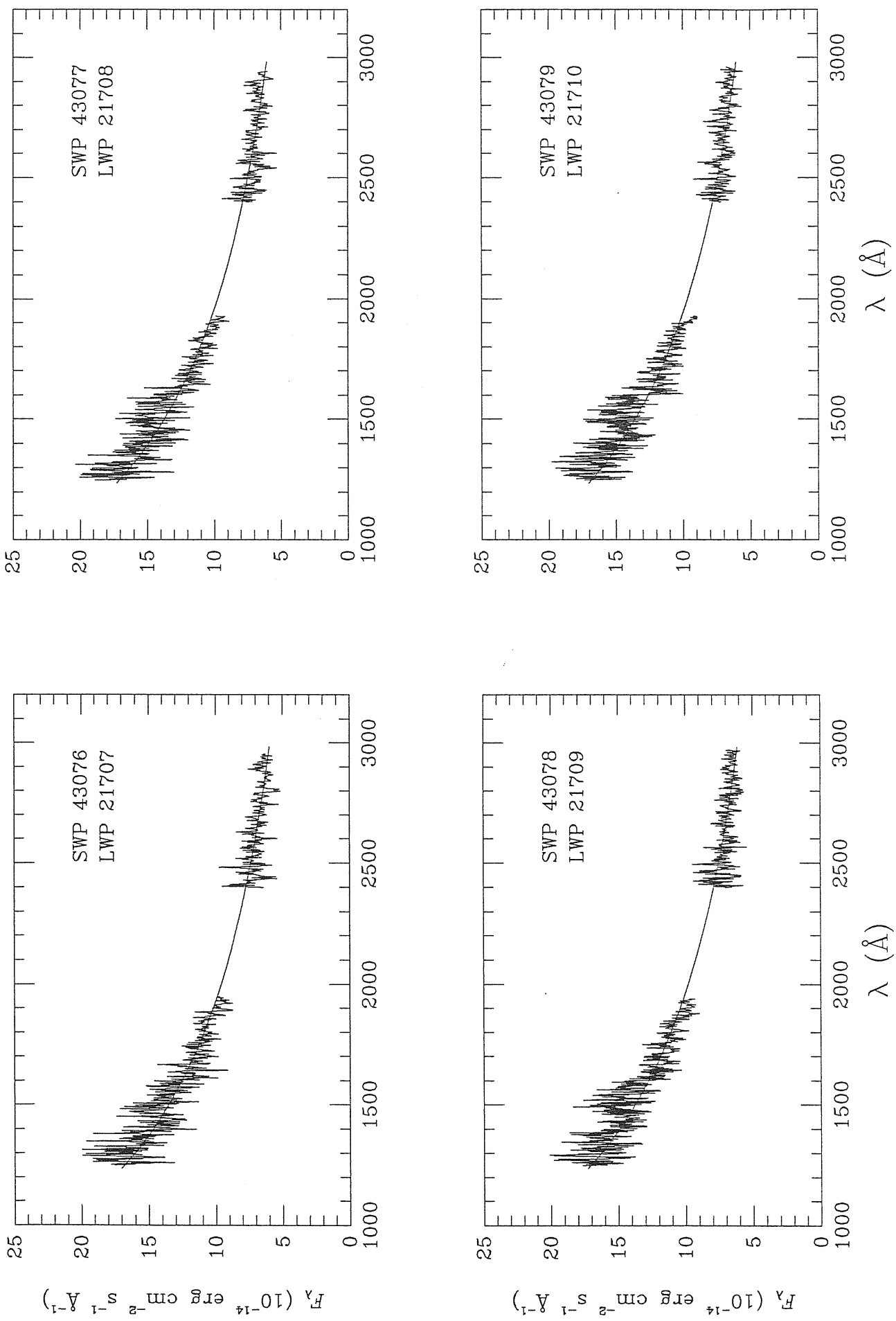

Fig. 3.1 (continued)

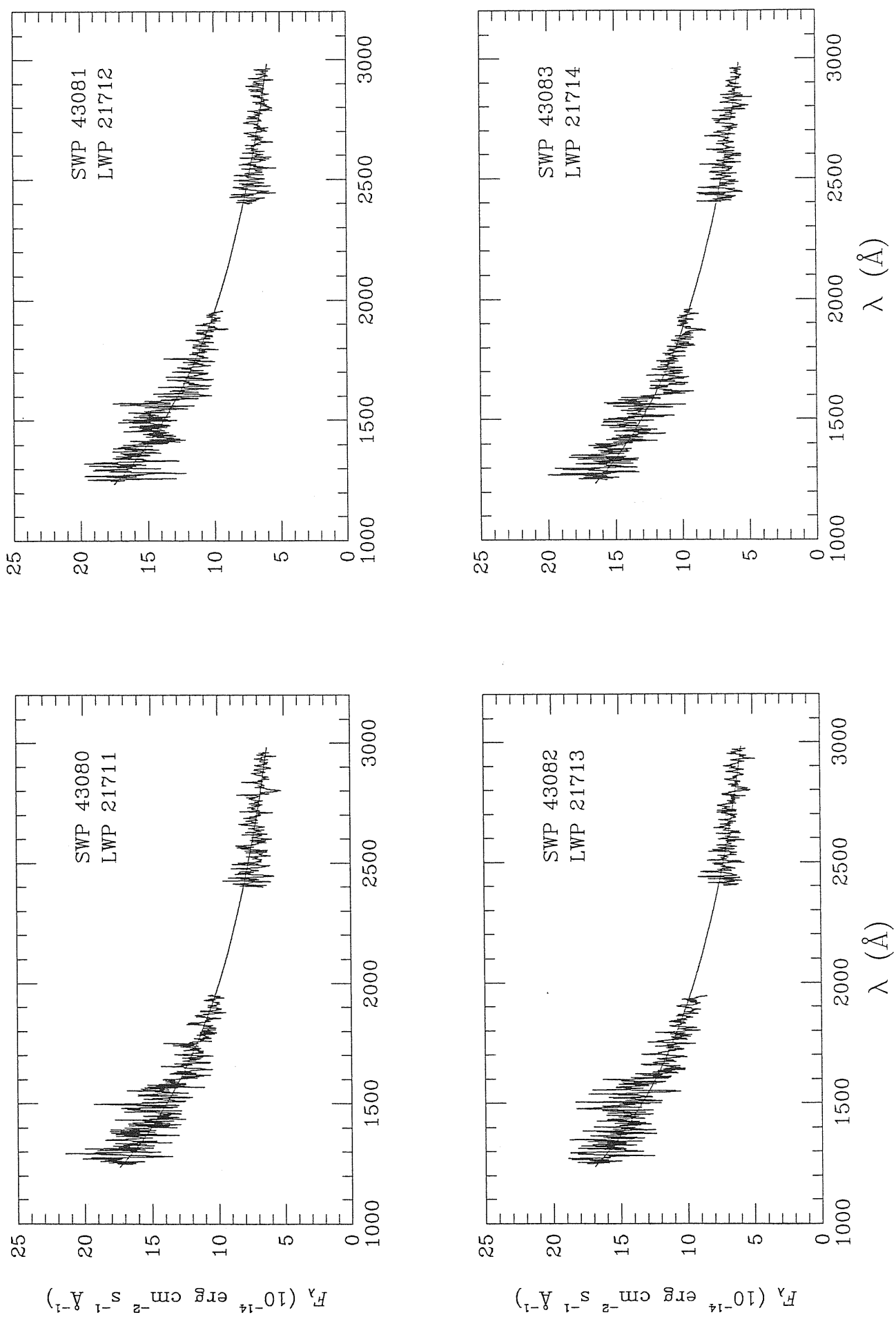

Fig. 3.1 (continued)

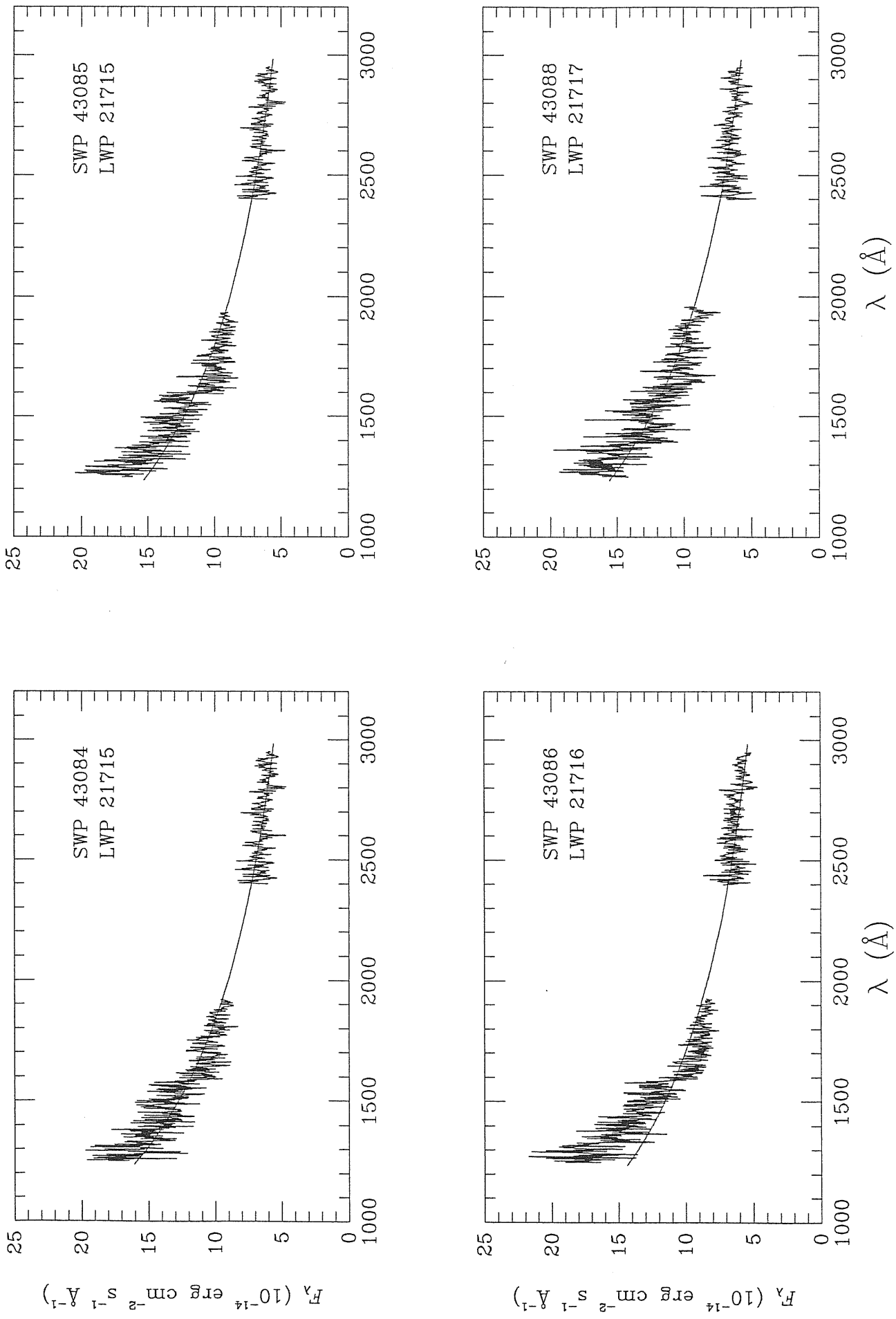

Fig. 3.1 (continued)

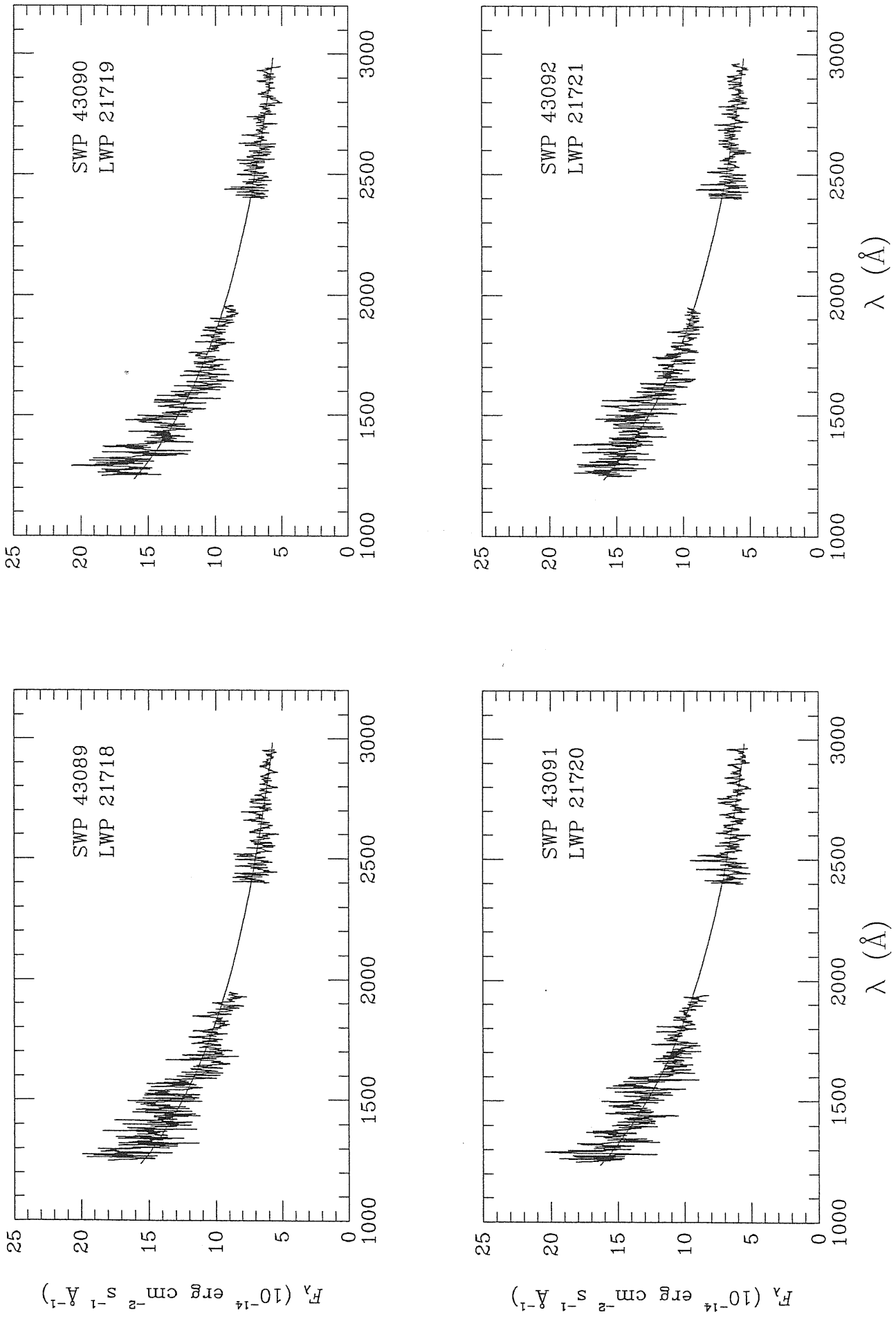

Fig. 3.1 (continued)

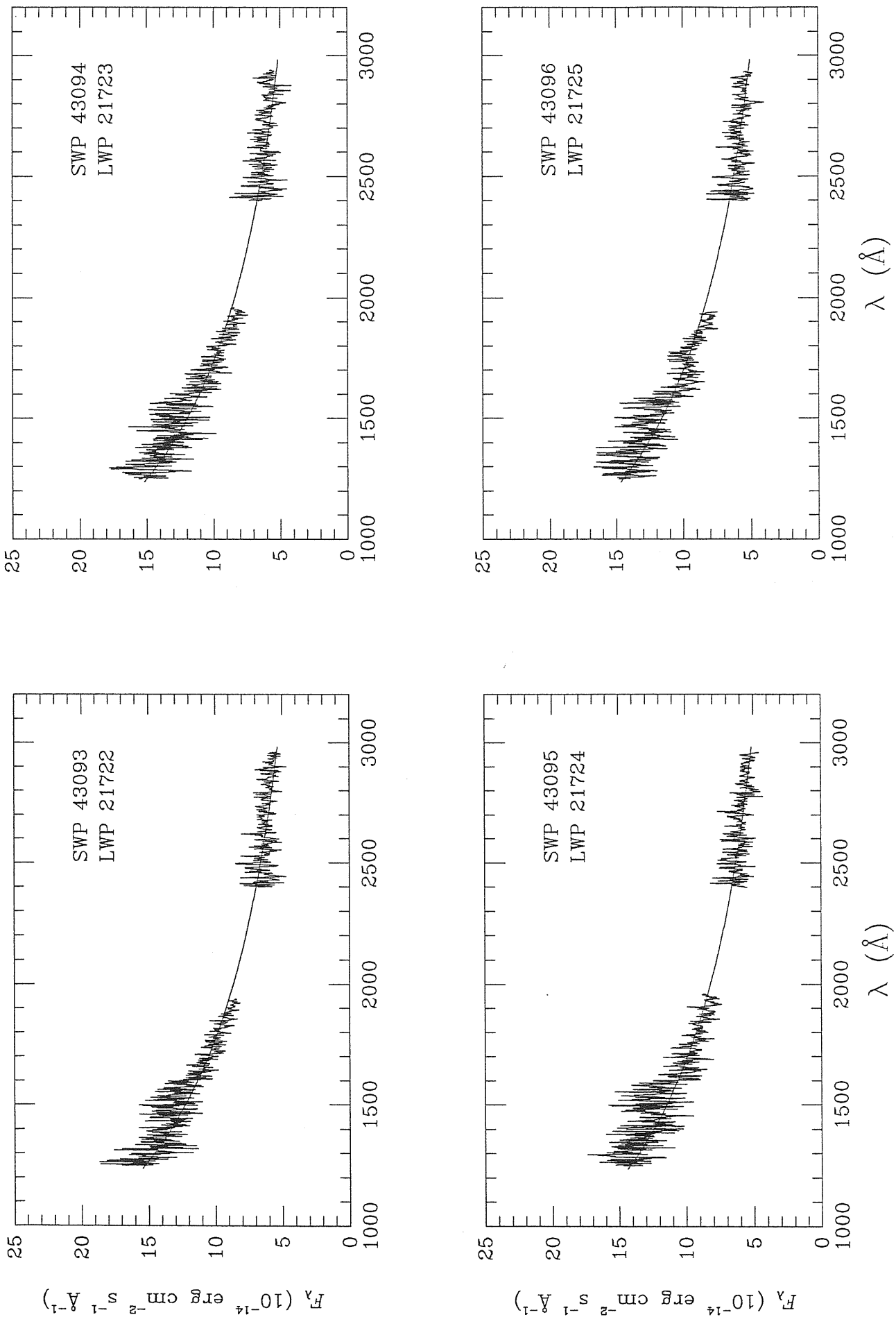

Fig. 3.1 (continued)

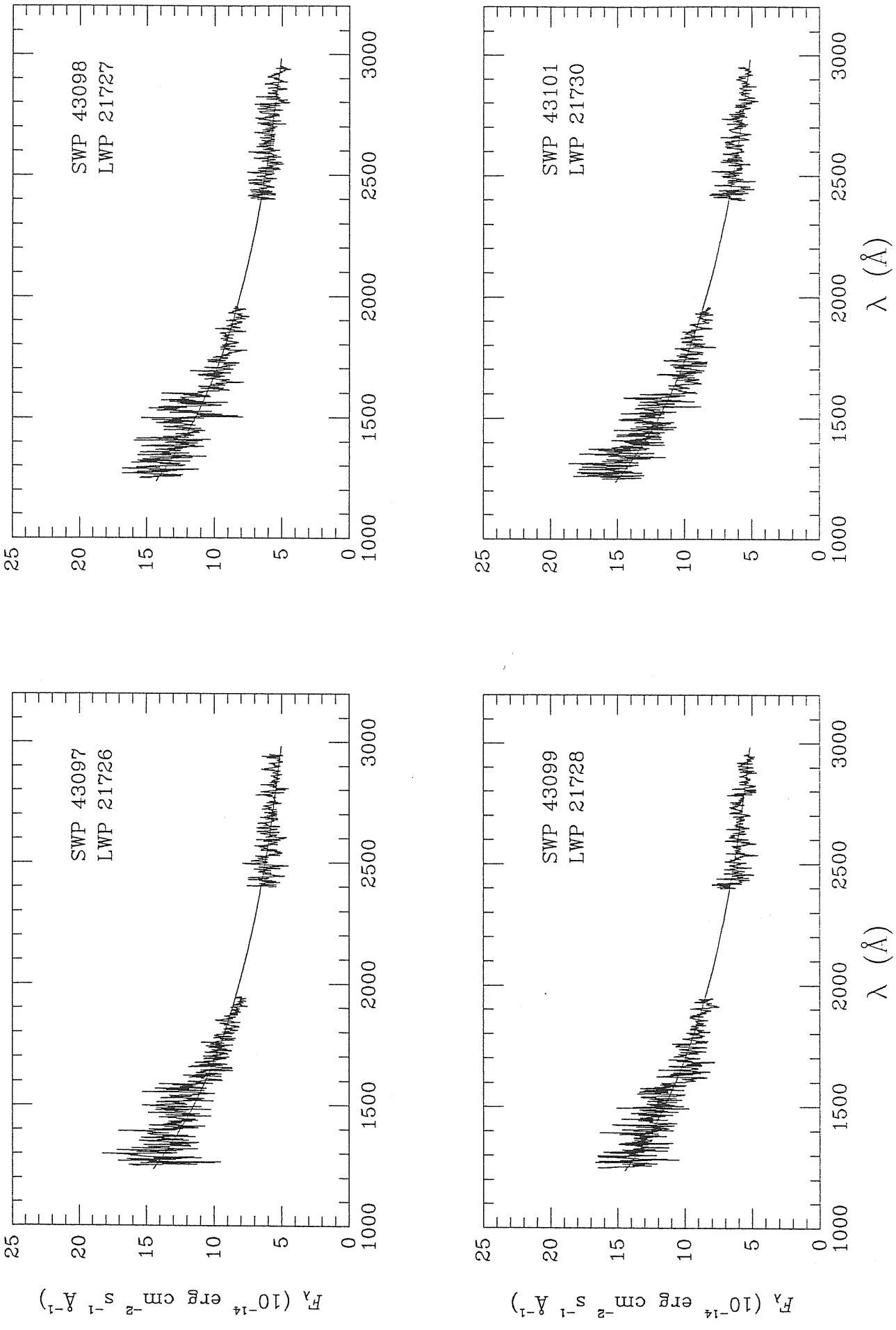

Fig. 3.1 (continued)

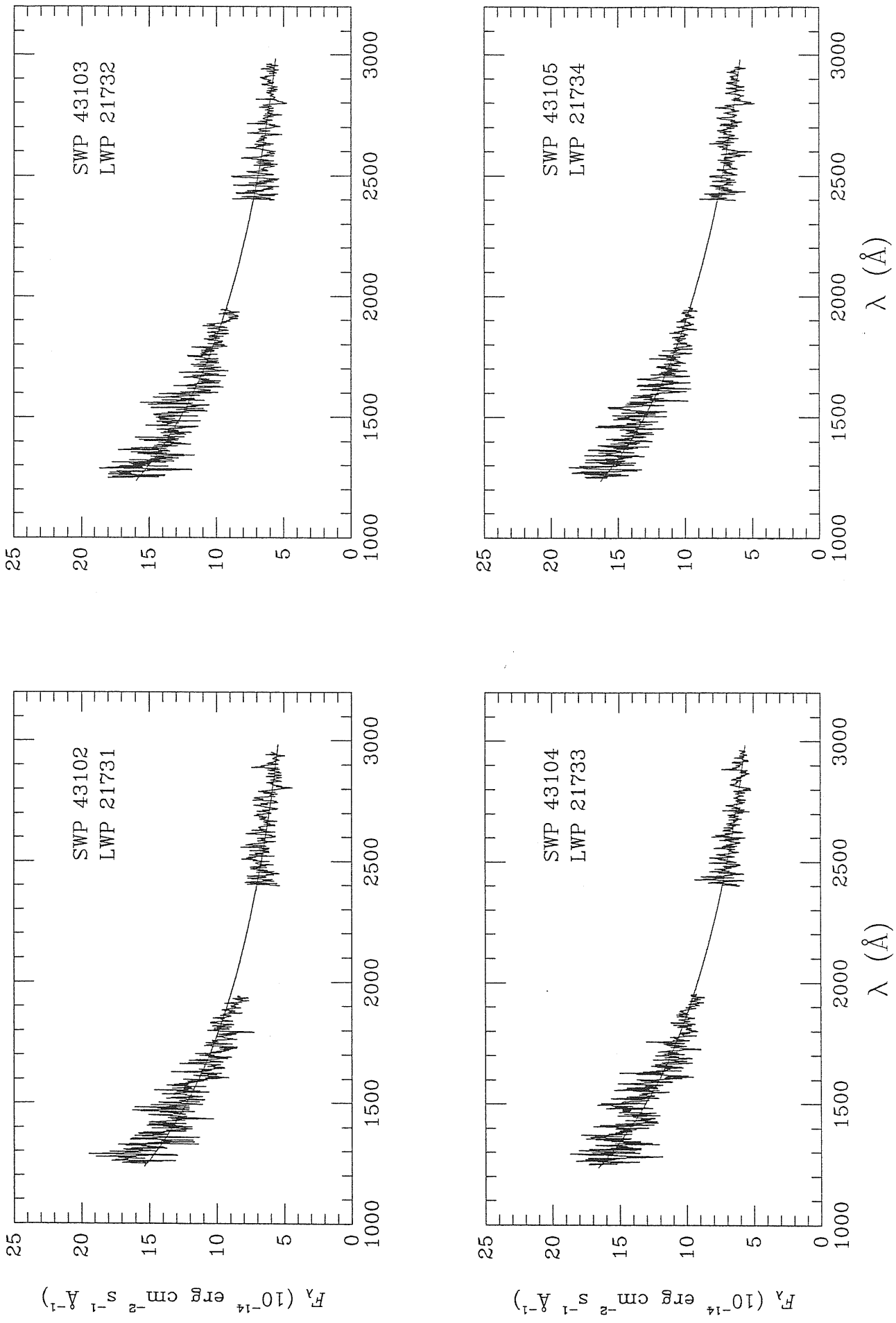

Fig. 3.1 (continued)

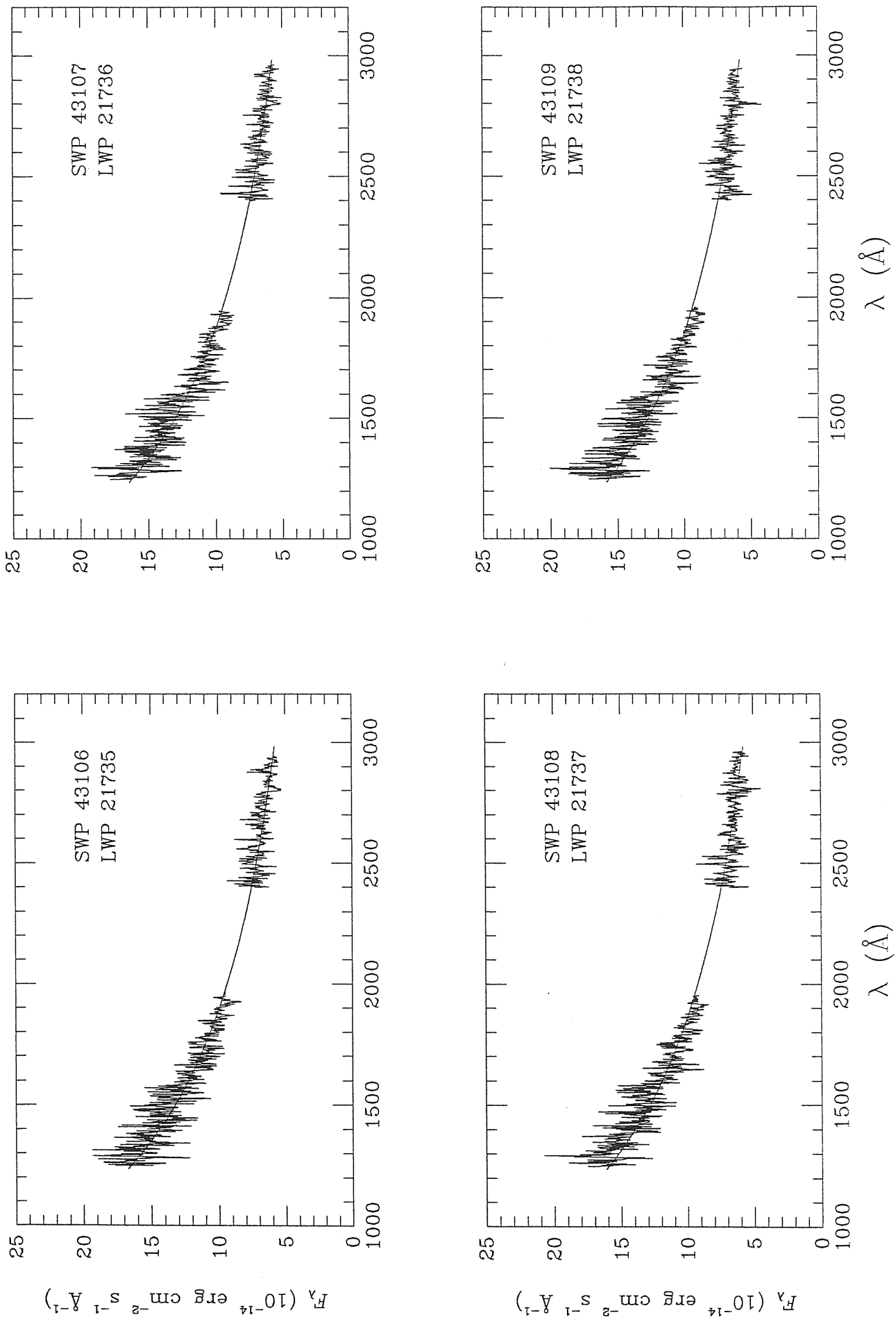

Fig. 3.1 (continued)

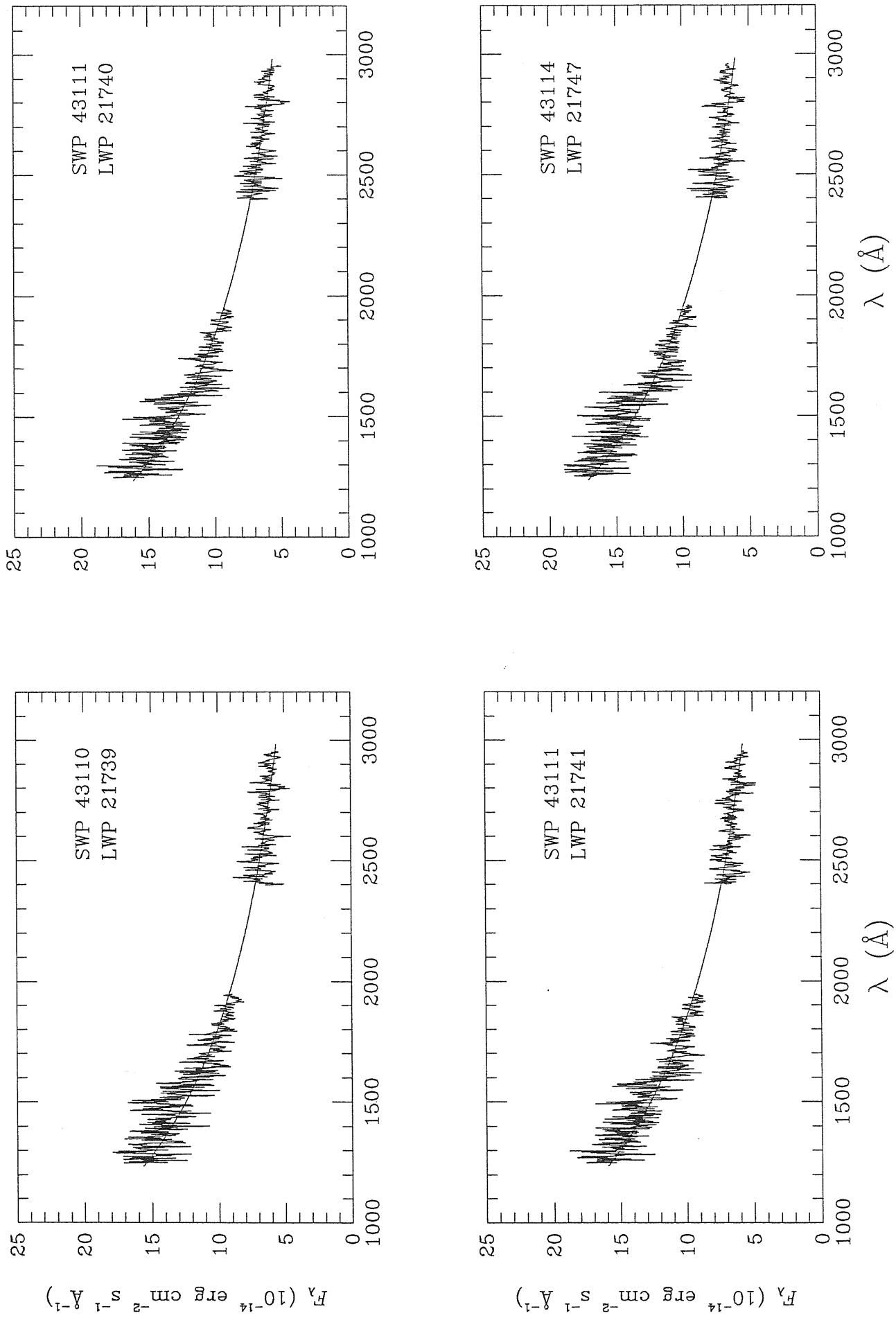

Fig. 3.1 (continued)

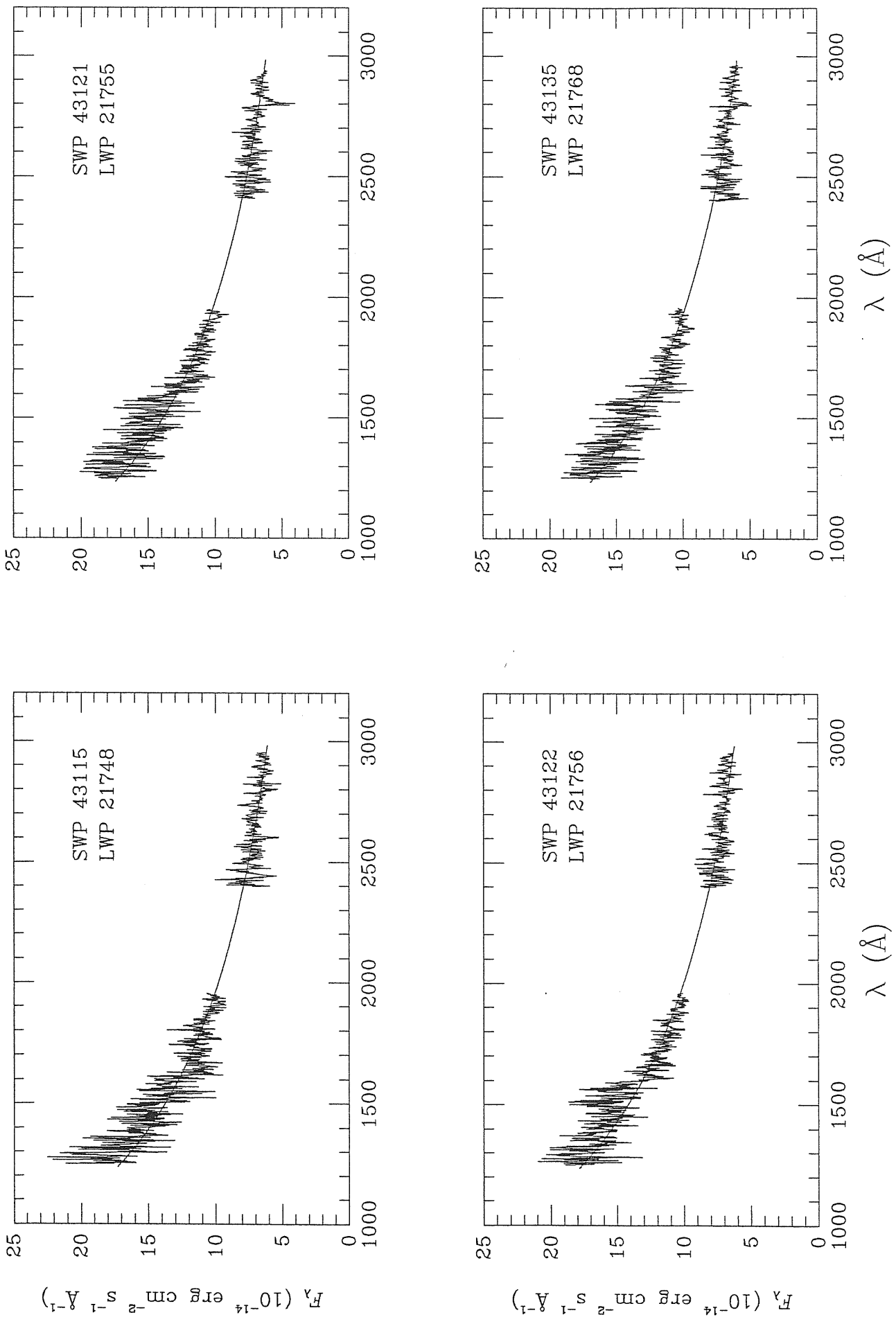

Fig. 3.1 (continued)

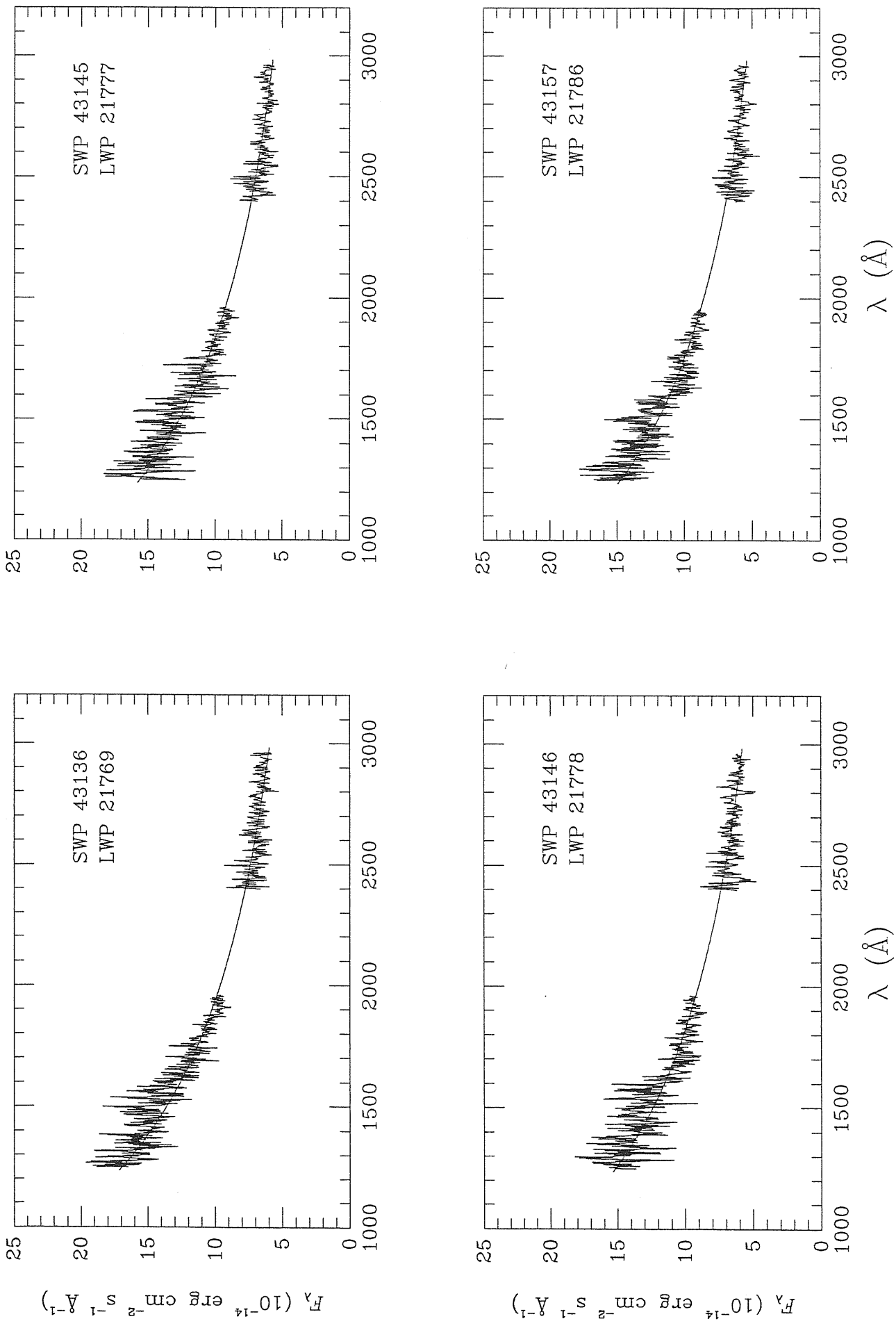

Fig. 3.1 (continued)

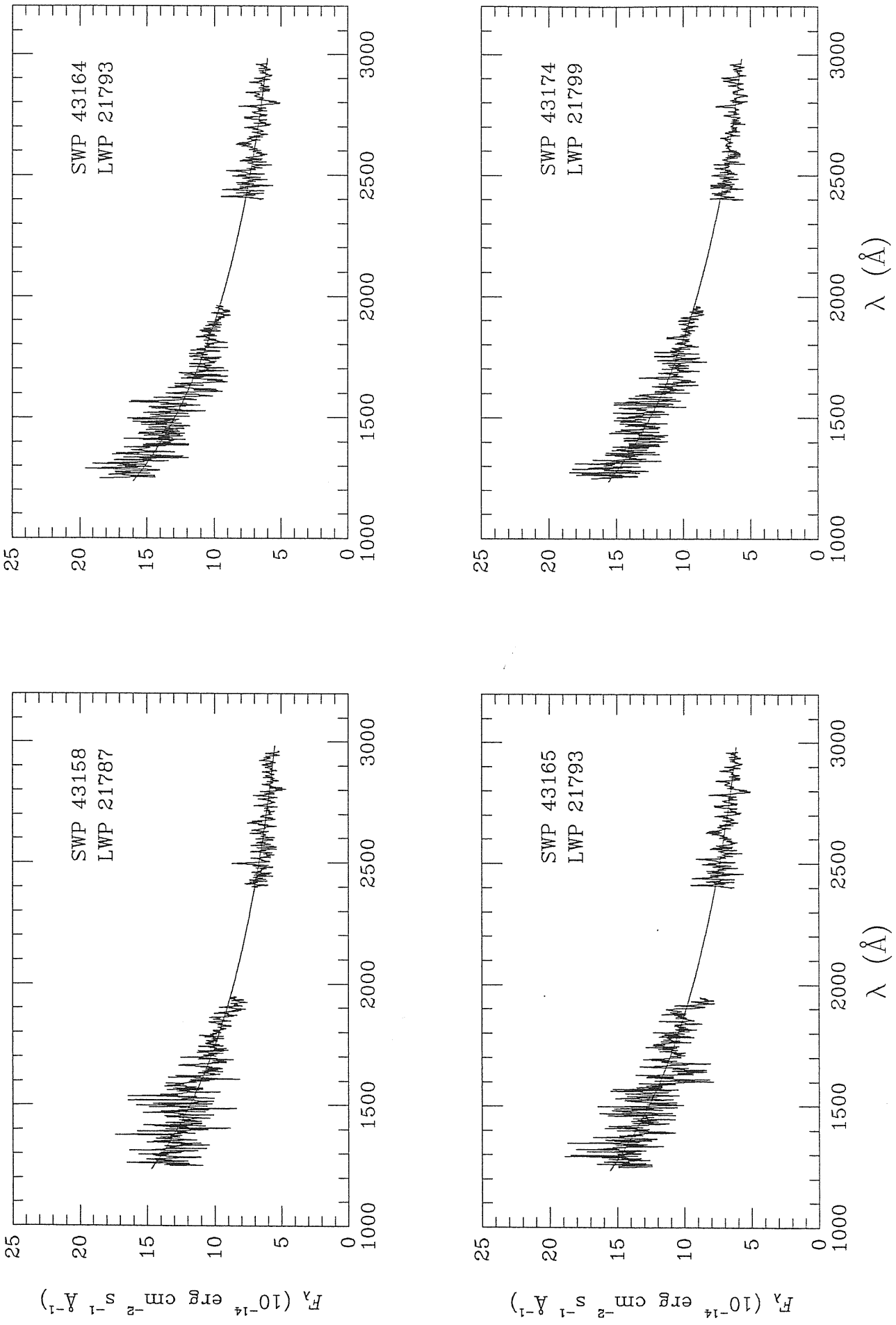

Fig. 3.1 (continued)

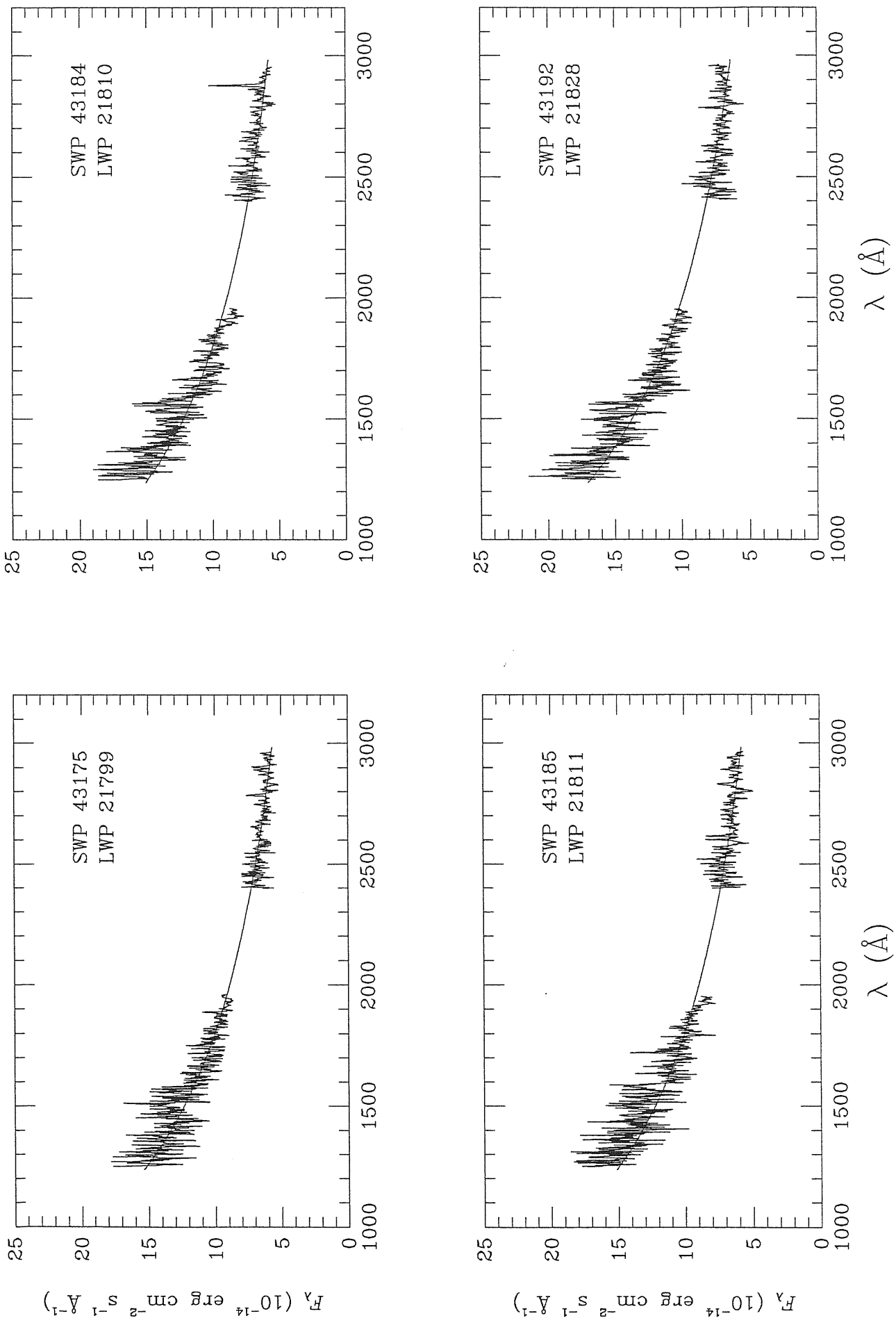

Fig. 3.1 (continued)

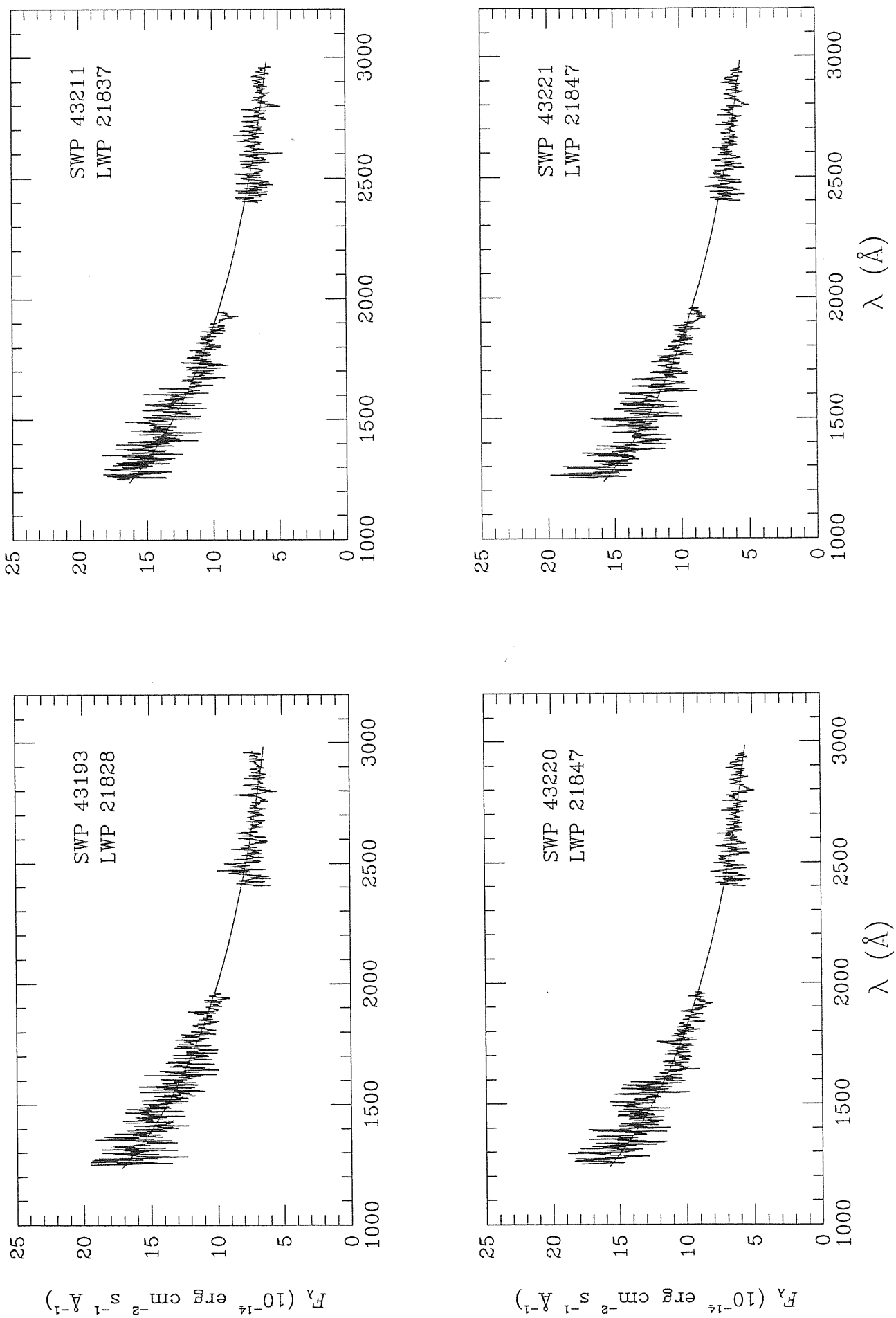

Fig. 3.1 (continued)

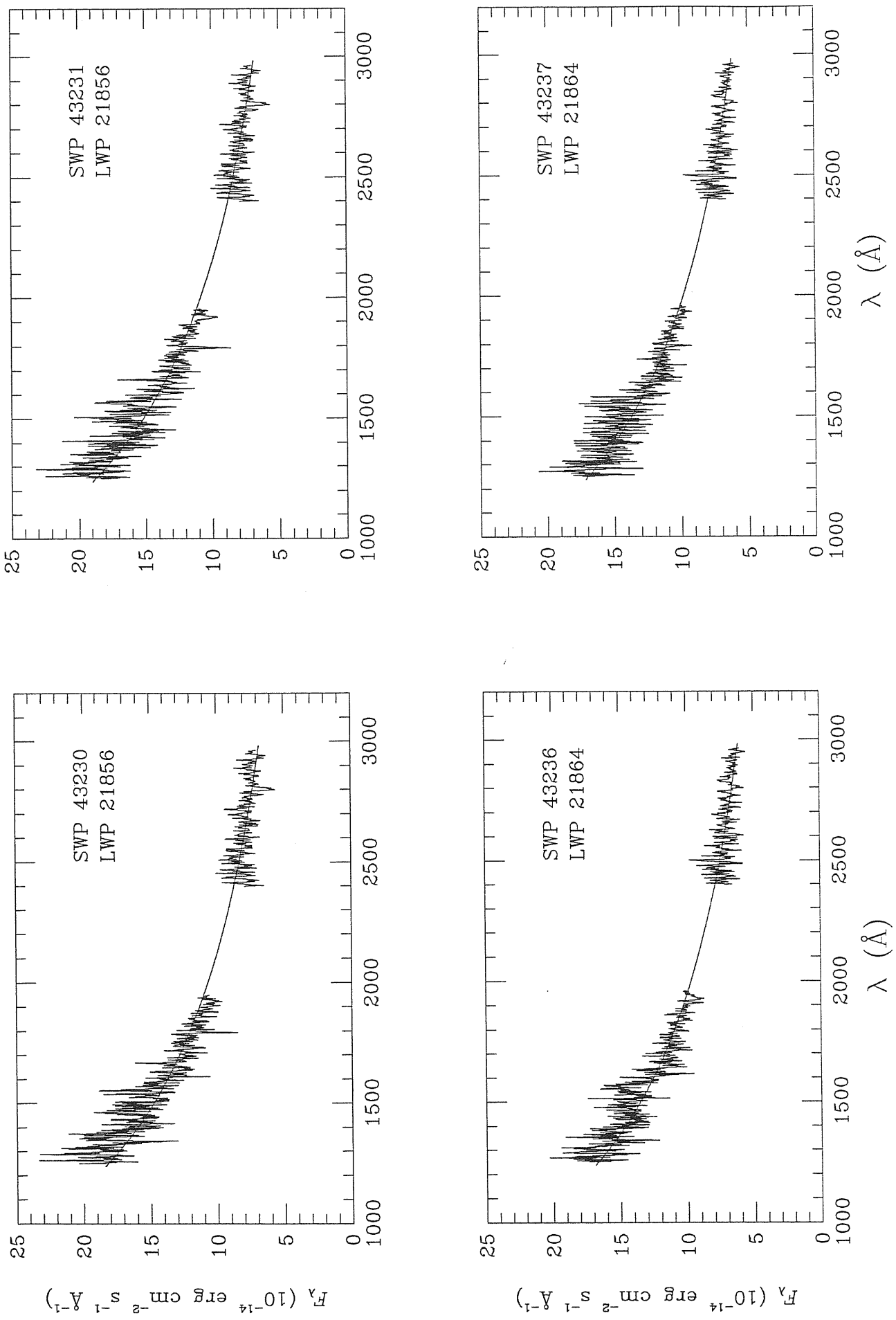

Fig. 3.1 (continued)

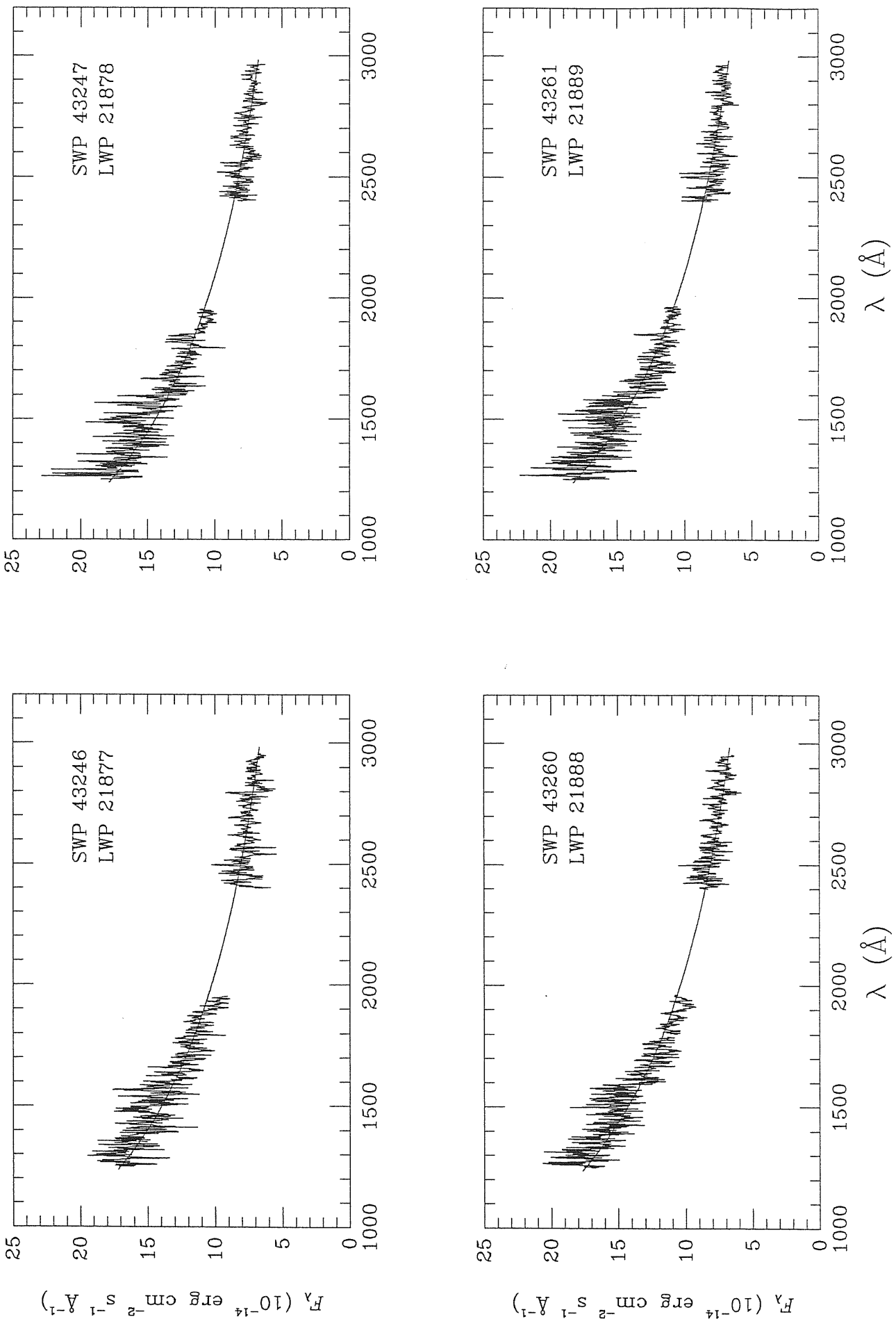

Fig. 3.2

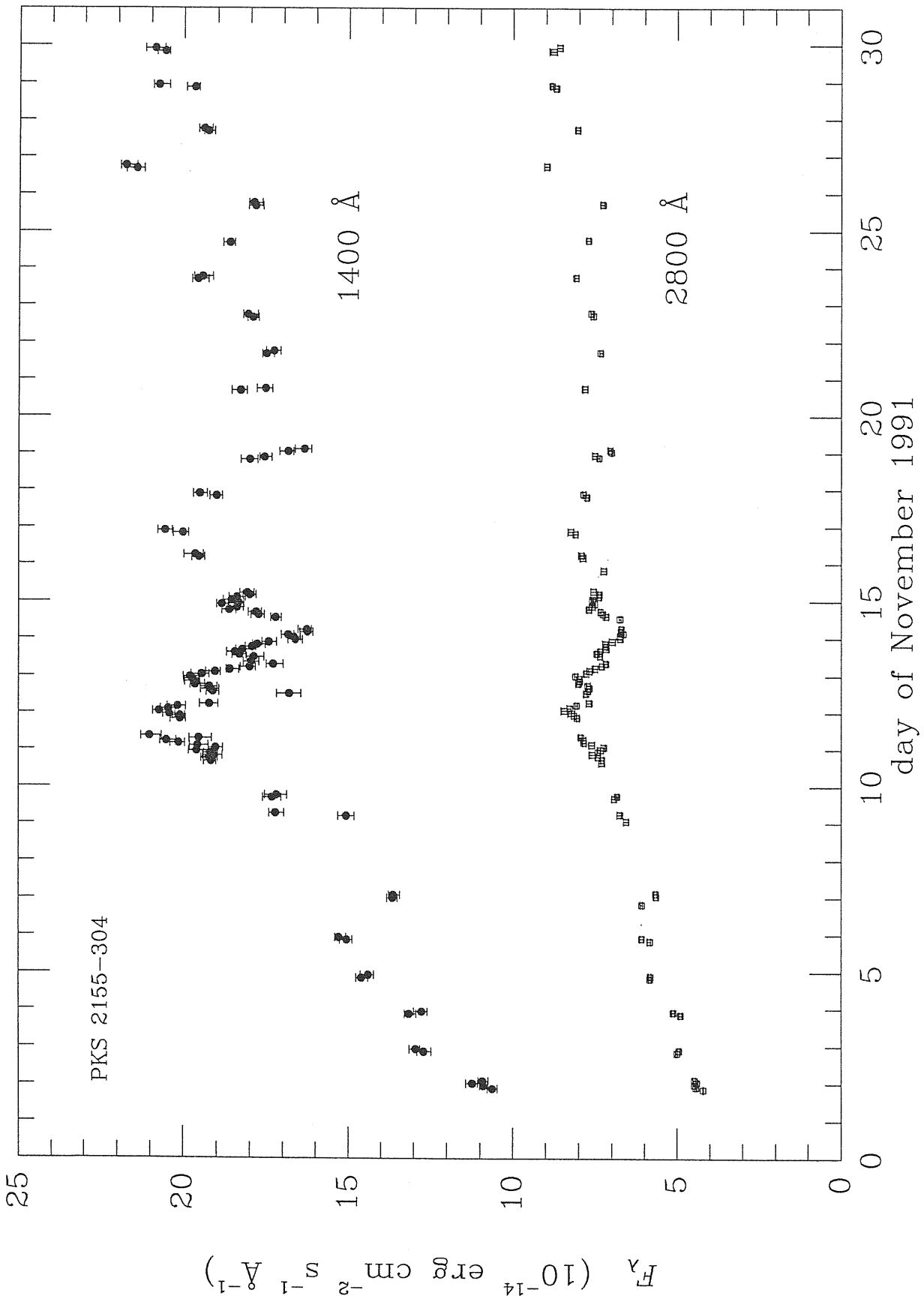
PKS 2155−304
1400 Å
2800 Å
day of November 1991
F_λ (10^{-14} erg cm^{-2} s^{-1} Å^{-1})

Fig. 3.3

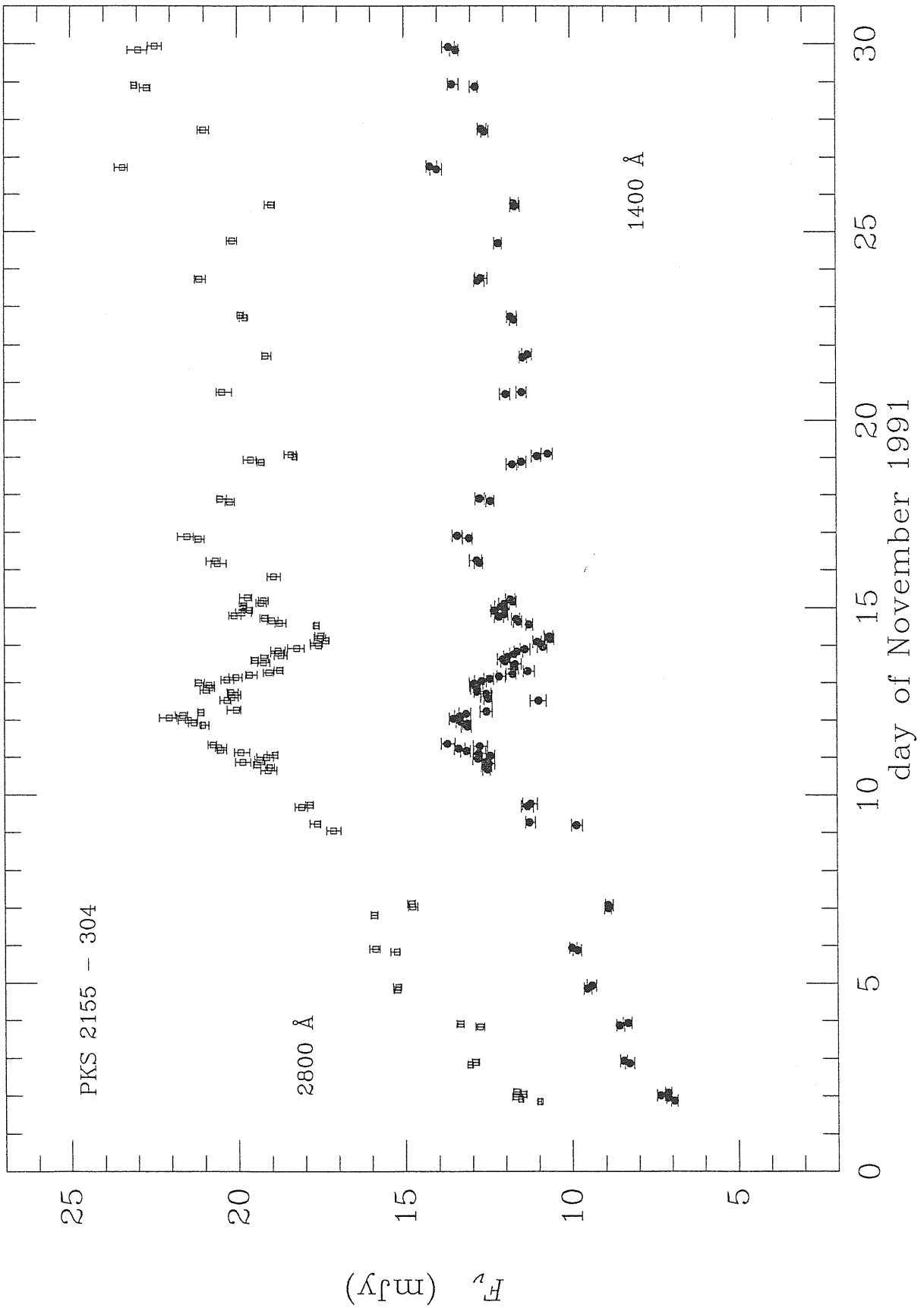
PKS 2155 − 304
2800 Å
1400 Å
F_ν (mJy)
day of November 1991
0
5
10
15
20
25
30

Fig. 3.4

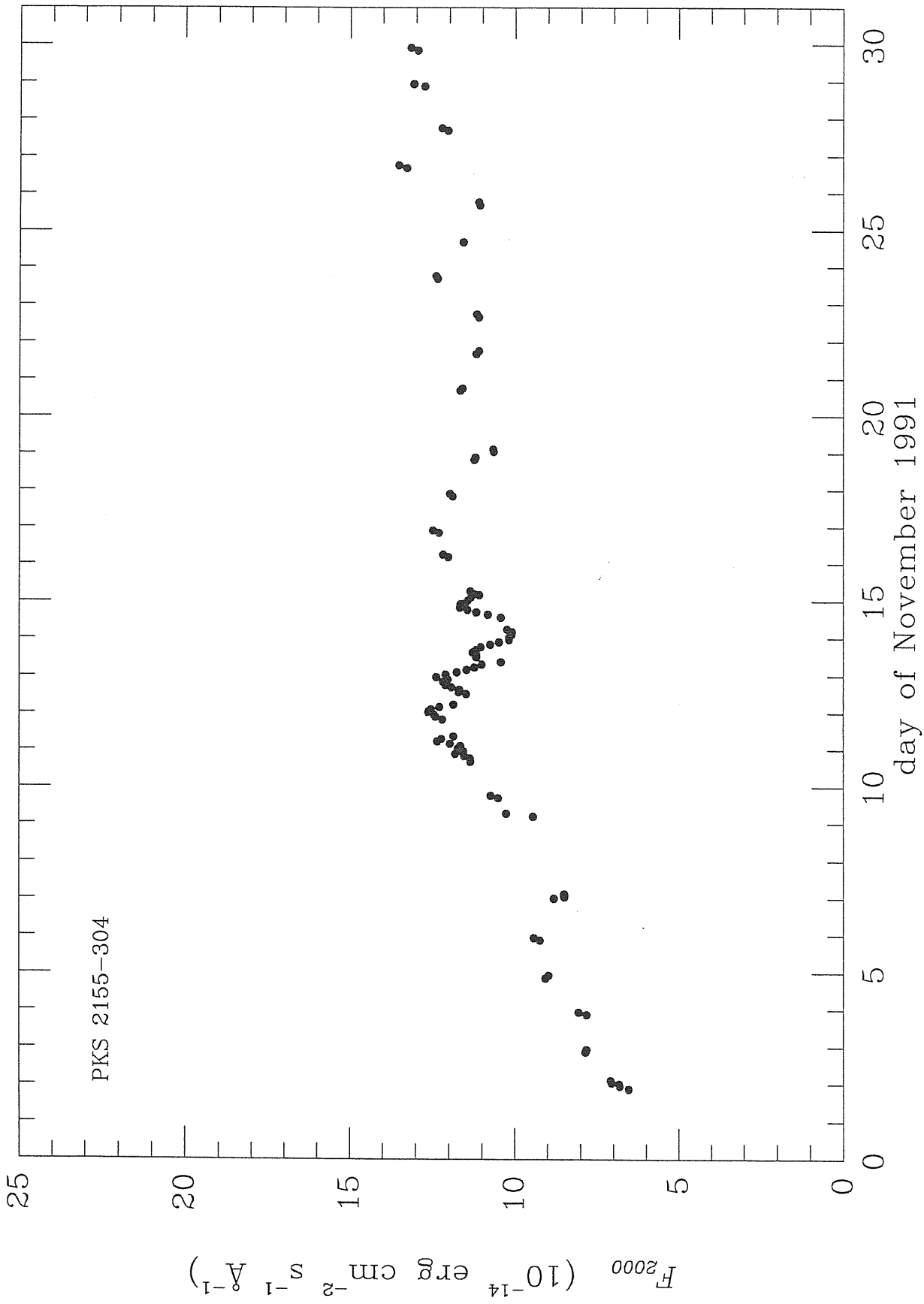
PKS 2155-304
F_{2000} (10^{-14} erg cm^{-2} s^{-1} Å^{-1})
day of November 1991
0
5
10
15
20
25
30

Fig. 3.5

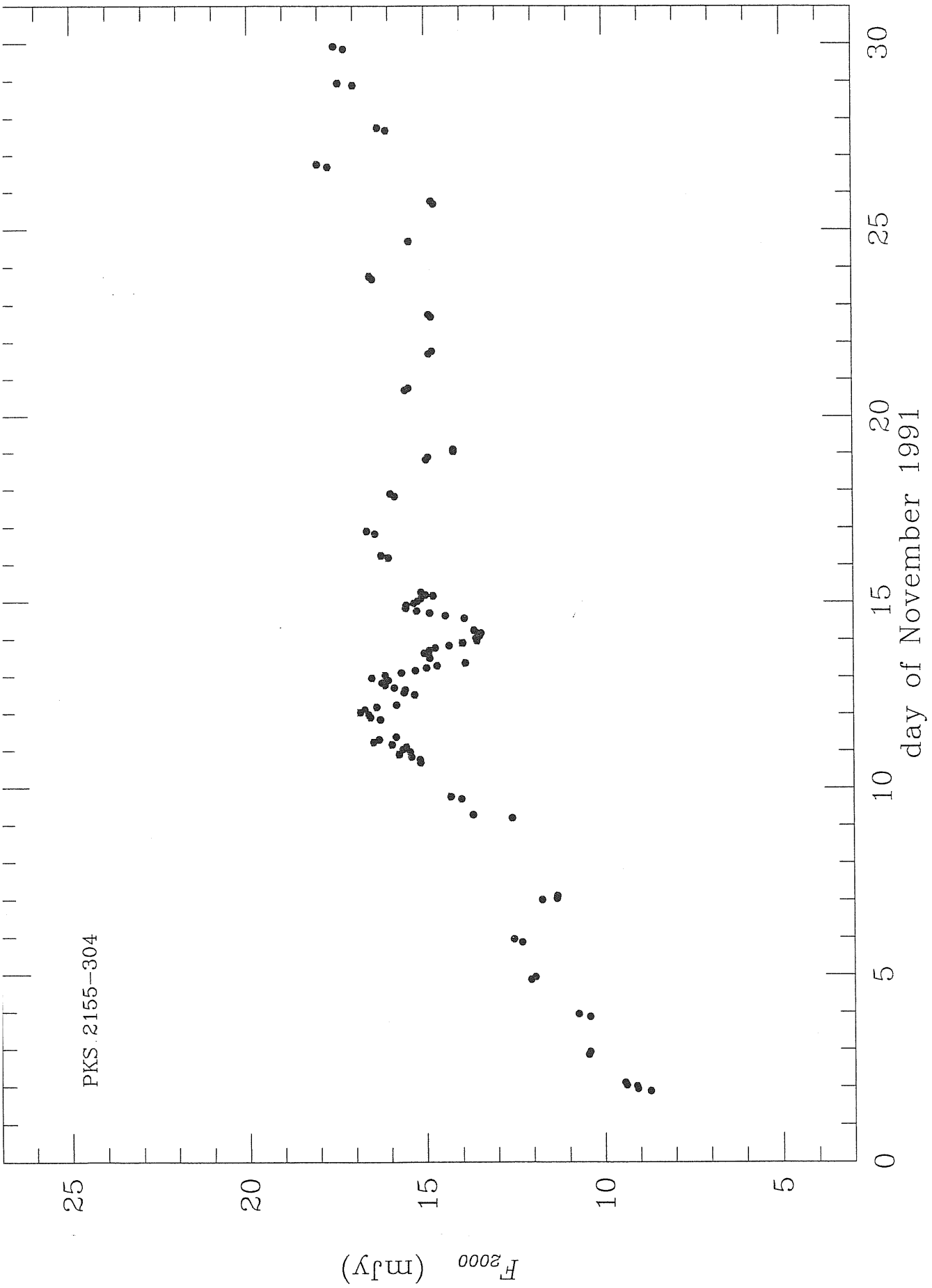
PKS 2155−304
F_{2000} (mJy)
25
20
15
10
5
0
5
10
15
20
25
30
day of November 1991

Fig. 3.6

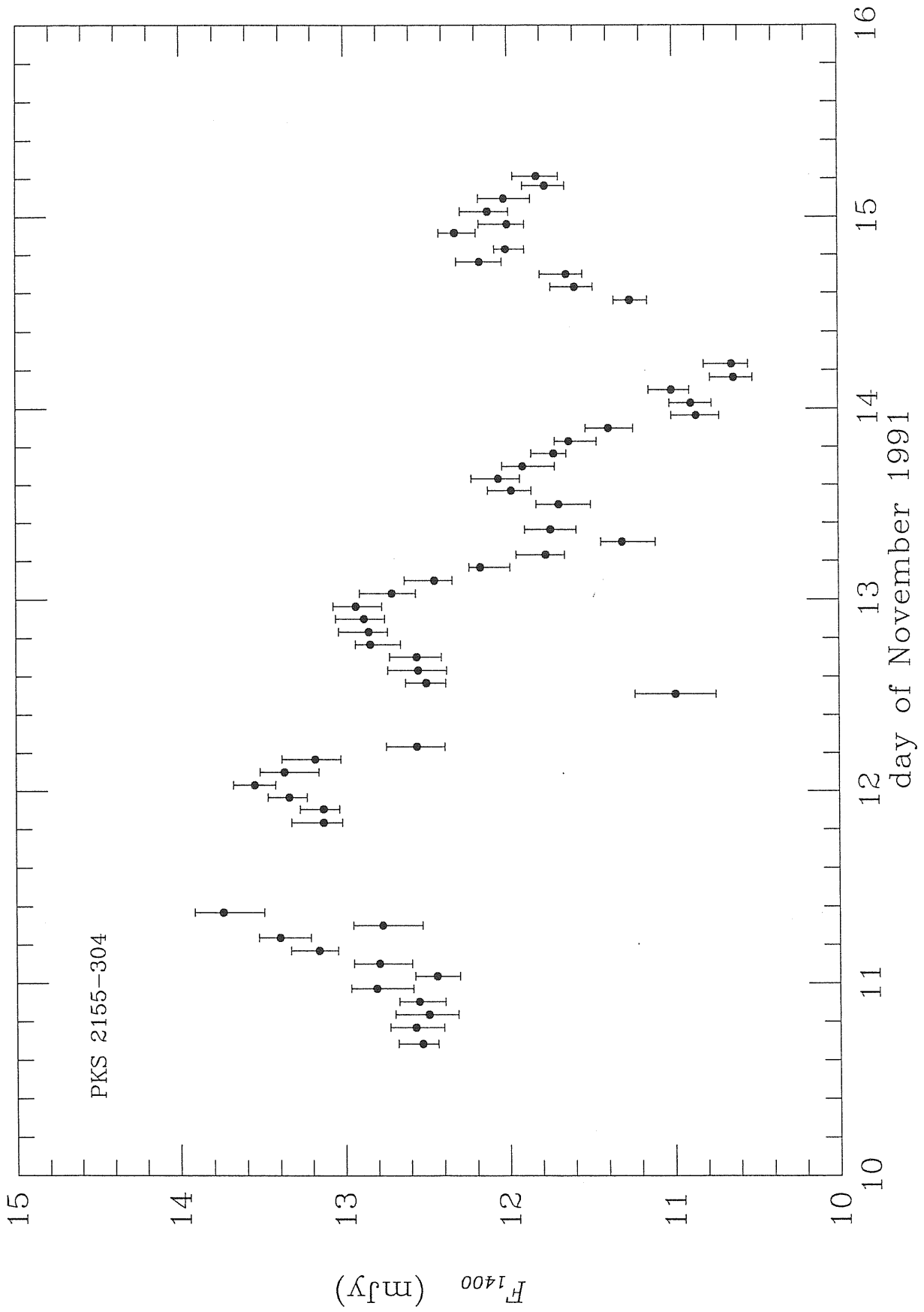

Fig. 3.7

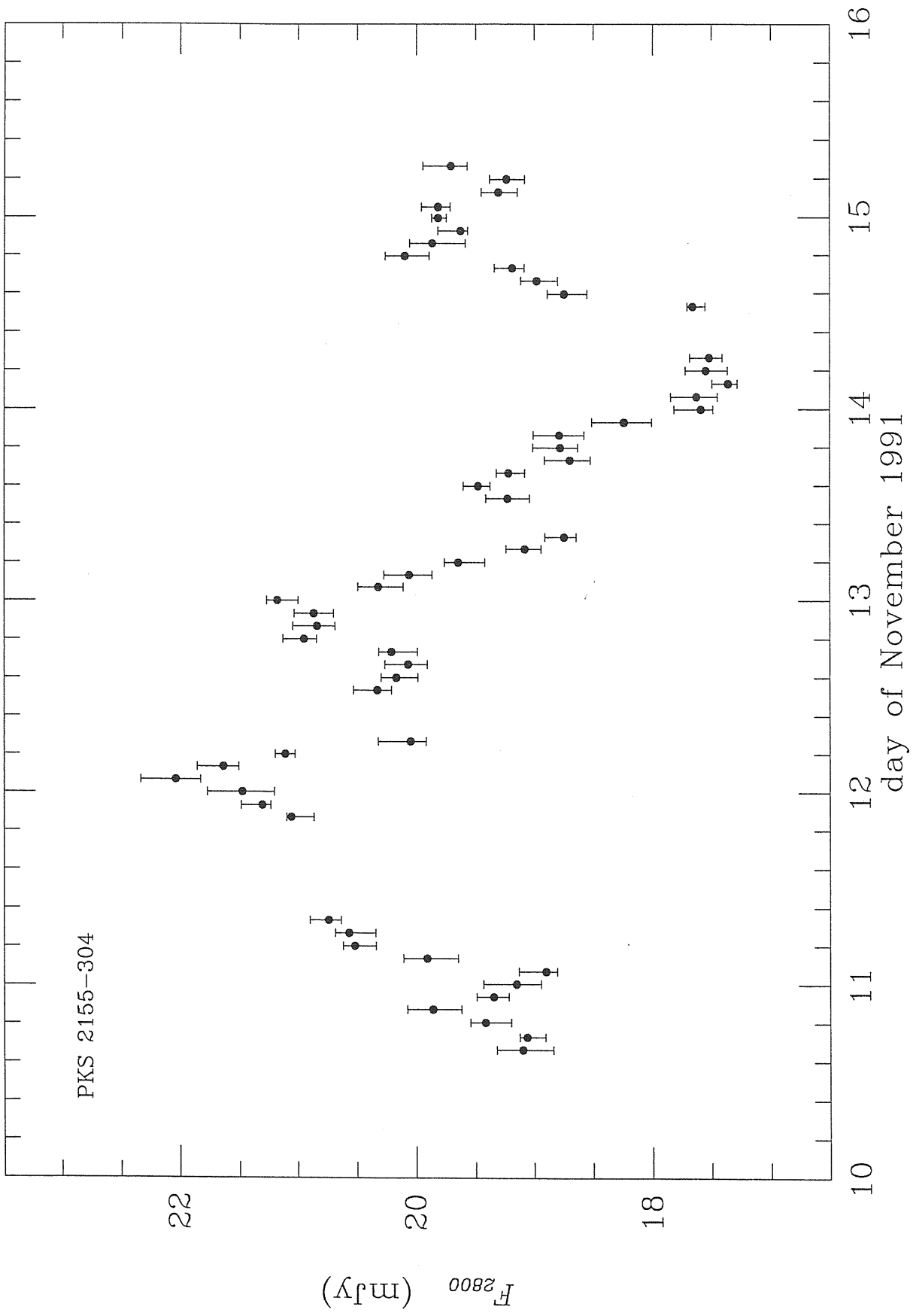
PKS 2155−304
F_{2800} (mJy)
22
20
18
10
11
12
13
14
15
16
day of November 1991

Fig. 3.8

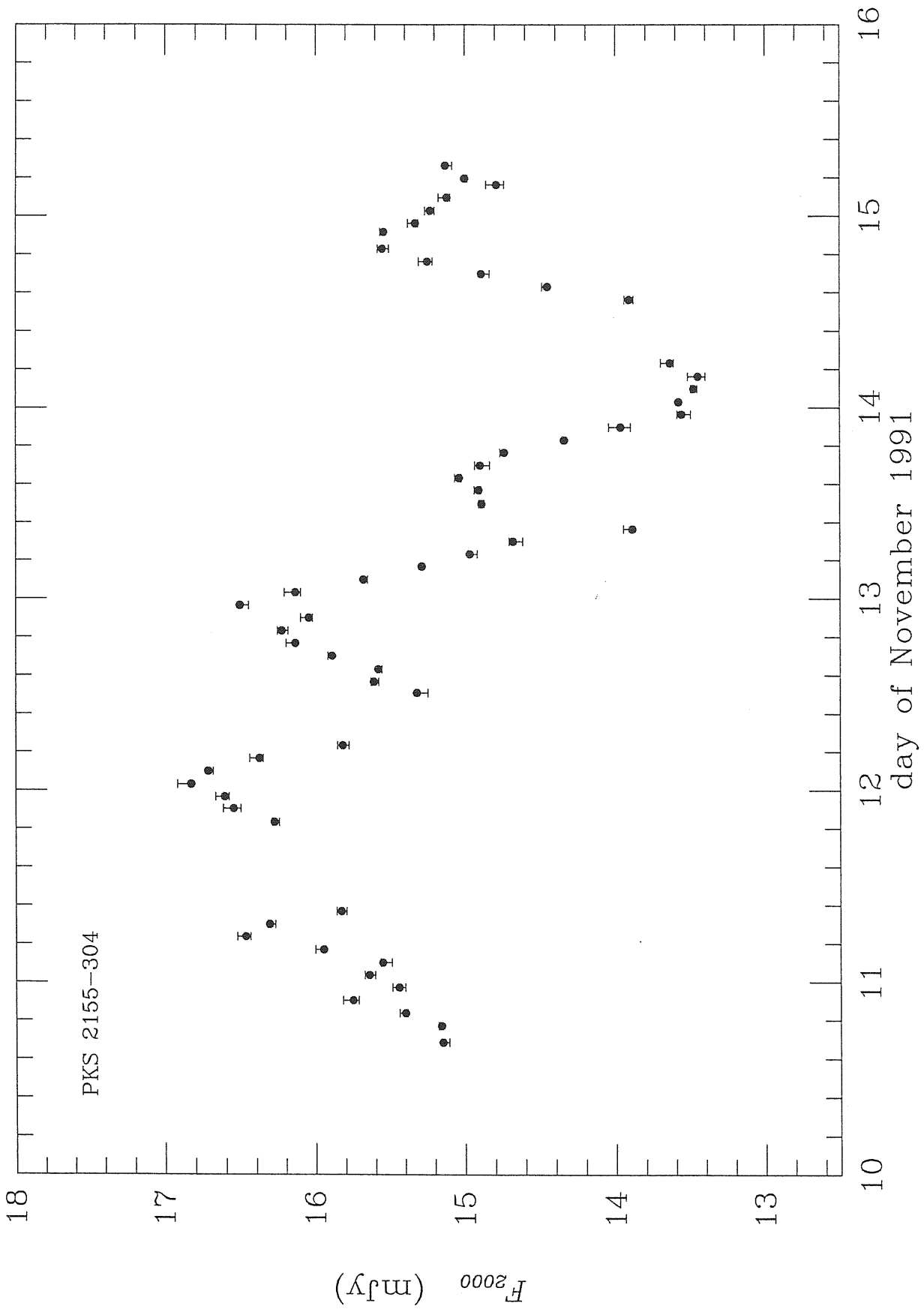
PKS 2155−304
F_{2000} (mJy)
day of November 1991
10
11
12
13
14
15
16
13
14
15
16
17
18

Fig. 3.9

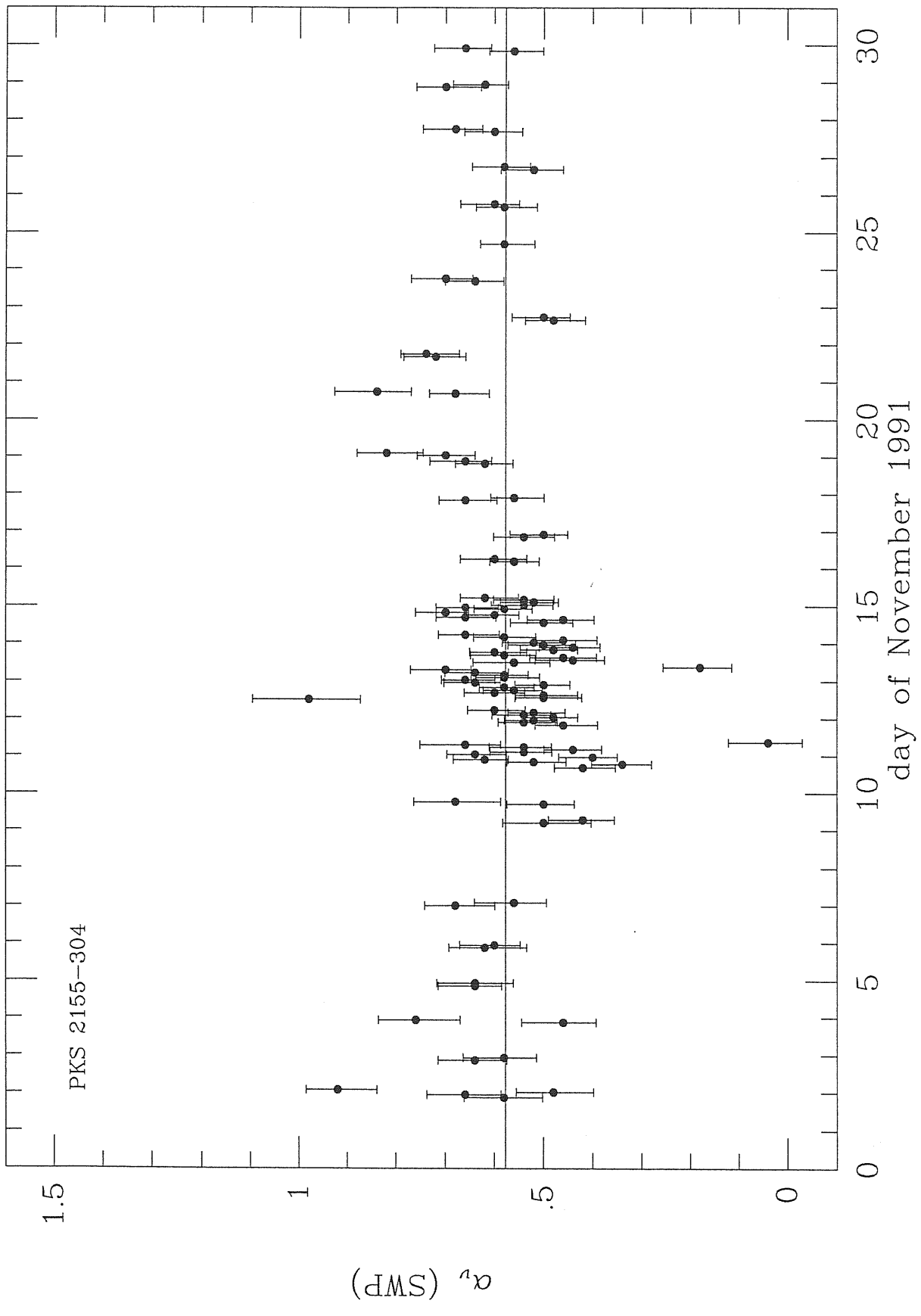
PKS 2155−304
α_ν (SWP)
1.5
1
.5
0
0
5
10
15
20
25
30
day of November 1991

Fig. 3.10

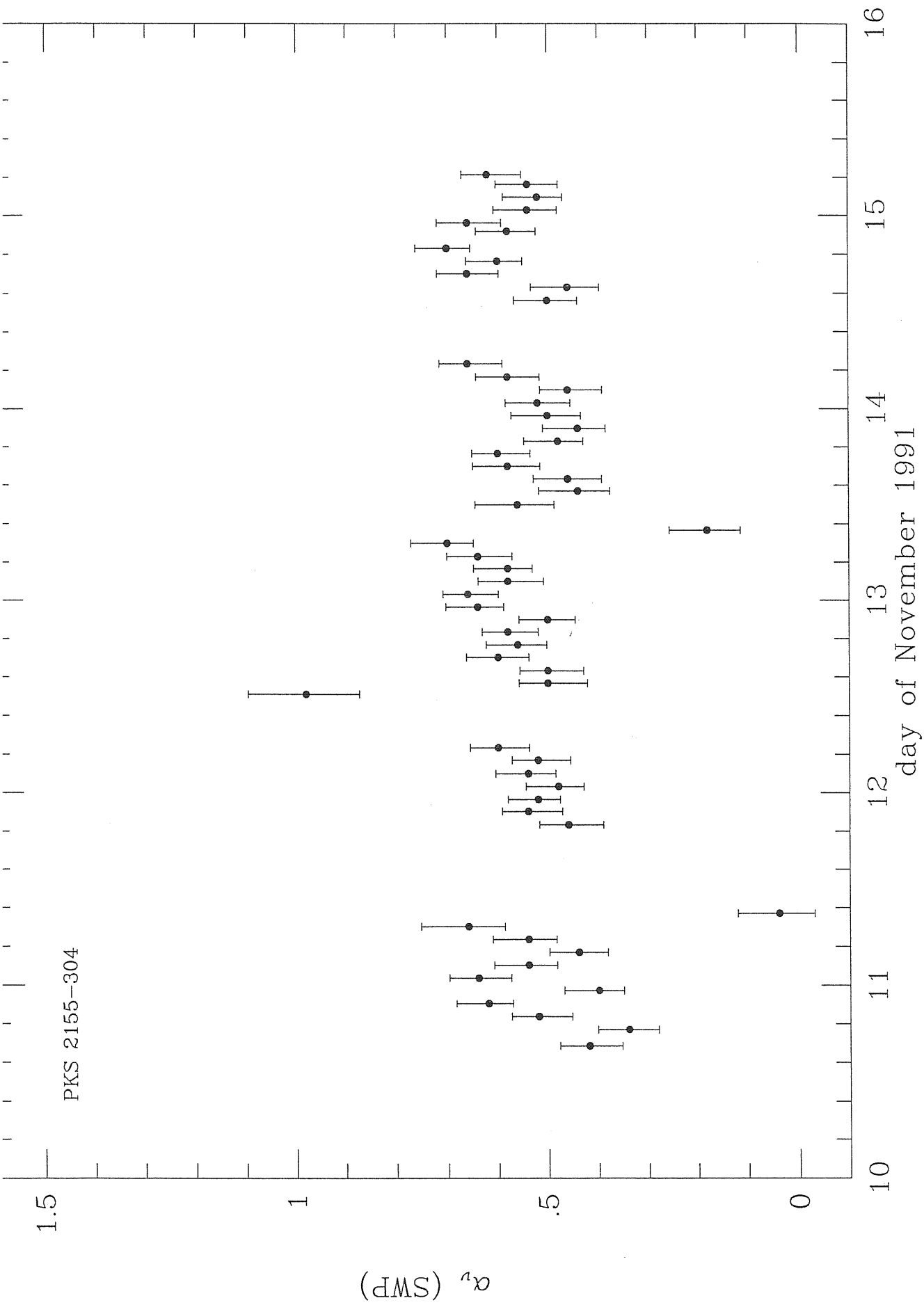
PKS 2155−304
α_ν (SWP)
1.5
1
.5
0
10
11
12
13
14
15
16
day of November 1991

Fig. 3.11

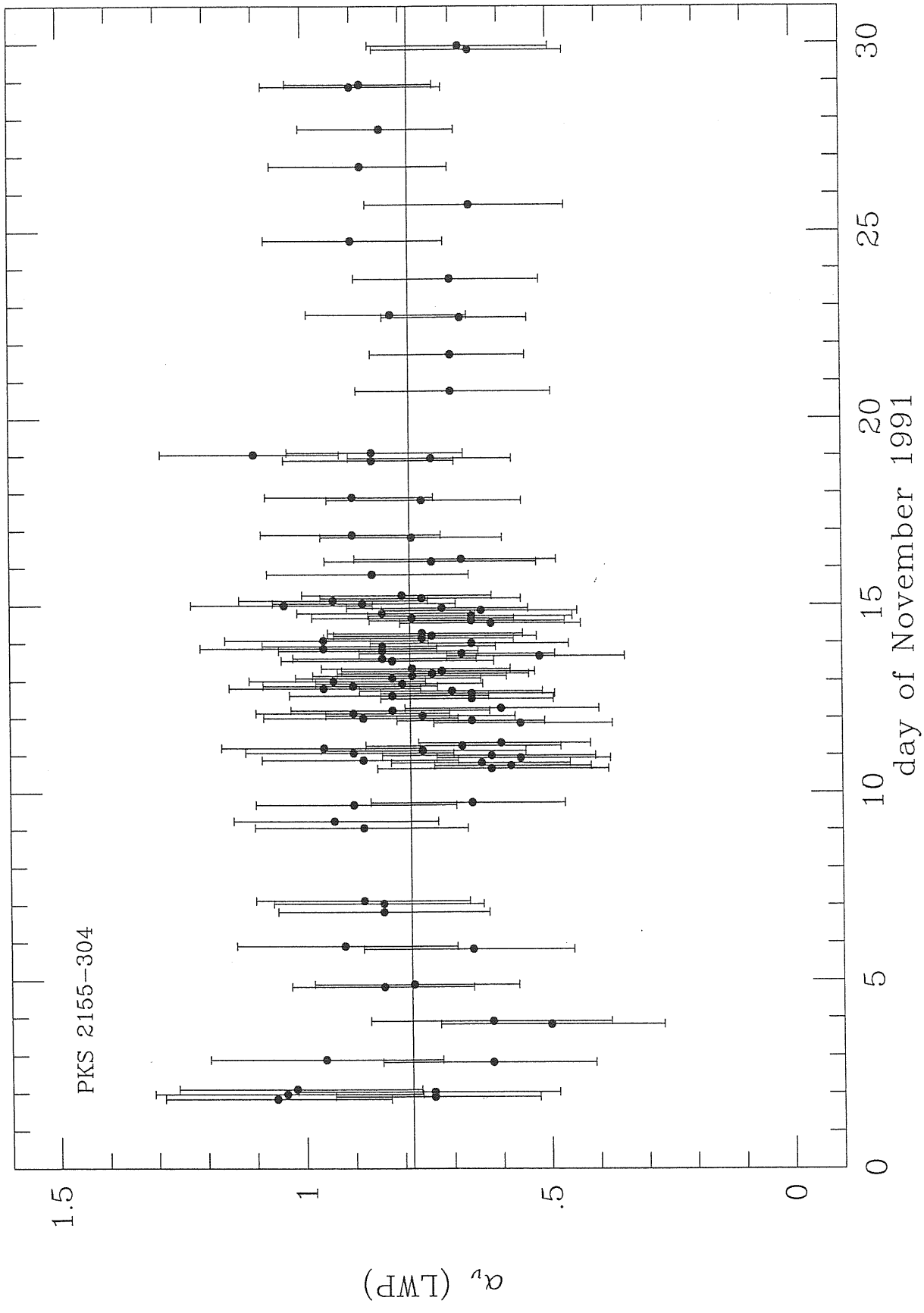
PKS 2155−304
1.5
1
.5
0
α_ν (LWP)
0
5
10
15
20
25
30
day of November 1991

Fig. 3.12

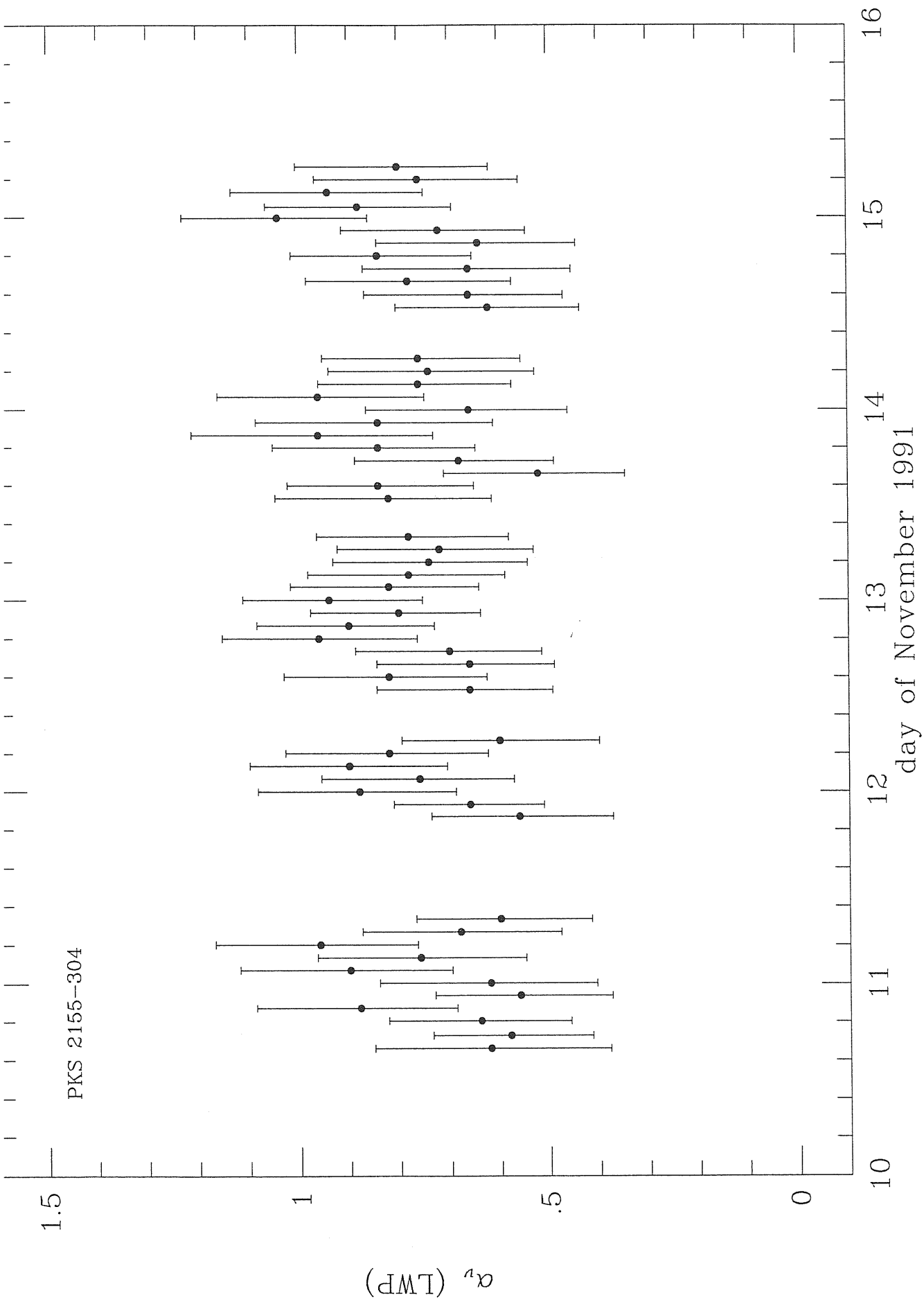
PKS 2155−304
α_ν (LWP)
1.5
1
.5
0
10
11
12
13
14
15
16
day of November 1991

Fig. 3.13

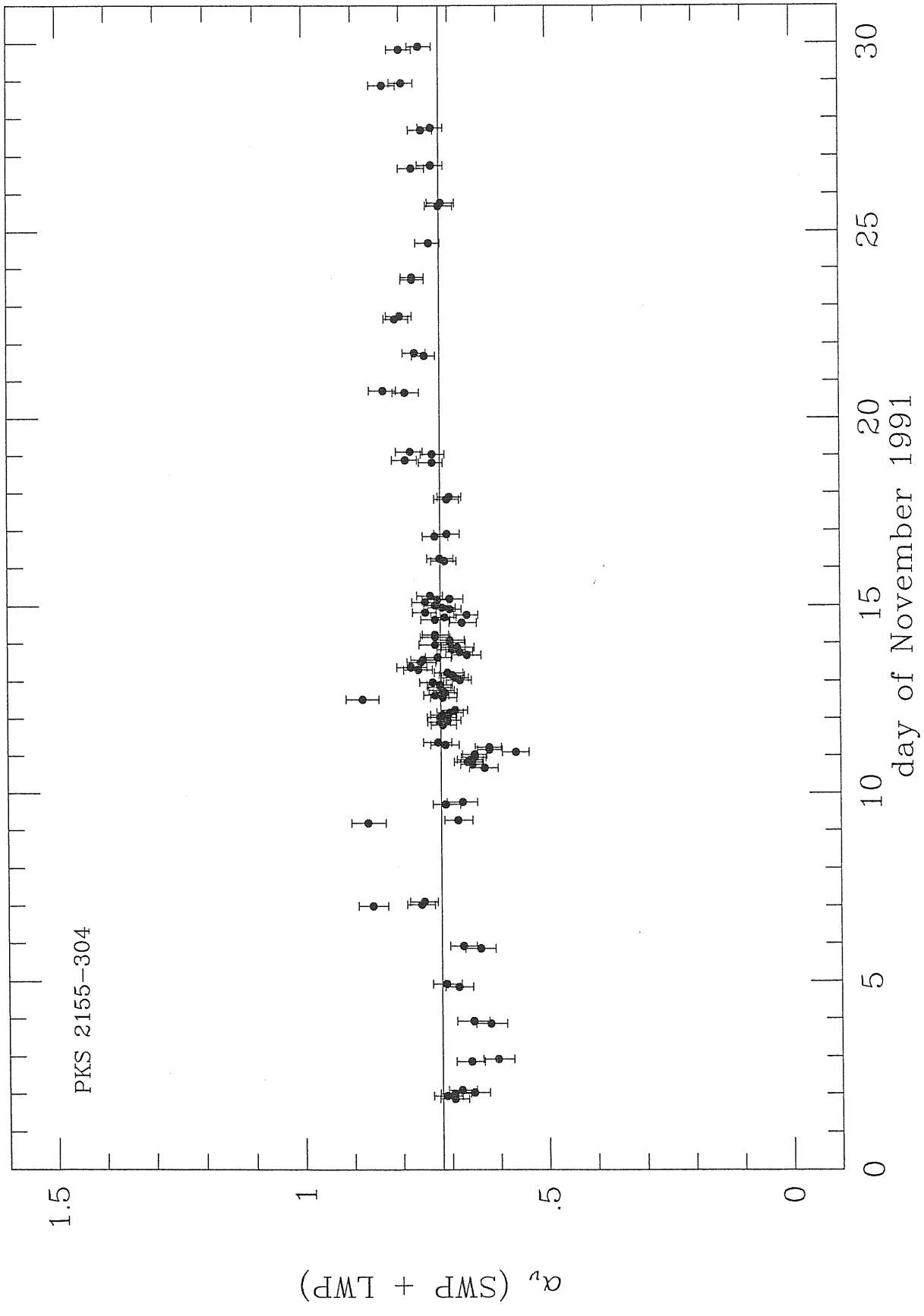
PKS 2155−304
1.5
1
.5
0
α_ν (SWP + LWP)
0
5
10
15
20
25
30
day of November 1991

Fig. 3.14

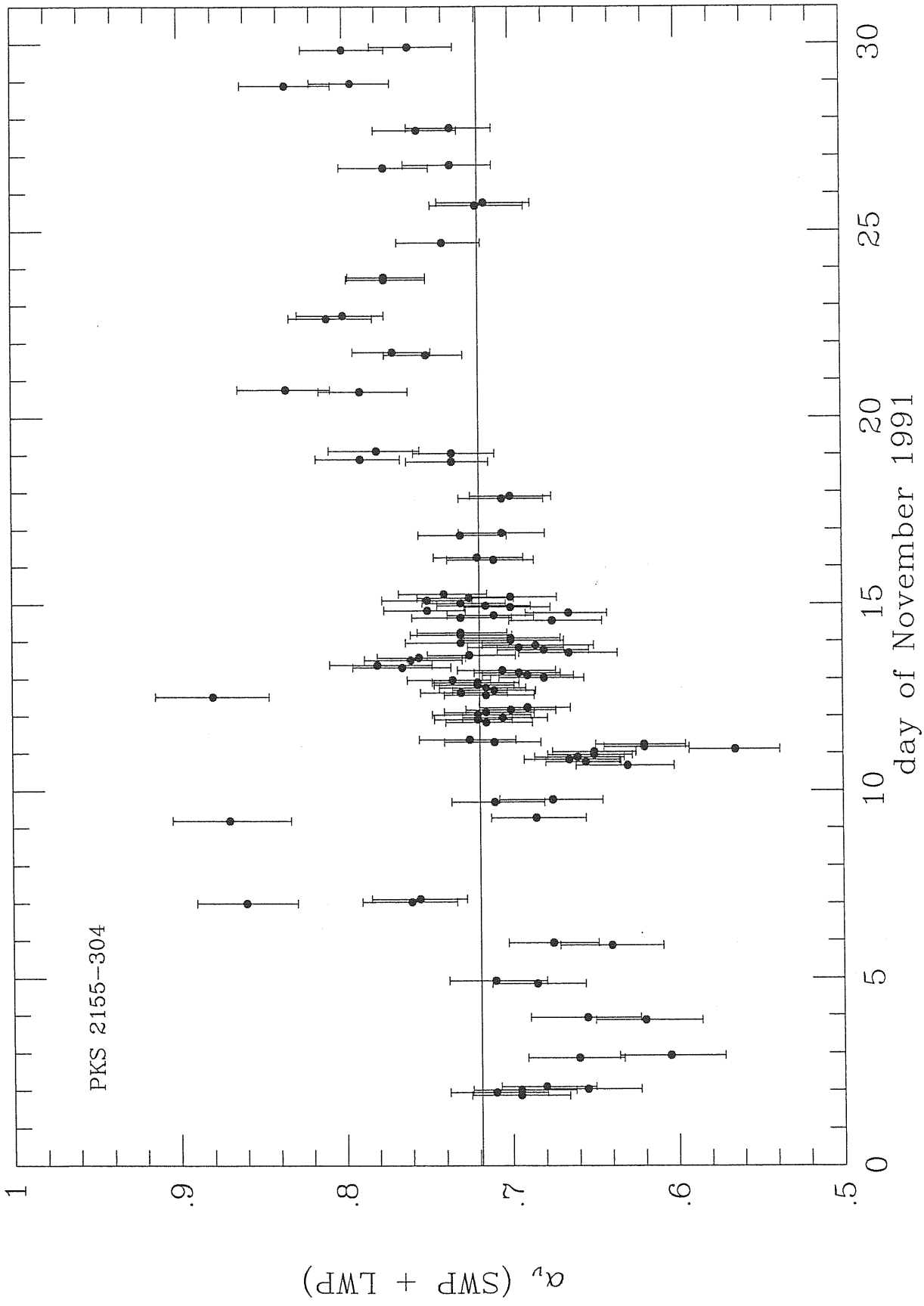

Fig. 3.15

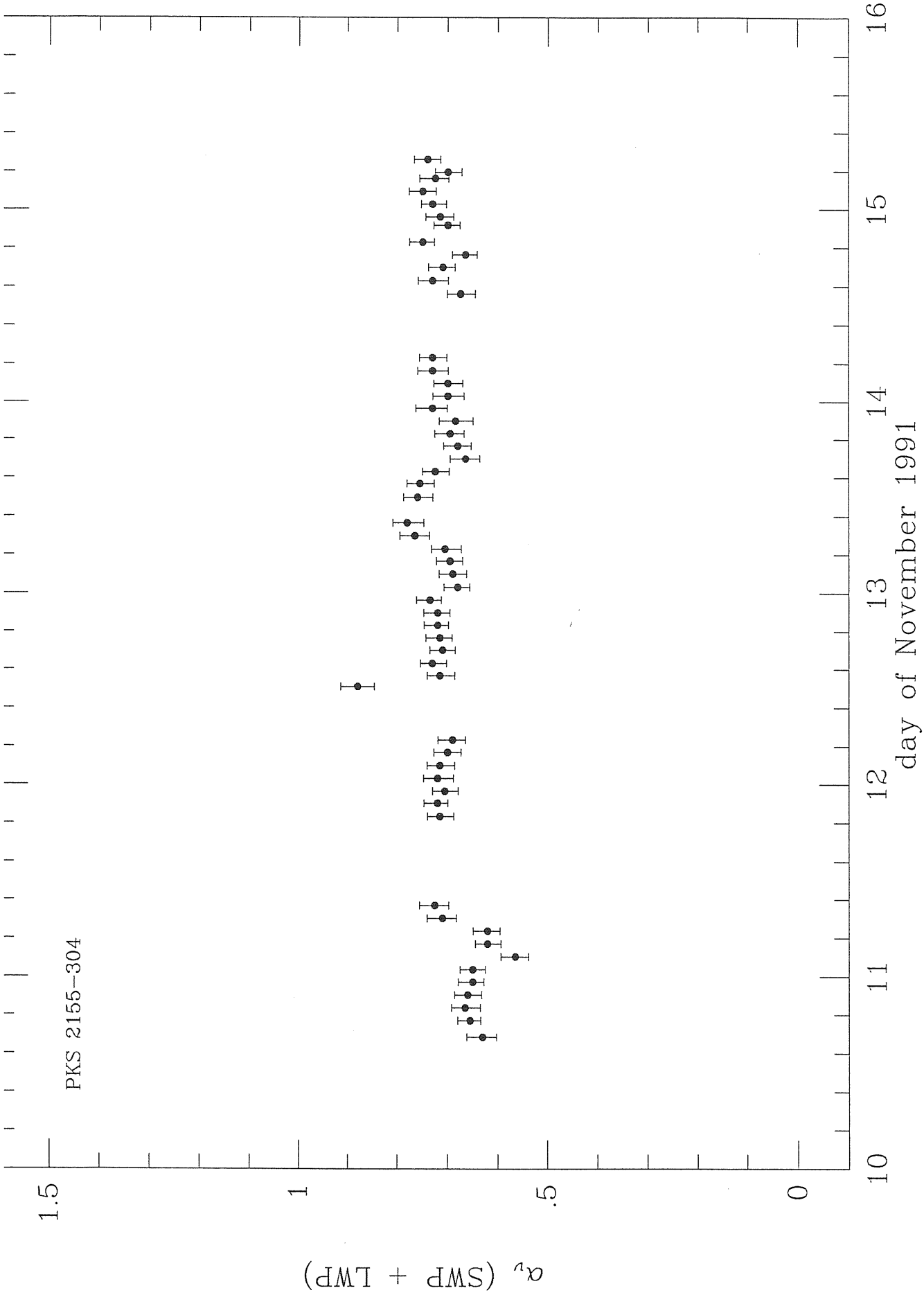
PKS 2155−304
α_v (SWP + LWP)
1.5
1
.5
0
10
11
12
13
14
15
16
day of November 1991

Fig. 3.16

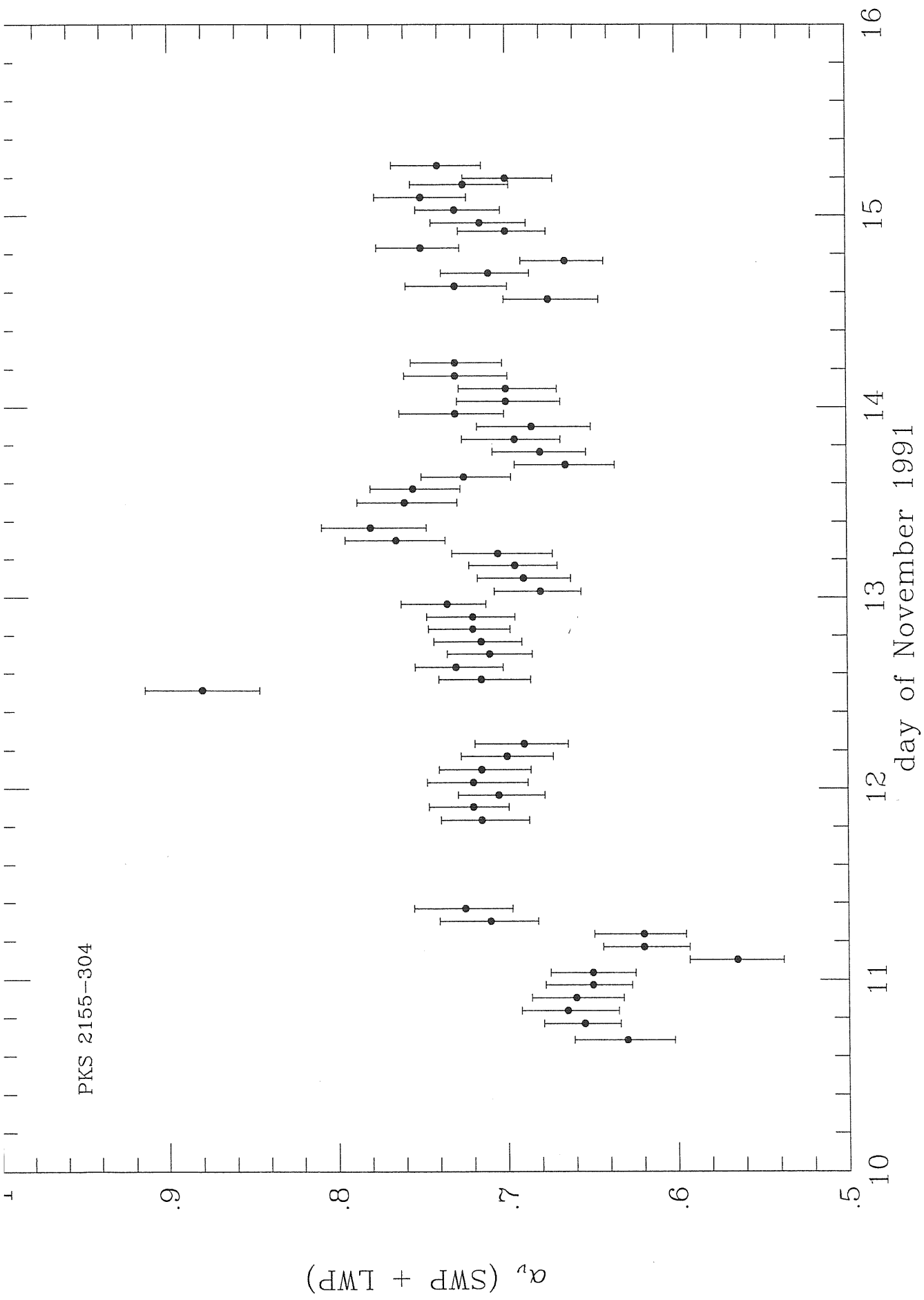
PKS 2155−304
α_v (SWP + LWP)
.5
.6
.7
.8
.9
1
10
11
12
13
14
15
16
day of November 1991

Fig. 3.17

PKS 2155−304

F_{2800} vs F_{1400}

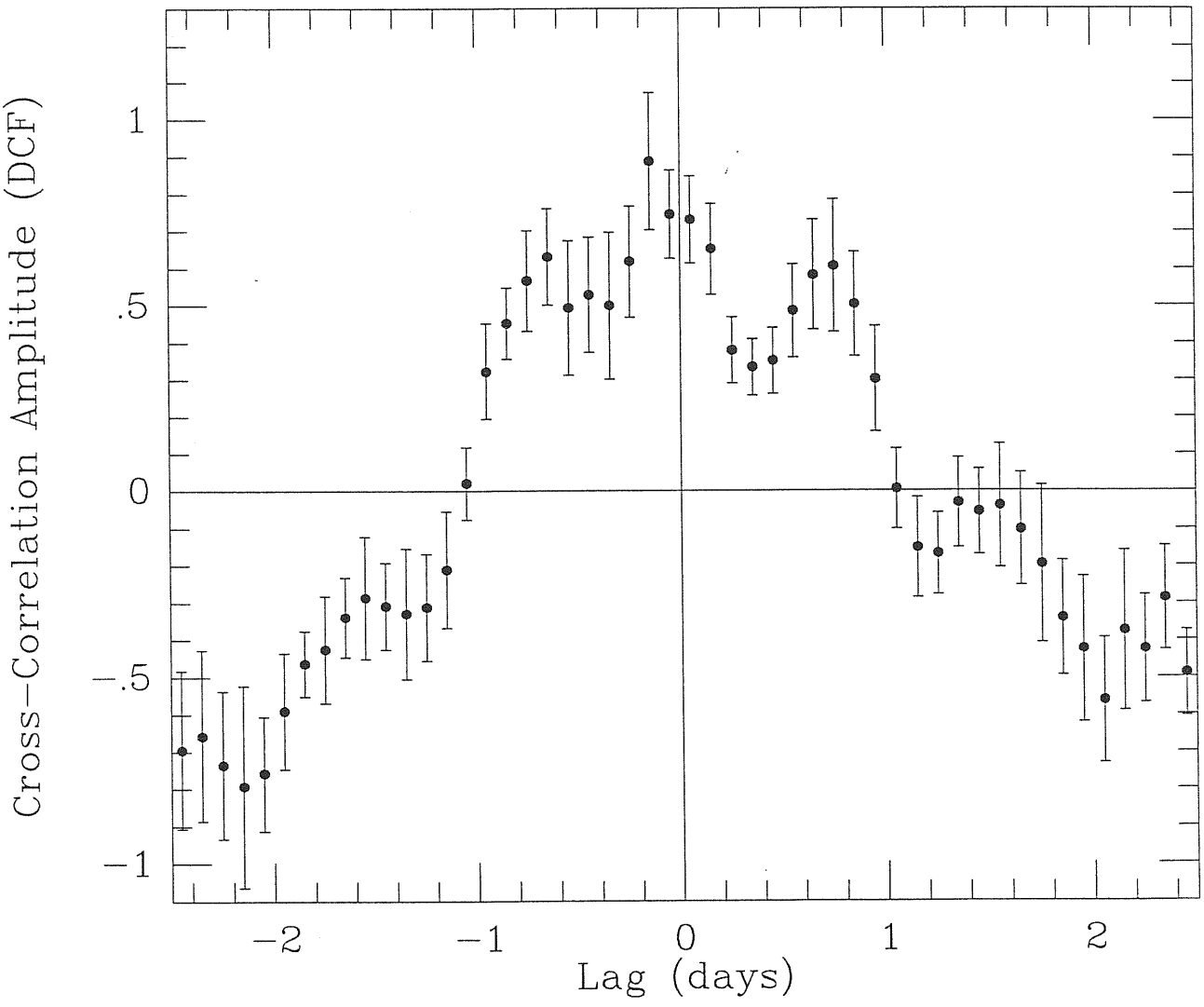

Fig. 3.18

PKS 2155−304

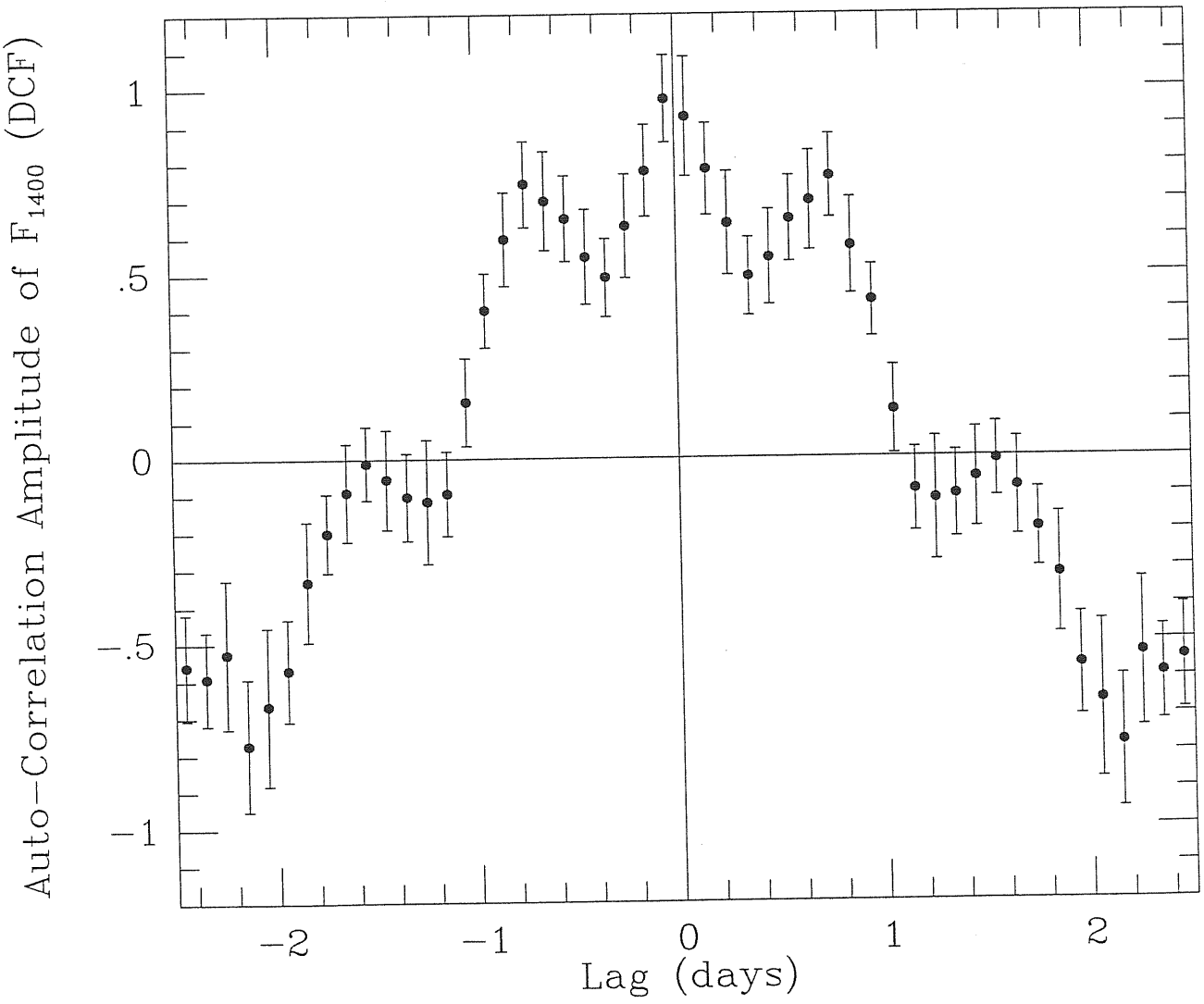

Fig. 3.19

PKS 2155−304

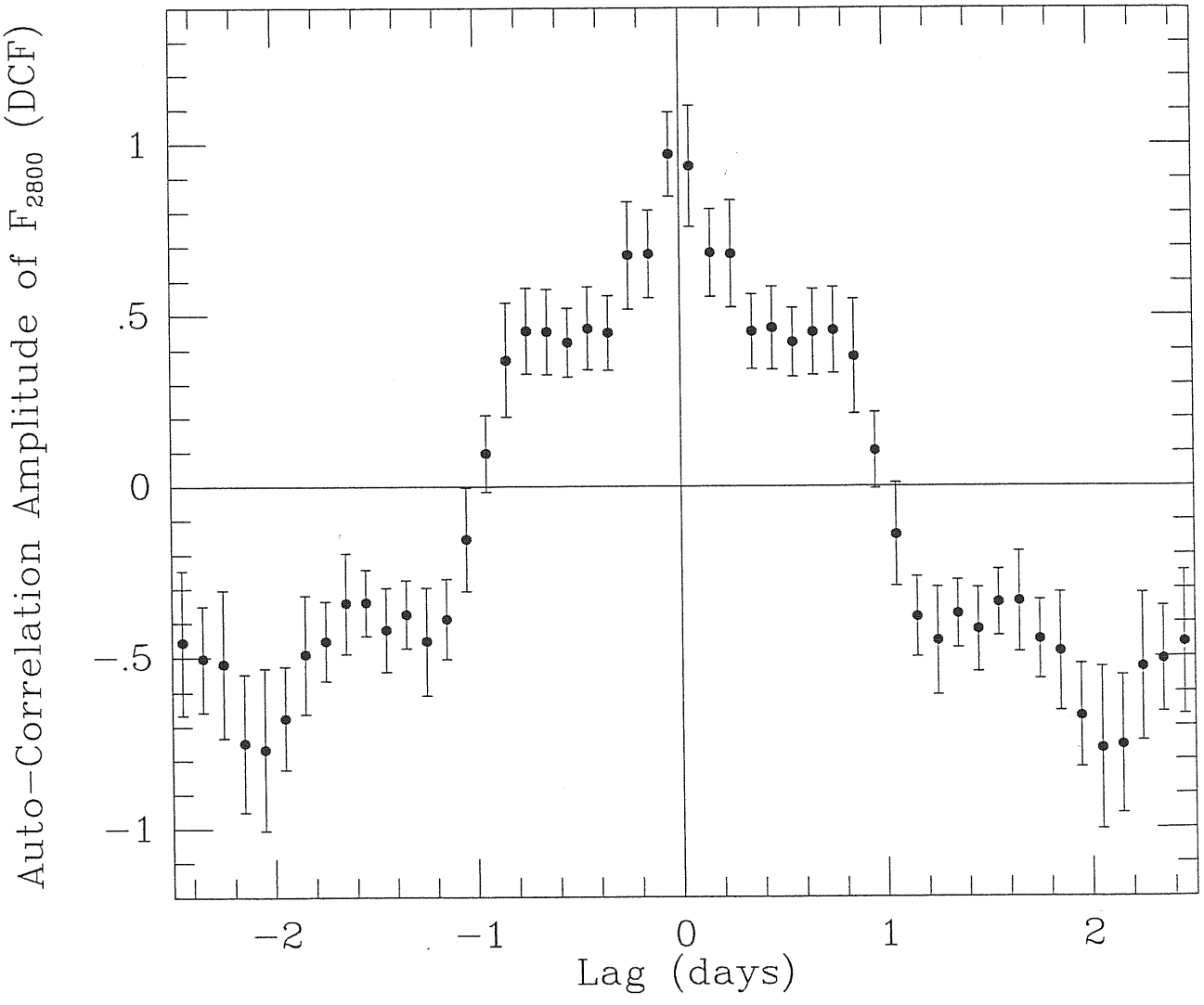

Fig. 3.20

PKS 2155−304

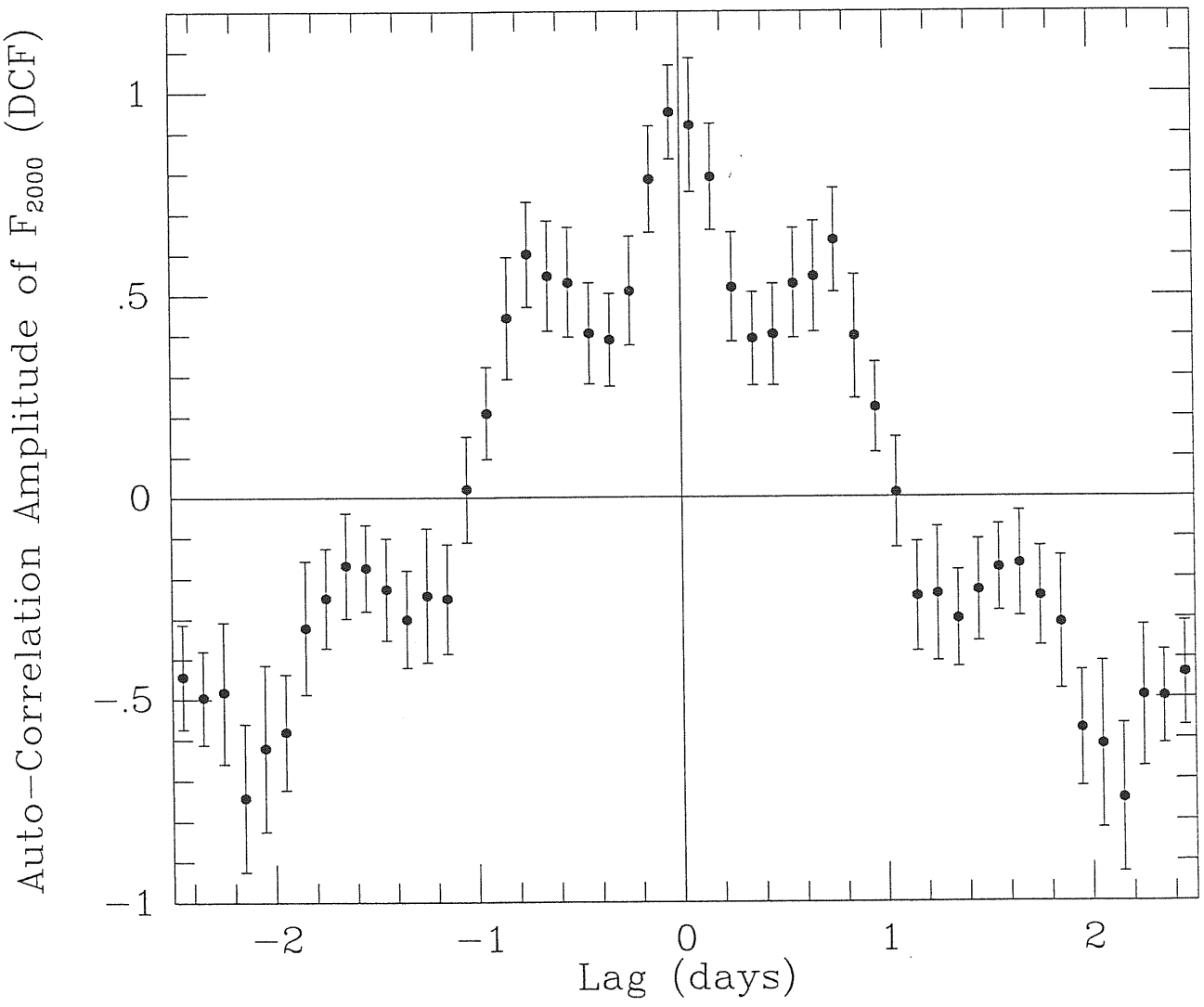

Fig. 3.21

PKS 2155−304

F_{1400} vs α_ν (SWP)

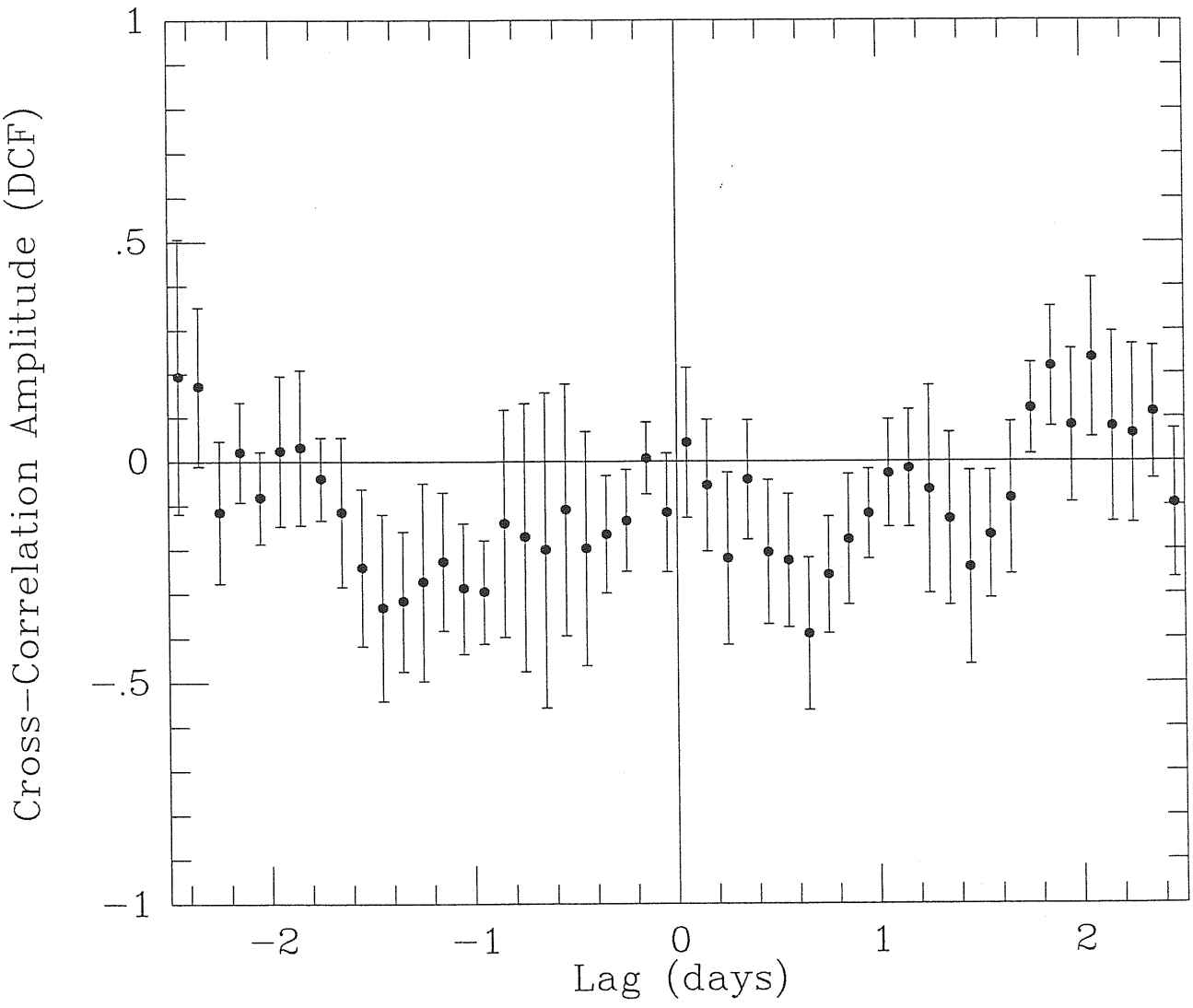

Fig. 3.22

PKS 2155−304

F_{2800} vs α_ν (LWP)

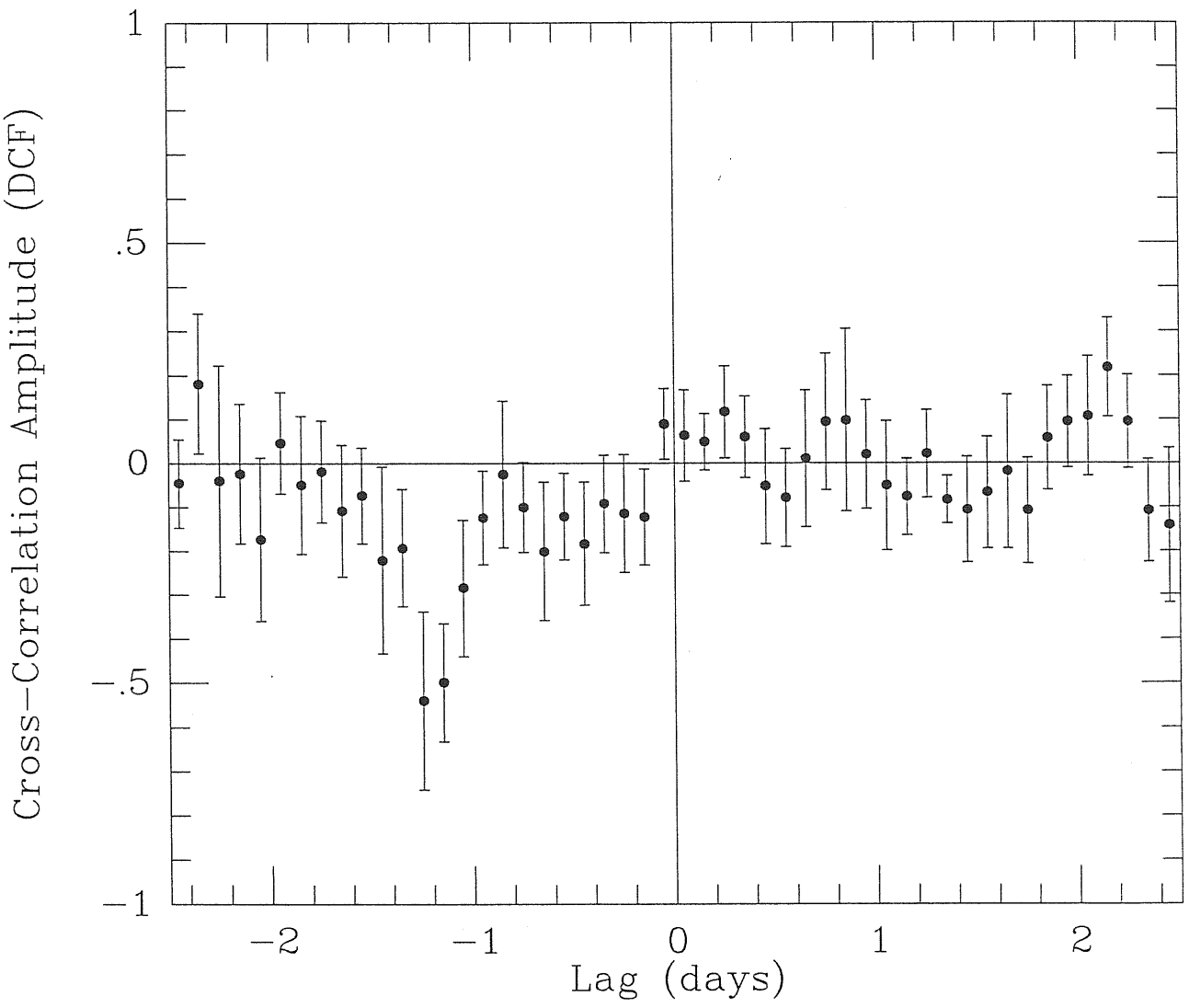

Fig. 3.23

PKS 2155−304

F_{2000} vs α_ν (SWP + LWP)

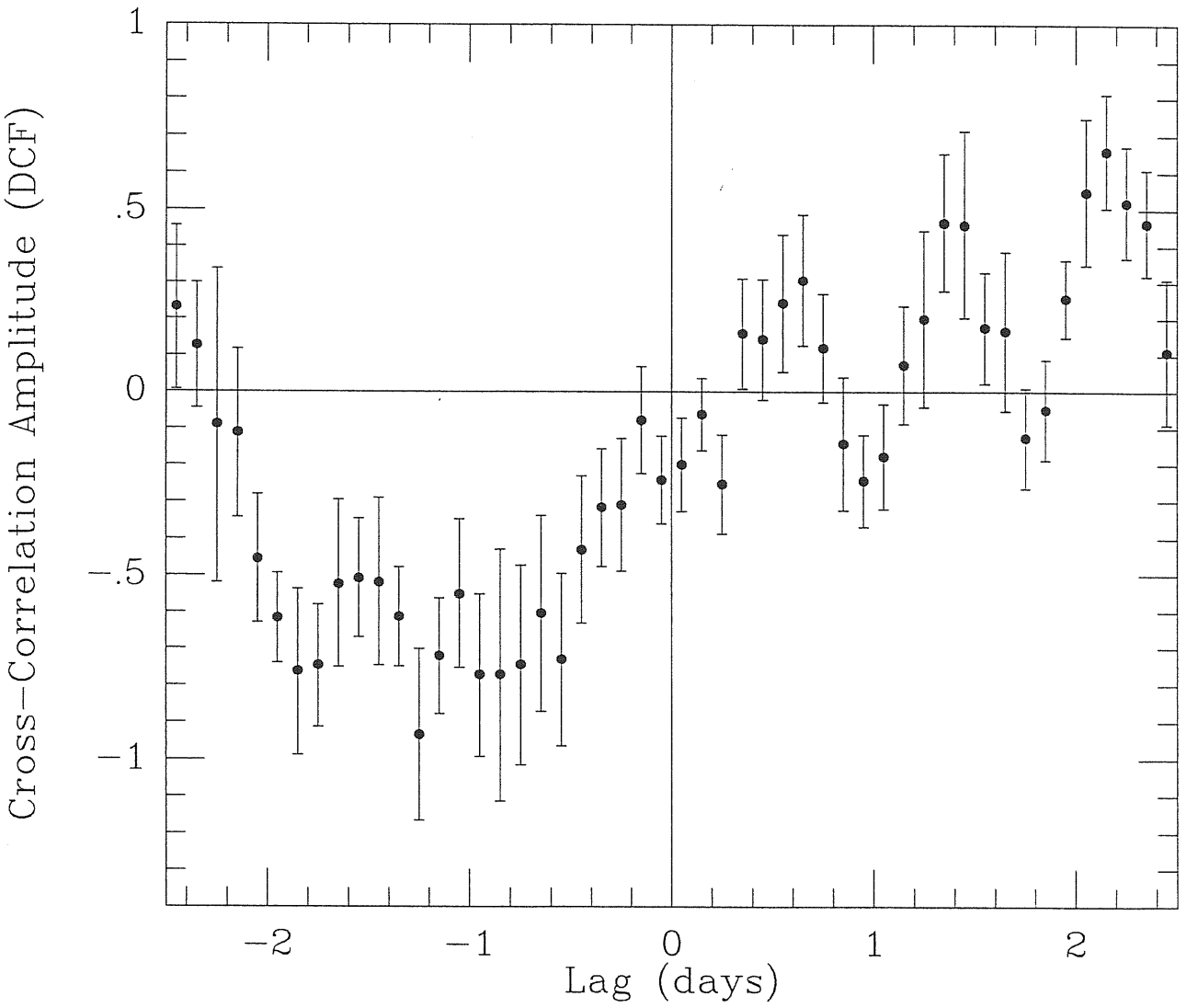

Fig. 3.24

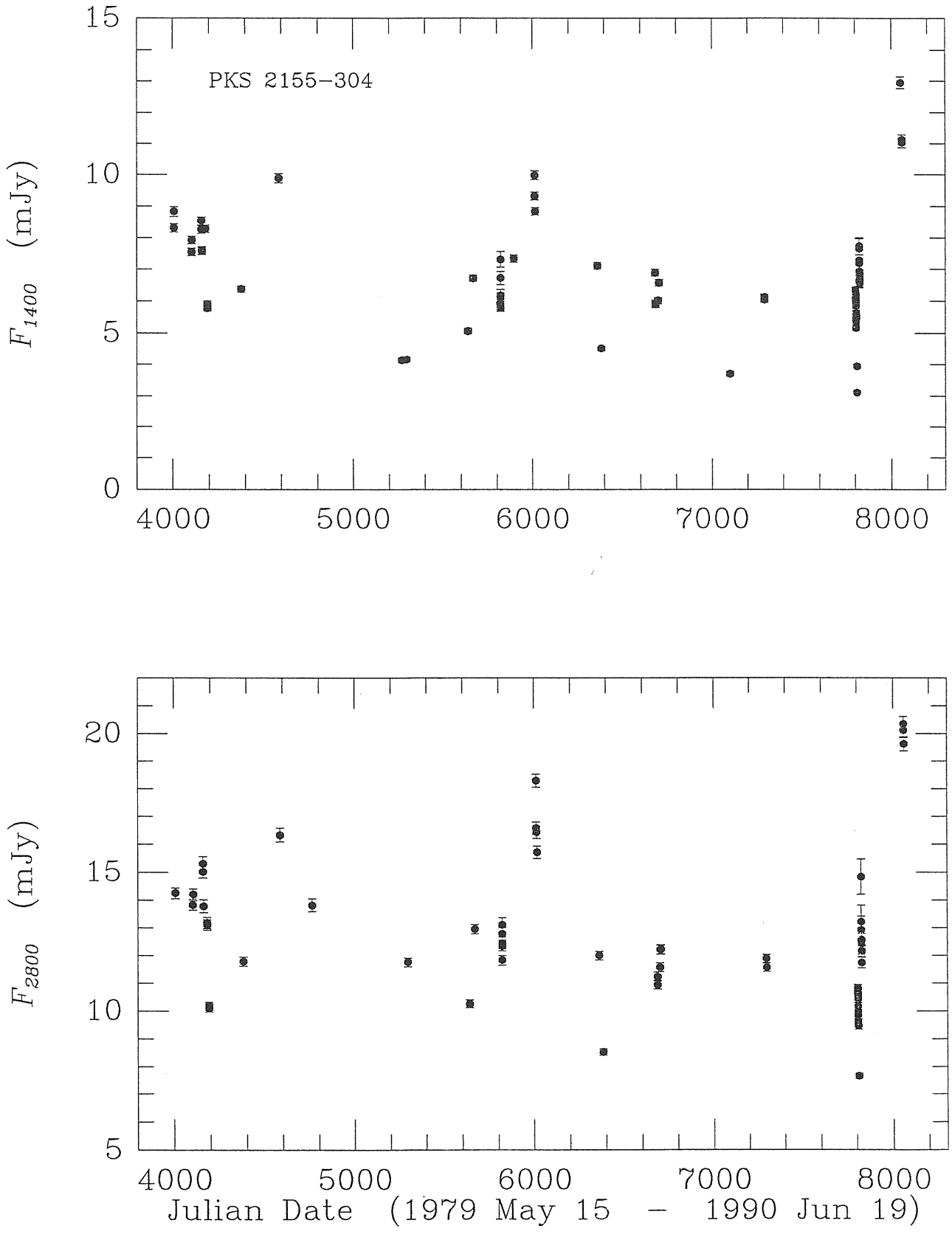
PKS 2155−304
F_{1400} (mJy)
F_{2800} (mJy)
0
5
10
15
20
4000
5000
6000
7000
8000
Julian Date (1979 May 15 − 1990 Jun 19)

Tables

Table 2.1: Journal of Observations

		PKS 0118–272	
1989 Aug	10.3	ESO 1.5 + BC + CCD	V = 16.1
	10.3	ESO 2.2 + IR phot	K = 12.5
1989 Aug	9.6	IUE + LWP	$F_\lambda^\dagger(2500Å) = 0.23 \pm 0.02$
		PKS 0301–243	
1989 Aug	7.4	ESO 1.5 + BC + CCD	V = 16.2
	11	ESO 2.2 + IR phot	K = 12.9
1989 Aug	8.6	IUE + SWP	$F_\lambda(1500Å) = 0.32 \pm 0.05$
1989 Aug	7.7	IUE + LWP	$F_\lambda(2500Å) = 0.29 \pm 0.02$
		PKS 1538+149	
1988 Aug	4.3	ESO 1.5 + BC + CCD	V = 17.4
	4.1	ESO 2.2 + IR phot	K = 13.4
1988 Aug	2.9	IUE + LWP	$F_\lambda(2700Å) = 0.06 \pm 0.01$
		H 0323+022	
1989 Aug	11.3	ESO 1.5 + BC + CCD	V = 16.7
	11.1	ESO 2.2 + IR phot	K = 13.5
1989 Aug	10.6	IUE + SWP	$F_\lambda(1500Å) = 0.19 \pm 0.02$
1989 Aug	8.8	IUE + LWP	$F_\lambda(2500Å) = 0.12 \pm 0.02$

† in units of 10^{-14} erg cm^{-2} s^{-1} Å^{-1}

Table 2.2: Ultraviolet Fluxes in Selected Wavelength Bands

$\Delta\lambda$	F_λ	ϵ_F
(1)	(2)	(3)
SWP 24010 (exposure = 26,400 s) + **LWP 4259** (exposure = 12,000 s)		
1250–1375	0.235	0.026
1375–1500	0.090	0.036
1705–1740	0.252	0.053
1770–1885	0.216	0.019
2500–2600	0.131	0.020
2600–2700	0.127	0.012
2700–2800	0.118	0.014
2800–2900	0.142	0.014
SWP 29319 (exposure = 18,000 s) + **LWP 9170** (exposure = 10,200 s)		
1470–1525	0.232	0.049
1690–1790	0.294	0.021
1790–1890	0.244	0.013
2400–2500	0.292	0.023
2500–2600	0.309	0.016
2600–2700	0.332	0.016
2700–2800	0.330	0.013
2800–2900	0.326	0.010
2900–3000	0.353	0.013

Table 2.2 (continued)

$\Delta\lambda$	F_λ	ϵ_F
(1)	(2)	(3)
SWP 30936 (exposure = 24,300 s) + **LWP 10705** (exposure = 15,000 s)		
1230–1360	0.238	0.032
1670–1750	0.190	0.023
1750–1850	0.182	0.014
1850–1930	0.157	0.011
2400–2500	0.163	0.020
2500–2600	0.188	0.011
2600–2700	0.203	0.090
2700–2800	0.184	0.007
2800–2900	0.186	0.007
2900–3000	0.200	0.008
SWP 34022 (exposure = 18,180 s)		
1230–1280	0.339	0.035
1280–1330	0.380	0.062
1330–1370	0.160	0.040
1690–1740	0.225	0.029
1740–1786	0.266	0.019
1795–1845	0.231	0.022
1845–1895	0.268	0.016
1895–1927	0.264	0.017

Table 2.2 (continued)

$\Delta\lambda$	F_λ	ϵ_F
(1)	(2)	(3)
SWP 34098 (exposure = 30,000 s) + **LWP 13873** (exposure = 11,040 s)		
1230–1300	0.183	0.021
1708–1758	0.180	0.017
1758–1808	0.152	0.015
1808–1858	0.130	0.015
1858–1908	0.117	0.011
1908–1935	0.131	0.009
2600–2700	0.086	0.007
2700–2800	0.098	0.006
2800–2900	0.105	0.007
SWP 35546 (exposure = 17,400 s) + **LWP 15037** (exposure = 5,340 s)		
1226–1247	0.208	0.047
1710–1760	0.189	0.026
1760–1810	0.173	0.017
1810–1860	0.198	0.013
1860–1910	0.214	0.010
1910–1950	0.259	0.012
2550–2650	0.135	0.018
2650–2750	0.137	0.015
2750–2850	0.140	0.012
2850–2950	0.107	0.010

Table 2.2 (continued)

$\Delta\lambda$	F_λ	ϵ_F
(1)	(2)	(3)
SWP 36809 (exposure = 10,800 s) + **LWP 16088** (exposure = 7,680 s)		
1250–1350	0.386	0.032
1475–1525	0.323	0.047
1650–1750	0.317	0.028
1750–1850	0.346	0.017
1850–1950	0.344	0.026
2400–2500	0.318	0.039
2500–2600	0.292	0.023
2600–2700	0.228	0.015
2700–2800	0.235	0.013
2800–2900	0.205	0.010
2900–3000	0.225	0.009
SWP 36820 (exposure = 22,080 s) + **LWP 16092** (exposure = 7,680 s)		
1250–1350	0.217	0.020
1350–1450	0.189	0.018
1450–1550	0.194	0.019
1600–1700	0.157	0.018
1700–1800	0.191	0.012
1800–1900	0.155	0.009
2400–2500	0.165	0.026
2500–2600	0.120	0.018
2600–2700	0.111	0.010
2700–2800	0.108	0.008
2800–2900	0.100	0.008

Table 2.2 (continued)

$\Delta\lambda$	F_λ	ϵ_F
(1)	(2)	(3)
LWP 10310 (exposure = 22,200 s)		
2635–2655	0.040	0.011
2665–2715	0.042	0.007
2715–2765	0.062	0.007
2765–2815	0.048	0.006
2815–2850	0.054	0.008
2872–2918	0.063	0.008
LWP 10697 (exposure = 7,500 s)		
2400–2500	0.146	0.014
2500–2600	0.142	0.016
2600–2700	0.175	0.011
2700–2800	0.183	0.013
2800–2900	0.215	0.010
2900–3000	0.204	0.011
LWP 13783 (exposure = 9,960 s)		
2650–2700	0.059	0.010
2700–2750	0.058	0.005
2750–2800	0.048	0.008
2800–2850	0.051	0.009
2850–2900	0.051	0.008

Table 2.2 (continued)

$\Delta\lambda$	F_λ	ϵ_F
(1)	(2)	(3)
LWP 15036 (exposure = 10,320 s)		
2400–2500	0.158	0.018
2500–2600	0.152	0.013
2600–2700	0.152	0.009
2700–2800	0.138	0.007
2800–2900	0.138	0.006
LWP 16089 (exposure = 6,000 s)		
2400–2500	0.169	0.029
2500–2600	0.110	0.020
2600–2700	0.095	0.009
2700–2800	0.114	0.009
2800–2900	0.139	0.009
2900–3000	0.143	0.011
LWP 16096 (exposure = 8,580 s)		
2500–2600	0.228	0.022
2650–2750	0.207	0.012
2750–2850	0.195	0.011
2850–2950	0.191	0.010

(1) Selected wavelength band in Å.
(2) UV flux in units of 10^{-14} erg cm^{-2} s^{-1} Å^{-1}.
(3) 1 σ statistical uncertainty divided by $\sqrt{(N/3)}$, where N is the number of pixels (see also text).

Table 2.3: Fitted UV Parameters

Date	Image	α_ν^0	Range	F_λ^0	Range	$(\chi^2/N)^0$	α_ν	Range	F_λ	Range	χ^2/N
(1)	(2)	(3)	(4)	(5)	(6)	(7)	(8)	(9)	(10)	(11)	(12)
					H 0323 + 022	*(A_V = 0.2)*					
1984 Sep 19	SWP 24010	2.260	[1.484, 3.069]	0.198	[0.173, 0.218]	4.07	2.080	[1.302, 2.907]	0.327	[0.284, 0.359]	4.28
1984 Sep 20	LWP 4259	2.740	[0.181, 5.281]	0.132	[0.120, 0.140]	0.42	2.180	[-0.352, 4.761]	0.187	[0.171, 0.199]	0.44
1988 Aug 18	SWP 34098	1.060	[0.616, 1.571]	0.176	[0.155, 0.195]	1.59	0.900	[0.434, 1.401]	0.294	[0.260, 0.328]	1.32
1988 Aug 19	LWP 13873	4.700	[2.469, 6.989]	0.101	[0.097, 0.104]	0.05	4.250	[1.983, 6.585]	0.143	[0.138, 0.148]	0.05
1989 Aug 10	SWP 36820	1.240	[0.836, 1.667]	0.200	[0.186, 0.212]	1.13	1.080	[0.670, 1.511]	0.328	[0.304, 0.348]	1.10
1989 Aug 8	LWP 16092	-0.360	[-1.994, 1.396]	0.102	[0.097, 0.107]	0.37	-0.920	[-2.574, 0.838]	0.145	[0.137, 0.152]	0.42
					H 1722 + 119	*(A_V = 0.51)*					
1986 Sep 28	SWP 29319	1.520	[0.319, 2.941]	0.289	[0.202, 0.387]	2.01	1.450	[0.200, 2.877]	0.940	[0.656, 1.267]	1.46
1986 Sep 25	LWP 9170	2.720	[2.200, 3.262]	0.332	[0.329, 0.333]	0.43	1.360	[0.807, 1.888]	0.811	[0.803, 0.816]	0.45
1897 May 5	LWP 10697	4.120	[3.371, 4.908]	0.193	[0.190, 0.194]	0.83	2.740	[1.971, 3.536]	0.473	[0.468, 0.477]	0.76
1987 May 8	SWP 30936	0.940	[0.353, 1.599]	0.225	[0.192, 0.256]	0.35	0.500	[-0.098, 1.197]	0.820	[0.694, 0.933]	0.05
1987 May 7	LWP 10705	2.300	[1.688, 2.905]	0.191	[0.189, 0.192]	1.23	0.960	[0.338, 1.583]	0.467	[0.463, 0.470]	1.18
					H 0414 - 009	*(A_V = 0.48)*					
1987 Mar 10	LWP 10310	6.000	[2.337, 9.670]	0.054	[0.052, 0.054]	0.84	4.900	[1.212, 8.564]	0.124	[0.121, 0.125]	0.84

Table 2.3 (continued)

Date	Image	α_ν^0	Range	F_λ^0	Range	$(\chi^2/N)^0$	α_ν	Range	F_λ	Range	χ^2/N
(1)	(2)	(3)	(4)	(5)	(6)	(7)	(8)	(9)	(10)	(11)	(12)
					PKS 1538 + 149	*(A_V = 0.1)*					
1988 Aug 2	LWP 13783	-0.900	[-4.400, 3.485]	0.052	[0.044, 0.055]	0.19	-1.200	[-4.301, 3.252]	0.062	[0.051, 0.066]	0.19
					PKS 0048 - 097						
1988 Aug 3	SWP 34022	1.760	[1.345, 2.218]	0.274	[0.246, 0.300]	2.56					
					PKS 0422 + 004						
1989 Feb 13	SWP 35546	4.400	[2.821, 6.482]	0.109	[0.059, 0.172]	2.85					
1989 Feb 14	LWP 15037	-0.080	[-2.099, 2.005]	0.125	[0.121, 0.126]	0.93					
1989 Aug 7	LWP 16089	4.580	[3.142, 6.061]	0.124	[0.123, 0.124]	2.36					
					PKS 0521 - 365						
1989 Feb 14	LWP 15036	0.960	[-0.018, 1.988]	0.139	[0.135, 0.143]	0.15					
					PKS 0301 - 243	*(A_V = 0.1)*					
1989 Aug 7	LWP 16088	0.500	[-0.262, 1.301]	0.228	[0.227, 0.228]	2.03	0.260	[-0.520, 1.048]	0.272	[0.271, 0.272]	2.11
1989 Aug 8	SWP 36809	1.740	[1.306, 2.209]	0.363	[0.330, 0.393]	0.51	1.650	[1.213, 2.125]	0.466	[0.423, 0.505]	0.63

Table 2.3 (continued)

Date	Image	α_ν^0	Range	F_λ^0	Range	$(\chi^2/N)^0$	α_ν	Range	F_λ	Range	χ^2/N
(1)	(2)	(3)	(4)	(5)	(6)	(7)	(8)	(9)	(10)	(11)	(12)
					PKS 0118 - 272	*(A_V = 0.1)*					
1989 Aug 9	LWP 16096	0.700	[-0.555, 2.008]	0.198	[0.196, 0.199]	0.05	0.440	[-0.809, 1.759]	0.236	[0.233, 0.237]	0.06

(1) Observing Date.
(2) IUE image identification number.
(3) Spectral index ($F_\nu^0 \propto \nu^{-\alpha_\nu^0}$) derived from the undereddened spectrum.
(4) Interval of confidence at 90% probability level associated to α_ν^0.
(5) Fitted ($F_\lambda^0 \propto \lambda^{-\alpha_\lambda^0}$) spectral flux (in units of 10^{-14} erg cm^{-2} s^{-1} Å^{-1}) at 1400 Å for SWP spectra and 2800 Å for LWP spectra. No reddening correction has been applied.
(6) Interval of confidence at 90% probability level associated to F_λ^0.
(7) Reduced χ^2 associated to the fitted parameters α_ν^0 and F_λ^0.
(8) Spectral index ($F_\nu \propto \nu^{-\alpha_\nu}$) derived after correcting the spectrum for the extinction A_V.
(9) Interval of confidence at 90% probability level associated to α_ν.
(10) Fitted ($F_\lambda \propto \lambda^{-\alpha_\lambda}$) spectral flux (in units of 10^{-14} erg cm^{-2} s^{-1} Å^{-1}) at 1400 Å for SWP spectra and 2800 Å for LWP spectra. No reddening correction has been applied.
(11) Interval of confidence at 90% probability level associated to F_λ.
(12) Reduced χ^2 associated to the fitted parameters α_ν and F_λ.

Table 2.4: Fitted UV Parameters of Combined Spectra

Images	α_ν^0	Range	F_λ^0	Range	$(\chi^2/N)^0$	α_ν	Range	F_λ	Range	χ^2/N
(1)	(2)	(3)	(4)	(5)	(6)	(7)	(8)	(9)	(10)	(11)
				H 0323 + 022	*(A_V = 0.2)*					
SWP 24010 + LWP 4259	1.290	[1.043, 1.533]	0.164	[0.159,0.167]	2.76	1.080	[0.837, 1.326]	0.252	[0.244,0.257]	2.83
SWP 34098 + LWP 13873	1.140	[0.949, 1.327]	0.127	[0.124,0.129]	1.87	0.870	[0.699, 1.074]	0.197	[0.193,0.200]	1.60
SWP 36820 + LWP 16092	1.050	[0.907, 1.216]	0.145	[0.145,0.146]	0.95	0.870	[0.702, 1.009]	0.225	[0.224,0.225]	1.08
				H 1722 + 119	*(A_V = 0.51)*					
SWP 29319 + LWP 9170	2.580	[2.417, 2.745]	0.272	[0.260,0.284]	0.99	1.920	[1.775, 2.090]	0.835	[0.797,0.866]	1.13
SWP 30936 + LWP 10705	2.160	[1.991, 2.344]	0.180	[0.171,0.188]	1.73	1.470	[1.314, 1.653]	0.558	[0.531,0.580]	1.53
				PKS 0422 + 004						
SWP 35546 + LWP 15037	0.930	[0.739, 1.118]	0.193	[0.192,0.193]	5.18					

Table 2.4 (continued)

Images	α_ν^0	Range	F_λ^0	Range	$(\chi^2/N)^0$	α_ν	Range	F_λ	Range	χ^2/N
(1)	(2)	(3)	(4)	(5)	(6)	(7)	(8)	(9)	(10)	(11)
					PKS 0301 - 243	*(A_V = 0.1)*				
SWP 36809 + LWP 16088	1.200	[1.096, 1.334]	0.299	[0.292,0.304]	1.86	1.110	[0.980, 1.217]	0.369	[0.361,0.377]	2.07

(1) IUE image identification numbers.
(2) Spectral index ($F_\nu^0 \propto \nu^{-\alpha_\nu^0}$) derived from the combined undereddened spectra.
(3) Interval of confidence at 90% probability level associated to α_ν^0.
(4) Fitted ($F_\lambda^0 \propto \lambda^{-\alpha_\lambda^0}$) spectral flux (in units of 10^{-14} erg cm^{-2} s^{-1} Å^{-1}) at 2000 Å.
No reddening correction has been applied.
(5) Interval of confidence at 90% probability level associated to F_λ^0.
(6) Reduced χ^2 associated to the fitted parameters α_ν^0 and F_λ^0.
(7) Spectral index ($F_\nu \propto \nu^{-\alpha_\nu}$) derived after correcting both spectra for the extinction A_V.
(8) Interval of confidence at 90% probability level associated to α_ν.
(9) Fitted ($F_\lambda \propto \lambda^{-\alpha_\lambda}$) spectral flux (in units of 10^{-14} erg cm^{-2} s^{-1} Å^{-1}) at 2000 Å.
No reddening correction has been applied.
(10) Interval of confidence at 90% probability level associated to F_λ.
(11) Reduced χ^2 associated to the fitted parameters α_ν and F_λ.

Table 3.1: IUE Log of Observations of PKS 2155-304

SWP #	UT (edelson)	Expo	Day	UT (pike)	Day (Vilspa)	UT(Vilsp	Expo(	HANDWRITTEN L
42969	1.8791	55	1	20 38 26				
42970	1.9489	55	1	22 18 53				
42971	2.0125	55	1	23 50 34				
42972	2.0777	55	2	01 24 26				
42979	2.866	55	2	20 19 36				
42980	2.9321	55	2	21 54 40				
42995	3.8764	55	3	20 34 34				
42996	3.9409	35	3	22 17 25				
43008	4.861	55	4	20 12 21				
43009	4.9319	55	4	21 54 30				
43017	5.8717	55	5	20 27 41	91110520	202700	5500	
43018	5.9473	55	5	22 16 35	91110522	221600	5500	
43025	7.004	55	6	23 38 19	91110623	233800	5500	
43026	7.0755	55	7	01 21 11	91110701	012100	5500	
43040	9.1964	55	9	04 15 21				
43041	9.2706	55	9	06 02 12				
43047					91110916	164721	5500	
43048					91110918	182219	2500	
43054					91111016	162602	5500	
43055	10.7701	55	10	18 01 26				
43056	10.8387	51	10	19 42 15				
43057	10.9053	55	10	21 16 05				
43058	10.9714	52	10	22 52 46				
43059	11.0373	55	11	00 26 09				
43060	11.1029	52	11	02 02 14				
43061	11.1698	51	11	03 39 01				
43062	11.237	51	11	05 15 49				
43063	11.3037	55	11	06 49 51				
43064	11.3705	50	11	08 28 30				
43065	11.8345	57	11	19 33 09				
43066	11.9045	45	11	21 20 02				
43067	11.9669	58	11	22 43 19				
43068	12.0336	57	12	00 19 51				
43069	12.1008	57	12	01 56 39				
43070	12.1684	54	12	03 35 29				
43071	12.2343	55	12	05 09 52				
43073					91111212	121441	1300	
43074	12.5679	55	12	13 10 15	91111213	131015	5500	
43075	12.6337	55	12	14 45 00	91111214	144500	5500	
43076	12.7025	49	12	16 27 10	91111216	162710	4900	
43077	12.7669	55	12	17 56 47				
43078	12.8336	55	12	19 32 50				
43079	12.8993	55	12	21 07 29				
43080	12.9659	57	12	22 42 22				
43081	13.0334	53	13	00 21 39				
43082	13.1009	51	13	01 59 50				
43083	13.1681	51	13	03 36 30	91111303	033600	5100	
43084	13.2313	55	13	05 05 32	91111305	050500	5500	
43085	13.2991	55	13	06 43 10	91111306	064300	5500	
43086	13.3659	65	13	08 14 28	91111308	081400	6500	
43088					91111311	115651	2700	

Table 3.1 (continued)

43089	13.5689	42	13	13 18 16	91111313	131816	4200		
43090	13.6315	55	13	14 41 54	91111314	144154	5500		
43091	13.6981	55	13	16 17 44	91111316	161744	5500		
43092	13.766	52	13	17 57 01	91111317	175700	5200		
43093	13.8308	56	13	19 28 25	91111319	192800	5600		
43094	13.8971	57	13	21 03 18	91111321	210300	5700		
43095	13.9657	52	13	22 44 36	91111322	224400	5200		
43096	14.0303	57	14	00 15 09	91111400	001500	5700		
43097	14.0965	57	14	01 50 29	91111401	015000	5700		
43098	14.1634	57	14	03 26 45	91111403	032600	5700		
43099	14.2313	53	14	05 06 38	91111405	050600	5300		
43101	14.563	55	14	13 03 09	91111413	130309	5500		
43102	14.629	55	14	14 38 18	91111414	143818	5500		
43103	14.6981	49	14	16 20 49	91111416	162049	4900		
43104	14.7628	55	14	17 50 55					
43105	14.8291	55	14	19 26 20					
43106		57	14					220023	
43107	14.9617	57	14	22 36 25					
43108	15.0284	57	15	00 12 26					
43109	15.0945	58	15	01 47 07					
43110	15.1623	54	15	03 26 41					
43111	15.2133	57	15	04 38 39					
43113								high resolution	
43114		55	16					043303	
43115		40	16					060621	
43121		55	16					201111	
43122		65	16					214025	
43135		55	17					201059	
43136		60	17					214743	
43145		55	18					193354	
43146		55	18					211318	
43157		55	19					005058	
43158		33	19					022741	
43164					91112016	164123	5500		
43165					91112018	182241	2500		
43174					91112116	160833	5500		
43175					91112117	175556	5500		
43184					91112215	155244	5500		
43185					91112217	173105	4700		
43192					91112316	162329	5500		
43193					91112318	180405	4400		
43211					91112416	162520	5500		
43220					91112516	161758	5500		
43221					91112517	175915	5000		
43230					91112616	161642	5500		
43231					91112618	180138	4500		
43236					91112716	161524	5500		
43237					91112717	175553	5000		
43246	28.8738	45	28	20 35 48	91112820	203500	4500		
43247	28.9349	45	28	22 03 45	91112822	220300	4500		
43260	29.8434	55	29	19 46 57					
43261	29.91	50	29	21 25 23					

Table 3.1 (continued)

LWP #	UT (edelson)	Expo	Day	UT (pike)	Day (Vilspa)	UT(Vilsp	Expo(	HANDWRITTEN	
21607	1.8424	30	1	19 58 07					
21608	1.9151	30	1	21 42 44					
21609	1.9797	25	1	23 18 13					
21610	2.0445	25	2	00 51 34					
21611	2.1093	25	2	02 24 57					
21616	2.8338	25	2	19 48 14					
21617	2.8977	25	2	21 20 13					
21625	3.8423	25	3	20 00 29					
21626	3.9132	25	3	21 42 29					
21636	4.826	25	4	19 36 56					
21637	4.897	25	4	21 19 07					
21644	5.8368	25	5	19 52 26	91110519	195200	2500		
21645	5.9118	25	5	21 40 30	91110521	214000	2500		
21652	6.822	25	6	19 31 12	91110619	193100	2500		
21653	7.0395	25	7	00 44 20	91110700	004400	2500		
21654	7.1114	25	7	02 27 54	91110702	022800	2500		
21667	9.0493	25	9	00 58 29					
21668	9.2325	25	9	05 22 21					
21673					91110916	161233	2500		
21674					91110917	174836	2500		
21683					91111015	155406	2500		
21684					91111017	172832	2500		
21685	10.8059	25	10	19 08 00					
21686	10.8724	25	10	20 43 46					
21687	10.9381	25	10	22 18 25					
21688	11.0048	25	10	23 54 21					
21689	11.0709	25	11	01 29 33					
21690	11.1364	25	11	03 03 57					
21691	11.2031	23	11	04 40 54					
21692	11.269	25	11	06 14 49					
21693	11.3367	25	11	07 52 21					
21696	11.8704	25	11	20 40 56					
21697	11.9335	27	11	22 10 46					
21698	12.0015	25	11	23 49 38					
21699	12.0672	27	12	01 23 14					
21700	12.1344	27	12	03 00 05					
21701	12.201	25	12	04 36 59					
21702	12.2674	28	12	06 11 03					
21704	12.534	25	12	12 36 24	91111212	123624	2500		
21705	12.6009	25	12	14 12 44	91111214	141244	2500		
21706	12.6671	25	12	15 48 06	91111215	154806	2500		
21707	12.7336	25	12	17 23 53	91111217	172353	2500		
21708	12.7999	25	12	18 59 22					
21709	12.8665	25	12	20 35 13					
21710	12.9322	28	12	22 08 18					
21711	13	25	12	23 47 34					
21712	13.0692	25	13	01 27 13					
21713	13.1321	25	13	02 57 46					
21714	13.1981	25	13	04 32 46	91111304	043200	2500		
21715	13.2664	25	13	06 11 08	91111306	061100	2500		
21716	13.3311	25	13	07 44 13	91111307	074400	2500		

Table 3.1 (continued)

21717	13.5316	25	13	12 33 00	91111312	123300	2500		
21718	13.5987	25	13	14 09 41	91111314	140941	2500		
21719	13.6647	25	13	15 44 40	91111315	154440	2500		
21720	13.7314	25	13	17 20 42	91111317	172042	2500		
21721	13.7974	26	13	18 55 15	91111318	185500	2600		
21722	13.8636	27	13	20 30 01	91111320	203000	2700		
21723	13.9306	27	13	22 06 34	91111322	220600	2700		
21724	13.9969	27	13	23 42 00	91111323	234200	2700		
21725	14.063	27	14	01 17 11	91111401	011700	2700		
21726	14.1299	27	14	02 53 32	91111402	025300	2700		
21727	14.1975	25	14	04 31 56	91111404	043200	2500		
21728	14.265	30	14	06 06 37	91111406	060600	3000		
21730	14.5295	25	14	12 30 00	91111412	123000	2500		
21731	14.5955	25	14	14 05 01	91111414	140501	2500		
21732	14.6627	25	14	15 41 47	91111415	154147	2500		
21733	14.7296	25	14	17 18 10	91111417	171810	2500		
21734	14.7957	27	14	18 52 21					
21735	14.8614	27	14	20 26 55					
21736	14.9282	27	14	22 03 06					
21737	14.9947	27	14	23 38 50					
21738		27	15					011401	
21739	15.1279	27	15	02 50 42					
21740	15.1944	27	15	04 26 23					
21741	15.2624	35	15	06 00 24					
21744	15.8248	25	15	19 35 14					
21747		25	16					040154	
21748		25	16					053437	
21755		25	16					194214	
21756		25	16					211039	
21768		25	17					193158	
21769	17.892	25	17	21 11 55					
21777	18.8679	27	18	20 36 18					
21778	18.9392	33	18	22 15 56					
21786	19.0222	25	19	00 19 32					
21787		27	19					015206	
21793					91112017	174522	2500		
21799					91112117	171352	2500		
21810					91112216	165748	2500		
21811					91112218	182421	2500		
21828					91112317	172928	2500		
21837					91112418	180029	3200		
21847					91112517	172048	2500		
21856					91112617	172206	2500		
21864					91112717	172342	2500		
21877	28.8407	25	28	19 58 04	91112819	195800	2500		
21878	28.9033	25	28	21 28 18	91112821	212800	2500		
21888	29.833	25	29	19 46 57					
21889	29.9411	25	29	22 22 43					

Table 3.2: Fitted Parameters of PKS 2155-304

Date (1991 Nov)	Image	α_ν^0	F_λ^0	$(\chi^2/N)^0$	α_ν	F_λ	χ^2/N
(1)	(2)	(3)	(4)	(5)	(6)	(7)	(8)
1.8424	LWP 21607	$1.38^{+0.22}_{-0.23}$	$3.53^{+0.01}_{-0.04}$	1.88	$1.06^{+0.23}_{-0.23}$	$4.21^{+0.02}_{-0.02}$	2.23
1.8791	SWP 42969	$0.64^{+0.09}_{-0.07}$	$8.33^{+0.12}_{-0.10}$	4.55	$0.58^{+0.08}_{-0.08}$	$10.63^{+0.15}_{-0.15}$	5.34
1.9151	LWP 21608	$1.06^{+0.20}_{-0.21}$	$3.72^{+0.03}_{-0.03}$	0.82	$0.74^{+0.20}_{-0.22}$	$4.43^{+0.02}_{-0.02}$	0.91
1.9489	SWP 42970	$0.72^{+0.08}_{-0.07}$	$8.53^{+0.12}_{-0.12}$	2.21	$0.66^{+0.08}_{-0.07}$	$10.90^{+0.12}_{-0.13}$	2.69
1.9797	LWP 21609	$1.36^{+0.28}_{-0.26}$	$3.76^{+0.04}_{-0.03}$	0.33	$1.04^{+0.27}_{-0.28}$	$4.48^{+0.04}_{-0.06}$	0.43
2.0125	SWP 42971	$0.54^{+0.09}_{-0.07}$	$8.81^{+0.11}_{-0.10}$	3.77	$0.48^{+0.08}_{-0.08}$	$11.24^{+0.19}_{-0.16}$	3.55
2.0445	LWP 21610	$1.08^{+0.26}_{-0.26}$	$3.69^{+0.03}_{-0.04}$	0.62	$0.74^{+0.28}_{-0.26}$	$4.39^{+0.03}_{-0.04}$	0.82
2.0777	SWP 42972	$0.96^{+0.08}_{-0.07}$	$8.58^{+0.11}_{-0.14}$	3.31	$0.92^{+0.07}_{-0.08}$	$10.92^{+0.14}_{-0.16}$	4.08
2.1093	LWP 21611	$1.32^{+0.25}_{-0.24}$	$3.76^{+0.02}_{-0.03}$	0.76	$1.02^{+0.24}_{-0.25}$	$4.47^{+0.04}_{-0.05}$	0.95
2.8338	LWP 21616	$0.96^{+0.22}_{-0.22}$	$4.20^{+0.04}_{-0.03}$	0.53	$0.62^{+0.22}_{-0.21}$	$5.01^{+0.03}_{-0.03}$	0.49
2.8660	SWP 42979	$0.70^{+0.07}_{-0.07}$	$9.94^{+0.13}_{-0.14}$	3.29	$0.64^{+0.07}_{-0.07}$	$12.70^{+0.19}_{-0.23}$	3.80
2.8977	LWP 21617	$1.28^{+0.23}_{-0.23}$	$4.15^{+0.03}_{-0.04}$	1.20	$0.96^{+0.24}_{-0.24}$	$4.95^{+0.04}_{-0.05}$	1.45
2.9321	SWP 42980	$0.66^{+0.07}_{-0.08}$	$10.10^{+0.14}_{-0.09}$	3.57	$0.58^{+0.08}_{-0.07}$	$12.94^{+0.19}_{-0.14}$	3.86
3.8423	LWP 21625	$0.84^{+0.23}_{-0.22}$	$4.11^{+0.05}_{-0.03}$	0.57	$0.50^{+0.23}_{-0.23}$	$4.89^{+0.05}_{-0.05}$	0.53
3.8764	SWP 42995	$0.54^{+0.07}_{-0.08}$	$10.24^{+0.12}_{-0.11}$	0.89	$0.46^{+0.08}_{-0.07}$	$13.14^{+0.14}_{-0.21}$	0.90
3.9132	LWP 21626	$0.98^{+0.24}_{-0.24}$	$4.30^{+0.03}_{-0.06}$	0.35	$0.62^{+0.25}_{-0.24}$	$5.12^{+0.04}_{-0.04}$	0.34
3.9409	SWP 42996	$0.82^{+0.08}_{-0.09}$	$9.98^{+0.22}_{-0.17}$	1.22	$0.76^{+0.08}_{-0.09}$	$12.77^{+0.23}_{-0.18}$	1.16
4.8260	LWP 21636	$1.18^{+0.19}_{-0.17}$	$4.90^{+0.04}_{-0.02}$	0.77	$0.84^{+0.19}_{-0.18}$	$5.83^{+0.04}_{-0.03}$	0.89
4.8610	SWP 43008	$0.70^{+0.07}_{-0.06}$	$11.42^{+0.18}_{-0.17}$	3.53	$0.64^{+0.07}_{-0.06}$	$14.61^{+0.15}_{-0.21}$	4.45
4.8970	LWP 21637	$1.12^{+0.20}_{-0.21}$	$4.89^{+0.03}_{-0.04}$	0.79	$0.78^{+0.20}_{-0.21}$	$5.82^{+0.06}_{-0.03}$	0.93
4.9319	SWP 43009	$0.68^{+0.08}_{-0.07}$	$11.32^{+0.18}_{-0.19}$	3.35	$0.64^{+0.08}_{-0.08}$	$14.40^{+0.23}_{-0.18}$	3.05
5.8368	LWP 21644	$1.02^{+0.21}_{-0.22}$	$4.91^{+0.05}_{-0.06}$	0.81	$0.66^{+0.22}_{-0.21}$	$5.83^{+0.07}_{-0.03}$	0.91
5.8717	SWP 43017	$0.64^{+0.09}_{-0.07}$	$11.89^{+0.15}_{-0.20}$	1.64	$0.62^{+0.07}_{-0.09}$	$15.06^{+0.21}_{-0.18}$	1.69
5.9118	LWP 21645	$1.26^{+0.23}_{-0.22}$	$5.12^{+0.04}_{-0.06}$	0.76	$0.92^{+0.22}_{-0.23}$	$6.08^{+0.07}_{-0.05}$	0.94
5.9473	SWP 43018	$0.68^{+0.06}_{-0.07}$	$11.92^{+0.12}_{-0.17}$	1.47	$0.60^{+0.07}_{-0.05}$	$15.30^{+0.12}_{-0.23}$	1.69
6.8220	LWP 21652	$1.20^{+0.21}_{-0.22}$	$5.13^{+0.07}_{-0.04}$	0.76	$0.84^{+0.22}_{-0.21}$	$6.09^{+0.04}_{-0.04}$	0.81
7.0040	SWP 43025	$0.72^{+0.07}_{-0.07}$	$10.70^{+0.12}_{-0.13}$	2.72	$0.68^{+0.06}_{-0.08}$	$13.64^{+0.18}_{-0.14}$	3.63
7.0395	LWP 21653	$1.20^{+0.21}_{-0.21}$	$4.76^{+0.06}_{-0.04}$	1.04	$0.84^{+0.22}_{-0.20}$	$5.65^{+0.05}_{-0.06}$	1.23
7.0755	SWP 43026	$0.62^{+0.08}_{-0.06}$	$10.68^{+0.11}_{-0.15}$	2.71	$0.56^{+0.08}_{-0.07}$	$13.63^{+0.13}_{-0.21}$	2.68
7.1114	LWP 21654	$1.22^{+0.22}_{-0.21}$	$4.76^{+0.05}_{-0.02}$	0.34	$0.88^{+0.22}_{-0.21}$	$5.67^{+0.05}_{-0.04}$	0.40
9.0493	LWP 21667	$1.22^{+0.22}_{-0.21}$	$5.51^{+0.04}_{-0.03}$	0.66	$0.88^{+0.22}_{-0.21}$	$6.56^{+0.08}_{-0.08}$	0.85
9.1964	SWP 43040	$0.54^{+0.10}_{-0.08}$	$11.84^{+0.22}_{-0.24}$	5.44	$0.50^{+0.08}_{-0.10}$	$15.08^{+0.24}_{-0.26}$	4.84
9.2325	LWP 21668	$1.28^{+0.20}_{-0.21}$	$5.68^{+0.05}_{-0.04}$	0.94	$0.94^{+0.20}_{-0.21}$	$6.75^{+0.09}_{-0.04}$	1.09
9.2706	SWP 43041	$0.46^{+0.08}_{-0.06}$	$13.54^{+0.13}_{-0.22}$	3.16	$0.42^{+0.07}_{-0.06}$	$17.24^{+0.18}_{-0.27}$	4.11
9.6754	LWP 21673	$1.24^{+0.19}_{-0.21}$	$5.83^{+0.03}_{-0.03}$	0.84	$0.90^{+0.20}_{-0.21}$	$6.93^{+0.07}_{-0.07}$	1.02
9.6995	SWP 43047	$0.54^{+0.08}_{-0.06}$	$13.61^{+0.16}_{-0.17}$	1.65	$0.50^{+0.07}_{-0.06}$	$17.34^{+0.28}_{-0.29}$	2.45
9.7421	LWP 21674	$1.02^{+0.19}_{-0.20}$	$5.74^{+0.03}_{-0.05}$	0.48	$0.66^{+0.21}_{-0.19}$	$6.83^{+0.05}_{-0.04}$	0.59
9.7655	SWP 43048	$0.72^{+0.08}_{-0.09}$	$13.50^{+0.29}_{-0.24}$	2.60	$0.68^{+0.08}_{-0.09}$	$17.21^{+0.34}_{-0.33}$	2.17
10.6626	LWP 21683	$0.96^{+0.24}_{-0.22}$	$6.15^{+0.05}_{-0.09}$	0.39	$0.62^{+0.23}_{-0.24}$	$7.31^{+0.08}_{-0.10}$	0.45
10.6847	SWP 43054	$0.46^{+0.07}_{-0.06}$	$15.06^{+0.11}_{-0.23}$	3.82	$0.42^{+0.06}_{-0.07}$	$19.17^{+0.22}_{-0.14}$	3.66
10.7281	LWP 21684	$0.90^{+0.16}_{-0.15}$	$6.12^{+0.02}_{-0.01}$	0.47	$0.58^{+0.16}_{-0.17}$	$7.30^{+0.02}_{-0.06}$	0.61
10.7701	SWP 43055	$0.40^{+0.06}_{-0.06}$	$15.07^{+0.10}_{-0.12}$	5.01	$0.34^{+0.06}_{-0.06}$	$19.24^{+0.24}_{-0.26}$	4.13
10.8059	LWP 21685	$0.98^{+0.19}_{-0.17}$	$6.24^{+0.04}_{-0.05}$	0.64	$0.64^{+0.18}_{-0.18}$	$7.43^{+0.05}_{-0.09}$	0.79
10.8387	SWP 43056	$0.56^{+0.06}_{-0.06}$	$15.00^{+0.23}_{-0.16}$	1.56	$0.52^{+0.05}_{-0.07}$	$19.11^{+0.31}_{-0.27}$	1.37

Table 3.2 (continued)

Date (1991 Nov)	Image	α_ν^0	F_λ^0	$(\chi^2/N)^0$	α_ν	F_λ	χ^2/N
(1)	(2)	(3)	(4)	(5)	(6)	(7)	(8)
10.8724	LWP 21686	$1.24^{+0.20}_{-0.20}$	$6.40^{+0.06}_{-0.08}$	0.98	$0.88^{+0.21}_{-0.19}$	$7.60^{+0.08}_{-0.09}$	1.15
10.9053	SWP 43057	$0.68^{+0.05}_{-0.06}$	$15.01^{+0.20}_{-0.13}$	2.14	$0.62^{+0.06}_{-0.05}$	$19.21^{+0.18}_{-0.24}$	2.90
10.9381	LWP 21687	$0.90^{+0.17}_{-0.18}$	$6.22^{+0.02}_{-0.03}$	0.87	$0.56^{+0.17}_{-0.18}$	$7.41^{+0.06}_{-0.05}$	0.96
10.9714	SWP 43058	$0.46^{+0.05}_{-0.06}$	$15.30^{+0.16}_{-0.19}$	3.09	$0.40^{+0.07}_{-0.05}$	$19.60^{+0.24}_{-0.34}$	2.14
11.0048	LWP 21688	$0.98^{+0.22}_{-0.21}$	$6.17^{+0.06}_{-0.07}$	1.08	$0.62^{+0.22}_{-0.21}$	$7.33^{+0.11}_{-0.08}$	1.33
11.0373	SWP 43059	$0.68^{+0.07}_{-0.05}$	$14.97^{+0.16}_{-0.16}$	2.72	$0.64^{+0.06}_{-0.07}$	$19.04^{+0.20}_{-0.21}$	3.22
11.0709	LWP 21689	$1.26^{+0.20}_{-0.22}$	$6.08^{+0.05}_{-0.04}$	2.24	$0.90^{+0.22}_{-0.20}$	$7.23^{+0.09}_{-0.04}$	2.61
11.1029	SWP 43060	$0.60^{+0.07}_{-0.06}$	$15.33^{+0.19}_{-0.21}$	2.71	$0.54^{+0.07}_{-0.06}$	$19.57^{+0.24}_{-0.30}$	2.35
11.1364	LWP 21690	$1.12^{+0.20}_{-0.22}$	$6.40^{+0.04}_{-0.07}$	0.46	$0.76^{+0.21}_{-0.21}$	$7.62^{+0.08}_{-0.10}$	0.56
11.1698	SWP 43061	$0.50^{+0.05}_{-0.06}$	$15.75^{+0.19}_{-0.17}$	3.96	$0.44^{+0.06}_{-0.06}$	$20.14^{+0.26}_{-0.18}$	2.95
11.2031	LWP 21691	$1.32^{+0.19}_{-0.21}$	$6.61^{+0.04}_{-0.06}$	0.88	$0.96^{+0.21}_{-0.19}$	$7.85^{+0.04}_{-0.07}$	1.08
11.2370	SWP 43062	$0.60^{+0.06}_{-0.06}$	$16.05^{+0.25}_{-0.17}$	2.62	$0.54^{+0.07}_{-0.06}$	$20.51^{+0.19}_{-0.29}$	3.34
11.2690	LWP 21692	$1.00^{+0.20}_{-0.19}$	$6.61^{+0.06}_{-0.06}$	0.87	$0.68^{+0.19}_{-0.20}$	$7.87^{+0.04}_{-0.09}$	1.08
11.3037	SWP 43063	$0.72^{+0.08}_{-0.08}$	$15.31^{+0.30}_{-0.20}$	9.50	$0.66^{+0.09}_{-0.07}$	$19.54^{+0.28}_{-0.37}$	11.65
11.3367	LWP 21693	$0.92^{+0.18}_{-0.17}$	$6.66^{+0.03}_{-0.02}$	0.98	$0.60^{+0.17}_{-0.18}$	$7.94^{+0.06}_{-0.04}$	1.17
11.3705	SWP 43064	$0.10^{+0.08}_{-0.07}$	$16.48^{+0.23}_{-0.28}$	4.55	$0.04^{+0.08}_{-0.07}$	$21.03^{+0.26}_{-0.38}$	5.73
11.8345	SWP 43065	$0.52^{+0.06}_{-0.07}$	$15.76^{+0.17}_{-0.12}$	1.79	$0.46^{+0.06}_{-0.07}$	$20.10^{+0.30}_{-0.18}$	1.78
11.8704	LWP 21696	$0.90^{+0.18}_{-0.18}$	$6.77^{+0.02}_{-0.06}$	0.24	$0.56^{+0.18}_{-0.19}$	$8.06^{+0.02}_{-0.07}$	0.27
11.9045	SWP 43066	$0.60^{+0.05}_{-0.07}$	$15.71^{+0.18}_{-0.14}$	3.73	$0.54^{+0.05}_{-0.07}$	$20.10^{+0.22}_{-0.15}$	2.79
11.9335	LWP 21697	$0.98^{+0.16}_{-0.14}$	$6.84^{+0.01}_{-0.03}$	0.54	$0.66^{+0.15}_{-0.15}$	$8.15^{+0.07}_{-0.03}$	0.57
11.9669	SWP 43067	$0.58^{+0.05}_{-0.06}$	$15.96^{+0.23}_{-0.16}$	2.32	$0.52^{+0.06}_{-0.04}$	$20.42^{+0.20}_{-0.17}$	1.69
12.0015	LWP 21698	$1.24^{+0.19}_{-0.20}$	$6.92^{+0.04}_{-0.09}$	0.84	$0.88^{+0.20}_{-0.19}$	$8.22^{+0.11}_{-0.10}$	1.02
12.0336	SWP 43068	$0.54^{+0.05}_{-0.07}$	$16.21^{+0.19}_{-0.12}$	1.19	$0.48^{+0.06}_{-0.05}$	$20.74^{+0.19}_{-0.19}$	1.46
12.0672	LWP 21699	$1.12^{+0.20}_{-0.18}$	$7.10^{+0.07}_{-0.09}$	0.49	$0.76^{+0.20}_{-0.19}$	$8.44^{+0.11}_{-0.08}$	0.49
12.1008	SWP 43069	$0.60^{+0.06}_{-0.06}$	$16.01^{+0.15}_{-0.19}$	1.72	$0.54^{+0.07}_{-0.06}$	$20.46^{+0.23}_{-0.33}$	1.84
12.1344	LWP 21700	$1.26^{+0.19}_{-0.20}$	$6.96^{+0.06}_{-0.08}$	0.47	$0.90^{+0.20}_{-0.19}$	$8.28^{+0.08}_{-0.05}$	0.60
12.1684	SWP 43070	$0.56^{+0.06}_{-0.05}$	$15.83^{+0.17}_{-0.24}$	1.93	$0.52^{+0.05}_{-0.06}$	$20.17^{+0.32}_{-0.24}$	1.51
12.2010	LWP 21701	$1.18^{+0.19}_{-0.21}$	$6.79^{+0.02}_{-0.07}$	0.99	$0.82^{+0.21}_{-0.20}$	$8.08^{+0.03}_{-0.03}$	1.15
12.2343	SWP 43071	$0.64^{+0.06}_{-0.06}$	$15.10^{+0.15}_{-0.15}$	3.85	$0.60^{+0.06}_{-0.06}$	$19.23^{+0.28}_{-0.26}$	4.93
12.2674	LWP 21702	$0.96^{+0.19}_{-0.20}$	$6.46^{+0.04}_{-0.08}$	0.27	$0.60^{+0.19}_{-0.20}$	$7.67^{+0.10}_{-0.05}$	0.34
12.5102	SWP 43073	$1.04^{+0.12}_{-0.10}$	$13.18^{+0.23}_{-0.25}$	3.32	$0.98^{+0.12}_{-0.11}$	$16.83^{+0.37}_{-0.37}$	3.48
12.5340	LWP 21704	$1.02^{+0.17}_{-0.18}$	$6.54^{+0.04}_{-0.04}$	0.54	$0.66^{+0.18}_{-0.17}$	$7.78^{+0.08}_{-0.05}$	0.56
12.5679	SWP 43074	$0.54^{+0.07}_{-0.06}$	$15.03^{+0.21}_{-0.19}$	1.38	$0.50^{+0.06}_{-0.08}$	$19.13^{+0.19}_{-0.18}$	1.81
12.6009	LWP 21705	$1.18^{+0.20}_{-0.20}$	$6.50^{+0.06}_{-0.04}$	0.36	$0.82^{+0.21}_{-0.19}$	$7.72^{+0.05}_{-0.07}$	0.51
12.6337	SWP 43075	$0.54^{+0.06}_{-0.07}$	$15.09^{+0.16}_{-0.20}$	3.77	$0.50^{+0.06}_{-0.07}$	$19.20^{+0.28}_{-0.26}$	4.28
12.6671	LWP 21706	$1.02^{+0.17}_{-0.18}$	$6.46^{+0.06}_{-0.04}$	0.49	$0.66^{+0.18}_{-0.17}$	$7.68^{+0.07}_{-0.06}$	0.59
12.7025	SWP 43076	$0.64^{+0.07}_{-0.05}$	$15.11^{+0.15}_{-0.22}$	2.72	$0.60^{+0.06}_{-0.06}$	$19.23^{+0.25}_{-0.23}$	2.57
12.7336	LWP 21707	$1.04^{+0.19}_{-0.17}$	$6.50^{+0.06}_{-0.05}$	0.59	$0.70^{+0.19}_{-0.19}$	$7.73^{+0.04}_{-0.08}$	0.64
12.7669	SWP 43077	$0.62^{+0.06}_{-0.06}$	$15.39^{+0.13}_{-0.20}$	2.06	$0.56^{+0.06}_{-0.06}$	$19.65^{+0.14}_{-0.28}$	1.99
12.7999	LWP 21708	$1.30^{+0.19}_{-0.19}$	$6.74^{+0.07}_{-0.07}$	1.29	$0.96^{+0.19}_{-0.20}$	$8.01^{+0.07}_{-0.04}$	1.55
12.8336	SWP 43078	$0.62^{+0.06}_{-0.05}$	$15.45^{+0.11}_{-0.18}$	3.41	$0.58^{+0.05}_{-0.06}$	$19.67^{+0.29}_{-0.18}$	2.81
12.8665	LWP 21709	$1.22^{+0.18}_{-0.17}$	$6.70^{+0.03}_{-0.05}$	0.63	$0.90^{+0.18}_{-0.17}$	$7.98^{+0.08}_{-0.06}$	0.83
12.8993	SWP 43079	$0.54^{+0.07}_{-0.05}$	$15.46^{+0.18}_{-0.17}$	4.77	$0.50^{+0.06}_{-0.05}$	$19.72^{+0.26}_{-0.20}$	3.57
12.9322	LWP 21710	$1.14^{+0.17}_{-0.16}$	$6.71^{+0.03}_{-0.06}$	0.65	$0.80^{+0.18}_{-0.16}$	$7.99^{+0.06}_{-0.06}$	0.85

Table 3.2 (continued)

Date (1991 Nov)	Image	α_ν^0	F_λ^0	$(\chi^2/N)^0$	α_ν	F_λ	χ^2/N
(1)	(2)	(3)	(4)	(5)	(6)	(7)	(8)
12.9659	SWP 43080	$0.68^{+0.07}_{-0.05}$	$15.54^{+0.10}_{-0.16}$	1.97	$0.64^{+0.06}_{-0.05}$	$19.79^{+0.21}_{-0.24}$	2.76
13.0000	LWP 21711	$1.26^{+0.19}_{-0.17}$	$6.80^{+0.02}_{-0.07}$	0.67	$0.94^{+0.17}_{-0.19}$	$8.10^{+0.04}_{-0.07}$	0.72
13.0334	SWP 43081	$0.70^{+0.05}_{-0.06}$	$15.27^{+0.21}_{-0.15}$	2.18	$0.66^{+0.05}_{-0.06}$	$19.46^{+0.30}_{-0.22}$	2.71
13.0692	LWP 21712	$1.16^{+0.19}_{-0.18}$	$6.54^{+0.04}_{-0.04}$	0.49	$0.82^{+0.20}_{-0.18}$	$7.78^{+0.07}_{-0.08}$	0.66
13.1009	SWP 43082	$0.64^{+0.07}_{-0.06}$	$14.92^{+0.14}_{-0.13}$	1.26	$0.58^{+0.06}_{-0.07}$	$19.06^{+0.28}_{-0.17}$	1.05
13.1321	LWP 21713	$1.14^{+0.20}_{-0.19}$	$6.46^{+0.09}_{-0.06}$	0.47	$0.78^{+0.20}_{-0.19}$	$7.68^{+0.08}_{-0.07}$	0.57
13.1681	SWP 43083	$0.64^{+0.06}_{-0.05}$	$14.57^{+0.19}_{-0.12}$	4.76	$0.58^{+0.07}_{-0.05}$	$18.62^{+0.10}_{-0.28}$	5.96
13.1981	LWP 21714	$1.08^{+0.20}_{-0.19}$	$6.32^{+0.08}_{-0.05}$	0.48	$0.74^{+0.19}_{-0.20}$	$7.52^{+0.04}_{-0.09}$	0.57
13.2313	SWP 43084	$0.68^{+0.06}_{-0.07}$	$14.14^{+0.19}_{-0.18}$	3.21	$0.64^{+0.06}_{-0.07}$	$18.02^{+0.28}_{-0.17}$	4.41
13.2664	LWP 21715	$1.08^{+0.19}_{-0.20}$	$6.14^{+0.06}_{-0.07}$	0.39	$0.72^{+0.20}_{-0.19}$	$7.30^{+0.06}_{-0.05}$	0.50
13.2991	SWP 43085	$0.74^{+0.06}_{-0.07}$	$13.58^{+0.17}_{-0.20}$	11.05	$0.70^{+0.07}_{-0.05}$	$17.31^{+0.20}_{-0.31}$	14.59
13.3311	LWP 21716	$1.12^{+0.19}_{-0.19}$	$6.03^{+0.03}_{-0.07}$	0.90	$0.78^{+0.18}_{-0.20}$	$7.18^{+0.06}_{-0.04}$	0.91
13.3659	SWP 43086	$0.22^{+0.08}_{-0.06}$	$14.13^{+0.14}_{-0.24}$	11.17	$0.18^{+0.08}_{-0.07}$	$17.97^{+0.24}_{-0.24}$	13.69
13.4978	SWP 43088	$0.64^{+0.07}_{-0.08}$	$13.96^{+0.20}_{-0.13}$	3.25	$0.56^{+0.08}_{-0.07}$	$17.89^{+0.21}_{-0.30}$	3.84
13.5316	LWP 21717	$1.20^{+0.21}_{-0.22}$	$6.20^{+0.06}_{-0.08}$	0.97	$0.82^{+0.23}_{-0.21}$	$7.36^{+0.07}_{-0.07}$	0.95
13.5689	SWP 43089	$0.50^{+0.07}_{-0.07}$	$14.33^{+0.15}_{-0.19}$	3.77	$0.44^{+0.08}_{-0.06}$	$18.33^{+0.22}_{-0.19}$	3.87
13.5987	LWP 21718	$1.16^{+0.19}_{-0.18}$	$6.25^{+0.05}_{-0.04}$	0.50	$0.84^{+0.18}_{-0.19}$	$7.45^{+0.05}_{-0.04}$	0.56
13.6315	SWP 43090	$0.52^{+0.06}_{-0.07}$	$14.46^{+0.22}_{-0.12}$	2.56	$0.46^{+0.07}_{-0.07}$	$18.46^{+0.25}_{-0.20}$	3.14
13.6647	LWP 21719	$0.86^{+0.18}_{-0.18}$	$6.18^{+0.03}_{-0.03}$	0.55	$0.52^{+0.19}_{-0.17}$	$7.35^{+0.04}_{-0.05}$	0.64
13.6981	SWP 43091	$0.64^{+0.07}_{-0.07}$	$14.28^{+0.13}_{-0.21}$	3.18	$0.58^{+0.07}_{-0.07}$	$18.24^{+0.19}_{-0.30}$	3.75
13.7314	LWP 21720	$1.04^{+0.20}_{-0.20}$	$6.02^{+0.06}_{-0.05}$	0.86	$0.68^{+0.21}_{-0.19}$	$7.16^{+0.08}_{-0.07}$	1.01
13.7660	SWP 43092	$0.64^{+0.07}_{-0.05}$	$14.07^{+0.16}_{-0.22}$	1.64	$0.60^{+0.05}_{-0.07}$	$17.94^{+0.21}_{-0.12}$	1.97
13.7974	LWP 21721	$1.18^{+0.20}_{-0.20}$	$6.04^{+0.06}_{-0.06}$	0.77	$0.84^{+0.21}_{-0.19}$	$7.19^{+0.09}_{-0.06}$	0.83
13.8308	SWP 43093	$0.54^{+0.06}_{-0.06}$	$13.92^{+0.16}_{-0.19}$	3.38	$0.48^{+0.07}_{-0.05}$	$17.80^{+0.13}_{-0.26}$	2.32
13.8636	LWP 21722	$1.32^{+0.24}_{-0.23}$	$6.05^{+0.07}_{-0.07}$	0.39	$0.96^{+0.25}_{-0.23}$	$7.19^{+0.08}_{-0.08}$	0.47
13.8971	SWP 43094	$0.50^{+0.07}_{-0.06}$	$13.63^{+0.11}_{-0.18}$	2.77	$0.44^{+0.07}_{-0.06}$	$17.44^{+0.21}_{-0.23}$	1.61
13.9306	LWP 21723	$1.20^{+0.23}_{-0.23}$	$5.87^{+0.05}_{-0.08}$	0.69	$0.84^{+0.24}_{-0.23}$	$6.98^{+0.10}_{-0.09}$	0.77
13.9657	SWP 43095	$0.56^{+0.07}_{-0.07}$	$13.01^{+0.15}_{-0.22}$	2.01	$0.50^{+0.07}_{-0.07}$	$16.63^{+0.23}_{-0.22}$	1.66
13.9969	LWP 21724	$1.02^{+0.20}_{-0.20}$	$5.66^{+0.05}_{-0.05}$	0.52	$0.66^{+0.20}_{-0.20}$	$6.73^{+0.09}_{-0.04}$	0.57
14.0303	SWP 43096	$0.58^{+0.07}_{-0.06}$	$13.05^{+0.12}_{-0.13}$	3.92	$0.52^{+0.06}_{-0.07}$	$16.67^{+0.20}_{-0.19}$	3.55
14.0630	LWP 21725	$1.30^{+0.20}_{-0.20}$	$5.67^{+0.03}_{-0.03}$	0.77	$0.96^{+0.20}_{-0.21}$	$6.75^{+0.08}_{-0.07}$	0.86
14.0965	SWP 43097	$0.50^{+0.05}_{-0.07}$	$13.21^{+0.20}_{-0.17}$	2.29	$0.46^{+0.06}_{-0.07}$	$16.85^{+0.21}_{-0.17}$	1.69
14.1299	LWP 21726	$1.12^{+0.19}_{-0.19}$	$5.58^{+0.02}_{-0.03}$	0.17	$0.76^{+0.20}_{-0.19}$	$6.64^{+0.05}_{-0.03}$	0.22
14.1634	SWP 43098	$0.64^{+0.06}_{-0.07}$	$12.73^{+0.14}_{-0.17}$	3.20	$0.58^{+0.06}_{-0.06}$	$16.27^{+0.22}_{-0.18}$	3.60
14.1975	LWP 21727	$1.08^{+0.20}_{-0.20}$	$5.64^{+0.04}_{-0.04}$	0.46	$0.74^{+0.20}_{-0.21}$	$6.72^{+0.07}_{-0.07}$	0.47
14.2313	SWP 43099	$0.72^{+0.06}_{-0.07}$	$12.74^{+0.19}_{-0.18}$	2.06	$0.66^{+0.05}_{-0.07}$	$16.28^{+0.26}_{-0.15}$	2.33
14.2650	LWP 21728	$1.10^{+0.20}_{-0.20}$	$5.64^{+0.06}_{-0.07}$	0.92	$0.76^{+0.19}_{-0.21}$	$6.70^{+0.06}_{-0.04}$	0.96
14.5295	LWP 21730	$0.96^{+0.18}_{-0.19}$	$5.67^{+0.04}_{-0.01}$	0.52	$0.62^{+0.18}_{-0.19}$	$6.76^{+0.02}_{-0.04}$	0.57
14.5630	SWP 43101	$0.54^{+0.07}_{-0.06}$	$13.52^{+0.11}_{-0.17}$	3.15	$0.50^{+0.07}_{-0.06}$	$17.23^{+0.15}_{-0.17}$	4.08
14.5955	LWP 21731	$1.02^{+0.20}_{-0.19}$	$6.04^{+0.05}_{-0.09}$	0.99	$0.66^{+0.21}_{-0.19}$	$7.17^{+0.05}_{-0.07}$	0.88
14.6290	SWP 43102	$0.52^{+0.07}_{-0.07}$	$13.90^{+0.16}_{-0.15}$	2.14	$0.46^{+0.07}_{-0.06}$	$17.75^{+0.22}_{-0.17}$	2.41
14.6627	LWP 21732	$1.12^{+0.20}_{-0.20}$	$6.10^{+0.04}_{-0.05}$	1.01	$0.78^{+0.20}_{-0.21}$	$7.26^{+0.05}_{-0.07}$	1.09
14.6981	SWP 43103	$0.70^{+0.07}_{-0.05}$	$14.01^{+0.12}_{-0.16}$	2.19	$0.66^{+0.06}_{-0.06}$	$17.82^{+0.24}_{-0.15}$	1.89
14.7296	LWP 21733	$1.00^{+0.21}_{-0.20}$	$6.18^{+0.03}_{-0.07}$	0.78	$0.66^{+0.21}_{-0.21}$	$7.34^{+0.06}_{-0.04}$	0.74

Table 3.2 (continued)

Date (1991 Nov)	Image	α_ν^0	F_λ^0	$(\chi^2/N)^0$	α_ν	F_λ	χ^2/N
(1)	(2)	(3)	(4)	(5)	(6)	(7)	(8)
14.7628	SWP 43104	$0.64^{+0.07}_{-0.05}$	$14.61^{+0.13}_{-0.17}$	3.40	$0.60^{+0.06}_{-0.05}$	$18.63^{+0.22}_{-0.21}$	3.07
14.7957	LWP 21734	$1.18^{+0.18}_{-0.17}$	$6.46^{+0.05}_{-0.04}$	0.72	$0.84^{+0.17}_{-0.19}$	$7.69^{+0.06}_{-0.08}$	0.80
14.8291	SWP 43105	$0.76^{+0.05}_{-0.05}$	$14.37^{+0.13}_{-0.14}$	1.10	$0.70^{+0.06}_{-0.05}$	$18.39^{+0.11}_{-0.18}$	1.85
14.8614	LWP 21735	$1.02^{+0.19}_{-0.20}$	$6.41^{+0.09}_{-0.06}$	0.83	$0.64^{+0.20}_{-0.20}$	$7.60^{+0.07}_{-0.11}$	0.75
14.9169	SWP 43106	$0.64^{+0.06}_{-0.06}$	$14.76^{+0.20}_{-0.18}$	1.42	$0.58^{+0.06}_{-0.06}$	$18.86^{+0.15}_{-0.20}$	1.29
14.9282	LWP 21736	$1.08^{+0.18}_{-0.18}$	$6.31^{+0.04}_{-0.03}$	0.39	$0.72^{+0.19}_{-0.18}$	$7.51^{+0.07}_{-0.02}$	0.38
14.9617	SWP 43107	$0.70^{+0.06}_{-0.06}$	$14.44^{+0.14}_{-0.16}$	2.95	$0.66^{+0.06}_{-0.07}$	$18.36^{+0.27}_{-0.16}$	2.82
14.9947	LWP 21737	$1.38^{+0.18}_{-0.18}$	$6.38^{+0.04}_{-0.05}$	0.84	$1.04^{+0.19}_{-0.18}$	$7.58^{+0.02}_{-0.03}$	1.17
15.0284	SWP 43108	$0.58^{+0.07}_{-0.06}$	$14.57^{+0.14}_{-0.20}$	0.93	$0.54^{+0.07}_{-0.06}$	$18.56^{+0.26}_{-0.20}$	0.88
15.0514	LWP 21738	$1.22^{+0.19}_{-0.17}$	$6.37^{+0.05}_{-0.03}$	0.51	$0.88^{+0.18}_{-0.19}$	$7.58^{+0.05}_{-0.04}$	0.51
15.0945	SWP 43109	$0.58^{+0.06}_{-0.06}$	$14.38^{+0.21}_{-0.14}$	1.72	$0.52^{+0.07}_{-0.05}$	$18.39^{+0.24}_{-0.25}$	1.49
15.1279	LWP 21739	$1.30^{+0.18}_{-0.20}$	$6.21^{+0.07}_{-0.04}$	0.66	$0.94^{+0.19}_{-0.19}$	$7.39^{+0.05}_{-0.06}$	0.74
15.1623	SWP 43110	$0.60^{+0.06}_{-0.06}$	$14.08^{+0.20}_{-0.17}$	1.61	$0.54^{+0.06}_{-0.06}$	$18.01^{+0.21}_{-0.18}$	1.37
15.1944	LWP 21740	$1.12^{+0.21}_{-0.20}$	$6.19^{+0.06}_{-0.08}$	0.42	$0.76^{+0.21}_{-0.20}$	$7.36^{+0.06}_{-0.06}$	0.57
15.2133	SWP 43111	$0.68^{+0.05}_{-0.07}$	$14.15^{+0.21}_{-0.10}$	1.65	$0.62^{+0.05}_{-0.07}$	$18.09^{+0.22}_{-0.20}$	2.27
15.2624	LWP 21741	$1.16^{+0.20}_{-0.18}$	$6.35^{+0.09}_{-0.04}$	0.98	$0.80^{+0.20}_{-0.18}$	$7.54^{+0.09}_{-0.05}$	1.05
15.8248	LWP 21744	$1.22^{+0.20}_{-0.21}$	$6.09^{+0.04}_{-0.05}$	0.52	$0.86^{+0.21}_{-0.19}$	$7.24^{+0.08}_{-0.07}$	0.65
16.1680	LWP 21747	$1.10^{+0.22}_{-0.20}$	$6.64^{+0.08}_{-0.04}$	0.30	$0.74^{+0.22}_{-0.21}$	$7.88^{+0.07}_{-0.10}$	0.46
16.1896	SWP 43114	$0.62^{+0.05}_{-0.05}$	$15.26^{+0.15}_{-0.09}$	3.69	$0.56^{+0.05}_{-0.05}$	$19.54^{+0.22}_{-0.17}$	3.37
16.2324	LWP 21748	$1.04^{+0.21}_{-0.20}$	$6.66^{+0.09}_{-0.08}$	0.72	$0.68^{+0.22}_{-0.19}$	$7.91^{+0.11}_{-0.06}$	0.67
16.2544	SWP 43115	$0.64^{+0.07}_{-0.07}$	$15.43^{+0.24}_{-0.25}$	3.41	$0.60^{+0.07}_{-0.07}$	$19.65^{+0.33}_{-0.24}$	4.41
16.8210	LWP 21755	$1.12^{+0.19}_{-0.18}$	$6.81^{+0.03}_{-0.05}$	0.22	$0.78^{+0.19}_{-0.18}$	$8.10^{+0.04}_{-0.07}$	0.25
16.8411	SWP 43121	$0.60^{+0.06}_{-0.06}$	$15.68^{+0.17}_{-0.18}$	2.05	$0.54^{+0.06}_{-0.06}$	$20.02^{+0.28}_{-0.17}$	2.43
16.8824	LWP 21756	$1.26^{+0.19}_{-0.17}$	$6.93^{+0.06}_{-0.06}$	0.94	$0.90^{+0.19}_{-0.18}$	$8.24^{+0.10}_{-0.08}$	1.06
16.9031	SWP 43122	$0.56^{+0.05}_{-0.06}$	$16.09^{+0.23}_{-0.12}$	2.06	$0.50^{+0.07}_{-0.05}$	$20.56^{+0.21}_{-0.22}$	2.53
17.8139	LWP 21768	$1.12^{+0.19}_{-0.20}$	$6.52^{+0.07}_{-0.07}$	0.83	$0.76^{+0.19}_{-0.20}$	$7.74^{+0.05}_{-0.06}$	0.91
17.8410	SWP 43135	$0.70^{+0.06}_{-0.05}$	$14.94^{+0.19}_{-0.17}$	2.54	$0.66^{+0.05}_{-0.07}$	$19.02^{+0.20}_{-0.19}$	3.57
17.8920	LWP 21769	$1.26^{+0.16}_{-0.17}$	$6.61^{+0.05}_{-0.07}$	1.21	$0.90^{+0.18}_{-0.16}$	$7.86^{+0.03}_{-0.08}$	1.42
17.9081	SWP 43136	$0.60^{+0.06}_{-0.05}$	$15.32^{+0.19}_{-0.15}$	3.27	$0.56^{+0.05}_{-0.06}$	$19.52^{+0.19}_{-0.22}$	2.34
18.8152	SWP 43145	$0.68^{+0.05}_{-0.06}$	$14.08^{+0.15}_{-0.17}$	1.21	$0.62^{+0.06}_{-0.06}$	$18.01^{+0.26}_{-0.24}$	0.83
18.8679	LWP 21777	$1.20^{+0.17}_{-0.17}$	$6.20^{+0.03}_{-0.04}$	1.34	$0.86^{+0.18}_{-0.17}$	$7.38^{+0.05}_{-0.03}$	1.63
18.8842	SWP 43146	$0.74^{+0.06}_{-0.07}$	$13.71^{+0.16}_{-0.13}$	3.06	$0.66^{+0.07}_{-0.05}$	$17.58^{+0.14}_{-0.22}$	3.89
18.9392	LWP 21778	$1.12^{+0.16}_{-0.17}$	$6.31^{+0.06}_{-0.07}$	0.94	$0.74^{+0.17}_{-0.16}$	$7.50^{+0.09}_{-0.06}$	1.08
19.0222	LWP 21786	$1.44^{+0.18}_{-0.18}$	$5.88^{+0.05}_{-0.06}$	1.30	$1.10^{+0.19}_{-0.17}$	$7.00^{+0.02}_{-0.03}$	1.49
19.0354	SWP 43157	$0.74^{+0.06}_{-0.06}$	$13.23^{+0.13}_{-0.14}$	2.79	$0.70^{+0.06}_{-0.06}$	$16.86^{+0.26}_{-0.17}$	3.53
19.0778	LWP 21787	$1.20^{+0.18}_{-0.17}$	$5.92^{+0.06}_{-0.07}$	0.68	$0.86^{+0.17}_{-0.19}$	$7.04^{+0.08}_{-0.06}$	0.79
19.1026	SWP 43158	$0.88^{+0.07}_{-0.07}$	$12.81^{+0.14}_{-0.19}$	4.22	$0.82^{+0.06}_{-0.07}$	$16.36^{+0.29}_{-0.23}$	2.84
20.6954	SWP 43164	$0.72^{+0.06}_{-0.06}$	$14.36^{+0.22}_{-0.20}$	2.24	$0.68^{+0.05}_{-0.07}$	$18.30^{+0.26}_{-0.20}$	2.73
20.7398	LWP 21793	$1.04^{+0.20}_{-0.19}$	$6.58^{+0.07}_{-0.08}$	0.69	$0.70^{+0.19}_{-0.21}$	$7.82^{+0.06}_{-0.11}$	0.75
20.7505	SWP 43165	$0.92^{+0.08}_{-0.08}$	$13.70^{+0.16}_{-0.15}$	2.49	$0.84^{+0.09}_{-0.07}$	$17.55^{+0.25}_{-0.22}$	1.89
21.6726	SWP 43174	$0.78^{+0.06}_{-0.06}$	$13.70^{+0.19}_{-0.18}$	2.03	$0.72^{+0.07}_{-0.06}$	$17.51^{+0.14}_{-0.21}$	2.23
21.7180	LWP 21799	$1.06^{+0.15}_{-0.16}$	$6.18^{+0.05}_{-0.05}$	1.17	$0.70^{+0.16}_{-0.15}$	$7.33^{+0.04}_{-0.07}$	1.20
21.7472	SWP 43175	$0.78^{+0.05}_{-0.07}$	$13.57^{+0.20}_{-0.19}$	2.28	$0.74^{+0.05}_{-0.07}$	$17.29^{+0.24}_{-0.21}$	1.97
22.6616	SWP 43184	$0.52^{+0.06}_{-0.06}$	$14.05^{+0.12}_{-0.17}$	3.53	$0.48^{+0.06}_{-0.07}$	$17.92^{+0.17}_{-0.16}$	3.14

Table 3.2 (continued)

Date (1991 Nov)	Image	α_ν^0	F_λ^0	$(\chi^2/N)^0$	α_ν	F_λ	χ^2/N
(1)	(2)	(3)	(4)	(5)	(6)	(7)	(8)
22.7068	LWP 21810	$1.04^{+0.14}_{-0.15}$	$6.35^{+0.01}_{-0.02}$	0.65	$0.68^{+0.16}_{-0.14}$	$7.56^{+0.07}_{-0.02}$	0.49
22.7299	SWP 43185	$0.56^{+0.05}_{-0.07}$	$14.10^{+0.17}_{-0.17}$	3.70	$0.50^{+0.06}_{-0.05}$	$18.07^{+0.16}_{-0.29}$	2.79
22.7670	LWP 21811	$1.18^{+0.16}_{-0.17}$	$6.40^{+0.05}_{-0.03}$	0.55	$0.82^{+0.17}_{-0.15}$	$7.62^{+0.03}_{-0.04}$	0.66
23.6830	SWP 43192	$0.68^{+0.06}_{-0.06}$	$15.36^{+0.17}_{-0.21}$	1.44	$0.64^{+0.06}_{-0.06}$	$19.57^{+0.17}_{-0.30}$	2.06
23.7288	LWP 21828	$1.06^{+0.19}_{-0.18}$	$6.80^{+0.06}_{-0.04}$	0.76	$0.70^{+0.19}_{-0.18}$	$8.08^{+0.05}_{-0.07}$	0.95
23.7528	SWP 43193	$0.76^{+0.07}_{-0.06}$	$15.22^{+0.12}_{-0.16}$	1.13	$0.70^{+0.07}_{-0.06}$	$19.44^{+0.25}_{-0.30}$	0.95
24.6843	SWP 43211	$0.62^{+0.06}_{-0.05}$	$14.62^{+0.16}_{-0.14}$	3.64	$0.58^{+0.05}_{-0.06}$	$18.62^{+0.20}_{-0.14}$	2.85
24.7503	LWP 21837	$1.24^{+0.18}_{-0.18}$	$6.47^{+0.03}_{-0.05}$	0.50	$0.90^{+0.18}_{-0.19}$	$7.71^{+0.07}_{-0.06}$	0.54
25.6791	SWP 43220	$0.62^{+0.07}_{-0.05}$	$14.03^{+0.13}_{-0.18}$	2.73	$0.58^{+0.06}_{-0.07}$	$17.86^{+0.20}_{-0.25}$	2.73
25.7228	LWP 21847	$1.02^{+0.20}_{-0.20}$	$6.11^{+0.06}_{-0.05}$	0.67	$0.66^{+0.21}_{-0.20}$	$7.26^{+0.07}_{-0.05}$	0.87
25.7495	SWP 43221	$0.66^{+0.06}_{-0.06}$	$14.01^{+0.13}_{-0.20}$	3.10	$0.60^{+0.07}_{-0.05}$	$17.90^{+0.15}_{-0.25}$	2.43
26.6783	SWP 43230	$0.58^{+0.05}_{-0.07}$	$16.76^{+0.24}_{-0.20}$	1.17	$0.52^{+0.07}_{-0.06}$	$21.44^{+0.31}_{-0.23}$	1.11
26.7237	LWP 21856	$1.24^{+0.17}_{-0.18}$	$7.54^{+0.06}_{-0.03}$	0.28	$0.88^{+0.18}_{-0.18}$	$8.97^{+0.09}_{-0.06}$	0.28
26.7511	SWP 43231	$0.64^{+0.06}_{-0.05}$	$17.02^{+0.19}_{-0.15}$	2.05	$0.58^{+0.07}_{-0.05}$	$21.77^{+0.15}_{-0.33}$	1.57
27.6774	SWP 43236	$0.66^{+0.05}_{-0.07}$	$15.09^{+0.18}_{-0.16}$	2.39	$0.60^{+0.06}_{-0.06}$	$19.28^{+0.13}_{-0.19}$	2.17
27.7248	LWP 21864	$1.20^{+0.16}_{-0.15}$	$6.75^{+0.04}_{-0.04}$	0.73	$0.84^{+0.17}_{-0.15}$	$8.04^{+0.06}_{-0.07}$	0.77
27.7471	SWP 43237	$0.74^{+0.06}_{-0.06}$	$15.17^{+0.18}_{-0.16}$	1.58	$0.68^{+0.07}_{-0.06}$	$19.39^{+0.16}_{-0.23}$	1.70
28.8407	LWP 21877	$1.24^{+0.19}_{-0.17}$	$7.30^{+0.04}_{-0.03}$	0.46	$0.90^{+0.18}_{-0.19}$	$8.69^{+0.08}_{-0.04}$	0.41
28.8738	SWP 43246	$0.76^{+0.06}_{-0.07}$	$15.39^{+0.19}_{-0.12}$	1.59	$0.70^{+0.06}_{-0.07}$	$19.68^{+0.24}_{-0.13}$	1.08
28.9033	LWP 21878	$1.22^{+0.16}_{-0.14}$	$7.42^{+0.08}_{-0.03}$	0.64	$0.88^{+0.15}_{-0.15}$	$8.83^{+0.04}_{-0.03}$	0.64
28.9349	SWP 43247	$0.68^{+0.05}_{-0.06}$	$16.22^{+0.26}_{-0.18}$	3.43	$0.62^{+0.07}_{-0.05}$	$20.76^{+0.18}_{-0.31}$	2.69
29.8330	LWP 21888	$1.02^{+0.20}_{-0.19}$	$7.39^{+0.07}_{-0.10}$	0.78	$0.66^{+0.19}_{-0.19}$	$8.78^{+0.13}_{-0.10}$	0.71
29.8434	SWP 43260	$0.62^{+0.05}_{-0.06}$	$16.09^{+0.22}_{-0.16}$	2.55	$0.56^{+0.05}_{-0.06}$	$20.57^{+0.25}_{-0.13}$	1.76
29.9100	SWP 43261	$0.70^{+0.06}_{-0.06}$	$16.37^{+0.17}_{-0.18}$	1.73	$0.66^{+0.06}_{-0.05}$	$20.88^{+0.29}_{-0.29}$	2.41
29.9411	LWP 21889	$1.04^{+0.19}_{-0.18}$	$7.23^{+0.09}_{-0.08}$	0.54	$0.68^{+0.18}_{-0.19}$	$8.59^{+0.08}_{-0.08}$	0.69

(1) Date of observation (days).
(2) IUE image identification number.
(3) Spectral index ($F_\nu^0 \propto \nu^{-\alpha_\nu^0}$) derived from the undereddened spectrum.
(4) Fitted ($F_\lambda^0 \propto \lambda^{-\alpha_\lambda^0}$) spectral flux (in units of 10^{-14} erg cm^{-2} s^{-1} Å^{-1}) at 1400 Å for SWP spectra and 2800 Å for LWP spectra. No reddening correction has been applied.
(5) Reduced χ^2 associated to the fitted parameters α_ν^0 and F_λ^0.
(6) Spectral index ($F_\nu \propto \nu^{-\alpha_\nu}$) derived after correcting the spectrum for the extinction $A_{1'} = 0.1$.
(7) Fitted ($F_\lambda \propto \lambda^{-\alpha_\lambda}$) spectral flux (in units of 10^{-14} erg cm^{-2} s^{-1} Å^{-1}) at 1400 Å for SWP spectra and 2800 Å for LWP spectra. The dereddening for $A_{1'} = 0.1$ has been applied.
(8) Reduced χ^2 associated to the fitted parameters α_ν and F_λ.

Table 3.3: Combined Spectra of PKS 2155-304

Combined images	α_ν^0	F_λ^0	$(\chi^2/N)^0$	α_ν	F_λ	χ^2/N
(1)	(2)	(3)	(4)	(5)	(6)	(7)
SWP 42969 + LWP 21607	0.80±0.03	5.279±0.004	4.85	0.70±0.03	6.542±0.004	4.66
SWP 42970 + LWP 21608	0.81±0.03	5.499±0.012	1.54	0.71±0.03	6.819±0.023	1.56
SWP 42971 + LWP 21609	0.79±0.03	5.511±0.010	3.21	0.70±0.03	6.832±0.019	2.59
SWP 42972 + LWP 21610	0.75±0.03	5.682±0.009	2.94	0.65±0.03	7.053±0.014	3.61
SWP 42972 + LWP 21611	0.78±0.03	5.708±0.009	3.10	0.68±0.03	7.084±0.017	3.53
SWP 42979 + LWP 21616	0.76±0.03	6.324±0.010	1.71	0.66±0.03	7.850±0.008	1.75
SWP 42980 + LWP 21617	0.70±0.03	6.304±0.014	2.67	0.60±0.03	7.823±0.040	2.53
SWP 42995 + LWP 21625	0.72±0.03	6.297±0.014	1.52	0.62±0.03	7.821±0.021	1.20
SWP 42996 + LWP 21626	0.76±0.03	6.479±0.010	0.79	0.65±0.03	8.055±0.022	0.82
SWP 43008 + LWP 21636	0.78±0.03	7.282±0.021	2.54	0.68±0.03	9.055±0.023	2.41
SWP 43009 + LWP 21637	0.81±0.03	7.226±0.005	2.25	0.71±0.03	8.970±0.010	1.78
SWP 43017 + LWP 21644	0.74±0.03	7.442±0.018	1.48	0.64±0.03	9.238±0.020	1.23
SWP 43018 + LWP 21645	0.77±0.03	7.576±0.016	2.03	0.68±0.03	9.416±0.020	1.60
SWP 43025 + LWP 21652	0.96±0.03	7.083±0.016	2.78	0.86±0.03	8.814±0.018	2.67
SWP 43026 + LWP 21653	0.86±0.03	6.854±0.006	2.91	0.76±0.03	8.503±0.019	2.43
SWP 43026 + LWP 21654	0.85±0.03	6.848±0.012	2.39	0.76±0.03	8.496±0.005	1.88
SWP 43040 + LWP 21667	0.97±0.04	7.591±0.010	4.61	0.87±0.04	9.441±0.017	3.92
SWP 43041 + LWP 21668	0.78±0.03	8.252±0.015	4.47	0.68±0.03	10.260±0.013	3.87
SWP 43047 + LWP 21673	0.81±0.03	8.460±0.007	3.09	0.71±0.03	10.510±0.027	2.57
SWP 43048 + LWP 21674	0.78±0.03	8.638±0.038	1.69	0.68±0.03	10.730±0.030	1.30
SWP 43054 + LWP 21683	0.72±0.03	9.137±0.011	4.04	0.63±0.03	11.360±0.021	3.28
SWP 43055 + LWP 21684	0.76±0.02	9.172±0.021	5.59	0.65±0.02	11.370±0.008	4.45
SWP 43056 + LWP 21685	0.76±0.03	9.277±0.008	2.33	0.66±0.03	11.550±0.021	1.76
SWP 43057 + LWP 21686	0.75±0.03	9.481±0.017	2.18	0.66±0.03	11.810±0.041	1.92
SWP 43058 + LWP 21687	0.76±0.03	9.310±0.015	4.46	0.65±0.03	11.580±0.033	3.10
SWP 43059 + LWP 21688	0.75±0.03	9.451±0.044	2.52	0.65±0.03	11.730±0.026	2.38
SWP 43060 + LWP 21689	0.66±0.03	9.390±0.011	3.57	0.57±0.03	11.660±0.029	2.91
SWP 43061 + LWP 21690	0.72±0.03	9.637±0.013	3.77	0.62±0.03	11.970±0.026	2.47
SWP 43062 + LWP 21691	0.72±0.03	9.940±0.016	3.21	0.62±0.03	12.350±0.033	2.69
SWP 43063 + LWP 21692	0.81±0.03	9.856±0.024	4.66	0.71±0.03	12.230±0.019	5.37
SWP 43064 + LWP 21693	0.83±0.03	9.564±0.023	10.79	0.73±0.03	11.870±0.025	10.45
SWP 43065 + LWP 21696	0.81±0.03	9.847±0.016	3.15	0.71±0.03	12.210±0.018	2.75
SWP 43066 + LWP 21697	0.83±0.02	9.993±0.009	3.32	0.72±0.02	12.410±0.044	2.38
SWP 43067 + LWP 21698	0.79±0.03	10.010±0.022	3.92	0.71±0.03	12.460±0.035	2.60
SWP 43068 + LWP 21699	0.81±0.03	10.130±0.019	3.49	0.72±0.03	12.620±0.035	2.65
SWP 43069 + LWP 21700	0.81±0.03	10.090±0.020	2.64	0.71±0.03	12.540±0.016	1.88
SWP 43070 + LWP 21701	0.80±0.03	9.881±0.009	3.31	0.70±0.03	12.290±0.034	2.26
SWP 43071 + LWP 21702	0.79±0.03	9.538±0.004	2.45	0.69±0.03	11.870±0.029	2.55
SWP 43073 + LWP 21704	0.99±0.03	9.245±0.031	1.74	0.88±0.03	11.490±0.030	1.97
SWP 43074 + LWP 21705	0.81±0.03	9.427±0.006	2.57	0.71±0.03	11.710±0.019	2.08
SWP 43075 + LWP 21706	0.83±0.03	9.402±0.004	3.99	0.73±0.03	11.690±0.011	3.39
SWP 43076 + LWP 21707	0.81±0.02	9.593±0.018	2.39	0.71±0.03	11.920±0.012	1.82
SWP 43077 + LWP 21708	0.81±0.03	9.748±0.027	2.98	0.71±0.03	12.110±0.027	2.32
SWP 43078 + LWP 21709	0.82±0.02	9.796±0.024	3.71	0.72±0.02	12.170±0.026	2.52

Table 3.3 (continued)

Combined images	α_ν^0	F_λ^0	$(\chi^2/N)^0$	α_ν	F_λ	χ^2/N
(1)	(2)	(3)	(4)	(5)	(6)	(7)
SWP 43079 + LWP 21710	0.82±0.03	9.666±0.013	4.74	0.72±0.03	12.040±0.030	3.34
SWP 43080 + LWP 21711	0.84±0.03	9.960±0.020	2.78	0.74±0.03	12.380±0.023	2.16
SWP 43081 + LWP 21712	0.78±0.03	9.730±0.035	1.94	0.68±0.03	12.100±0.042	1.64
SWP 43082 + LWP 21713	0.79±0.03	9.467±0.023	1.47	0.69±0.03	11.760±0.012	1.05
SWP 43083 + LWP 21714	0.79±0.03	9.233±0.030	3.02	0.70±0.03	11.470±0.003	3.08
SWP 43084 + LWP 21715	0.80±0.03	9.025±0.028	1.96	0.71±0.03	11.230±0.023	2.12
SWP 43085 + LWP 21715	0.86±0.03	8.838±0.020	5.06	0.76±0.03	11.010±0.034	6.13
SWP 43086 + LWP 21716	0.88±0.03	8.377±0.006	13.30	0.78±0.03	10.420±0.023	13.00
SWP 43088 + LWP 21717	0.86±0.03	8.991±0.015	3.10	0.76±0.03	11.170±0.014	2.77
SWP 43089 + LWP 21718	0.86±0.03	9.010±0.026	4.96	0.76±0.03	11.180±0.017	4.01
SWP 43090 + LWP 21719	0.82±0.03	9.088±0.016	3.48	0.73±0.03	11.280±0.017	3.26
SWP 43091 + LWP 21720	0.76±0.03	8.995±0.021	2.27	0.66±0.03	11.170±0.037	2.18
SWP 43092 + LWP 21721	0.78±0.03	8.882±0.013	1.91	0.68±0.03	11.050±0.011	1.55
SWP 43093 + LWP 21722	0.79±0.03	8.648±0.022	3.94	0.70±0.03	10.750±0.006	2.67
SWP 43094 + LWP 21723	0.77±0.03	8.414±0.021	3.86	0.68±0.03	10.480±0.055	2.73
SWP 43095 + LWP 21724	0.83±0.03	8.180±0.013	2.74	0.73±0.03	10.170±0.034	2.14
SWP 43096 + LWP 21725	0.79±0.03	8.192±0.032	3.50	0.70±0.03	10.180±0.008	2.76
SWP 43097 + LWP 21726	0.80±0.03	8.124±0.006	3.97	0.70±0.03	10.110±0.016	2.59
SWP 43098 + LWP 21727	0.82±0.03	8.108±0.021	2.60	0.73±0.03	10.090±0.044	2.37
SWP 43099 + LWP 21728	0.83±0.03	8.238±0.021	1.81	0.73±0.03	10.230±0.032	1.57
SWP 43101 + LWP 21730	0.77±0.03	8.386±0.026	3.00	0.68±0.03	10.430±0.023	2.81
SWP 43102 + LWP 21731	0.82±0.03	8.709±0.006	3.52	0.73±0.03	10.830±0.014	3.02
SWP 43103 + LWP 21732	0.81±0.03	8.993±0.007	1.90	0.71±0.03	11.170±0.024	1.43
SWP 43104 + LWP 21733	0.77±0.03	9.192±0.028	2.59	0.66±0.02	11.440±0.035	1.92
SWP 43105 + LWP 21734	0.85±0.02	9.379±0.005	1.56	0.75±0.02	11.660±0.030	1.29
SWP 43106 + LWP 21735	0.80±0.03	9.374±0.030	1.81	0.70±0.03	11.650±0.014	1.39
SWP 43107 + LWP 21736	0.81±0.03	9.257±0.004	1.88	0.71±0.03	11.500±0.026	1.43
SWP 43108 + LWP 21737	0.83±0.03	9.193±0.017	3.10	0.73±0.03	11.420±0.024	2.02
SWP 43109 + LWP 21738	0.85±0.03	9.118±0.016	3.47	0.75±0.03	11.340±0.028	2.37
SWP 43110 + LWP 21739	0.83±0.03	8.915±0.017	2.88	0.73±0.03	11.090±0.045	1.98
SWP 43111 + LWP 21740	0.80±0.03	9.054±0.024	1.56	0.70±0.03	11.250±0.010	1.50
SWP 43111 + LWP 21741	0.84±0.03	9.130±0.028	2.16	0.74±0.03	11.350±0.017	1.95
SWP 43114 + LWP 21747	0.81±0.03	9.665±0.010	3.67	0.71±0.03	12.030±0.043	2.77
SWP 43115 + LWP 21748	0.82±0.03	9.790±0.012	2.86	0.72±0.03	12.180±0.040	2.59
SWP 43121 + LWP 21755	0.83±0.03	9.909±0.024	2.69	0.73±0.03	12.310±0.020	2.12
SWP 43122 + LWP 21756	0.80±0.03	10.030±0.020	3.73	0.71±0.03	12.480±0.033	2.80
SWP 43135 + LWP 21768	0.81±0.03	9.570±0.015	1.98	0.71±0.03	11.900±0.008	2.01
SWP 43136 + LWP 21769	0.80±0.03	9.629±0.024	3.90	0.70±0.02	11.970±0.020	2.51
SWP 43145 + LWP 21777	0.84±0.02	9.035±0.017	2.57	0.74±0.02	11.230±0.025	1.78
SWP 43146 + LWP 21778	0.89±0.03	9.013±0.018	2.47	0.79±0.03	11.200±0.012	2.52
SWP 43157 + LWP 21786	0.84±0.03	8.558±0.020	3.35	0.74±0.02	10.650±0.023	2.73
SWP 43158 + LWP 21787	0.88±0.03	8.570±0.017	2.66	0.78±0.03	10.660±0.022	1.75
SWP 43164 + LWP 21793	0.89±0.03	9.377±0.023	2.09	0.79±0.03	11.660±0.027	1.95
SWP 43165 + LWP 21793	0.94±0.03	9.348±0.009	1.39	0.84±0.03	11.610±0.033	1.24
SWP 43174 + LWP 21799	0.85±0.02	8.979±0.020	1.71	0.75±0.02	11.170±0.027	1.58

Table 3.3 (continued)

Combined images	α_ν^0	F_λ^0	$(\chi^2/N)^0$	α_ν	F_λ	χ^2/N
(1)	(2)	(3)	(4)	(5)	(6)	(7)
SWP 43175 + LWP 21799	0.87±0.02	8.916±0.006	1.91	0.77±0.02	11.100±0.023	1.50
SWP 43184 + LWP 21810	0.91±0.03	8.931±0.018	5.98	0.81±0.03	11.110±0.006	4.74
SWP 43185 + LWP 21811	0.91±0.03	8.953±0.027	5.37	0.80±0.03	11.160±0.029	3.91
SWP 43192 + LWP 21828	0.88±0.02	9.935±0.016	2.99	0.77±0.02	12.350±0.024	2.43
SWP 43193 + LWP 21828	0.88±0.02	9.994±0.027	2.18	0.77±0.02	12.400±0.042	1.60
SWP 43211 + LWP 21837	0.84±0.03	9.321±0.022	3.77	0.74±0.03	11.580±0.029	2.49
SWP 43220 + LWP 21847	0.81±0.03	8.906±0.018	2.49	0.72±0.03	11.070±0.017	2.22
SWP 43221 + LWP 21847	0.81±0.03	8.932±0.025	2.38	0.71±0.03	11.110±0.025	1.86
SWP 43230 + LWP 21856	0.87±0.03	10.680±0.017	3.27	0.77±0.03	13.280±0.043	2.29
SWP 43231 + LWP 21856	0.84±0.03	10.870±0.025	2.52	0.74±0.03	13.510±0.028	1.56
SWP 43236 + LWP 21864	0.85±0.03	9.704±0.026	2.89	0.76±0.03	12.050±0.026	1.95
SWP 43237 + LWP 21864	0.84±0.03	9.832±0.021	1.78	0.74±0.03	12.220±0.025	1.18
SWP 43246 + LWP 21877	0.93±0.03	10.260±0.024	1.95	0.84±0.03	12.750±0.047	1.22
SWP 43247 + LWP 21878	0.90±0.03	10.500±0.032	3.65	0.79±0.02	13.070±0.040	2.35
SWP 43260 + LWP 21888	0.90±0.03	10.410±0.019	4.27	0.80±0.03	12.950±0.017	3.26
SWP 43261 + LWP 21889	0.86±0.03	10.570±0.024	2.34	0.76±0.03	13.160±0.013	1.89

(1) IUE image identification numbers of combined spectra.
(2) Spectral index ($F_\nu^0 \propto \nu^{-\alpha_\nu^0}$) derived from the undereddened spectrum.
(3) Fitted ($F_\lambda^0 \propto \lambda^{-\alpha_\lambda^0}$) spectral flux (in units of 10^{-14} erg cm^{-2} s^{-1} Å^{-1}) at 2000 Å.
No reddening correction has been applied.
(4) Reduced χ^2 associated to the fitted parameters α_ν^0 and F_λ^0.
(5) Spectral index ($F_\nu \propto \nu^{-\alpha_\nu}$) derived after correcting the spectrum for the extinction $A_{V'} = 0.1$.
(6) Fitted ($F_\lambda \propto \lambda^{-\alpha_\lambda}$) spectral flux (in units of 10^{-14} erg cm^{-2} s^{-1} Å^{-1}) at 2000 Å.
The reddening correction for $A_{V'} = 0.1$ has been applied.
(7) Reduced χ^2 associated to the fitted parameters α_ν and F_λ.

Appendix A

Multifrequency observations of BL Lac Objects

The UV to near IR spectral flux distribution of four BL Lac objects.[a]

R. Falomo[1], A. Treves[2], L. Chiappetti[3], L. Maraschi[4], E. Pian[2], and E.G. Tanzi[3]

[1] Osservatorio Astronomico di Padova, v. Osservatorio 5, 35122, Padova, Italy

[2] Scuola Internazionale Superiore di Studi Avanzati, Strada Costiera 11, 34014 Trieste, Italy

[3] Istituto di Fisica Cosmica, CNR, via Bassini 15, 20133 Milano, Italy

[4] Dipartimento di Fisica Universitá di Genova, Italy

Accepted for publication on The Astrophysical Journal

1992 June

[a] *Based on observations obtained at the European Southern Observatory, La Silla, Chile, and with the International Ultraviolet Explorer collected at the ESA Tracking Station at Villafranca*

ABSTRACT

We report on simultaneous UV, optical and near–IR observations of four BL Lac objects. For three objects (PKS 0118–27, PKS 0301–24 and PKS 1538+14) we find that the spectral flux distribution from 8×10^{13} to 2.5×10^{15} Hz is well described by a single power law with spectral index $\alpha_\nu = 1.2$, $\alpha_\nu = 1.0$ and $\alpha_\nu = 1.3$ respectively. For H 0323+02, after subtraction of the contribution due to the host galaxy, the spectral emission is again consistent with a single, flatter power law, $\alpha_\nu = 0.78$.

1. INTRODUCTION

In general the overall spectral flux distribution (SFD) of BL Lac objects cannot be described by a single power law ($f_\nu \propto \nu^{-\alpha}$). More complex forms, like broken power laws or a continuous steepening with increasing frequency (e.g. Landau et al. 1986, Cruz-Gonzales and Huchra 1984, Ballard et al. 1990, Brown et al. 1989) are used depending on the considered energy range. Spectral "breaks" are seen to occur between near-IR and optical or between optical and UV frequencies (*e.g.* Ghisellini et al. 1986). These observed "features" may be intrinsic to the non-thermal emission component or be due to other causes like reddening, a contribution from the host galaxy and/or lack of simultaneity among observations in different bands. The contribution of starlight from the galaxy, if non negligible with respect to the non-thermal emission, produces a steepening of the energy distribution in the optical and a flattening in the near-IR, while reddening introduces a steepening of the continuum at optical - UV frequencies. For instance the spectral break observed in some objects between near-IR and optical is completely removed when proper reddening corrections are applied (*e.g.* Tanzi et al. 1989).

The non-thermal emission is usually interpreted as due to the synchrotron or synchrotron self-Compton processes. A detailed study of the spectral shape of the non thermal component is clearly important in order to understand the physics of the emission region. In fact the observed "features" (as spectral breaks) if intrinsic to the emission may be associated to energy losses of the relativistic electrons.

We report here on quasi simultaneous (within days) UV, optical and near-IR observations of four BL Lac objects obtained in the course of our system-

atic multifrequency study of BL Lacs (see *e.g.* Tanzi et al.1986; Falomo et al. 1988, 1989; Treves et al.1989; Falomo and Treves 1990). For the three objects PKS 0118–27, PKS 0301–24 and PKS 1538+14 the UV observations are the first obtained thus far, while for H 0323+02 the UV spectrum is of higher quality than reported before.

2. TARGET OBJECTS

Three of the objects are bright, compact (flat spectrum) radio sources identified as BL Lac objects (variable, polarized, featureless continuum), while the fourth one derives from the $HEAO-1$ X-ray survey.

a) PKS 0118–27

The optical magnitude ranges between $m_V = 15.5$ and $m_V = 17.0$ (Condon Hicks and Jauncey 1977; Thompson Djorgovski and De Carvalho 1990). The polarization has been measured by Impey and Tapia (1988, 1990) who report the value of 17.4%. IR optical photometry is given by Adam (1985), Tanzi et al. (1989), Allen et al. (1982), Ballard et al. (1990) and Mead et al. (1990), who also observed a high and constant polarization. The X-ray flux observed by the *Einstein* satellite is 0.14 μJy at 1 keV (Ledden and O' Dell 1985). An absorption redshift $z = 0.559$ was recently determined by Falomo (1991) from an intervening absorption feature attributed to the MgII doublet.

b) PKS 0301–24

The optical magnitude ranges between 16.0 and 17.0 (Condon Hicks and Jauncey 1977; Pica et al. 1980, 1988). Optical polarimetry by Impey and

Tapia (1988, 1990) gave an average polarization of 10.6%. Near-IR observations were gathered by Allen et al. (1982), Wright Ables and Allen (1983) and Bersanelli et al. (1992). Thus far there is no X-ray detection, nor a redshift estimate.

c) PKS 1538+14

The optical identification ($m_V = 15.5$) and the spectroscopic confirmation are due to Wills and Wills (1974) who have been led to recognize it as a BL Lac object. Optical monitoring of the source by Kinman (1976) and Pica et al. (1988) evidenced a variability in the visual band of almost 2 mag ($17.2 \leq m_V \leq 19$) and a weaker one in the blue band (Kidger, 1988). The maximum optical polarization measured by Impey and Tapia (1990) was of 20%. The results of *IRAS* far IR observations are reported by Impey and Neugebauer (1988) who also give the overall energy distribution which is peaked in the far infrared. Observations in the millimetric spectral range are reported by Edelson (1987) and near IR measurements have been performed by Allen et al. (1982) and Bersanelli et al. (1992). The X-ray flux detected by *Einstein* is 0.15 μJy at 1 keV (Ledden and O'Dell 1985). The redshift $z = 0.605$ is reported by Stickel et al. (1992).

d) H 0323+02

The flaring X-ray source H 0323+02 was independently noted by Doxsey et al. (1981) and Piccinotti et al. (1982) because of its dramatic variability and is well studied at all frequencies (Feigelson et al. 1986, and references therein). The redshift $z = 0.147$ has been measured by Filippenko et al. (1986). The near infrared flux emission has been studied by Ballard et al. (1990). The visual magnitude ranges from 15.5 to 17.5 (Doxsey et

al. 1983; Feigelson et al. 1986 and Pica et al. 1988) with short term fluctuations.

The X-ray flux in the energy range 2-10 keV varied by about a factor of 3 between $\simeq 1\ \mu Jy$ and $3\ \mu Jy$ with an occasional flare up to $10\ \mu Jy$ during a 6 month period (Doxsey et al. 1983), whereas the *Einstein* IPC data exhibited a 60 seconds dip of a factor of ~ 11 at X-ray energies greater than 0.6 keV but not at 1/4 keV. The data following the 60 seconds dip showed that the X-ray emission at 1 keV varied smoothly between 4.8 and $6.4\ \mu Jy$. *GINGA* observations by Ohashi (1989) in the range 2-30 keV yielded a dramatic variation of the flux in 5 hours from $1.1\ \mu Jy$ to $0.4\ \mu Jy$.

3. OBSERVATIONS

a) Ultraviolet spectra

UV observations (see Table 1 for a journal of observations) were obtained using both the Short Wavelength Primary (SWP; range: 1200-1950 Å) and the Long Wavelength Primary (LWP; range: 2000-3200 Å) cameras onboard of the *International Ultraviolet Explorer* (IUE). The sources were centered in the blind offset mode in the large aperture ($10'' \times 20''$ oval) at coordinates measured on a blue POSS paper copy or on ESO plates. IUE line-by-line images have been calibrated in flux using curves provided by Bohlin and Holm (1980) for the SWP camera and Cassatella Lloyd and Gonzales (1989) for the LWP camera. Net spectra have been extracted using an implementation of the Gaussian extraction procedure GEX (Urry and Reichert, 1988) developed by one of us (LC) and running within the *MIDAS* interactive analysis system produced at ESO.

The spectrum of PKS 1538+14 was at the limit of detectability, but still clearly visible in the line-by-line spectrum. For this case only the extraction criteria of Urry and Reichert have been relaxed: the default procedure first makes a fit of the background and computes the rms of the residuals around this fit in the region where signal is expected, then proceeds to signal extraction only if the average signal is > rms/2. In our case we have loosened this constraints to be > rms/3 to give evidence to the very faint signal.

Fig. 1 shows the extracted UV spectra of the four objects. For the purpose of fitting the flux data were binned in wavelength intervals of 50 Å or 100 Å, after some spectral regions, heavily affected by camera artifacts and cosmic rays hits, had been excluded. The associated errors are the standard deviations in the considered wavelength intervals divided by $\sqrt{N/3}$, where N is the number of pixels contained in each wavelength interval. This follows from the finding of a correlation length of $\simeq 3$ pixels in the cameras response, which roughly corresponds to their resolution (see Edelson et al. 1991 and Kinney et al. 1991). The UV spectrum of each object (jointly in LWP and SWP cameras when observations from both were available) was fitted by a single power law $F_\lambda \propto \lambda^{-\alpha}$ (see Fig. 1). The interval of confidence at the 90 % level associated to the spectral index has been evaluated after Avni (1976) and Lampton et al. (1976). Spectral indices are reported in the caption of Figure 1.

Besides these UV spectra we retrieve from IUE archive two previous observations of H 0323+02 obtained in 1984 and 1988. These spectra, processed using the same procedure described above, are reported in Fig 2.

b) Optical spectrophotometry

Optical spectrophotometry of the sources was obtained at the European

Southern Observatory (ESO) 1.5m telescope equipped with a Boller and Chivens spectrograph and CCD detector. Spectra were taken at a resolution of $\approx$ 15 Å (FWHM) through a long slit of 8 arcsec width. Standard reduction procedures were applied to obtain flux calibrated spectra. From repeated observations of standard stars (Stone 1977; Baldwin and Stone 1984) during each night, we derive a photometric accuracy better than 10 %. To increase the signal-to-noise ratio we obtained fluxes at intervals spaced of $\sim$ 100 Å binning the spectra over bands of 100 Å.

c) Near IR photometry

J,H,K and L photometry was obtained (see Table 1) at the ESO 2.2m telescope (+ InSb photometer). A 15 arcsec circular aperture with chopper throw of 20 arcsec in the E–W direction was used. Statistical 1-σ errors are less than 0.1 mag in all bands. Conversion to flux units is made according to the zero–magnitude fluxes given in Bersanelli, Bouchet and Falomo (1991).

4. OVERALL SPECTRA

A composite spectral flux distribution (SFD) was constructed for each object from quasi simultaneous IR, optical and UV observations. Errors in the UV were computed combining the statistical errors of each band (see previous paragraph) with a 10% systematic error. Data were corrected for interstellar reddening using A_V as deduced from the hydrogen column density (Stark et al. 1984) and assuming $N_H/E_{B-V} = 5.8 \times 10^{21}$ (Bohlin, Savage and Drake 1978). The interstellar extinction curve of Savage and Mathis (1979) for the optical-UV region and its extension to the IR by Whittet (1988) were used. The adopted values of A_V are given in the captions of

figures 3, 4 and 5 and 6.

a) PKS 0118–27

The spectral flux distribution of PKS 0118–27 is reported in Fig. 3. We find that a single power law of $\alpha_\nu = 1.17 \pm 0.03$ is a good representation of the non thermal emission from 8×10^{13} to 1.2×10^{15} Hz. There is no spectral signature in the SFD of the presence of a host galaxy.

b) PKS 0301–24

The overall spectral flux distribution of PKS 0301–24 from 1.2×10^{14} to 2.4×10^{15} Hz (see Fig. 4) can be described by a single power law of index $\alpha = 1.01 \pm 0.03$ ($\chi^2_\nu \sim 1.9$). Although the data appear to be consistent with a single power law model there are some deviations which could be real.

The near-IR to optical region exhibits a small curvature. Spectral indices in the optical and near-IR regions indicate that some curvature (break ?) may be present at 5×10^{14} Hz ($\alpha_{opt} = 1.17 \pm 0.04$; $\alpha_{IR} = 0.83 \pm 0.22$). This could arise from the thermal contribution due to the host galaxy. To test this hypothesis we decomposed the spectrum into a power law plus an elliptical galaxy (assuming $z = 0.2$). We find the data are well fitted ($\chi^2_\nu \sim 0.9$) by the model with $\alpha_\nu = 0.84$ and a galaxy contributing 10% of total flux at 5500 Å. This corresponds to a galaxy of $M_V \sim -22$.

c) PKS 1538+14

This is the faintest source among those observed and in fact it is at the limit of detectability with IUE, In the observed spectral range (1.2×10^{14} to 1.2×10^{15} Hz the dereddened SFD (see fig 5) is consistent with a simple

power law model of $\alpha = 1.33 \pm 0.08$ ($\chi^2_\nu \sim 0.2$). We note, however, that a fit to the optical spectrum alone gives a significant steeper spectral index ($\alpha \sim 1.8$). This steeper value was repeatedly observed also at different other epochs (Falomo et al.1992).

d) H 0323+02

The X-ray selected BL Lac object H 0323+02 (Doxsey et al. 1983) is known to reside in a giant elliptical galaxy of $M_V \sim -22$ (Feigelson et al. 1986; Fillipenko et al.1986) which contributes substantially to the observed flux in the near-IR and optical range. Our overall spectrum (see Fig. 6) shows in fact a clear signature of a stellar population which flattens the energy distribution in the near-IR with respect to the optical.

To study the non thermal component, we decomposed the UV–optical to IR spectral flux distribution into a giant elliptical superposed onto a single power law emission. We assumed the standard elliptical of Yee and Oke (1978) with the near–IR colors of Arimoto and Yoshii (1987) for the thermal component and a single power law ($f_\nu \propto \nu^{-\alpha}$) for the non thermal source.

We found that the observations can be well fitted by the superposition of the (standard) elliptical galaxy, contributing 25% of the observed flux at 5500 Å, plus a flat non thermal component of spectral index $\alpha_\nu = 0.78$. The absolute magnitude of the host galaxy as derived from the decomposition of the SFD is $M_V = -21.6$ assuming $H_0 = 50$; $q_0 = 0$. This decomposition is consistent with that performed by Filippenko et al. (1986) using only optical spectrum and indicates that the non thermal component described by a flat power law extends from 2×10^{14} to 5×10^{15} Hz.

The source was observed with IUE at previous epochs (see Figure 2 and Table 2). It is apparent that no significant variability in the intensity and

spectral shape is present within the errors.

5. DISCUSSION AND CONCLUSIONS

We obtained quasi-simultaneous observations at various wavelengths for 4 BL Lac objects. This allows to study the broad band continuum from IR to UV taking into account the reddening correction and the contribution from the host galaxy.

We found that in all cases observed the SFD is well accounted for either by a single power law ($f_\nu \propto \nu^{-\alpha}$) or by a power law plus an elliptical galaxy. The large polarization observed in the optical together with the continuity of the spectral shape strongly suggests that in the entire IR to UV range the dominant emission mechanism is synchrotron radiation. There is no clear signature in the overall spectra observed of a steepening of the non thermal continuum, indicating that energy losses of relativistic electrons would occur at higher frequencies than UV.

It may be noticeable that the slope for H 0323+02, $\alpha_\nu = 0.78$, which is an X-ray selected object is flatter than that of PKS 0118–27 and PKS 0301–24 and PKS 1538+14, which instead are radio-selected. This agrees with our findings based on the examination of archival data of a collection of 33 IUE observed BL Lacs (Maraschi et al. 1986; Ghisellini et al. 1986) and confirmed by Bersanelli et al (1992) for a large set of homogeneous IR measurements of BL Lacs.

The power law which describes the non thermal component in the IR–UV domain can be extrapolated to the X-ray band and compared with the observed flux. In the case of PKS 1538+14 and H 0323+02 the extrapolation

is consistent, within the uncertainty, with the *Einstein* fluxes at 1 keV. The expected flux for PKS 0118–27 is a factor $\sim$ 5 higher than the observed one, which may be attributed to a steepening of the spectrum or to non simultaneous observations. We note that the optical UV observations were taken during a high state of the source. Finally, the extrapolated flux for PKS 0301-24 is $\sim$ 2.7 μJy at 1 keV. Therefore the source should be successfully detected with the *ROSAT* satellite.

References

Adam 1985, A&AS, **61**, 225.

Allen, D.A., Ward, M.J., and Hyland, A.R. 1982, MNRAS, **199**, 969.

Arimoto and Yoshii 1987, A&A, **173**, 23.

Avni, Y. 1976, ApJ, **210**, 642.

Baldwin, J.A., and Stone, R.P.S. 1984 MNRAS, **206**, 241.

Ballard, K.R., Mead, A.R.G., Brand, P.W.J.L., and Hough, J.H. 1990, MNRAS, **243**, 640.

Bersanelli, M., Bouchet, P., and Falomo, R. 1991, A&A, 252, 854.

Bersanelli, M. Bouchet, P., Falomo, R., and Tanzi, E. G. 1992, AJ , in press.

Bohlin, R.C., and Holm, A.V. 1980, *IUE NASA Newsletter*, 10, 37

Bohlin, R.C., Savage, B.D., and Drake, J.F. 1978, ApJ,**224**, 132.

Brown et al.1989 ApJ, **340**, 129.

Cassatella, A., Lloyd, C., and Gonzales Riestra,R. 1988, IUE ESA Newsletter 35,225.

Condon, J.J., Hicks, P.D., and Jauncey, D.L. 1977, AJ , **82**, 692.

Cruz-Gonzalez I., Huchra J.P. 1984, AJ , **89**, 441.

Doxsey, R.E., McClintock, J.E., Petro, L., Remillard, R., and Schwartz, D.A. 1981, Bull. AAS, **13**, 558.

Doxsey, R., Bradt, H., McClintock, J., Petro, L., Remillard, R., Ricker, G., Schwartz, D., and Wood, K. 1983, ApJ, **264**, L43.

Edelson, R.A. 1987, AJ , **94**, 1150.

Edelson, R., Pike, G.F., Saken, J.M., Kinney, A., and Shull, J.M. 1991, ApJS, *submitted*

Elvis, M., Lockman, F. J., and Wilkes, B. J. 1989, AJ , **97**, 777.

Falomo,R., Bouchet, P., Maraschi,L., Tanzi,E.G., Treves,A. 1988, ApJ, **335**, 122.

Falomo, R., Bouchet, P., Maraschi, L. , Tanzi, E.G., Treves,A. 1989, ApJ, **345**, 148.

Falomo, R., Melnick, J., and Tanzi, E. G. 1990, Nat, **345**, 692.

Falomo, R. 1991, AJ , 102, 1991.

Falomo, R. and Treves, A. 1991, PASP, .

Feigelson, E.D., Bradt, H., McClintock, J., Remillard, R., Urry, C.M., Tapia, S., Geldzahler, B., Johnston, K., Romanishin, W., Wehinger, P.A., Wyckoff, S., Madejski, G., Schwartz, D.A., Thorstensen, J., and Schaefer, B.E. 1986, ApJ, **302**, 337.

Filippenko, A.V., Djorgovski, S., Spinrad, H., and Sargent, W. L. W. 1986, AJ , **91**, 49.

Ghisellini, G., Maraschi, L., Tanzi, E.G., and Treves, A. 1986, ApJ, **310**, 317.

Impey, C.D. and Neugebauer, G. 1988, AJ , **95**, 307.

Impey, C.D. and Tapia, S. 1988, ApJ, **333**, 666.

Impey, C.D. and Tapia, S. 1990, ApJ, **354**, 124.

Kidger, M. R. 1988, PASP, **100**, 1248.

Kinman, T.D. 1976, ApJ, **205**, 1.

Kinney, A., Bohlin, R., and Neill, J. 1991, PASP, **103**, 694.

Lampton, M., Margon, B., and Bowyer, S. 1976, ApJ, **208**, 177.

Landau, R. et al. 1986, ApJ, **308**, 78.

Ledden, J.E., and O'Dell, S.L. 1985, ApJ, **298**, 630.

Margon, B., and Jacoby, G.H. 1984, ApJ, **286**, L31.

Maraschi L., Ghisellini G., Tanzi E.G., Treves A. 1986, ApJ, **310**, 325

Mead, A. R. G., Ballard, K. R., Brand P. W. J. L., Hough, J. H., Brindle, C., and Bailey, J. A. 1990, A&AS, **83**, 183.

Ohashi, T. 1989, in *BL Lac Objects*, ed. L. Maraschi, T. Maccacaro, and M.-H. Ulrich (Berlin: Springer), p. 96.

Pica, A.J., Pollock, J.T., Smith, A.G., Leacock, R.J., Edwards, P.L., and Scott, R.L. 1980, AJ , **85**, 1442.

Pica, A.J., Smith, A.G., Webb, J.R., Leacock, R.J., Clements, S., and Gombola, P.P. 1988, AJ , **96**, 1215.

Piccinotti, G., Mushotzky, R.F., Boldt, E.A., Holt, S.S., Marshall, F.E., Serlemitsos, P.J., and Shafer, R.A. 1982, AJ , **253**, 485.

Savage, B.D., and Mathis, J.S. 1979, ARA&A, **17**, 73.

Stark, A.A., Heiles, C., Bally, J., and Linde, R. 1984, Bell Labs. privately distributed tape.

Stickel, M., Padovani, P., Urry, C.M., Fried, J.W., and Kühr, H. 1991, ApJ, **374**, 431.

Stone, R.P.S. 1977, ApJ, **218**, 767.

Tanzi, E.G., Falomo, R., Bouchet, P., Bersanelli, M., Maraschi, L., and Treves, A. 1989, in *BL Lac Objects*, ed. L. Maraschi, T. Maccacaro, and M.-H. Ulrich (Berlin: Springer), p. 171.

Thompson, D.J., Djorgovski, S., and De Carvalho, R. 1990, PASP, **102**, 1235.

Treves, A., Morini, M., Chiappetti, L., Fabian, A., Falomo, R., Maccagni, D., Maraschi, L., Tanzi, E.G., and Tagliaferri, G. 1989, ApJ, **341**, 733.

Ulrich, M-H. 1989, in *BL Lac Objects*, ed. L. Maraschi, T. Maccacaro, and M.-H. Ulrich (Berlin: Springer), p. 92.

Urry, C.M. and Reichert, G. 1988, *IUE NASA Newsletter*, 34, 96

Wills, D. and Wills, B.J. 1974, ApJ, **190**, 271.

Whittet, D.C.B. 1988, in *Dust in the Universe*, eds. Bailey, M.E. and Williams, D.A., p. 25.

Wright, A.E., Ables, J.G., and Allen, D.A. 1983, MNRAS, **205**, 793.

Yee and Oke 1978, ApJ, **226**, 769.

Captions to figures

Fig. 1 IUE extracted spectra of 4 BL Lacs: a) PKS 0118–27 $\alpha_\lambda = 1.31$, [-0.03,2.57]; b) PKS 0301–24. $\alpha_\lambda = 0.76$, [0.65,0.88]; c) PKS 1538+14. $\alpha_\lambda = 3.0$, [-1.5,6.3]; d) H 0323+02. $\alpha_\lambda = 0.96$, [0.80,1.11]. The spectral index α_λ is given with the error interval at the 90% confidence level in square brackets. The fitting power law curve is superimposed to each spectrum.

Fig 2. IUE extracted spectra of H 0323+02 obtained from IUE archive: a) SWP 24010 (exp. = 26,400 s) + LWP 4259 (exp. = 12,000 s) $\alpha_\lambda = 0.80$, [0.57,1.01]; b) SWP 34098 (exp. = 30000 s) + LWP 13873 (exp. = 11040 s) $\alpha_\lambda = 1.08$, [0.87,1.28].

Fig. 3 Spectral flux distribution of PKS 0118–27. Data have been dereddened with $A_V = 0.1$. Only errors larger than 5% are plotted. Solid line represents the fitted power law of $\alpha = 1.17$.

Fig. 4 Spectral flux distribution of PKS 0301–24. Data have been dereddened with $A_V = 0.1$. Only errors larger than 5% are plotted. Solid line is the composition of a power law *dashed line)* of $\alpha = 0.84$ plus an elliptical galaxy *(dotted line)* contributing to 10% of total flux at 5500 Å.

Fig. 5 Spectral flux distribution of PKS 1538+14. Data have been dereddened with $A_V = 0.1$. Only errors larger than 5% are plotted. Solid line represents the fitted power law of $\alpha = 1.33$.

Fig. 6 The near-IR to UV spectral flux distribution of H 0323+02 in the 100 Å rebinning (filled squares), is decomposed into a power law (*dashed line*) with $\alpha_\nu = 0.65$ plus a standard elliptical galaxy (*dotted line*) redshifted at z

$= 0.147$. The open squares represent the standard elliptical after rebinning as the observed data points and the solid line is the sum of the two components. All data are dereddened with $A_V = 0.2$. Only errors larger than 5% are plotted.

Table 1

Journal of Observations

PKS 0118–27			
1989 Aug	10.3	ESO 1.5 + BC + CCD	V = 16.1
	10.3	ESO 2.2 + IR phot	K = 12.5
1989 Aug	9.6	IUE + LWP	$F_\lambda^\dagger(2500Å) = 0.23 \pm 0.02$
PKS 0301–24			
1989 Aug	7.4	ESO 1.5 + BC + CCD	V = 16.2
	11	ESO 2.2 + IR phot	K = 12.9
1989 Aug	8.6	IUE + SWP	$F_\lambda(1500Å) = 0.32 \pm 0.05$
1989 Aug	7.7	IUE + LWP	$F_\lambda(2500Å) = 0.29 \pm 0.02$
PKS 1538+14			
1988 Aug	4.3	ESO 1.5 + BC + CCD	V = 17.4
	4.1	ESO 2.2 + IR phot	K = 13.4
1988 Aug	2.9	IUE + LWP	$F_\lambda(2700Å) = 0.06 \pm 0.01$
H 0323+02			
1989 Aug	11.3	ESO 1.5 + BC + CCD	V = 16.7
	11.1	ESO 2.2 + IR phot	K = 13.5
1989 Aug	10.6	IUE + SWP	$F_\lambda(1500Å) = 0.19 \pm 0.02$
1989 Aug	8.8	IUE + LWP	$F_\lambda(2500Å) = 0.12 \pm 0.02$

† in units of 10^{-14} erg cm^{-2} s^{-1} Å^{-1} (see also text)

Table 2

Archival IUE Observations

H 0323+02			
1984 Sep	19.9	IUE + SWP	$F_\lambda^\dagger(1500\text{Å}) = 0.18 \pm 0.05$
1984 Sep	20.25	IUE + LWP	$F_\lambda(2600\text{Å}) = 0.12 \pm 0.02$
1988 Aug	18.9	IUE + SWP	$F_\lambda(1700\text{Å}) = 0.18 \pm 0.02$
1988 Aug	19.00	IUE + LWP	$F_\lambda(2500\text{Å}) = 0.09 \pm 0.01$

† in units of 10^{-14} erg cm^{-2} s^{-1} Å^{-1} (see also text)

Fig. 1

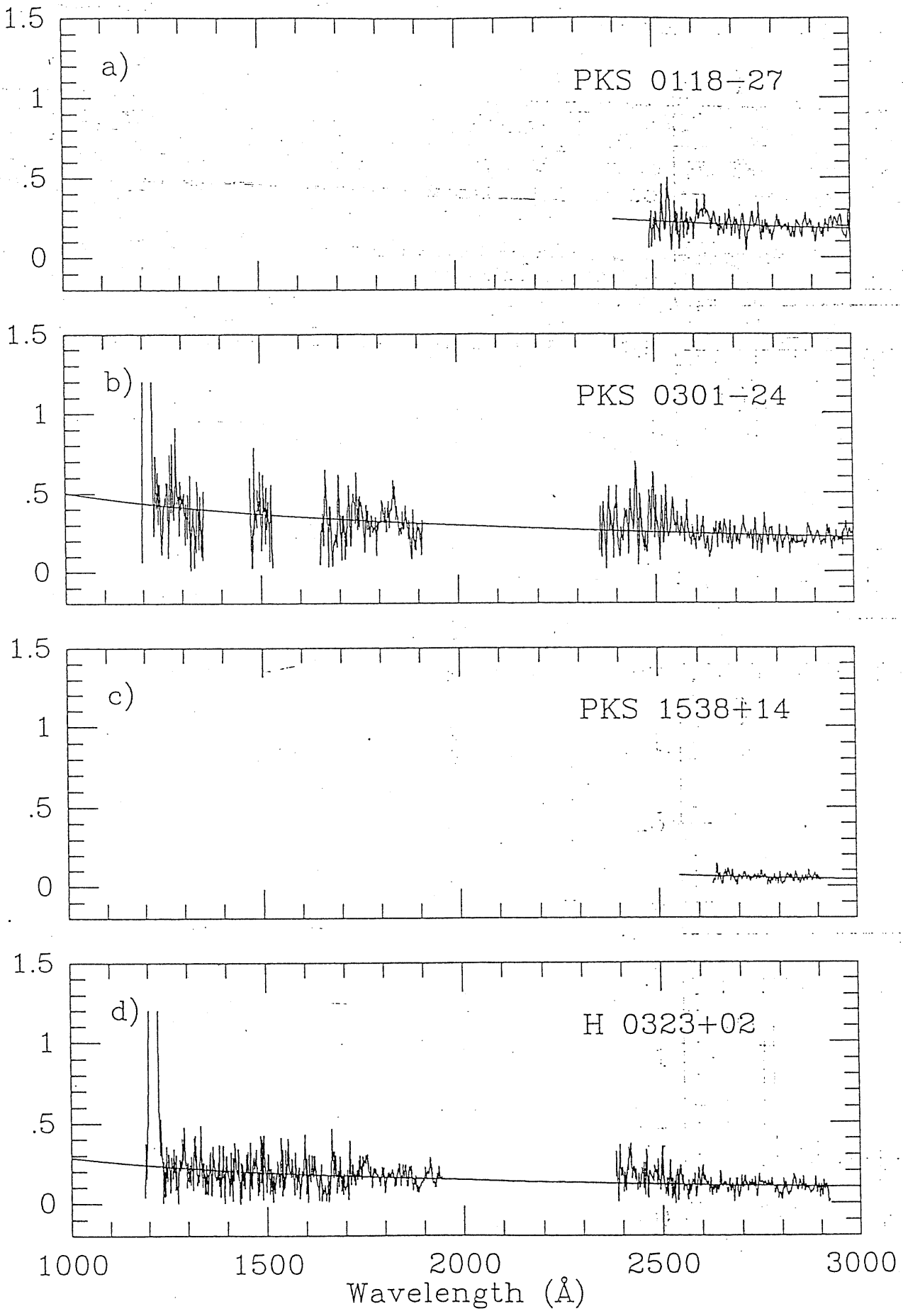
a)
PKS 0118−27
b)
PKS 0301−24
c)
PKS 1538+14
d)
H 0323+02
1.5
1
.5
0
1000
1500
2000
2500
3000
Wavelength (Å)

Fig. 2

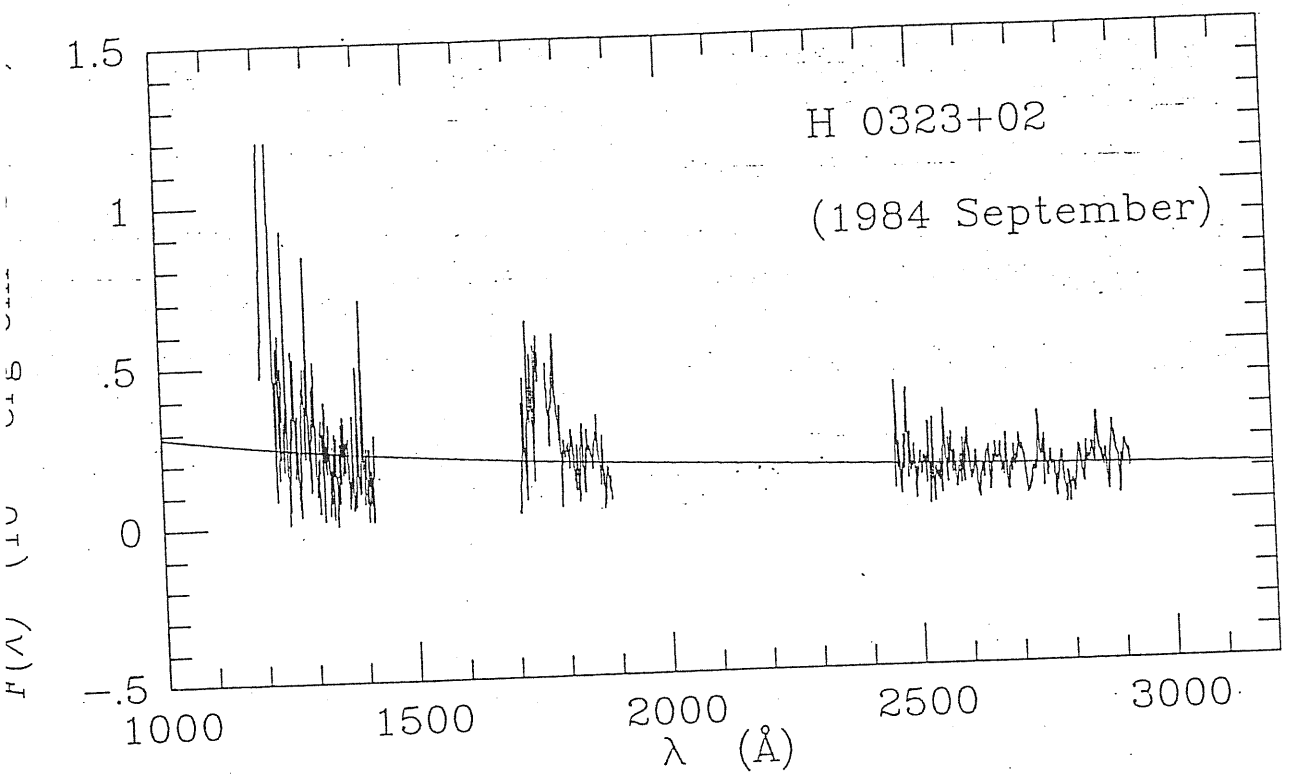
H 0323+02
(1984 September)
1.5
1
.5
0
-.5
1000
1500
2000
2500
3000
λ (Å)

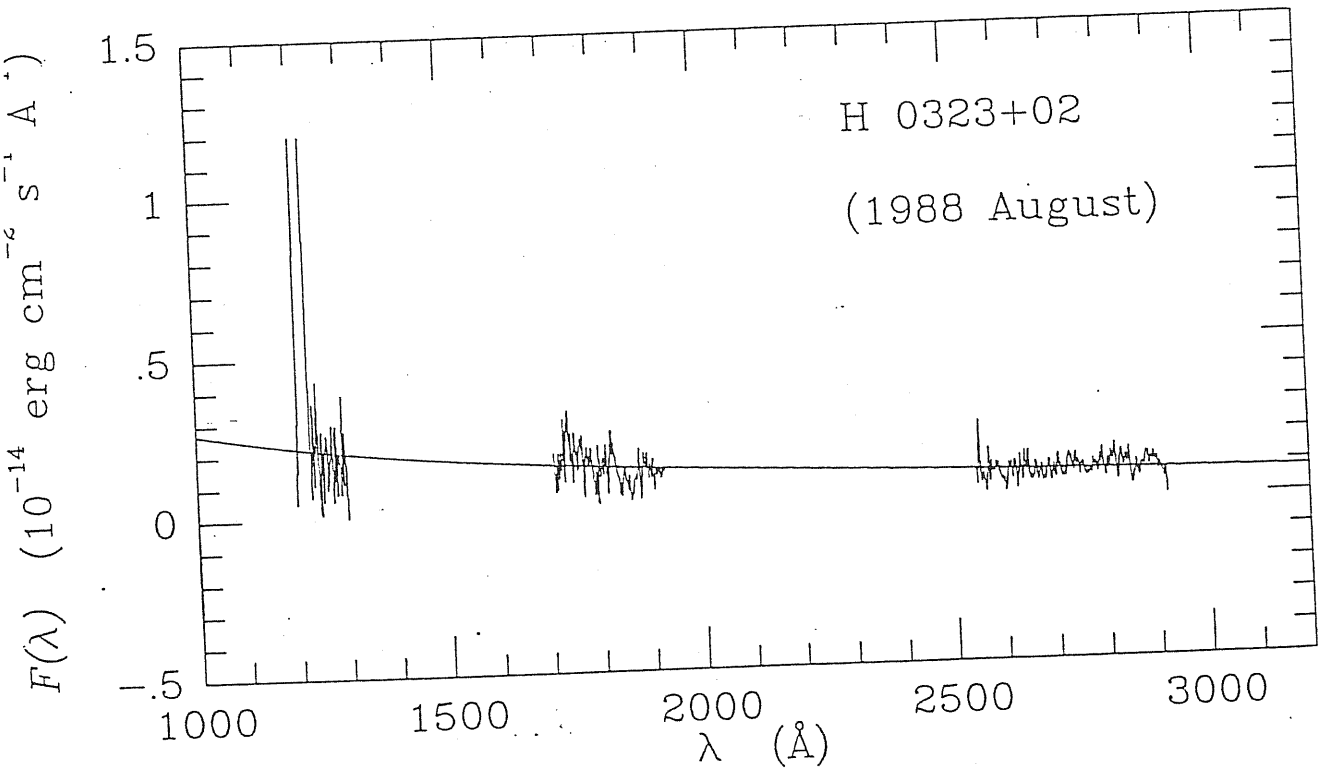
H 0323+02
(1988 August)
1.5
1
.5
0
-.5
1000
1500
2000
2500
3000
λ (Å)
F(λ) (10^-14 erg cm^-2 s^-1 A^-1)

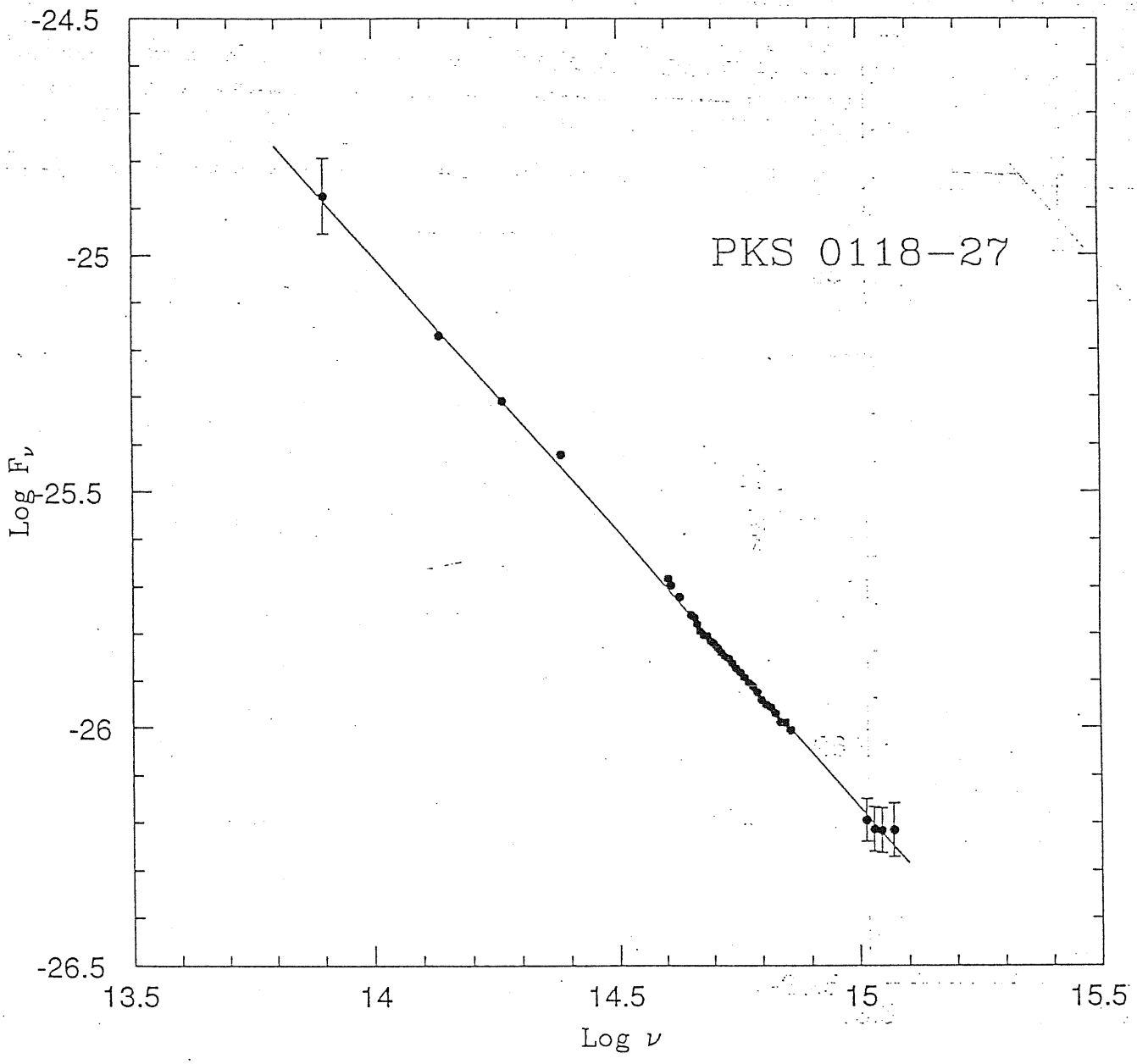

Fig 3

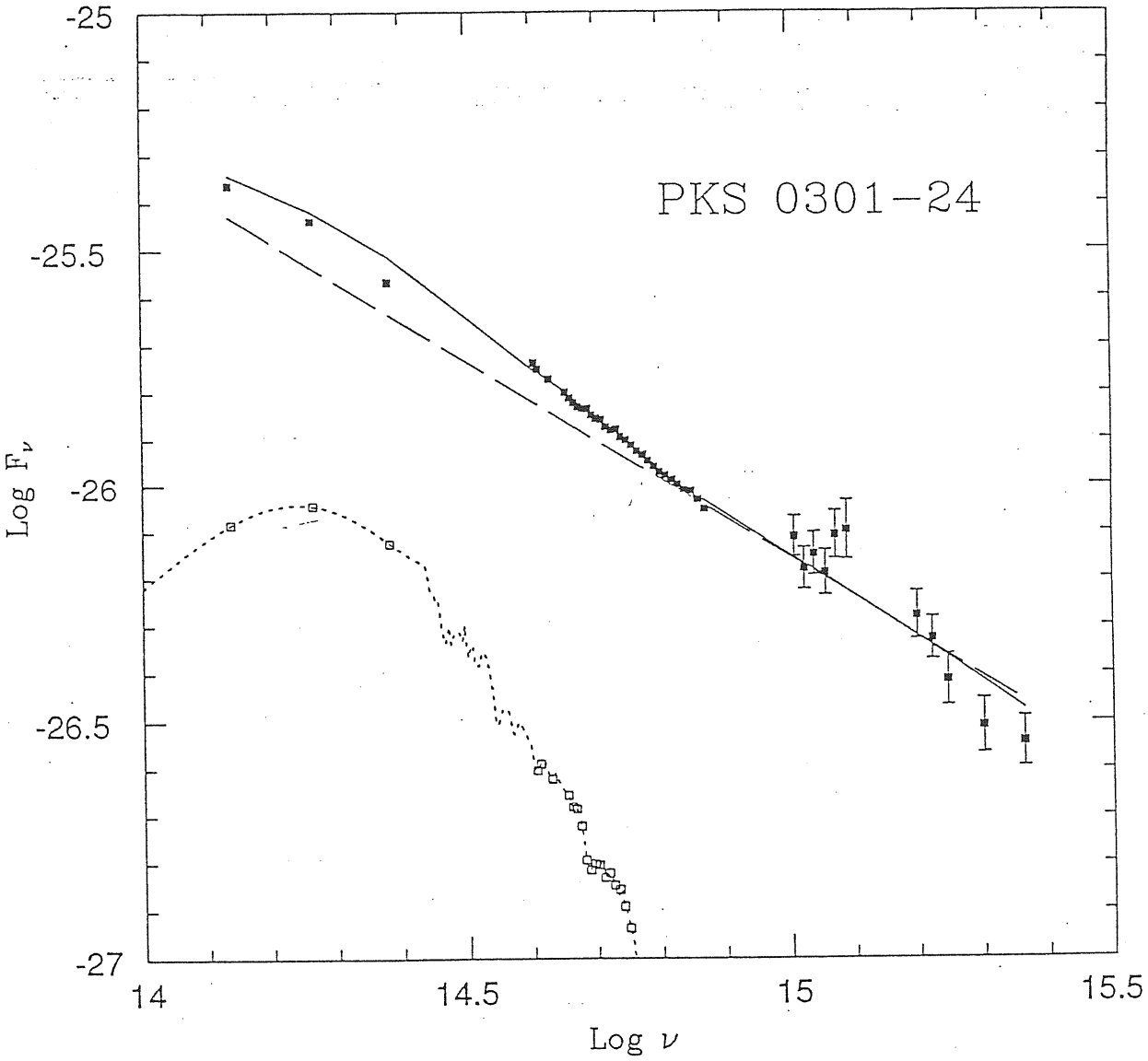
PKS 0301-24
-25
-25.5
-26
-26.5
-27
Log F_ν
14
14.5
15
15.5
Log ν

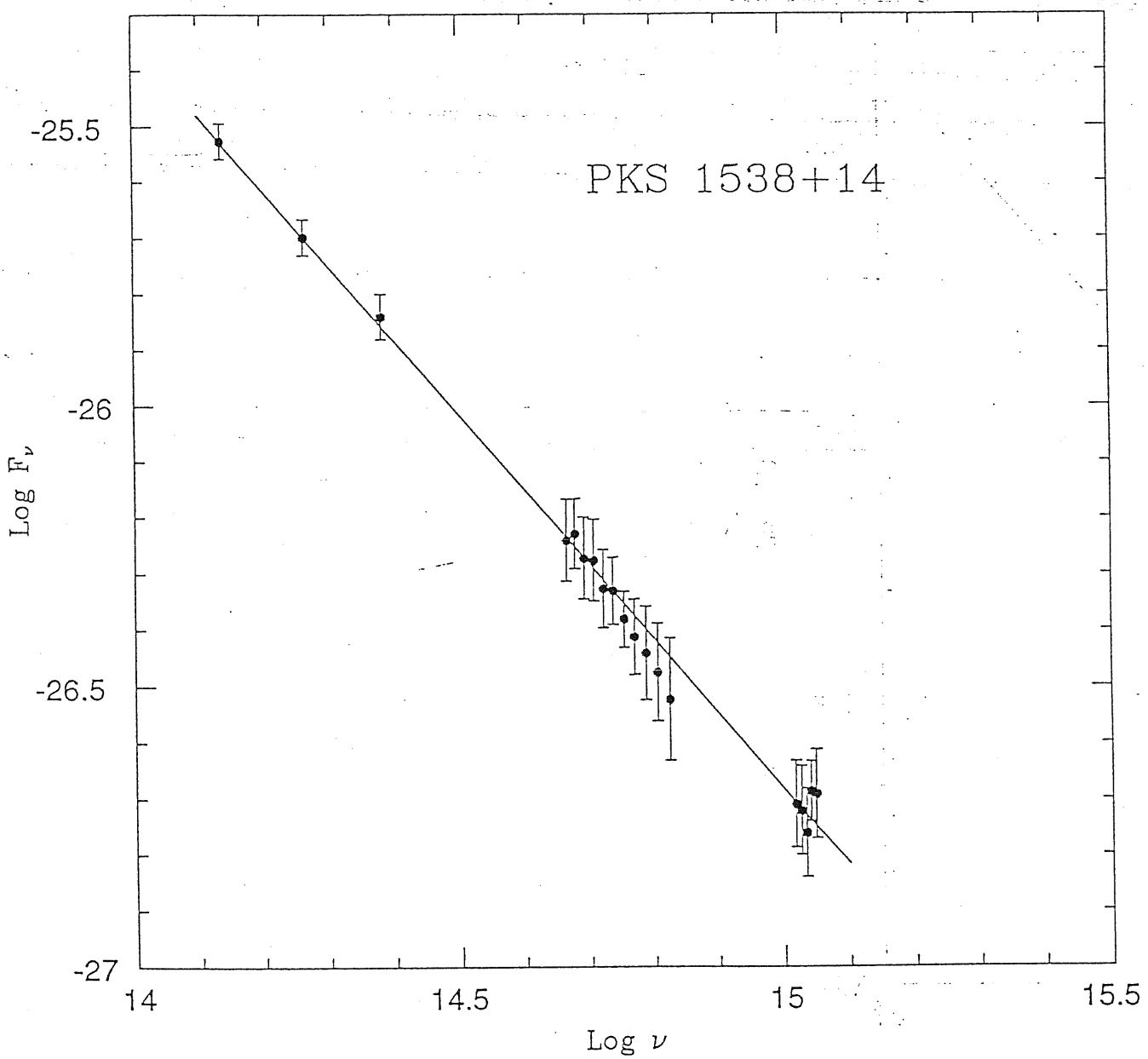

Fig 5

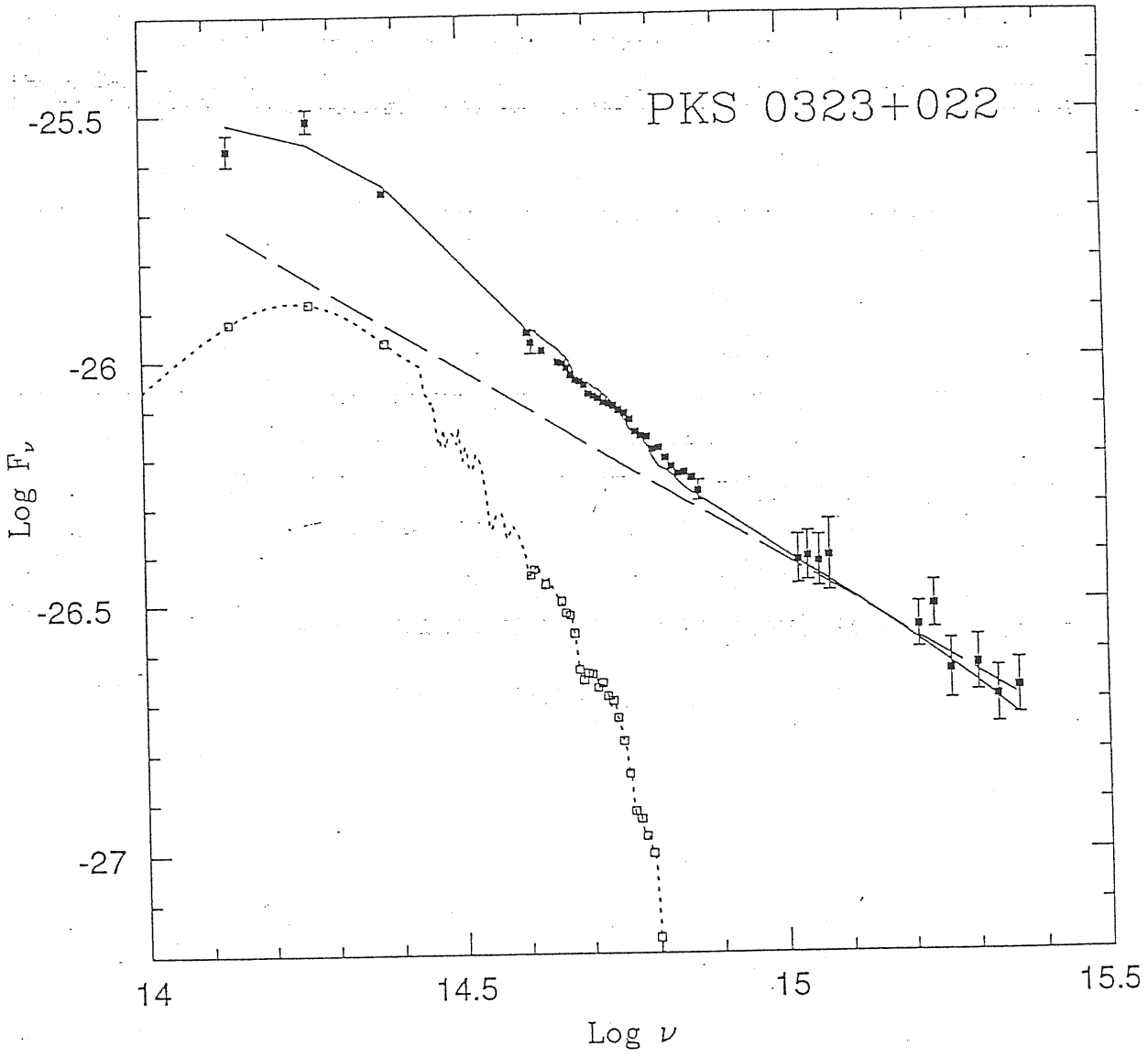

g 6

Appendix B

IUE monitoring of PKS 2155-204

Multiwavelength Monitoring of the BL Lac Object PKS 2155-304.

I. IUE Observations

C. M. Urry[1,2], L. Maraschi[2,3], R. Edelson[4], A. Koratkar[1], G. Madejski[4], E. Pian[5], G. Pike[4], G. Reichert[4], A. Treves[5] W. Wamsteker[6], R. Bohlin[1], W. Brinkmann[7], L. Chiappetti[8], T. Courvoisier[9], A. V. Filippenko[10], H. Fink[7], I. M. George[4], Y. Kondo[11], J. Krolik[12], P. O'Brien[13], M. Shull[14], M. Sitko[15], A. E. Szymkowiak[4], G. Tagliaferri[16], S. Wagner[17], R. Warwick[18]

[1]Space Telescope Science Institute, 3700 San Martin Drive, Baltimore, MD 21218

[2]Guest Observer with the International Ultraviolet Explorer

[3]Department of Physics, University of Milan, via Celoria 16, I-20133 Milan, Italy

[4]Laboratory for High Energy Astrophysics, Code 660, NASA/GSFC, Greenbelt, MD 20771

[5]SISSA/ISAS International School for Advanced Studies, Trieste, Italy

[6]ESA *IUE* Observatory, P.O. Box 50727, 28080 Madrid, Spain

[7]MPE, Giessenbachstrasse, D-8046 Garching bei München

[8]Istituto di Fisica Cosmica CNR, via Bassini 15, I-20133 Milan, Italy

[9]Observatory of Geneva, Ch-1290 Sauverny, Switzerland

[10]Department of Astronomy, University of California, Berkeley, CA 94720

[11]Laboratory for Astronomy and Solar Physics, NASA/GSFC, Greenbelt, MD 20771

[12]The Johns Hopkins University, Department of Physics and Astronomy, Baltimore, MD 21218

[13]Department of Physics and Astronomy, University College London, Gower STreet, London WC1E 6BT, England

[14]JILA, University of Colorado, Campus Box 440, Boulder, CO 80309

[15]Department of Physics, University of Cincinnati, 210 Braunstein M1 11, Cincinnati, OH 45221

[16]ESTEC, Space Science Department, Astrophysics Division, Postbus 299, NL-2200 AG Noordwijk, Netherlands

[17]Landessternwarte Heidelberg-Königstuhl, Königstuhl, D-6900 Heidelberg 1, Germany

[18]Department of Physics, University of Leicester, University Road, Leicester LE1 7RH, England

Presented at the conference *Science with the Hubble Space Telescope*,
Baia Chia (Italy), June 29-July 7 1992
E.Schreier and P.Benvenuti eds.

SUMMARY

Daily monitoring of PKS 2155-304 with the IUE satellite throughout November 1991 has revealed dramatic, large-amplitude, rapid variations in the ultraviolet flux of this BL Lac object. Many smaller, rapid flares are superimposed on a general doubling of the intensity in 30 days. During the four-day period when sampling was roughly continuous, the rapid flaring has a quasi-periodic nature, with peaks repeating every ~ 0.7 days. Short- and long-wavelength ultraviolet light curves are well correlated with each other, and with the optical light curve deduced from the Fine Error Sensor (FES) on IUE.

1. INTRODUCTION

The most puzzling aspect of AGN has always been their high power output coupled with the small emission region inferred from rapid variability. By definition blazars (the collective name for BL Lac objects and Optically Violently Variable quasars) are the most rapidly variable AGN. Blazars are radio-loud and have a smooth continuum (especially compared to Seyfert galaxies and radio-quiet quasars) spanning the wavelength range from the radio through the soft X-ray.

In the last decade, considerable progress has been made interpreting the fast variability and the broad-band spectra of blazars as emission from relativistic jets (Blandford & Rees 1978; Königl 1981; Urry & Mushotzky 1982; Ghisellini, Maraschi & Treves 1985; Worrall *et al.* 1986; Hutter & Mufson 1986; George, Warwick & Bromage 1988). These models have been very successful, in the sense that they usually fit the continuum spectrum over nearly 10 decades in wavelength. Unfortunately, the parameters of the model are rarely well-determined because acceptable fits can be produced with a number of assumptions which are to some extent arbitrary.

The missing ingredient is variability. The degeneracy of multiple model solutions vanishes or is greatly reduced when variability information is added because the derived size limits represent strong constraints for the models. Although some studies have recognized this (George *et al.* 1988, Mufson *et al.* 1990, Treves *et al.* 1989), the available sampling to date — only a few spectra, spaced far apart in time – has been sparse, uneven, and inadequate.

For this reason, we designed a monitoring program that would produce high-quality light curves in several bands, including ultraviolet, optical, and X-ray. The object selected for our study, PKS 2155-304, is one of the brightest extragalactic objects in the ultraviolet and X-ray sky. It was discovered with the HEAO1 X-ray satellite (Schwartz *et al.* 1979) and identified as a BL Lac object because of its radio emission and polarized optical continuum (Griffiths *et al.* 1979). The redshift is not well established but is probably close to $z = 0.1$ (Bowyer *et al.* 1979; Falomo *et al.* 1991). PKS 2155-304 has previously been observed to be highly variable at both ultraviolet (Maraschi, Tanzi, & Treves 1986; Urry *et al.* 1988; Edelson *et al.* 1991) and X-ray (Snyder *et al.* 1980, Morini *et al.* 1986, Treves *et al.* 1989, Sembay *et al.* 1992) wavelengths.

The campaign was carried out in 1991 November. Unprecedented spectral coverage in the ultraviolet, extreme ultraviolet, and soft-X-ray was provided by the combination of IUE, the Rosat Wide Field Camera (WFC), and the Rosat Position Sensitive Proportional Counter. Ground based observations covered optical to radio frquencies. The IUE data set itself is of exceptional quality, with about 100 spectra in each of the two IUE cameras and daily sampling for a month plus 4 days of quasicontinuous observations. Here we present some preliminary results of the ultraviolet part of the monitoring campaign. The observations and data analysis are described in § 2, and the results in § 3. The results are briefly discussed in § 4.

2. OBSERVATIONS AND DATA ANALYSIS

2.1 Observing Strategy

The variability time scales of BL Lac objects in general, and even this best-studied object PKS 2155-304 in particular, were not well measured, so the observing plan bracketed a range of time scales. In order to measure moderate time scale variations (days to a week) we scheduled at least one half IUE shift daily from 1 November to 29 November (except on November 8, due to a scheduling conflict). In order to study short-term variability,

four and a half days in the middle of the campaign (10.7 - 15.3 November) were devoted to nearly continuous coverage using ~3 shifts per day.

The short-wavelength (SWP) and long-wavelength (LWP) IUE cameras were exposed alternately, with typical integration times of 55 and 25 minutes, respectively. This allowed us to get two pairs of spectra during each half IUE shift, absent any operational problems.

Just before each SWP or LWP exposure, counts from the Fine Error Sensor (FES), the optical monitor on IUE, were measured on target and on background.

2.2 Spectral Extraction

Spectra were extracted from each of the 202 IUE images using the Slit-Weighted Extraction Technique (SWET) of Kinney, Bohlin & Neill (1991). which is publicly available through the IUE Regional Data Analysis Facility. Details of the SWET procedure can be found in Kinney *et al.* (1991).

There is another well-known slit-weighted technique, the Gaussian extraction or GEX method (Urry & Reichert 1988), which assumes the cross-dispersion profile is a Gaussian. We have also extracted all the spectra using GEX, and compared this to the SWET results. Differences found using the two extraction methods do not affect the results significantly.

The FES counts were converted to optical magnitudes using the recently developed algorithm of Perez and Loomis (1991), which takes into account the background due to scattered light. PKS 2155-304 was assumed to have color B–V=0.26 throughout the month, which is the mean value measured contemporaneously with ground-based optical telescopes, and did not change much during the monitoring period (Smith *et al.* 1992).

2.3 Spectral Corrections

The extracted net fluxes were converted to absolute flux using the recent IUE calibration of Bohlin *et al.* (1990). A correction was made for degradation in the SWP sensitivity (Bohlin & Grillmair 1988, as updated through 1990 by Bohlin, private communication); the extrapolation beyond 1990 is somewhat uncertain (but not by more than 1%). No sensitivity correction was made to the LWP net flux.

There is no evidence for internal reddening in PKS 2155-304; in particular, the soft X-ray spectrum (e.g., Canizares and Kruper 1984, Madejski 1985) indicates the column density of absorbing cool gas along the line of sight is commensurate with the interstellar medium in our Galaxy in that direction. Using a standard conversion (Burstein & Heiles 1984), this column density of $N_H = 1.78 \times 10^{20}$ atoms cm^{-2} (Stark *et al.* 1992) corresponds to $E(B-V) \sim 0.03$. Therefore spectra were dereddened using $E(B-V) = 0.03$ and the standard curve from Seaton (1979). The dereddened flux is 27% greater at 1400 Å and 19% greater at 2800 Å than the observed flux, and the fitted energy spectral index is typically 0.06 flatter in the SWP and 0.28 flatter in the LWP. Further discussion focuses on the dereddened spectra.

2.4 Spectral Fitting

Using an iterative, chi-squared minimization fitting routine, the dereddened IUE spectra were fitted to a simple power–law model of the form:

$$f_\lambda = b_1 \left(\frac{\lambda}{\lambda_0} \right)^{b_2} \quad . \tag{1}$$

The fit parameters are the normalization, b_1, at fiducial wavelength λ_0, and slope b_2. We will however give the more commonly used energy index, α, where $F_\nu \propto \nu^{-\alpha}$, which is

related to b_2 via $\alpha = 2 + b_2$. The wavelength ranges over which the data were fitted were 1230–1950 Å for the SWP camera (which excludes the geo-coronal Lyman-α region) and 2100–3100 for the LWP camera. Wavelength regions affected by SWP camera artifacts (Crenshaw, Bruegman & Norman 1990), at 1277–1281 Å, 1286–1290 Å, and 1660–1666 Å, were excluded, as was the region 1470–1540 Å, in which unusual features were apparent in many of the spectra. The power–law fit is generally good for all the spectra. The normalization is at 1400 Å for SWP spectra and 2800 Å for LWP spectra. These wavelengths are close to the flux-weighted means of each band ($\sim$ 1560 Å and $\sim$ 2568 Å, respectively, for $\alpha = 1$), so that the uncertainty on the derived flux is small.

2.5 Error Analysis

The detection and evaluation of variability requires an accurate treatment of errors. A continuum estimate from direct measurement would have a relatively large error bar (the variance in some interval around that wavelength), including both local statistical noise and fixed-pattern noise. Like most BL Lac objects, however, PKS 2155-304 has a smooth and approximately featureless spectrum which is well fitted by a simple power–law model. The flux calculated from a fitted power law gives a much smaller error bar than direct measurement because information from the full band is used.

The estimation of errors in the flux and spectral index involved several steps: First, the SWET error vector was propagated through the fitting procedure to get initial uncertainties for the parameters of the power-law fit, b_1 and b_2. Next, both Δb_1 and Δb_2 were increased by a factor equal to the mean of the reduced chi-squared distribution, $\sqrt{\langle \chi^2_\nu \rangle}$ ($\langle \chi^2_\nu \rangle = 3.76$ for the SWP and ($\langle \chi^2_\nu \rangle = 2.42$ for the LWP). This is equivalent to scaling up the SWET error vector so that $\langle \chi^2_\nu \rangle = 1$ in both cases. The final error estimate on the flux at λ_0 is equal to the quadrature sum of the scaled error on b_1 and 1.25% of b_1. (The power-law models were normalized at 1400 Å for the SWP and 2800 Å for the LWP.) The final error estimate on the spectral index was derived by increasing the scaled error on b_2 by 1.95 for the SWP, 2.46 for the LWP, and 2.48 for the combined SWP-LWP fits, so that it represents the 1 σ error for the observed differences between adjacent measurements of α. Since this assumes no intrinsic variation between adjacent measurements, it is if anything an overestimate of the error on the spectral index.

A procedure similar to that used for determining $\Delta\alpha$ was used to estimate the global mean uncertainty in the FES-derived magnitude. The normalized error distribution for $\Delta V = 0.08$ mag had variance equal to one and was consistent with a Gaussian distribution centered on zero. This is therefore a good estimate of the mean uncertainty in the FES magnitudes; it does not take into account relative errors among FES measurements or any systematic offset from other optical measurements (e.g., Smith *et al.* 1992, Courvoisier *et al.* 1992), such as might be due to incorrect color corrections.

3. RESULTS

3.1 Ultraviolet Light Curves

The light curves for the full month and for the central period are shown in Figure 1. During the intensive monitoring, the ultraviolet flux varied by $\sim$30% in several distinct flares that are well-sampled apart from a possible dip during the 7-hour gap on 11 November. The width of these rapid flares is roughly half a day; if we define a doubling time scale as $\tau_D = \Delta t(\overline{F}/\Delta F)$, then values for these flares are typically less than 5 days. There are no obvious differences between the time scales for flaring or decaying intensity. The

fastest ultraviolet variations seen previously in this or any other object were of order 10% over a few days (e.g., Edelson *et al.* 1991).

The fractional variability is comparable for the two bands: both light curves show a doubling of flux, and in both bands the variance is about 15% of the mean flux. The optical light curve shows exactly the same trends as the ultraviolet light curves, on both long and short time scales, albeit with larger error bars.

The SWP, LWP, and FES light curves are all highly correlated, with no discernable lag (the upper limit is $\lesssim 0.1$ days). The discrete cross-correlation functions (Edelson & Krolik 1988) for SWP versus LWP and SWP versus FES are shown in Figure 2. Both cross-correlation functions are asymmetric, in the sense of higher correlation at positive lags, which correspond to the longer wavelength emission following the short-wavelength emission.

The autocorrelation functions of the SWP, LWP and FES fluxes were also computed. The SWP and LWP give similar results, while the FES amplitude is generally smaller, probably because the relative errors are larger. (For the SWP and LWP, the behavior of the autocorrelation functions suggests the estimates of flux errors were about right.) On long time scales, the autocorrelation functions suggest smooth "red" power spectra, with relatively more power on longer time scales. However, on shorter time scales (using the data from the well-sampled, five-day intensive monitoring) they are modulated strongly with a period of $\sim$0.7 days. The SWP and LWP autocorrelations for this case are shown in Figure 3. This quasi-periodic behavior can be seen going through a full five cycles directly in the light curves (Fig. 1b), despite the uncertainty introduced by the gap at 11.5 November. Further runs of intensive monitoring are needed to verify whether this is a repeatable, possibly periodic or quasiperiodic phaenomenon.

3.3 Spectral Shape

Taking the reddening into account, the spectrum in the SWP and LWP ranges is well described by a single power law, i.e. there is no spectral "curvature" in the ultraviolet band,. The flatness of the UV spectral index means that the peak of the luminosity emitted from this BL Lac object is in the far-ultraviolet, as noted by previous authors. PKS 2155-304 is one of the few extragalactic objects detected in the Rosat WFC survey (Pounds 1991), thus using the simultaneous data from IUE and Rosat we will be able to actually measure the total luminosity and spectral shape from 10^{15} to 510^{17} Hz.

The spectral index of the SWP did change significantly during the monitoring campaign. A non-parametric Spearman Rank-Order Correlation test shows a likely correlation between F_{1400} and α_{SWP} ($P = 1.7 \times 10^{-3}$) The correlation improves when one looks at change in spectral index versus change in flux; $\Delta\alpha$ and ΔF are correlated with probabilities 6.6×10^{-7}. The sense of the correlation is that the spectrum hardens as it brightens, as found previously (Maraschi *et al.* 1986, Urry *et al.* 1988, Edelson 1992). The improvement of the correlation when one looks at *changes* in F and α indicates there is little long-term memory of spectral shape. Further analysis of the spectral behavior is in progress.

4. CONCLUSION

The campaign has up to now demonstrated at least the need of frequent sampling for these rapidly variable extragalactic objects. For the first time, after more than a decade of observations of this object, a definite timescale of 0.7 days has become apparent. Its significance should be confirmed by further observations. It is tempting to believe that it may be real in the sense that it may be associated to some physical time scale, perhaps

to a periodic or quasiperiodic phaenomenon. The associated $\frac{\Delta L}{\Delta t} \simeq 310^{40} erg/sec^2$ is not extreme, but does not take into account a bolometric correction which will be determined from the simultaneous Rosat data.

In BL Lac objects the UV emission is supposed to be non thermal, due to synchrotron emission from relativistic electrons. The radiative loss times of such particles are estimated to be much shorter then the observed timescale so the latter should be associated to some non stationary macroscopic process of acceleration and/or confinment of the relativistic particles. These mechanisms must be closely related to the "central engine" possibly through a magnetohydrodinamic wind driven by a spinning black hole. Similar timescales are observed in the X-ray emission of Seyfert galaxies, which is also thought to originate close to the central engine. We expect that the combined information from the multiwavelength campaign will allow further progress in the understanding of BL Lac objects.

Acknowledgements —

We are grateful to the IUE project, to the schedulers, the Telescope Operators and Resident Astronomers who made important contributions to the realization of the campaign. The IUE Regional Data Analysis Facility was instrumental in making prompt access to the data possible. CMU acknowledges Rick Shafer and Jerry Kriss for helpful discussions about error analysis. This work was supported in part by NASA Grant NAG 5-1034.

REFERENCES

Blandford, R., & Rees, M. J. 1978, in Pittsburgh Conference on BL Lac Objects, ed. A. M. Wolfe, (U. of Pittsburgh), p. 328

Bohlin, R. 1988, NASA IUE Newsletter, 35, 141

Bohlin, R., & Grillmair, C. J. 1988, ApJS, 66, 209

Bohlin, R., Harris, A. W., Holm, A. V., & Gry, C. 1990, ApJS, 73, 413

Burstein, D., & Heiles, C. 1984, ApJS, 54, 33

Canizares, C. R., & Kruper, J. S. 1984, ApJ, 278, L99

Courvoisier, T., *et al.* 1992, in preparation

Crenshaw, M. D., Bruegman, O. W., & Norman, D. J. 1990, PASP, 102, 463

Edelson, R. A. 1992, ApJ, in press

Edelson, R. A., *et al.* 1991, ApJ, 372, L9

Edelson, R. A., & Krolik, J. H. 1988, ApJ, 333, 646

Fabian, A. C. 1979, Proc. Roy. Soc., 366, 449

Falomo, R., *et al.* 1991, ApJ, 380, L67

Feigelson, E., *et al.* 1986, ApJ, 302, 337

George, I. M., Warwick, R. S., & Bromage, G. E. 1988, MNRAS, 232, 793

Ghisellini, G., Maraschi, L., & Treves, A. 1985, A&A, 146, 204

Griffiths, R. E., Tapia, S., Briel, U., & Chaisson, L. 1979, ApJ, 234, 810

Hutter, D. J., & Mufson, S. L. 1986, ApJ, 301, 50

Kinney, A. L., Bohlin, R. C., & Neill, J. D. 1991, PASP, 103, 694

Königl, A. 1981, ApJ, 243, 700

Madejski, G. 1985, Ph.D. Thesis, Harvard University.

Maraschi, L., Tanzi, E. G., & Treves, A. 1986, ApJ, 304, 637
Morini, M., *et al.* 1986, ApJ, 306, L71
Mufson, S. L., Hutter, D. J., Kondo, Y., Urry, C. M., & Wisniewski, W. Z. 1990, ApJ, 354, 116
Perez, M., & Loomis, C. 1991, Record of the Meeting of the International Ultraviolet Explorer User's Committee, (CSC/TM-91/6142), p. I-3
Schwartz, D. A., Doxsey, R. E., Griffiths, R. E., Johnston, M. D., & Schwarz, J. 1979, ApJ, 229, L53
Seaton, M. J. 1979, MNRAS, 187, 73p
Makino, F., & Ohashi, T. 1992, ApJ, submitted
Smith, P., *et al.* 1992, ApJ, submitted
Snyder, W. A., *et al.* 1980, ApJ, L11
Stark, A. A., Gammie, C. F., Wilson, R. W., Bally, J., Linke, R. A., Heiles, C., & Hurwitz, M. 1992, ApJS, 79, 77
Treves, A., *et al.* 1989, ApJ, 341, 733
Urry, C. M., Kondo, Y., Hackney, K. R. H., & Hackney, R. L. 1988, ApJ, 330, 791
Urry, C. M., & Mushotzky, R. F. 1982, ApJ, 253, 38
Urry, C. M., & Reichert, G. A. 1988, IUE Newsletter, 34, 95
Worrall, D. M., *et al.* 1986, ApJ, 303, 589

FIGURE CAPTIONS

Fig. 1. — Ultraviolet light curves of PKS 2155-304. *(a)* The full light curve, with fitted fluxes at 2800 Å (*open squares*) and 1400 Å (*filled circles*) on the same scale. Both long- and short-wavelength fluxes doubled during the month, with no apparent lag. *(b)* Expanded view of the intensive monitoring period, during which IUE observations were nearly continuous. The LWP scale is at left, the SWP scale at right. Many rapid flares, with duration of about half a day, have clearly been well-sampled. Five cycles of a quasi-periodic nature can be seen, but true periodicity cannot be established without a longer data train.

Fig. 2. — Cross-correlations of SWP (1400 Å) flux versus LWP (2800 Å) flux and SWP versus FES flux. The light curves are highly correlated, with zero lag (with an upper limit of less than a few hours), and the curves are asymmetric in the sense of the short-wavelength emission leading the longer wavelength emission.

Fig. 3. — Auto-correlation functions for SWP (1400 Å) and LWP (2800 Å) light curves calculated for the 5-day intensive monitoring period only. The SWP and LWP autocorrelation functions are very similar, and both show a peak at a lag of about 0.7 days.

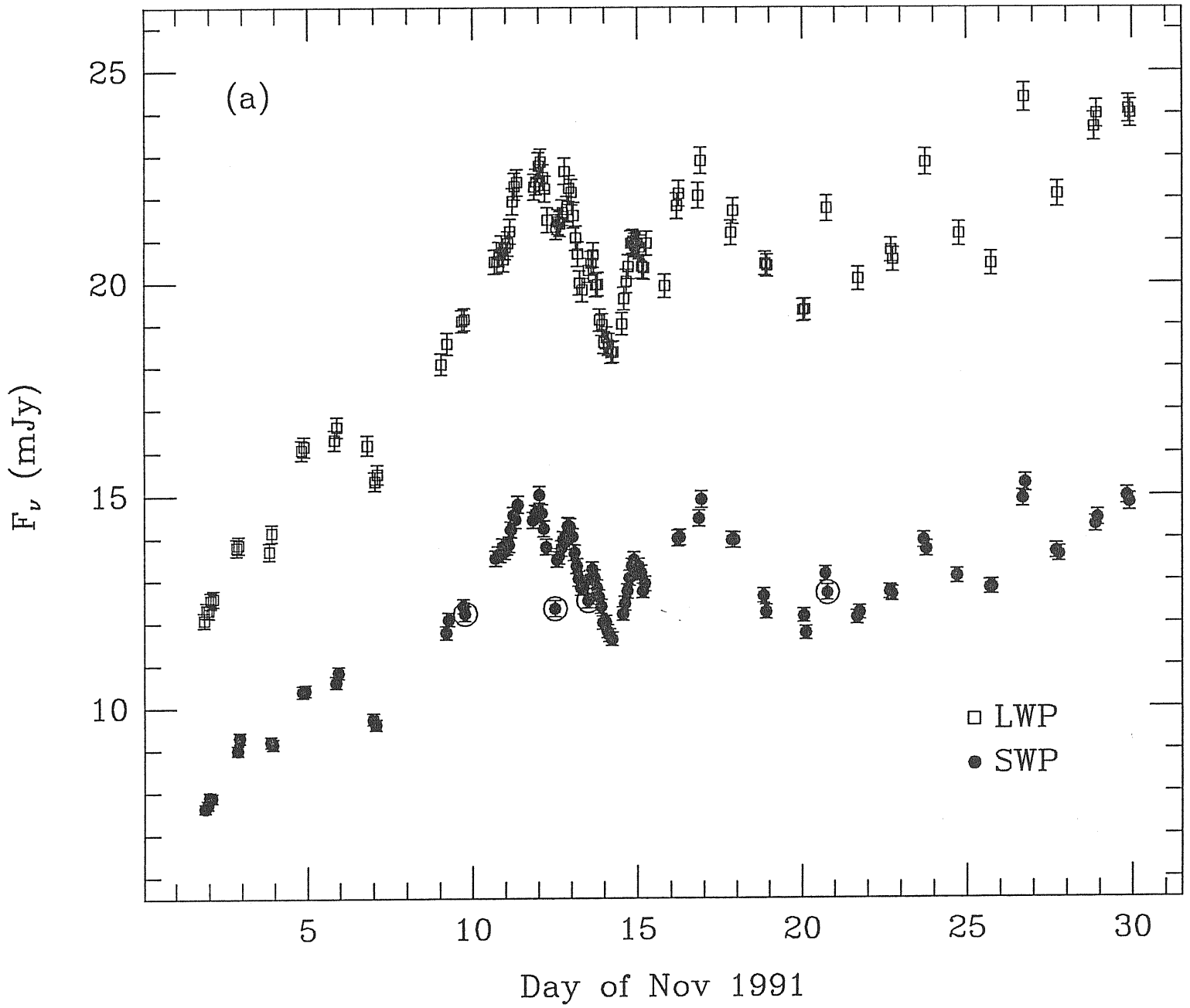

Fig.1a

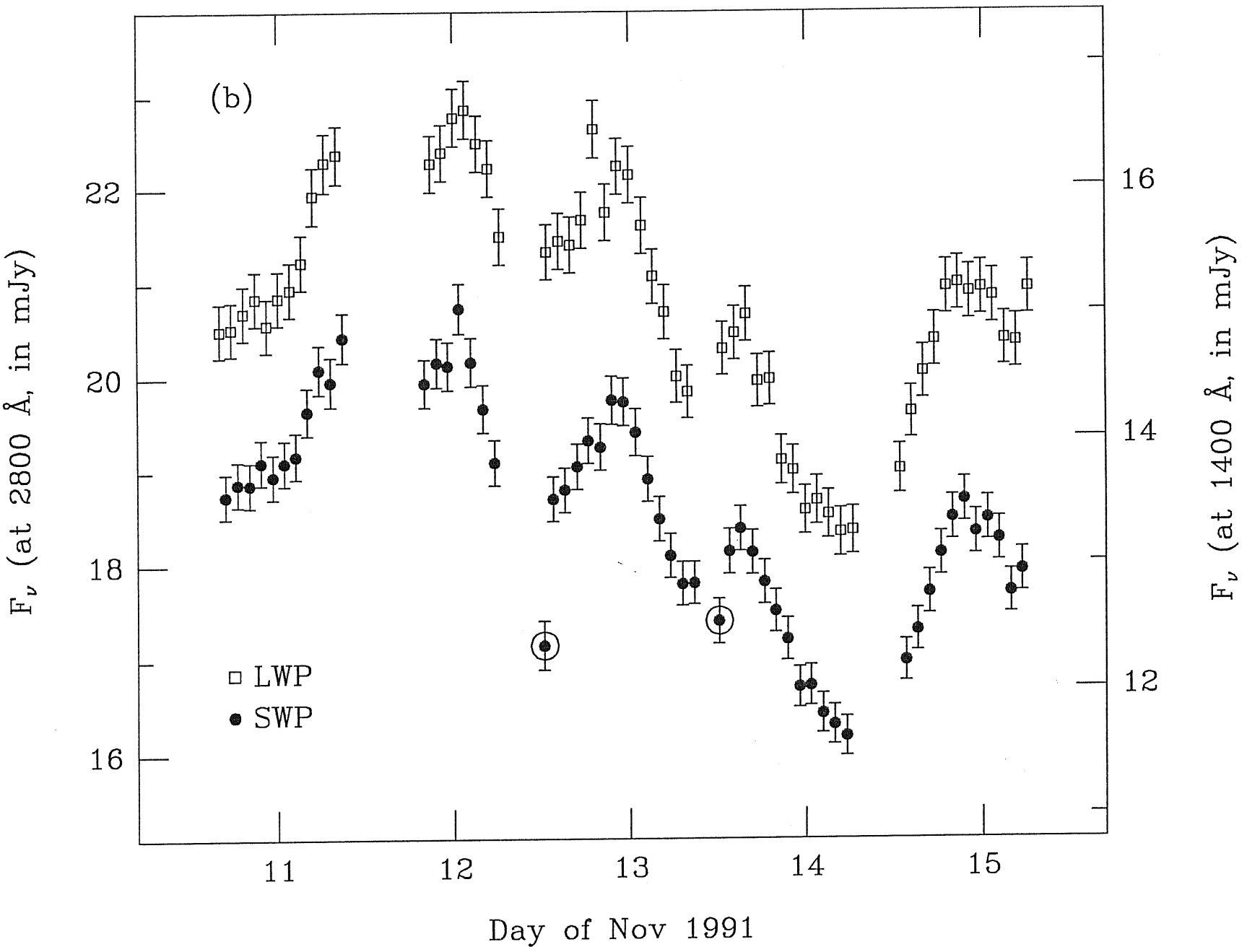
(b)
22
20
18
16
16
14
12
11
12
13
14
15
LWP
SWP
F_ν (at 2800 Å, in mJy)
F_ν (at 1400 Å, in mJy)
Day of Nov 1991

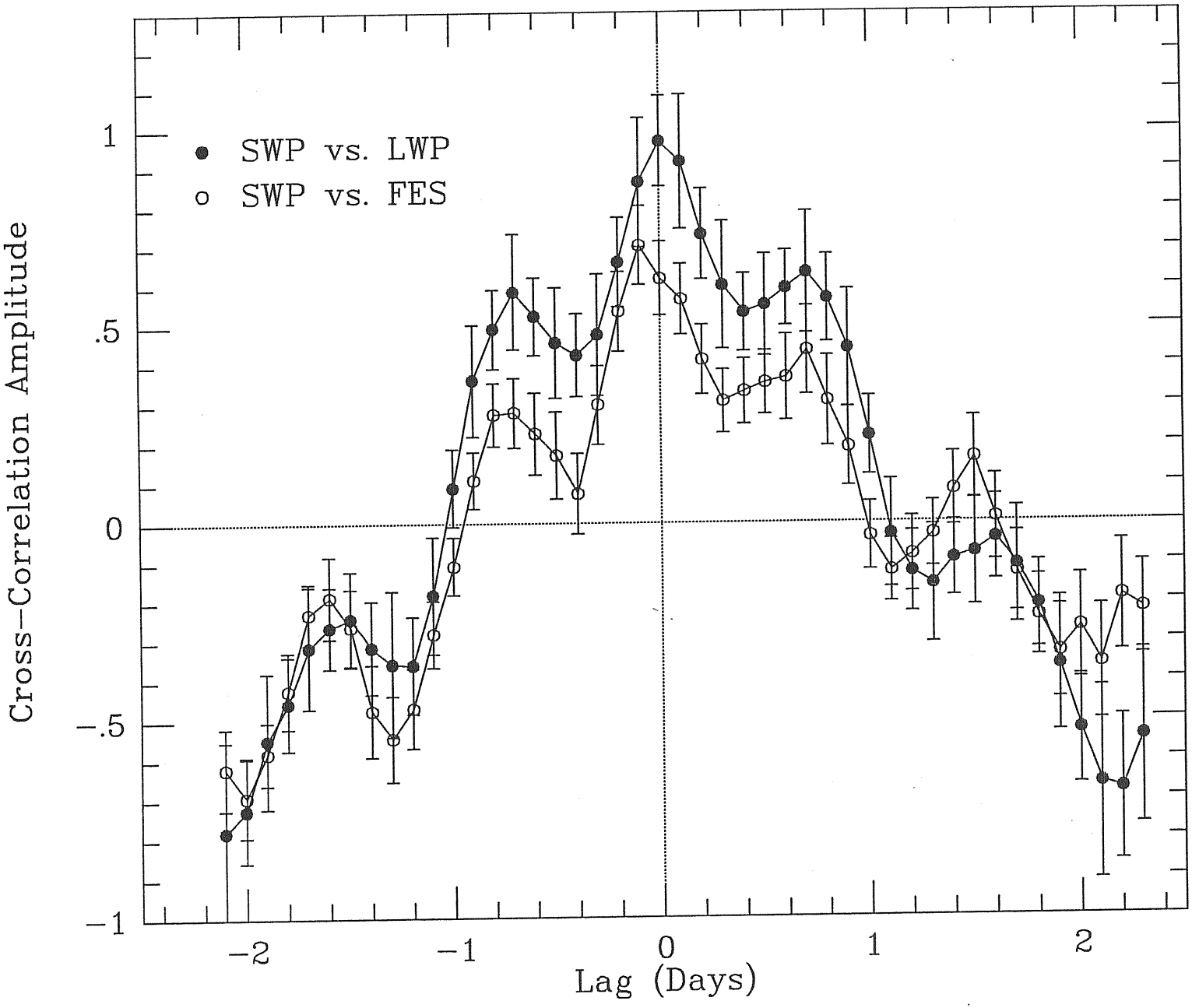
SWP vs. LWP
SWP vs. FES
Cross-Correlation Amplitude
1
.5
0
-.5
-1
-2
-1
0
1
2
Lag (Days)

Fig.2

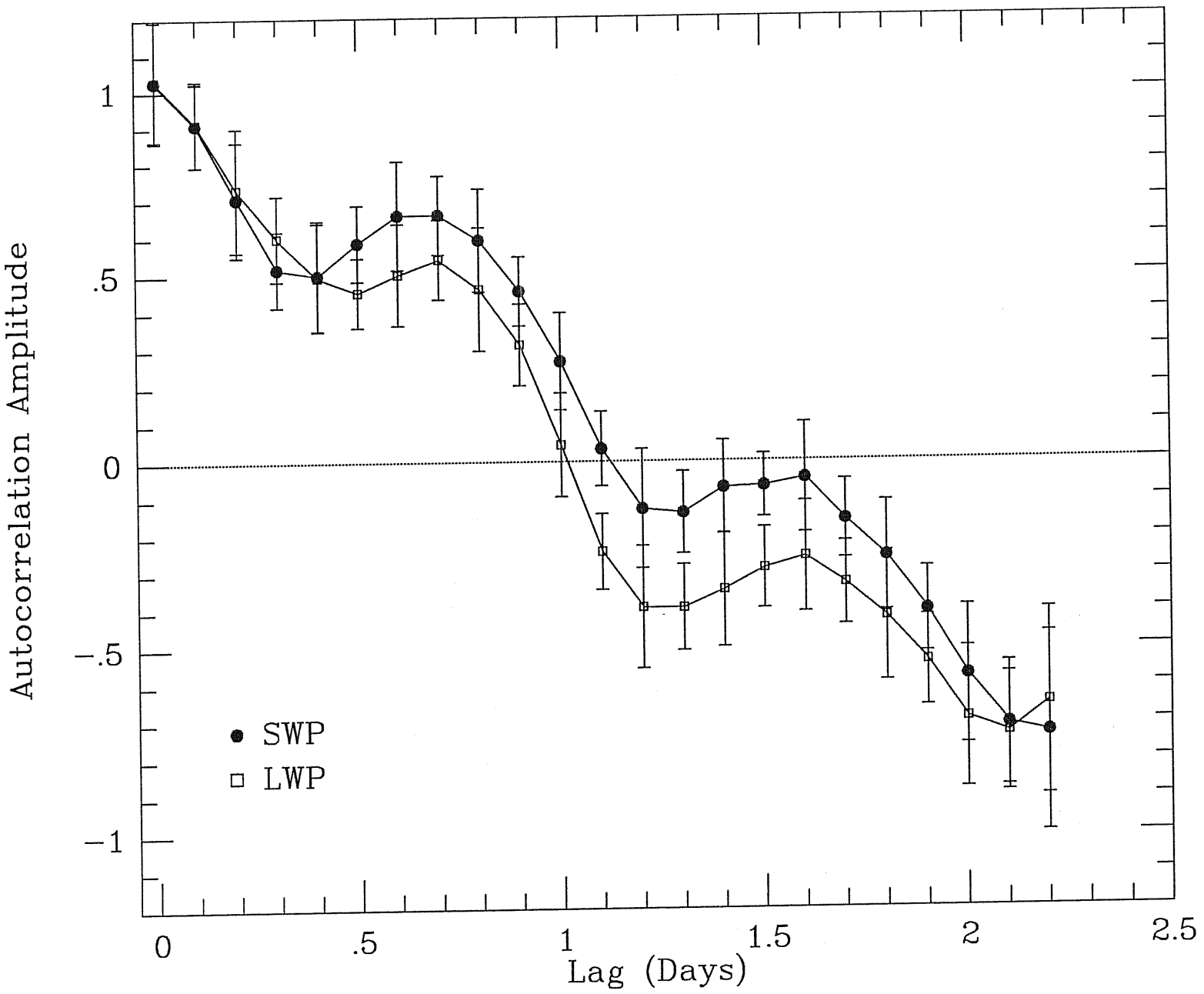
Autocorrelation Amplitude
1
.5
0
−.5
−1
0
.5
1
1.5
2
2.5
Lag (Days)
SWP
LWP

Appendix C

Notes on IUE data reduction software

IUE data reduction

note and software prepared by
L.Chiappetti - IFCTR & E.Pian - SISSA

"così per li gran savi si confessa
che la fenice muore e poi rinasce
quando al cinquecentesimo anno appressa"
(Inf. XXIV 106-108)

"rifatto sì come piante novelle
rinovellate di novella fronda,
puro e disposto a salire alle stelle"
(Purg. XXX 143-145)

Table of content

1. Introduction
2. The standard extraction
   2.1 Prerequisites
   2.2 The procedure
3. The Gaussian extraction
   3.1 Prerequisites
   3.2 The procedure
4. Hints for reduction and analysis
   4.1 Tape analysis commands
   4.2 Reduction commands
      4.2.1 rebinning
      4.2.2 sum, rescaling and algebra on images/spectra
      4.2.3 joining images/spectra
      4.2.4 smoothing
      4.2.5 rigid shift and change of coordinates
      4.2.6 extraction of a region, truncation, extension of an image
      4.2.7 maximum and minimum
   4.3 Dereddening
   4.4 File handling
   4.5 Analysis commands
      4.5.1 computation of fluxes
      4.5.2 generation of wide-band spectra (SIGMA files)
5. Spectral fitting
   5.1 Generation of SIGMA files from MIDAS spectra
   5.2 Generation of FLUX files from MIDAS spectra
   5.3 Conversion of FLUX files into MIDAS spectra
   5.4 Conversion of SIGMA files into MIDAS tables
   5.5 Recommended procedure
   5.6 Utilities for file transfer to and from the IBM
6. Graphics
   6.1 Vector graphics
      6.1.1 Graphics control

6.1.2 Graphics hardcopy
6.1.3 Interactive graphics
6.2 Image display
6.2.1 Display control
6.2.2 Display hardcopy
6.2.3 Interactive display
Appendix A.
Instructions for installation of MIDAS procedures
A.1 Introduction
A.2 Material to be retrieved
A.3 Instructions for retrieval
A.4 Common procedure installation
A.4.1 Main and auxiliary procedures
A.4.2 Calibration table installation
A.5 IUEX specific notes
A.6 GEX specific notes and installation
Appendix B.
Instructions for installation of IUEFITS
B.1 Introduction
B.2 Material to be retrieved
B.3 Instructions for retrieval
B.4 Common procedure installation
B.4.1 load and go installation
B.4.2 installation with relink
B.4.3 full reinstallation
B.4.4 IFCTR specific instructions

1. Introduction

The software runs on the Institute's Unix workstation within the framework of MIDAS .

This note is intended as a **complement** to previous documentation, including:

[1] Belloni and Chiappetti, 1987, Sistema di analisi IUE. Manuale per l'uso (IFCTR, Milano).

[2] Chiappetti, 1989, GEX. An IHAP implementation of the Gaussian Extraction for IUE (IFCTR, Milano).

therefore extensive description of basic IUE concepts are not presented here, but just the changes and updates to previous procedures. The reader is referred to the documentation quoted above for more information.

2. The standard extraction

The standard extraction is currently implemented as a MIDAS procedure. At the moment only 4-th files are processed.

c.2.1 Prerequisites

The procedure assume the files have an identifier of the same form used by the old IHAP extraction (Ref. [1], sect. 3.5.1) The convention is that the first character of the identifier be a `4` followed by a *blank* followed by the *camera* and image number (e.g. `4 SWP22553`). As in the case of the previous procedure, only 55 or 110 line spectra are processed. The user should take care that the `IDENT` descriptor is set appropriately.

It is also assumed to have the exposure time in seconds stored in a descriptor `EXPOTIME`. The user can write it manually, or wait to be prompted by the procedure.

2.2 The procedure

The procedure is called `IUEX` and currently processes a single 4-th file stored in MIDAS format (read in as described in 2 above). It is invoked as:

`@@ /pian/midas/iuex` *`name`* `[D] [N]`[1] ,

where

`name` is the name of the image

the optional argument `D` is used if one wants to follow the procedure step by step on the display. In this case it is recommended to create two image displays (size e.g. 1024×110) and one graphics display (size e.g. 1024×400) in advance, as the procedure does not take care of it.

the optional argument `N` is used to inhibit deletion of temporary files, which are otherwise automatically deleted (they are listed below).

The procedure is the exact analogue of the IHAP `DISK4` batch (see [1] 3.5.3.4). **Note however that presently no filtering is performed yet and the original image is used unchanged.** A minor difference is represented by the fact that the calibration curves are kept in MIDAS tables (and not read in from ASCII tables all the times). The latest calibration curves used in IHAP (i.e. the

---

[1] You might invoke it as `IUEX` *`filename`* `[D] [N]` in the case you have previously issued (e.g. in your `login.prg`) the MIDAS command:

CREATE/COMMAND IUEX @@ /pian/midas/iuex

Cassatella, Lloyd & Gonzalez 1988 for camera LWP) are used. There is some minor difference in the way the spline-interpolation of the calibration curve is done, in particular in the wavelength range outside that of the table the curve is set to zero, instead of extrapolating as IHAP did. Anyhow the difference is in general less than 2%.

The procedure produces two MIDAS files, a 4-th file calibrated in flux and an extracted 1-d spectrum. They are labelled accordingly using the same identifier of the input file followed by the word `calibrated` or `extracted`. The extracted file has the date of extraction in the `HISTORY` descriptor. The files are named appending a suffix to the original *name*, namely:

name`_calib` for the calibrated 4-th file
name`_iuex` for the extracted spectrum

In the case the extraction is repeated several times, and files with the same name exist already, a further 4-digit sequence number is appended to the file name, e.g. *name*`_calib_0001`.

The *name*`_calib` and *name*`_iuex` files correspond respectively to the files labelled `CALIB` and `EXTRA` on IHAP (ref. [1], 3.5.3).

All other files produced by the procedure are temporary files (accessible within MIDAS as `&A,&B...&H` : they are known on disk as `middumma.bdf` etc., see MIDAS manual). They can be deleted with `DELETE/TEMP`.

The temporary files are, in order of production :

`&A` filtered 4th file (currently copy of input file)
`&B` background in lower strip
`&C` background in upper strip
`&D` average background
`&E` smoothed background
`&F` 2-d smoothed background
`&G` interpolated calibration curve
`&H` 2-d calibration curve
`&I` calibrated 4th file, later renamed to *name*`_calib`
`&J` extracted spectrum, later renamed to *name*`_iuex`

In the case you enable the Display option, you will be shown the following (in time sequence):

In image 0:	the original file with standard cuts
In image 1:	the filtered file (&A) with the same cuts
In graphics :	the background (upper, lower, average, smoothed) upper (&C) and lower (&B) in cyan and magenta, average (&D) in black, smoothed (&E) in red : note that the upper and lower background refers to 8-16 scan lines and the average is reported to 1 line)
In graphics :	the calibration points with the interpolation (&G)
In image 1:	the calibrated 4-th file (`_calib`) with cuts 1-10
In graphics :	the extracted spectrum (`_iuex`)

. The Gaussian extraction

3.1 Prerequisites

They are the same reported in section 3.1 above

3.2 The procedure

The procedure is called GEX and currently processes a single 4-th file stored in MIDAS format (read in as described in 2 above). It is invoked as:

`@@ /pian/midas/gex` *`name step1 step2`* `[D] [N]`[1]

where

name is the name of the image and *step1, step2* are the binning factors for the two GEX passes (see [2])

the optional argument D is used if one wants to follow the procedure step by step on the display and to enable verbose mode.

the optional argument N is used to inhibit deletion of temporary files, which are otherwise automatically deleted (they are listed below).

The procedure is the exact analogue of the IHAP GEX batch (see [2] and reference therein for the details of the algorithm.).. A minor difference is represented by the fact that the calibration curves are kept in MIDAS tables and in the way the spline-interpolation of the calibration curve is done (for this refer to 2.2 above since the same calibration code is used). Also the binning procedure in MIDAS is aligned to the original bins, while in IHAP it is offset by half new bin.

The procedure takes (for a 55-line spectrum on a DECStation 5000) 0.2 s for the first pass and about 20 s for the second pass, plus the time needed to MIDAS for binning and calibration.

The procedure produces two MIDAS files, the raw result of GEX 2nd pass (which is a 1-d file scaled 0 to 1) and an extracted 1-d spectrum. They are labelled accordingly using the same identifier of the input file followed by the wording `GEX 2nd pass output 0-1` or `Gauss s1:`*`step1`* `s2:`*`step2`*. The extracted file has the date of extraction in the HISTORY descriptor. The files are named appending a suffix to the original *name*, namely:

---

[1] You might invoke it as `GEX` *`filename`* `[D] [N]` in the case you have previously issued (e.g. in your `login.prg`) the MIDAS command:

CREATE/COMMAND GEX @@ /pian/midas/gex

*name*_gex for the raw result of GEX 2nd pass
*name*_gauss for the extracted spectrum

In the case the extraction is repeated several times, and files with the same name exist already, a further 4-digit sequence number is appended to the file name, e.g. *name*_gauss_0001.

The *name*_gex and *name*_gauss files correspond respectively to the files labelled GEX and GAUSS on IHAP (ref. [2], pag. 4)

All other files produced by the procedure are temporary files (accessible within MIDAS as &A,&B...&H : they are known on disk as middumma.bdf etc., see MIDAS manual). They can be deleted with DELETE/TEMP.

The temporary files are, in order of production :

&A	the input file scaled 0 to 1
&B	&A rebinned according to coarse *step1*
&C	&A rebinned according to fine *step2* (only if not equal 1)
&D	result of GEX pass 2, later renamed to *name*_gex
&E	&D rescaled back to flux numbers
&F	integration of &E perpendicular to dispersion
&G	interpolated calibration curve
&I	extracted spectrum, later renamed to *name*_gauss

In the case you enable the Display option, **you will so far not be shown any plot** (it is planned to add such option later). This option only enables verbose mode in pass 2 (in this case for each wavelength been processed, the resulting flux is shown in a one-line status area on the screen). Pass 1 is always semi-verbose, showing a status line with the current wavelength, and messages about wavelength bins ignored because of insufficient signal, as well as the result of the final parabolic fit to the Gaussian width.

. Hints for reduction and analysis

This section will be filled with a brief reminder of the most useful MIDAS and IRAF commands.

.1 Tape analysis commands

The only equivalent to the commands described in [1], sect. 3.2 is the IRAF command `mtexamine`. Refer to [1], sect. 3.3 for the typical format of IUE, IHAP and FITS tapes.

Beware that the new FITS standard allows blocking factors and data formats (IEEE floating points) incompatible with IHAP. Check for the default formats used by MIDAS and IRAF (they are different) when planning to export data, and eventually change them as wished (it should always be possible to revert explicitly to the old format if needed).

.2 Reduction commands

This section shall describe replacements for commands listed in [1], sect 3.6, 3.7 etc. (to be written)

4.2.1 rebinning

4.2.2 sum, rescaling and algebra on images/spectra

See help for `COMPUTE/IMA`

4.2.3 joining images/spectra

4.2.4 smoothing

4.2.5 rigid shift and change of coordinates

4.2.6 extraction of a region, truncation, extension of an image

4.2.7 maximum and minimum

See help for `STATISTICS/IMA` and `FIND/MINMAX`

.3 Dereddening

.4 File handling

MIDAS files (images and tables) can be copied, renamed and deleted with the variants of the `COPY`, `RENAME` and `DELETE` commands (see the MIDAS help for use of qualifiers).

External files can be manipulated from within MIDAS using the `$` command followed by a system command. Unix users shall note that this gives access only to `sh` commands. To access `csh` commands (including the *Uniq interface*) one can define a `SYS` command as follows (typically do this in `login.prg`):

```
CREATE/COMMAND SYS $ csh -c
```

and then issue any csh command prefixing it with `SYS`.

There is no obvious facility to handle a directory of images (as done in IHAP with DLIST) unless perhaps one uses MIDAS catalogues. One could note the following commands:

`SHOW/DESC` *`file`*	to list all descriptors of a file (verbose)
`READ/DESC` *`file descriptor`*	to look at the value of one descriptor
`READ/DESC` *`file`* `IDENT`	to look at the image identifier

4.5 Analysis commands

This section shall describe replacements for commands listed in [1], sect [5.1 and 5.2 etc. (to be written : see also graphics in section 7 below)

4.5.1 computation of fluxes

The following MIDAS procedure (WARNING! this temporarily resides in /pian/midas) can be useful to compute the flux in an extracted spectrum (it assumes the usual IUE convention that units for data are 10^{-14} erg/cm^2/s/Å):

```
@@ flux file start end
```

This will use `STATISTICS/IMA` to compute the mean flux (in erg/cm^2/s/Å) of *`file`* between wavelength *`start`* and *`end`* (in Å). It will also compute the wide band flux (in erg/cm^2/s) multiplying by the band width.

The error shown is the *standard deviation* computed by MIDAS, which has been verified to be

$$\sqrt{\sum_{1}^{n} \frac{(x_i - \bar{x})^2}{n-1}}$$

Former IHAP users shall note that, while this standard deviation is numerically the same as the RMS returned by IHAP `SAMP` command, there may be an *inconsistency in usage* if one was accustomed to divide the IHAP RMS by the number of points `n` to obtain the error (this was done

systematically by several of our procedures). The current convention uses the raw standard deviation without dividing by n.

The following trick is useful to record the results of repeated invocations of flux into MIDAS logfile and to print it :

`log/on` to enable logging
issue all relevant commands
`log/off` to disable logging
with a system command (`$`) rename or print file `$MID_WORK/FORGR00.LOG` (capital letters !!) then delete it (otherwise new stuff will be appended to the previous log file)
`log/on` to re-enable logging

4.5.2 generation of wide-band spectra (SIGMA files)

Since the `makesigma` MIDAS procedure is mainly used as interface to the fitting programs, it is described in section 5 below.

6. Spectral fitting

At the moment the spectral fitting programs run unchanged on an IBM machine in Milan, which is accessible via internet.(see [1], sect. 4.3, and 6.7 below). Here are given only hints on the way to generate input files for them and to import results back to MIDAS. It might be possible that on a later date the fitting programs are ported to Unix.

One should note that the transfer of files between the workstation and the IBM is greatly enhanced by the use of ftp, and that it is possible to keep a window open on the IBM while on the workstation.

All procedures listed below reside temporarily in /pian/midas from where shall be copied.

5.1 Generation of SIGMA files from MIDAS spectra

A simple MIDAS procedure replaces the awkward IHAP procedure described in [1] 6.5. This procedure is invoked as :

```
@@ makesigma file (start end step) mode
```

where `file.bdf` shall be an extracted IUE spectrum. `mode` can be `AUTO` or `NOAUTO` (default) The remaining parameters are wavelengths in Å and are optional. The default is to use as `start` and `end` the start and end of the file, and as `step` a value of 50 Å. `mode=AUTO` disables interactive prompting.

As default operation the procedure will produce a file with fluxes and errors computed in bands `step` Å wide, covering with continuity the interval from `start` to `end`. This is however easily changed (typically to reject regions with noise or lines, *previously* identified e.g. in a graphical way) interactively : in fact the procedure (in `NOAUTO` mode) will prompt the user for the start and end wavelength of each bin as follows :

The start wavelength of the *first* bin will be suggested to be `start`. The user can however change it (and generally *must* change it : it is obvious that there is no sense in analysing a SWP spectrum from less than 1230 Å, or a LW spectrum from less than 2100 or 2400 Å, but the raw files will start at 1000 or 1700 Å respectively).

The start wavelength of *each next* bin will be the end of the previous bin. The user shall change it to introduce gaps (reject regions).

The end wavelength of *each* bin will be `step` Å more than its start. The user shall normally not change it, unless the bin is affected by a line (in which case one would make it *smaller*) or the next bin is affected by a line (in which case one would *extend* the current bin to include the line-free portion of the next one)

The user is prompted for bins a number of times determined in advance. This is 5 more than the number of bins *step* Å wide necessary to cover the range from *start* to *end*, to take into account the possibility of shorter bins specified by the user. The user can however terminate the input at any time by:

specifying a negative start wavelength
specifying a start wavelength shorter than the end of the previous bin
specifying an end wavelength beyond the file end

The following tracing of a typical run illustrates the way `makesigma` operates. Boldface indicates user input. <CR> indicates a plain carriage return.

```
Midas 003> @@ makesigma swp24010_iuex
Table prova will be created with max 0024 fluxpoints
Enter a NEGATIVE or out-of-range value to terminate
Point 0001 From lambda (df 1.00000E+03) 1250                    [1]
Point 0001 To   lambda (df 1.30000E+03) <CR>
Mean flux is 3.66367E-01 +/- 2.38836E-01 *E-14 erg/cm2/s/A
Point 0002 From lambda (df 1.30000E+03) <CR>
Point 0002 To   lambda (df 1.35000E+03) <CR>
Mean flux is 1.99881E-01 +/- 1.90026E-01 *E-14 erg/cm2/s/A
Point 0003 From lambda (df 1.35000E+03) 1500                    [2]
Point 0003 To   lambda (df 1.55000E+03) 1525
Mean flux is 3.67966E-01 +/- 2.46752E-01 *E-14 erg/cm2/s/A
Point 0004 From lambda (df 1.52500E+03) 1575                    [1]
Point 0004 To   lambda (df 1.62500E+03) <CR>
Mean flux is 2.12177E-01 +/- 2.53506E-01 *E-14 erg/cm2/s/A
Point 0005 From lambda (df 1.62500E+03) -1
Only 0004 points entered
Midas 004> read/tab swp24010_iuex
```

Sequence	LAMBDA	FLUX	ERROR	DELTA	NPTS
1	1.27500e+03	3.66367e-01	2.38836e-01	2.50000e+01	4.30000e+01
2	1.32500e+03	1.99881e-01	1.90026e-01	2.50000e+01	4.40000e+01
3	1.51250e+03	3.67966e-01	2.46752e-01	1.25000e+01	2.20000e+01
4	1.60000e+03	2.12177e-01	2.53506e-01	2.50000e+01	4.40000e+01

```
Midas 005>
```

[1] : change the start wavelength of the bin

[2] : change both the start and end wavelength of the bin

The procedure computes the flux *and error* as described in 5.5.1 above.

The procedure will produce two files (both in the current MIDAS data directory, the same where the input `file.bdf` resides) :

`file.sigma` is a SIGMA file in the old format (the choice of the old format is to make easier plotting it with programs like SMONGO), that is:

5 header lines (inclusive of the image identification)
n records with three columns (wavelength, flux, error respectively)

file.tbl is a MIDAS table. The only use of this is to plot the data within MIDAS using the PLOT/TAB or OVER/TAB commands. The table has 5 columns (the *first three* are the same as in the SIGMA file), that is:

#1 (LAMBDA) :	the central wavelength of each bin
#2 (FLUX) :	the flux
#3 (ERROR) :	the associated error
#4 (DELTA) :	the half width of the bin in Å
#5 (NPTS) :	the number of data points used in the bin

the purpose of the additional information is to allow, *should it prove necessary*, generation of a SIGMA file in the new format (including DELTA), or recomputing the error according to the old convention (dividing by NPTS) just using standard MIDAS table manipulation.

Limitations: the command used to transfer the table data outside MIDAS is PRINT/TABLE. This implies resetting the current ASSIGN/PRINT. Since the way the assignment is coded is not clearly documented, it is impossible to restore it. Therefore a default ASSIGN/PRINT is made at the end : in the case this *does not repristinate* the previous assignment a *warning* is issued and the user shall take care of it manually.

A further limitation is that the way used to transform the output of PRINT/TAB into the wished format (particularly appending the header) is strongly *dependent on Unix* commands.

5.2 Generation of FLUX files from MIDAS spectra

A simple MIDAS procedure replaces the IHAP procedure described in [1] 6.4. This procedure is invoked as :

```
@@ makeflux file
```

where *file*.bdf shall be an extracted IUE spectrum.

The procedure will produce *file*.flux (in the current MIDAS data directory, the same where the input *file*.bdf resides), in the standard FLUX format, that is :

5 header lines (inclusive of the image identification)
n records with two columns (wavelength, flux respectively)

This procedure is essentially a wrapper around the COPY/IT command to convert a MIDAS .bdf image into an intermediate MIDAS table. The table is then written out to ASCII using PRINT/TAB in a way similar to makesigma. Any intermediate files are deleted.

Limitations: the same described in 5.1 above.

5.3 Conversion of FLUX files into MIDAS spectra

A simple MIDAS procedure replaces the IHAP procedure described in [1] 6.3. This procedure is invoked as :

```
@@ fromflux file reffile (KEEP)
```

where *file*.flux shall be a standard FLUX file, and *reffile*.dbf an existing spectrum in MIDAS .bdf format used as reference to determine the wavelength range and the step in wavelength necessary to create *file*.bdf.

The procedure works reading in the ASCII FLUX file into an intermediate table (using CREATE/TABLE) and converting this into an image (with CONVERT/TABLE). This second step requires the reference image. Normally one should use as a reference image a spectrum from which the parent of *file*.flux was generated (therefore with the same step), however the MIDAS command is capable of interpolating the FLUX file on any other binning (but cannot extrapolate outside the wavelength range of the FLUX file and will set to zero the flux there).

There is generally no sense in keeping and using the intermediate table (which can be quite large), but if wished this is accomplished specifying the optional keyword KEEP. In this latter case the table will be named *file*.tbl.

Limitations: there are two *Unix dependent* commands used to chop off the header of the FLUX file and dispose of a temporary file.

5.4 Conversion of SIGMA files into MIDAS tables

This will be needed very seldom, but can be done straight away with the MIDAS CREATE/TABLE command. It is recommended to chop off the 5 header lines from the SIGMA file before.

6.5 Recommended procedure

This is the recommended procedure to run a fitting session using MIDAS to produce the SIGMA files and to plot the results, and the IBM for fitting.

a extract the IUE spectra according to the procedures in sections 3 or 4, the file selected for processing be e.g. good.bdf

b plot good.bdf and note down the regions to be rejected

c use makesigma (see 5.1) to produce good.sigma

d use makeflux (see 5.2) to produce good.flux

e transfer good.sigma and good.flux to the IBM (see 5.6) : note they will be named GOOD SIGMA and GOOD FLUX

f on the IBM do not forget to use SETMODE (see [1] 2.1) and make sure that GOOD SIGMA and GOOD FLUX have RECFM F (see 5.6)

g run the fitting program UVFIT (see [1] 4.3) on GOOD SIGMA and print the final results in FIT PRINT; eventually rename such file if you want to keep it

h in order to have a visual impression of the fit (optional), you might (it could be not necessary to save the intermediate files):

h1 transfer FIT FLUX from IBM to the workstation with MIDAS

h2 use fromflux (see 5.3) with option KEEP to create a table fit.tbl

h3 use OVER/TAB to overplot both the input and the output of the fitting procedure, that is good.tbl and fit.tbl over good.bdf

i on the IBM run UVGRID or multiple runs of UVFIT to find the confidence range of the parameters of the best fit, and/or to refine the best fit

j once you have determined the final best fit parameters, run again UVFIT on GOOD FLUX in dummy mode, that is do not fit the initial guesses (reply NO to all questions)

k throw away FIT PRINT but rename FIT FLUX to some name reminding you of the original (e.g. to GOODFIT FLUX)

l transfer GOODFIT FLUX from IBM to the workstation with MIDAS

m use fromflux in default mode to create goodfit.bdf

n use OVER/IMA to overplot the fitted curve from goodfit.bdf over the original spectrum good.bdf (or equivalent, e.g. it might be convenient to use the result of a Gaussian extraction for generating the SIGMA files, but the result of the default extraction, without gaps, for plotting)

So far there are no facilities to plot the results of UVGRID within MIDAS.

5.6 Utilities for file transfer to and from the IBM

It is suggested to have an IBM window open on the same workstation running MIDAS and to get the SIGMA and FLUX file via ftp invoking the ftp session from the IBM (this is easier than making a put from Unix which requires the IBM disk passwords). Similarly the results of the fit can be put to the workstation opening the ftp session from the IBM.

See HELP FTP and HELP FTP MENU for details (e.g. for the use of mget to get multiple files). In general you shall open an interactive ftp session as listed below (this is typically done if you want to get more files in a session) or issue a special command to invoke one of the automatic unsupported procedures also listed below.

```
ftp  tsmix3.sissa.it
 [1]
VM TCP/IP FTP R1.2.1
Connecting to tsmix3.sissa.it 147.122.2.255, port 21
220 tsmix3.sissa.it FTP server (..........) ready.
USER (identify yourself to the host):
pian                                                          [2]
>>>USER pian
331 Password required for pian.
Password:
typeyourpasswordhere                                          [2]
>>>PASS ********
230 User pian logged in.
Command:
cd  /pian/midas                                    [3]
>>>CWD /pian/midas
250 CWD command successful.
Command:
get  swp36820_iuex.flux                                       [4]
>>>PORT 147,122,2,255
200 PORT command successful.
>>>RETR swp36820_iuex.flux
150 Opening data connection for swp36820_iuex.flux (192.65.131.1,28725) (25962
bytes).
226 Transfer complete.
26802 bytes transferred. Transfer rate 5.46 Kbytes/sec.
Command:
quit
>>>QUIT
221 Goodbye.
Ready;
reform  swp36820  flux  a  f                                  [5]
COPY SWP36820 FLUX A = = = ( RECFM F REPLACE
Ready;
```

[1] : select your workstation

[2] : type your username and password

[3] : cd to the MIDAS data directory (*/user/midas* typically)

[4] : get the file : beware the name might be truncated to 8 characters

[5] : **important** : change the file format manually !!!!

Note that ftp will truncate any filename to 8 character. In the example above the IBM file will be called SWP36820 FLUX. If a file with the same name exists it will not be replaced by default. You shall (in an interactive ftp session) either issue a get *file.type* (REPLACE command or specify a new name on the IBM issuing get *file.type newfile.type*.

IMPORTANT! ftp transfers files with RECFM V, while UVFIT wants them with RECFM F. To change the record format use (if command available) :

```
REFORM filename filetype * F                    or otherwise do
COPY filename filetype * = = = (RECFM F REPLACE
```

where *filetype* is either FLUX or SIGMA. Do not forget to change record format or the fitting program will fail.

There are two unsupported utilities to automatically arrange for copies. These could be invoked as :

`FROMSISSA name type` **or** `TOSISSA name type`

They will copy file `name.type` from the VAX machine of S.I.S.S.A. to the IBM as `name type`, or viceversa copy `name type` from IBM to VAX as `name.type`. The arrangement will be such that one will be prompted for the username, password and directory on the remote machine only once at the beginning. One still have to make a `REFORM`.

```
fromsissa  swp36820_iuex  flux
Enter username
pian
Enter password
youwontexpectIlltypemypasswordheredontyou
Enter remote directory
[ap.pian....]
VM TCP/IP FTP R1.2.1
OPEN (name of foreign host):
Connecting to tsmi19.sissa.it 147.122.2.79, port 21
220 tsmi19 FTP server (......) ready.
USER (identify yourself to the host):
>>>USER pian
331 Password required for pian.
>>>PASS ********
230 User pian logged in.
Command:
Usage of SITE command with PUT is OFF
Command:
>>>CD [ap.pian....]
250 CWD command successful.
Command:
200 PORT command successful.
>>>RETR swp36820_iuex.flux
150 Opening data connection for swp36820_iuex.flux (192.65.131.1,29996) (25962
bytes).
226 Transfer complete.
Ready; T=0.10/0.18 09:28:52
reform  swp36820  flux  a  f
COPY SWP36820 FLUX A = = = ( RECFM F REPLACE
Ready; T=0.03/0.05 09:29:24
```

5.7 Unidimensional chi-square grids

A further (IBM) program has been added to UVFIT and UVGRID to allow to search for confidence intervals on a single interesting parameter in an easier and automatized way. This program is named UVGRID1D and is used exactly with the same calling sequence as UVGRID (see [1], 4.3.2). The only differences are :

Only one parameter (typically this is spectral index) can be stepped. The other parameters can be fitted (typically the normalization) or fixed (typically A_V). There are 100 steps in the 1-d grid (so the range is from the *value* given for the interesting parameter to *value*+99**step*

The program performs an auto search of the best fit (minimum of the chi-square profile vs interesting parameter), which is often more accurate than the one performed by UVFIT (which tends to get stuck in local minima) and of the 90% confidence limit (using a $\Delta\chi^2$ of 2.71 appropriate for one interesting parameter). The results are written to the terminal and to the output file GRID PRINT. *Note that if the confidence interval is larger than the stepped interval, suitable warnings are given.*

There is no 2-d chi-square grid image file. Instead one has a file GRID1D TABLE (2 header lines, 2 columns), which can be used to plot the chi-square (column 2) versus the single interesting parameter (column 1).

An additional file GRID1D RESULT contains a single line with the image id, the best fit value and the 90% interval extrema for the interesting parameter. Its purpose is to be appended (manually) to a "database" summary file, in case of fitting of multiple images.

One can still read the values of the uninteresting fitted parameters in the file GRID PRINT.

Programmer's note: in order to implement this program quickly with minimum disruptions the source file contains dedicated variants of routines READP and SETP which replace the official library version

6. Graphics

It is presently not planned to support officially any graphics program (although it might be possible that some of the old HP programs are converted). Users are referred to the plotting facilities available within MIDAS and IRAF, to the other plotting utilities available (e.g. Supermongo - it shall be noted that this is considered *unsupported*), or to their PC plotting facilities.

In particular for what concerns MIDAS it is recommended to create one or more image displays and one graphic display. The following is the arrangement assumed e.g. by the IUEX batch for displaying its results : two image windows of appropriate size (of which display 0 is used as default) and one graphic window.

```
create/display 0 1024,110,0,1000
create/display 1 1024,110,0,800
create/graphic 0 1024,400,0,600
load/lut rainbow
assign/display d,0
```

6.1 Vector graphics

6.1.1 Graphics control

Graphics command to look at spectra include `PLOT/IMA` and `OVER/IMA` (and the corresponding `PLOT/TAB` and `OVER/TAB`). The layout of the plot can be controlled by the `SET/PLOT` command : particularly useful are the following parameters :

`XAXIS` (set to `AUTO` or use it to control the wavelength range)
`YAXIS` (set to `AUTO` or use it to control the cuts in flux for plot)
`BIN=ON` (to have histogram-like, not spiky plots)
`PMODE` (use 2 as default, use 1 for hardcopies without long legenda)
`COLOUR` (useful for display on screen, 1=black 2=red 3=green etc.)
`LTYPE` (use 1=solid 2=dotted instead of colour for hardcopies)

6.1.2 Graphics hardcopy

To produce an hardcopy see section 6.1.6 of volume A of the MIDAS Users Guide: `SEND/PLOT` looks preferred to `ASSIGN/PLOT` to dispose of the plot. It appears that, selecting `LASERA` as hardcopy device, a file `pscrplot.0` is produced in the MIDAS data directory : however the PostScript previewer has some difficulty with it.

6.1.3 Interactive graphics

Interactive graphics can be used to read coordinates out of a plot. The standard MIDAS command to do this is `GET/GCURS`. However it has a problem, that is it accepts only filenames not longer than 12 characters (limit

which is generally violated by the naming convention used by the IUEX and Gaussian extraction) A replacement procedure (WARNING! temporarily this resides in /pian/midas) is provided and can be invoked as :

```
@@ gcur
```

This procedure retrieves the full name of the image currently plotted from keyword MID$PLOT and temporarily renames it to the first 12 characters of the name (if longer) while invoking GET/GCURS.

6.2 Image display

6.2.1 Display control

The typical command to look at an image is LOAD/IMA. Useful manipulation of the appearance of the image is obtained controlling the CUTS or via the lookup table (LOAD/LUT, DISP/LUT and MODI/LUT; also CLEAR/LUT). An useful command to be associated with a shortcut synonym is CLEAR/CHANNEL OVERLAY.

6.2.2 Display hardcopy

There are two commands which can be used to produce a gray scale hardcopy of an image (PLOT/GRAY and PLOT/PERSPECTIVE are not considered as they work only on a limited image size) : LOAD/IMA having done an ASSIGN/DISP to LASERA, and COPY/DISP from the current image display. It is however unclear and undocumented how to easily control the appearance of the hardcopy (e.g. black-on-white, white-on-black, position on the page etc.).

6.2.3 Interactive display

Interactive display can be used to read coordinates out of an image. The standard MIDAS command to do this is GET/CURS. However it has a problem, that is it accepts only filenames not longer than 12 characters (this limit is however not considered seriously, since normally one will use it on raw fourth files, whose names are 8 character long).

The best results are obtained using GET/CURS in a zoom window. Unfortunately the syntax is complex and also it is not possible to resize the zoom window once created. The following command string is a reasonable approach, and could be aliased to a shortcut synonym or a private procedure :

```
get/cursor ? ? NN ? W,8 512,220,0,400
```

Appendix A.
Instructions for installation of MIDAS procedures

A.1 Introduction

The MIDAS procedures IUEX and GEX (described in 2.2 and 3.2) are potentially available for distribution to external sites. They are distributed "as is" with no guarantee express or implied of fitness to any particular purpose. It is requested that the author of the procedure be duly acknowledged in each paper using results produced by these extraction codes, with a sentence like:

> The routines for the IUE spectral extraction are a local implementation within ESO MIDAS written by L.Chiappetti.

We give here instruction for installation of the procedures at a generic site running MIDAS (portable MIDAS version 91MAY or later), together with some programming information.

A.2 Material to be retrieved

The material to be retrieved for an installation is given in the table in the following page (for each the complete path name on the `poseidon` DECstation is given; see below for information about network retrieval).

A.3 Instructions for retrieval

If you have an Internet connection, you can retrieve all the above via `ftp` to `poseidon.mi.cnr.it` (192.65.131.49), with username `none` password `none`. Please do not retrieve the system dependent (optional) parts if you are not on a compatible system. The mandatory parts shall be retrieved in `ascii` mode, while the optional parts are to be retrieved in `binary` mode.

If you have only Decnet connections, you should be able to retrieve the material using IFCTR (= 39610) as gateway as in the following example :

```
COPY IFCTR::SUN"none none"::"/poseidon/lucio/iue/midas/gex.prg" *.*
```

There is of course no sense in retrieving the optional material on a VMS system.

Mandatory material	File name
ASCII source for calibration files	/poseidon/lucio/iue/calibration/twsp.ascii /poseidon/lucio/iue/calibration/tlwp.ascii /poseidon/lucio/iue/calibration/tlwr.ascii
Main IUEX procedure	/poseidon/lucio/iue/midas/iuex.prg
Main GEX procedure	/poseidon/lucio/iue/midas/gex.prg
Auxiliary procedures (for both)	/poseidon/lucio/iue/midas/iueaux_smo.prg /poseidon/lucio/iue/midas/iuerename.prg
Fortran sources for GEX	/poseidon/lucio/iue/source/gex1.for /poseidon/lucio/iue/source/gex2.for /poseidon/lucio/iue/source/gexco.for
Optional compilation csh script	/poseidon/lucio/iue/source/mcomp
Optional material	
MIDAS calibration tables (Ultrix)[1]	/poseidon/lucio/iue/midas/tswp.tbl /poseidon/lucio/iue/midas/tlwp.tbl /poseidon/lucio/iue/midas/tlwr.tbl
MIDAS calibration tables (Sun)[2]	/poseidon/lucio/iue/midas/sun/tswp.tbl /poseidon/lucio/iue/midas/sun/tlwp.tbl /poseidon/lucio/iue/midas/sun/tlwr.tbl
Executables for GEX (DEC Ultrix)[3]	/poseidon/lucio/iue/midas/gex1.exe /poseidon/lucio/iue/midas/gex2.exe
Executables for GEX (Sun)[4]	/poseidon/lucio/iue/midas/sun/gex1.exe /poseidon/lucio/iue/midas/sun/gex2.exe

A.4 Common procedure installation

A.4.1 Main and auxiliary procedures

a) Select a directory where you want to install everything (this is here `/poseidon/lucio/iue/midas`) and go there

b) copy there all *.`prg` files (`iuex.prg`, `gex.prg` and the auxiliary files)

c) edit the `iuex.prg` file, read the header, then go the `define/local` statement defining the `disk` variable and replace it with the name of

---

[1] to be retrieved only from another Ultrix system
[2] to be retrieved only from another Sun system
[3] to be retrieved only from another DECstation running Ultrix (RISC)
[4] to be retrieved only from another Sun system with `sun4` architecture

your directory (Unix or VMS syntax). Note you may have to change the length of the `disk` variable too if it is longer than the current value. You should also disable/delete the following statements which reset `disk` if an environment variable `DECSTATION` is not set to 1 (this is used locally for multiple architecture support on Decstation and Sun).

d) edit the `gex.prg` file and apply the same changes done to `iuex`.

e) do not forget to do a `CREATE/COMMAND` pointing to the new correct location of iuex and gex if you want to call them by name.

A.4.2 Calibration table installation

The calibration tables are supplied as ASCII files, since MIDAS table files are not portable among different systems. You should reinstall them by reading the ASCII file into a MIDAS table within MIDAS. The ASCII tables may reside anywhere, and can be deleted after the conversion (even if it is suggested to store them in some safe place out of the way). The MIDAS tables shall reside in the same directory where the .prg files are.

a) go into MIDAS
b) `create/tab` *name* `2` *n* `/poseidon/lucio/calibration/`*name*`.ascii`
c) assign names to columns (the units and formats are optional)
```
name/col name #1 :LAMBDA "Angstrom" G12.4
name/col name #2 :CALIB "S-1 FN ?" G12.4
```
d) make sure to repeat b-c for all three tables (*name* is `tswp,tlwp,tlwr` and *n* is `34,61,31` respectively)

A.5 IUEX specific notes

IUEX is a pure MIDAS procedure. Therefore it shall be available immediately if the above instructions have been followed correctly.

A.6 GEX specific notes and installation

GEX, similarly to his IHAP predecessor, calls two external Fortran programs GEX1 and GEX2. Unless you have a compatible DECstation or Sun system, you shall not install the corresponding `.exe` files but recompile them from the sources.

Both programs make reference to a common include file `gexco.for`, which shall be present on the same disk where `gex1.for` and `gex2.for` are.

You may copy the program sources to any directory you wish (possibily different from the one where the `.prg` files reside) and remove them once you have generated the `.exe` files and moved them to the same directory where you have the `.prg` and `.tbl` files.

Note that the source files shall have a `.for` extension even on an Unix system. The corresponding `.f` files will be created by the `esoext` preprocessor. The source files are compliant to the rules in the *MIDAS Environment* document (ESO 1991) with the exception that terminal output is handled via Fortran `WRITE`s.

To generate the `.exe` files on an Unix system and move them to the appropriate place, you may use the provided `mcomp` script.

```
mcomp gex1 destination
mcomp gex2 destination
```

where *destination* is the final directory where the `.exe` files are to be stored. Note that this csh script explicitly specifies to `esoext` to look for include files also in the current directory.

On VMS systems you compile and link as described on pag. 5-1 of the *MIDAS Environment* document, then manually move the files to their destination. Note that this has not been tested. If compilation fails, look for the `INCLUDE` statements referring to `:GEXCO.FOR` (which are in the unusual MIDAS syntax) and try removing the initial colon. Such statements are located in the main program and in `MID_GEX` routine. You might also have to comment out the calls and the code of the `CPUCLK` subroutine (or replace with one written by you).

Some notes for programmers. GEX1 and GEX2 retrieve information from the calling `gex.prg` via MIDAS keywords. They read and write MIDAS images using the STI interface routines. For the rest (apart the syntax of the INCLUDE statement) they are virtually unchanged w.r.t. the original HP sources. All debug statements are commented out (`esoext` does not like them)

Of course the main computation has been moved into a subroutine, since this is required by the STI pseudomapping mechanism.

Due to an unexplained deficiency in the STI routines on the DECstation (it appears not possible to have two images open at same time), the GEX2 works on a copy of the input image, opened in read/write mode (`F_IO_MODE`).

It was also necessary to protect the exponential for underflows, as the handling of floating point exceptions on DECstations is less robust than on HP.

At the moment GEX1 and GEX2 still communicate via a Fortran- written direct access file called `gexfin` (in current MIDAS data directory). It is planned to replace this with a MIDAS table and a set of keyword (for the parabolic fit coefficients). At the moment all debug plotting is disabled, but is planned to insert some plotting (either directly using plotlib or in the calling .prg files using intermediate tables).

Appendix B.
Instructions for installation of IUEFITS

B.1 Introduction

The program IUEFITS for reading IUE tapes is potentially available for distribution to external sites. It is distributed "as is" with no guarantee express or implied of fitness to any particular purpose. It is desirable that the author of the program be duly acknowledged in each paper using results produced by this program, with a sentence like:

> The routines for reading IUE tapes into FITS are a local implementation written by L.Chiappetti. The use of W.Pence's FITSIO library is gratefully acknowledged.

We give here instruction for installation of the program at a generic site, together with some programming information.

B.2 Material to be retrieved

The material to be retrieved for an installation is given in the table in the following page (for Unix files the complete path name on the `poseidon` DECstation is given, for VMS the path on disk `IFCTR::DUA0:` is given; see below for information about network retrieval).

Mandatory material	**File name**
Sun executable	/poseidon/lucio/iue/midas/sun/iuefits
VMS executable	[LUCIO.IUE]IUEFITS.EXE
Optional material for relink	
Main program sources (just one copy needed, they are *identical* for Unix and VMS)	/poseidon/lucio/iue/source/iuefits.f /poseidon/lucio/iue/source/iuefits.inc or [LUCIO.IUE.SOURCE]IUEFITS.FOR [LUCIO.IUE.SOURCE]IUEFITS.INC
Sun relocatable libraries	/poseidon/lucio/lib/libluciolib.a /poseidon/lucio/xas/lib/libfitsio.a /poseidon/lucio/xas/lib/libvos.a
VMS relocatable libraries	[LUCIO.LIB]LUCIOLIB.OLB [LUCIO.XAS.LIB]FITSIO.OLB [LUCIO.XAS.LIB]VOS.OLB

Continued in next page.

Optional material for full recompile

Sun sources for luciolib library	all files in in /poseidon/lucio/fortran/luciolib in /poseidon/lucio/xas/libsource/vos
Sun sources for fitsio library	all files in /poseidon/lucio/xas/libsource/fitsio
Sun source for vos library	from /poseidon/lucio/xas/libsource/vos : z_op_sys.f z_tape_open.f z_print_file.f
VMS sources for luciolib library	all files in [LUCIO.FORTRAN.LUCIOLIB]
VMS sources for fitsio library	all files in [LUCIO.XAS.LIBSOURCE.FITSIO]
VMS source for vos library	from [LUCIO.XAS.LIBSOURCE.VOS] : Z_OP_SYS.FOR Z_TAPE_OPEN.FOR Z_PRINT_FILE.FOR

B.3 Instructions for retrieval

If you have an Internet connection, you can retrieve all the above via `ftp` to `poseidon.mi.cnr.it` (192.65.131.49), with username `none` password `none`. Please retrieve only what you really need. Source files shall be retrieved in `ascii` mode, while executables and libraries are to be retrieved in `binary` mode.

If you have only Decnet connections, you should be able to retrieve the material using IFCTR (= 39610) as gateway as in the following example :

```
COPY IFCTR::DEC"none none"::"/poseidon/lucio/iue/pinco.f" *.*
```

B.4 Common procedure installation

B.4.1 load and go installation

This is the simplest case. You just retrieve the executables (mandatory material) and run them. You **do not need to recompile and relink.** Do this if you are not curious of what is inside.

Just select a directory *yourpath* where you want to install everything and copy there the Sun or VMS executable (**only** the one relevant for your system !!). Then define a command for it as :

```
alias iuefits 'yourpath/iuefits \!*'        on Unix)
IUEFITS == "$yourpath:IUEFITS"              (on VMS)
```

B.4.2 installation with relink

If you want to have a look at the source of `IUEFITS`, you can retrieve the source files (listed under optional material). The source code is identical for Unix and VMS, so you need just to retrieve them once.

If you want to modify the program, or for any other reason you need to relink it, you need also to retrieve the relocatable libraries already compiled (also listed as optional material). You can store all the libraries in the same directory, even if the arrangement in Milano is different. The simplest procedure for a generic site is :

a) select a directory `yourpath` where you put everything
b) retrieve source code *and* relocatable libraries
c) compile `iuefits.f` (or `IUEFITS.FOR`)
d) link it with the three libraries
e) delete the object files

B.4.3 full reinstallation

Only in exceptional cases you might need to retrieve all the sources. In general an installation with relink (B.4.2) *should suffice* to most sites. Since each site has local conventions about using libraries, and since the libraries used by `IUEFITS` are used at IFCTR for other projects, only *generic* guidelines can be given :

a) select a directory `yourpath` where you put everything
b) retrieve source code *and* the source for all library routines (you do not need to put library routines in different subdirectories, but you might find this helpful)
c) compile `iuefits.f` (or `IUEFITS.FOR`)
d) compile each library routine separately
e) put each object into a relocatable library (you can put all of them in a single library, or preserve the arrangement in three libraries as you wish) with a command like `ar` and `ranlib` (Unix) or `LIBRARY` (VMS).
f) link the main program with the library (or libraries)
g) delete all object files

B.4.4 IFCTR specific instructions

The following procedure is used to recompile `iuefits` at IFCTR. Please note that the source of the main program, and of the associated include file reside physically on `IFCTR::DUA0:[LUCIO.IUE.SOURCE]` while the files in `/poseidon/lucio/iue/source` are just links. Therefore all edits have to be done on the Vax.

Library routines have to be compiled separately on each system, using *the same* Real Programmer Tool commands. The example refers to the

`upcase.f` routine in library `luciolib`. The paths for `libsourcedir` and `libdir` in a generic case can be derived from the table above :

```
libsourcedir /poseidon/lucio/fortran
libdir /poseidon/lucio/lib
complib lucliolib upcase
```

On Sun proceed as follows for the relink of the main program :

login to `helios` **only** !

```
cd /poseidon/lucio/iue/source
configure
comlink iuefits iuefits [term]
```

Note that the file `iuefits.loader` contains indications on where to find the correct libraries. The executable is stored in `/poseidon/lucio/iue/midas/sun` together with all Sun-specific executables, even if it has nothing to do with MIDAS directly.

On Vax proceed as follows for the relink of the main program :

```
cd [lucio.iue.source]
@configure
comlink iuefits iuefits [term]
```

Here too the file `IUEFITS.LOADER` is used to locate the correct libraries. The executable is stored in `[LUCIO.IUE]` in lack of a better place.